

October 1966.

1119.56
Report SA-6

398506143

ANNUAL SUMMARY I

UPPER and LOWER BOUNDS TO
STRUCTURAL DEFORMATIONS
by DUAL ANALYSIS in FINITE ELEMENTS.

G. SANDER,
Assistant,
Laboratoire de Techniques
Aéronautiques et Spatiales.

Université de Liège
BST - Sciences Appliquées et Mathématiques
1, Chemin des Chevreuils; Bât. B52/4
S-4000 LIEGE

B. FRAEIJIS de VEUBEKE,
Professor of Aerospace Engineering.

UNIVERSITY of LIEGE,
75, rue du Val-Benoît, LIEGE, Belgium.

The research reported in this document has been sponsored by the Air Force Flight Dynamics Laboratory under CONTRACT AF 61(052)-892 through the EUROPEAN OFFICE of AEROSPACE RESEARCH (OAR) UNITED STATES AIR FORCE.

SUMMARY.

I. GENERAL THEORY.

I.0- Introduction.

I.1- Displacement models for lower bounds.

I.2- Equilibrium models for upper bounds.

2. MODELS LIBRARY.

2.1- Displacement models.

2.1.1- Bar elements 2.1.1.1- Linear displacement field.

2.1.1.2- Quadratic displacement field.

2.1.2- Skin elements 2.1.2.1- Turner triangle.

2.1.2.2- Quadratic triangle.

2.1.3- Spar elements 2.1.3.1- Linear spar cap displacements.

2.1.3.2- Quadratic spar cap displacements.

2.1.4- Plate elements : Quadrangle in oblique coordinates.

2.1.5- Rigid jointed frame element.

2.2- Equilibrium models.

2.2.1- Bar element with constant shear.

2.2.2- Skin element : the constant stress quadrangle.

2.2.3- Spar element 2.2.3.1- Upper bound version.

2.2.3.2- Direct approach.

2.2.4- Plate element : the triangle with linear moments distribution.

3. NUMERICAL RESULTS.

3.1- Spars.

3.2- Box beams.

3.3- Multiwebbed swept back wing.

3.4- Plates in bending.

APPENDIX : The A.S.E.F. computer program.

A.1- General description.

A.2- Substructure technique.

A.3- Description of the program.

A.4- Flow diagram.

A.5- Input data preparation.

A.6- Worked examples.

I. GENERAL THEORY.

I.0- Introduction.

In the analysis of a structure by decomposition into finite elements the initial emphasis has been almost exclusively directed towards the matrix operations by which the final displacement unknowns or redundant force unknowns can be determined. From there the name of "matrix structural analysis" and the broad classification of procedures in two classes :

The "Direct Stiffness Method" (see for instance References R.I.1 and R.I.2) which takes nodal displacements as the set of unknowns,

The "Redundant Force Method", sometimes simply called the Force Method, where a set of internal and external force redundancies is taken as the set of unknowns (see for instance References R.I.3 and R.I.4).

The two procedure are intuitively linked, the first to satisfaction of compatibility conditions, the second to satisfaction of equilibrium conditions. While this is true at the structural level, it must be emphasized that it is generally not true at the element level. Many of the models of element behavior used in the past do not comply with the existence of a continuous displacement field (they are not internally compatible) nor do they satisfy everywhere the local equilibrium conditions. The same can be said for conditions prevailing at the interfaces between adjacent elements.

The connections are often such that the displacements are not continuous across an interface, nor are the stresses transmitted continuously.

However, the correct representation of the structure depends fundamentally on the value of the models devised to represent element behavior and interface transmission. Once the models are chosen, progress in the mathematical techniques of matrix structural analysis cannot improve the resulting picture of deflections and stress distributions; they can only provide for reduced computer time and better accuracy in the figures for the idealized structure. More exactly, the only way that remains open to better approximate the real structure is by cutting it into finer pieces. The resulting multiplication in the number of unknowns makes this a costly procedure and eventually leads to loss in figure accuracy by accumulation in round off errors. As experience has shown, it is not even certain that, with crude element models, this procedure will succeed. This is the so-called "convergence" problem for which very few scientific guidelines are yet available.

As a consequence, after the development of satisfactory computer programs, progress in the approximation to the real structure will stem from a development of more sophisticated elements with an attendant reduction in the number of pieces and better convergence characteristics. The first realization of this and the first attempt at a systematic derivation of discrete element properties is due to GALLAGHER (Reference R.I.5).

The simplest approach, and the most easily visualized, is through the use of a parametric displacement field, the first few parameters to introduce representing the rigid body motions of the element, the others essential deformation modes. Internal compatibility is then automatically secured. Conformity, that is continuity of displacements at an interface, is less easily obtained, although some early skin elements of triangular shape (Ref. R.I.6) and rectangular shape (Ref. R.I.7), analyzed under the assumption of linear edge displacements, already had this advantage. The equivalent point loads associated to the set of nodal displacements are best derived from the minimum total potential principle (equivalent to Castiglione's theorem). This approach, which produces what we call "displacement models", puts the whole burden of the approximation on local violations of the equilibrium conditions.

The natural alternative approach, which concentrates on satisfying equilibrium properties, is decidedly more difficult. That is perhaps the reason why it has been so poorly represented and mostly in some indirect way. In Reference R.I.5 a swept quadrangular skin panel model is based on a parametric equilibrated stress field. The assumptions are simple enough to secure an integrable deformation field. The integrated displacement field is then determined by nodal displacements and the element properties of this compatible, but not conforming, model can be derived by the previous approach. In our terminology this model is a "hybrid". It is not a displacement model because it is not conforming, it is not an equilibrium model because, although internally equilibrated, the stresses are not transmitted continuously at the adjacent elements. Both types of inconsistencies occur in this case at the interfaces. All known "Force Methods", with their natural tendency to pay closer attention to the equilibrium properties, have relied on "shear panel" representations of the skin elements. This is a semi empirical approach in which the normal stress carrying capacity is obtained by lumping the material into edge stringers and a constant shear stress is assumed inside and determined by equilibrium considerations. It is not known whether this procedure can be justified by simultaneous assumptions on the displacement and stress fields, in which case its properties could be more logically derived by Reissner's variational principle.

The major justification for the development of equilibrium models, internally equilibrated and continuously stress transmitting, was put forward in Reference R.I.8. It was shown that, on the basis of variational principles, a set of displacement models produces lower bounds to local influence coefficients, a set of equilibrium models upper bounds. A dual analysis, based on a set of each type, then furnishes a direct measure of the accuracy of the idealizations by a simple assessment of the width of the brackets. The profound mathematical justification for the upper and lower bound character of equilibrium and displacement solutions is that, from the point of view of

functional analysis, they belong to orthogonal subspaces of an inner product space.

At the time the only equilibrium models devised to prove the point were those of a stringer, under uniform shear feed, and the constant stress triangular skin panel.

The general theory of equilibrium models was further elaborated in Reference R.I.9. It appears quite clearly from it that the major obstacle to the previous development of equilibrium models was the restriction to local (nodal) displacements as generalized unknowns. Except for simple cases in which the deformation field is integrable, the only information on displacements provided by equilibrium models is through weighted averages of the displacement field.

A spar web was amongst the new equilibrium elements produced.

In this reference appear also for the first time the quadratic type triangular skin panel and the associated spar element, both more sophisticated displacement types, which proved remarkably successful in the present numerical investigations. Plate bending elements for upper and lower bounds determination were developed in References R.I.10, II, I2 and I4. They were made operational during the course of the present investigation and, from the few testing cases in which they were compared to other available models, have been proved equally successful.

Comparison studies were run on different idealizations and on the use of different types of elements for structural analysis of

- a spar. This permitted separate evaluation of our displacement and equilibrium spar elements, considered to be a major ingredient to represent correctly in elongated structures. The results presented here are taken from Reference R.I.15.
- a box beam of simple rectangular cross section. This permitted to evaluate the capability of our skin elements to represent correctly the properties of the cover sheets.
- a multispar swept wing. This was taken as an example of an already complex structure. The choice was further dictated by the existence of previous finite element studies of this structure (References R.I.16 and I7) and of test results (Reference R.I.18).
- a rectangular plate, centrally loaded, with either simply supported or clamped edges.

The conclusions that emerge from the comparisons can be summarized as follows :

- The principle of a dual analysis, producing upper and lower bounds to structural deflections, is not only of theoretical but of great practical value. In the swept back wing case, for instance, the almost perfect agreement

between spar deflections, obtained in dual analyses, indicates that the discrepancies with test results must be due to difficulties in assessing the true boundary conditions at the root.

- Sophisticated displacement elements show remarkable convergence characteristics for deflections and dramatic improvements in accuracy and ease of interpretation of stress distributions.
- The present lack of equally sophisticated operational skin equilibrium elements leads sometimes to difficult interpretation of the stress output.
- For a given complexity (measured for instance by the total number of generalized coordinates) the best geometrical pattern of subdivision into given types of elements remains an art.

However, the more sophisticated the elements, the less important the influence of the pattern.

Finally we would not like to condemn the use of hybrid models of elements (violating both continuity of the stress field and of the displacement field) without further evaluation, though, of course, the deflections they produce cannot be predicted to be upper or lower bounds.

There is also a point we wish to emphasize : the conceptual distinction between displacement model and equilibrium model, valid at the element level, is completely independent of the conceptual distinction between the displacement method (or direct stiffness method) and the force method, which applies at the structural level. In fact our theory of equilibrium models produces a stiffness matrix for the element just as in the case of a displacement model.

This has the advantage that the same computer program (in our case the A.S.E.F. displacement type program developed by the junior author) can draw on all types of elements and run the dual analyses. By the same token it would be perfectly possible to set up a force type program using any of the dual elements. It is true however that the topology of connections is such that fewer generalized displacements are generated by arrays of displacement models and fewer redundant forces by arrays of equilibrium models.

Hence the application of the A.S.E.F. program to equilibrium type analyses is possibly less efficient and accurate than would be a good force program. A minimal self-straining type of force program is presently under study.

I.I- Displacement models for lower bounds.

The starting assumption is that the displacement field within the element can be approximated by a linear superposition of a finite number of displacement modes, including the rigid body modes. The unknown intensities α_1 of the assumed modes are the parameters of the field and form the coordinates of a

column matrix α .

In most applications, and in all the applications contained in this report, the assumed modes are described by low order polynomials. That is, in

$$\vec{u} = \sum_1^n \alpha_i \vec{U}_i(x_j) \quad j = 1, 2, 3$$

the modal vectors \vec{U}_i are represented by polynomials in the space coordinates x_j .

From the parameters of the field we pass to a set of generalized displacements q_j according to the following rules :

- Along each interface with an adjacent element, a complete set of interface displacement modes, generated by the parametric field, is chosen. The generalized displacements pertaining to this interface are defined to be the intensities of these interface modes. It often happens that local values of displacement components can be chosen as generalized coordinates (see example of Figure F.I.I). In that case they can belong to more than one interface.

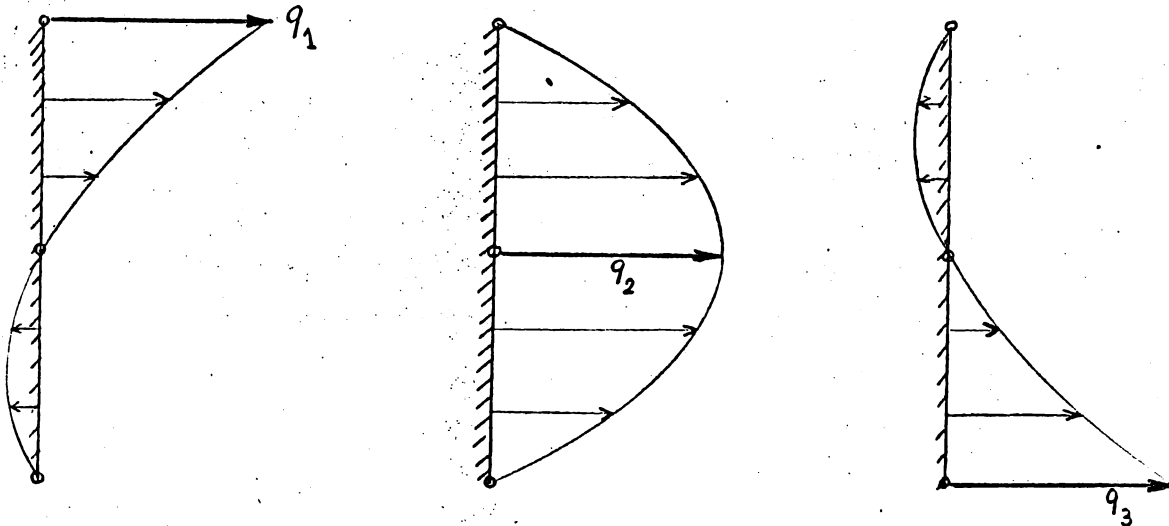


Figure F.I.I. Interface displacement modes defined by local displacement components. The superposition determines a general parabolic variation of the displacement component.

- The same interface modes must exist in the adjacent element, in which case the elements are said to be "conforming". If the elements are conforming, equating the corresponding generalized displacements by pair secures complete continuity of the displacement field across the interface.

The justification of these rules is that an array of conforming displacement models produces in the whole structure a continuous and piecewise differentiable displacement field. This results in lower bounds being as certain for the influence coefficients.

Since the interface modes are deduced from the parametric field, a linear relationship is always available between the parameters α_i and the generalized displacements q_j ; in matrix form, there is always a S matrix such that

$$q = S \alpha$$

Since however it is essential that the generalized coordinates be independent, their number may not exceed the number of parameters. This is the only source of difficulties in trying to build up new conforming models.

If the number of coordinates is inferior to the number of parameters, a complementary set of coordinates, represented by the column matrix r , can be so chosen that the transformation

$$\begin{pmatrix} q \\ r \end{pmatrix} = S \alpha$$

is non singular and has a reciprocal

$$\alpha = T_q q + T_r r$$

In complex cases it may be necessary to obtain the T_q and T_r matrices by numerical inversion of S , but it is always better, from the accuracy point of view, to obtain them in analytical form. Then the displacement field can be placed in the form

$$\vec{u} = \sum q_j \vec{w}_j(x_1) + \sum r_k \vec{v}_k(x_1) \quad (\text{I.I})$$

In a certain sense this means that the interface modes have been continued analytically in the interior of the element and auxiliary modes defined to complete the internal behaviour.

By differentiation the deformation tensor can be found and its elements replaced in the formula for the strain energy density of the element. After integration (analytical whenever possible) over the volume of the element, the strain energy turns out as a quadratic form in the generalized coordinates

$$U = \frac{1}{2} q' K_{qq} q + q' K_{qr} r + \frac{1}{2} r' K_{rr} r$$

The matrices (of numerical constants) of this form are the so-called "stiffness" matrices of the element.

By Castigliano's theorem, each partial derivative of this quadratic form with

respect to a generalized displacement produces the corresponding generalized load. Hence, if in matrix notation the virtual work of generalized loads on the corresponding displacements is noted

$$V = q' g_q + r' g_r \quad (I.2)$$

the column matrices of generalized loads are given by

$$g_q = K_{qq} q + K_{qr} r \quad (I.3)$$

$$g_r = K'_{qr} q + K_{rr} r$$

and $V = 2 U$ (Clapeyron's external theorem). The virtual work can also be calculated from the actual external loads applied to the element, either in the form of body loads \vec{X} (per unit volume) or surface traction loads \vec{p} (on the whole boundary surface of the element) :

$$V = \int \vec{X} \cdot \vec{u} \, dVol + \int \vec{p} \cdot \vec{u} \, dArea \quad (I.4)$$

Substitution of equ.(I.1) into (I.4) and identification with (I.2) produces the interpretation of the generalized loads :

$$g_j = \int \vec{X} \cdot \vec{W}_j \, dVol + \int \vec{p} \cdot \vec{W}_j \, dArea \quad (I.5)$$

$$g_k = \int \vec{X} \cdot \vec{V}_k \, dVol + \int \vec{p} \cdot \vec{V}_k \, dArea$$

This reveals another important role of the modal functions \vec{W}_j and \vec{V}_k : they act as weighting functions to translate any system of externally applied loads into generalized forces.

The discrete elastic properties of the element are now completely described by the stiffness relations (I.3). There is however an important difference in the subsequent treatment of the coordinates in the q -group and in the r -group. Those of the former group will be later identified with nodal displacements, a procedure which physically links the elements together and, if they are conforming, secures the continuity of displacements. The coordinates of the r -group need not and should not be subjected to any physical interelement constraint. In fact one has the possibility to eliminate the r -group by inversion of the last of equations (I.3)

$$r = K_{rr}^{-1} (g_r - K'_{qr} q)$$

The matrix K_{rr} is never singular because the rigid body modes belong to the q -group.

The first stiffness relation becomes simply

$$g = K q \quad (I.6)$$

with

$$K = K_{qq} - K_{qr} K_{rr}^{-1} K'_{qr} \quad (I.7)$$

and

$$g = g_q - K_{qr} K_{rr}^{-1} g_r \quad (I.8)$$

The last equation shows that the new generalized loads associated to the q group, after elimination, correspond to new weighting functions

$$g_j + \vec{W}_j - \sum_k f_{jk} \vec{V}_k \quad (I.9)$$

$$(f_{jk}) = K_{qr} K_{rr}^{-1} \quad (I.10)$$

In our spar element, for instance, there are two coordinates of the r type (the end slopes of the neutral axis) and, under general loading conditions, good results are obtained after elimination of those coordinates only if the weighting functions are correctly modified.

One has also the choice to work with the extended element stiffness matrix

$$\begin{pmatrix} K_{qq} & K_{qr} \\ K'_{qr} & K_{rr} \end{pmatrix}$$

and to eliminate the r group at the structural level. This presents some advantage in uniformity of the operations required to produce a stress output.

I.2- Equilibrium models for upper bounds.

The stress field within the element is approximated by a linear superposition of stress-modes. The modes should be subdivided into two groups :

Group 1 Satisfies homogeneous equilibrium equations in the volume (no body forces) and on the "external boundary" (e.b.) of the element.

By external boundary is meant the set of boundary surfaces which are not interfaces.

Hence if $\sigma_{ij} = S_{ij,r} (x_m)$

denotes such a stress field of mode index r ,

$$\sum_i \frac{\partial S_{ij,r}}{\partial x_i} = 0 \quad \text{and} \quad (I.II)$$

$$\sum_i \ell_i S_{ij,r} = 0 \quad \text{on e.b.}$$

where ℓ_i ($i = 1, 2, 3$) are the direction cosines of the outward normal to the boundary.

Group 2 Satisfies non homogeneous equilibrium equations, either in the volume, or on the external boundary, or both. If

$$\sigma_{ij} = T_{ij,s}(x_m)$$

is such a field, of mode index s

$$\sum_i \frac{\partial T_{ij,s}}{\partial x_i} = -X_{j,s}(x_m) \quad (I.I2)$$

$$\sum_i \ell_i T_{ij,s} = p_{j,s}(x_m) \quad \text{on e.b.}$$

The general parametric stress field is then

$$\sigma_{ij} = \sum_r \beta_r S_{ij,r}(x_m) + \sum_s \gamma_s T_{ij,s}(x_m) \quad (I.I3)$$

The presence of the second group opens the possibility of loading the structure by body forces and surface tractions on its external boundary. Those possibilities are naturally restricted to combinations of the body modes $X_{j,s}(x_m)$ and surface traction modes $p_{j,s}(x_m)$ if equilibrium is to be preserved.

This is an unavoidable disadvantage of the equilibrium approach in general as compared to the displacement approach; once a stress field approximation is adopted, the nature of the acceptable loads is limited.

The other loading possibilities occur at the interfaces, where continuity of the stress transmission must be preserved in order to build a true equilibrium model providing for upper bounds of the influence coefficients.

At an interface, the parametric field (I.I3) generates interface traction

modes. To each chosen mode we attach a generalized force coordinate g_t ; it can be a local value of a surface traction component or, preferably, a resultant of the surface traction diagram of the mode.

In general each generalized force coordinate belongs to a single interface. Exceptionally, as occurs in the Kirchhoff plate bending theory, it can belong to more than one interface.

Let $G_{i,t}(x_m)$ ($i = 1, 2, 3$)

be such an interface traction mode of index t . Then, the virtual work of the mode will be

$$g_t \int_{\text{interface}} \sum_i G_{i,t}(x_m) u_i(x_m) d\text{Area}$$

and, by definition of the associated generalized displacement q_t , can also be written as $q_t g_t$. Hence, by identification, the interpretation of the generalized displacement

$$q_t = \int_{\text{interface}} \sum_i G_{i,t}(x_m) u_i(x_m) d\text{Area} \quad (\text{I.14})$$

as a weighted average of the displacements at this interface.

Since the interface modes are generated by the field, each generalized force is a given combination of the parameters of the field:

$$g_t = \sum_r g_{tr} \beta_r + \sum_s g_{ts} \gamma_s \quad (\text{I.15})$$

It should also be noted that, in order to preserve equilibrium, the loads externally applied to the structure at an interface must correspond to a linear superposition of modes identical to the interface modes.

We now group all the generalized loads necessary to specify the interface traction modes in a single column matrix g , using a conventional sequence. The corresponding sequence is used to group the associated generalized displacements in the column matrix q . The scalar product

$$q'g$$

accounts for the complete virtual work of loads applied at the interfaces. The remainder is, from (I.12), equal to

$\sum_s \gamma_s p_s$ where

$$p_s = \int \sum_j X_{j,s} u_j dVolume + \int_{e.b.} \sum_j p_{j,s} u_j dArea \quad (I.16)$$

since only the γ_s parameters give rise to body forces and surface traction forces on the external boundary.

We are thus led to consider each γ_s as an additional generalized load with corresponding generalized displacement p_s . Grouping each set in corresponding column matrices γ and p , this additional virtual work is

$$p' \gamma$$

We also group all the relationships (I.15) in matrix form

$$g = C_\beta \beta + C_\gamma \gamma \quad (I.17)$$

where β is, in a chosen sequence, the column matrix of the first parameters. We further introduce the complete connection matrix C , partitioned as follows

$$C = \begin{pmatrix} C_\beta & C_\gamma \\ 0 & E \end{pmatrix}$$

where E is an identity matrix of dimensions equal to the number of γ_s parameters. This matrix connects the complete set of generalized loads to the complete set of parameters :

$$\begin{pmatrix} g \\ \gamma \end{pmatrix} = C \begin{pmatrix} \beta \\ \gamma \end{pmatrix} \quad (I.18)$$

The discrete element properties are now conveniently derived from the complementary energy principle, under the assumption that all the generalized displacements are specified. To this purpose the complementary energy density (in the present linear stress-strain case, the energy density expressed in terms of stresses) is calculated from the field assumption (I.13). After integration over the volume of the element it furnishes a quadratic and homogeneous form in the parameters :

$$U = \frac{1}{2} \beta' F_{\beta\beta} \beta + \beta' F_{\beta\gamma} \gamma + \frac{1}{2} \gamma' F_{\gamma\gamma} \gamma$$

The $F_{\beta\beta}$, $F_{\beta\gamma}$ and $F_{\gamma\gamma}$ matrices are known as the flexibility matrices of the element. The complementary energy principle states that

$$U - q'g - p'\gamma = U - q' C_{\beta} \beta - q' C_{\gamma} \gamma - p'\gamma$$

is a minimum under specified q and p values for all possible choices of the β and γ values. This requires that

$$F_{\beta\beta} \beta + F_{\beta\gamma} \gamma = C_{\beta}' q$$

$$F_{\beta\gamma}' \beta + F_{\gamma\gamma} \gamma = C_{\gamma}' q + p'$$

This is also expressed in a single matrix equation

$$F \begin{pmatrix} \beta \\ \gamma \end{pmatrix} = C' \begin{pmatrix} q \\ p \end{pmatrix} \quad (I.19)$$

with

$$F = \begin{pmatrix} F_{\beta\beta} & F_{\beta\gamma} \\ F_{\beta\gamma}' & F_{\gamma\gamma} \end{pmatrix}$$

The complete flexibility matrix is symmetrical and non singular. It can be inverted (numerically if not analytically) to give

$$\begin{pmatrix} \beta \\ \gamma \end{pmatrix} = F^{-1} C' \begin{pmatrix} q \\ p \end{pmatrix}$$

And this result, substituted into (I.18) gives

$$\begin{pmatrix} g \\ \gamma \end{pmatrix} = K \begin{pmatrix} q \\ p \end{pmatrix} \quad (I.20)$$

with

$$K = C F^{-1} C' \quad (I.21)$$

It is thus possible in any case to express the discrete element properties of an equilibrium model in terms of a stiffness matrix. This has the considerable advantage of making a direct stiffness program available for the treatment of the problem at the structural level.

One can then wonder why the same difficulties that can plague the build up of a conforming displacement element do not seem to appear here. The answer is that the corresponding difficulties are hidden in the perhaps too singular nature of the stiffness matrix obtained.

Let us look at the displacement modes which can leave the element unstressed ($g = 0$ and $\gamma = 0$). They are solutions of

$$K \begin{pmatrix} q \\ p \end{pmatrix} = 0$$

or, equivalently, of

$$C' \begin{pmatrix} q \\ p \end{pmatrix} = 0 \quad (I.22)$$

The rigid body modes must be solutions of (I.22) and this is always automatically satisfied. If, however, the number of generalized loads that had to be introduced exceeds the number of stress parameters by more than the number of rigid body modes, there are additional independent and non trivial solutions to (I.22).

This means that the element contains some deformation modes which do not generate stresses, they are appropriately called "spurious kinematical freedoms". The ideal case is that of an equilibrium model without such defects, but the difficulties inherent in this ideal are of the same nature as those of the conforming displacement model. It is also true that equilibrium models containing such kinematical freedoms, or generating them by grouping in subassemblies can be useful. We can either make choice of special geometrical characteristics to make them unharmed or modify them slightly to keep local violations to the exact stress transmission property insignificant by an appeal to the de Saint Venant principle. Details of those methods must be left to the individual cases (see sections 2.2.2 and 2.2.3).

References of Section I.

- R.I.1. M.J. TURNER, "The Direct Stiffness Method of Structural Analysis".
AGARD Meeting, Aachen, Germany, paper presented 17 September 1959.
- R.I.2. M.J. TURNER, M.C. MARTIN and R.C. WEIKEL, "Further Development and Applications of the Stiffness Method", in "Matrix Methods of Structural Analysis", AGARDograph 72, ed. F. de Veubeke, Pergamon Press, 1964
- R.I.3. P.H. DENKE, "A General Digital Computer Analysis of Statically Indeterminate Structures". Douglas Aircraft Company Engineering Paper N° 834, September 1959.
- R.I.4. P.H. DENKE, "Digital Analysis of non-linear Structures by the Force Method", in "Matrix Methods of Structural Analysis", AGARDograph 72, ed. F. de Veubeke, Pergamon Press, 1964.
- R.I.5. R.H. GALLAGHER, "A Correlation Study of Methods of Matrix Structural Analysis", AGARDograph 69, Pergamon Press, 1964.
- R.I.6. M.J. TURNER, R.J. CLOUGH, H.C. MARTIN and L.J. TOPP, "Stiffness and Deflection Analysis of Complex Structures", J. Aeronautics Sci., September 1956.
- R.I.7. J.H. ARGYRIS, "Energy Theorems and Structural Analysis".
Butterworths, London, 1960.
- R.I.8. B.M. FRAEIJIS de VEUBEKE, "Upper and Lower Bounds in Matrix Structural Analysis", in "Matrix Methods of Structural Analysis", AGARDograph 72, Pergamon Press, 1964.
- R.I.9. B.M. FRAEIJIS de VEUBEKE, "Displacement and Equilibrium Models in the Finite Element Method", in "Stress Analysis", ed. O.C. Zienkiewicz and G.S. Holister, John Wiley and Sons, 1965.
- R.I.10. G. SANDER, "Bornes Supérieures et Inférieures dans l'Analyse Matricielle des Plaques en Flexion-Torsion", Bull. Soc. Royale des Sciences de Liège, 33-7 et 8, 1964.
- R.I.11. B.M. FRAEIJIS de VEUBEKE, "Bending and Stretching of Plates".
Proc. Conf. Matrix Methods in Structural Analysis, Dayton, OHIO, October 1965.

- R.I.I2. B.M. FRAEIJIS de VEUBEKE, "A Conforming Finite Element for Plate Bending", Report SA-5, Laboratoire de Techniques Aéronautiques et Spatiales, Université de Liège, Belgium, 1966.
- R.I.I3. R.W. CLOUGH, "The Finite Element in Structural Mechanics", in "Stress Analysis", ed. O.C. Zienkiewicz and G.S. Holister, John Wiley and Sons, 1965.
- R.I.I4. B.M. FRAEIJIS de VEUBEKE, "An Equilibrium Model for a Plate Bending Element". Report SA-6, Laboratoire de Techniques Aéronautiques et Spatiales, Université de Liège, Belgium, 1966.
- R.I.I5. G. SANDER, "Upper and Lower Bounds in Spar Matrix Analysis", Report SA-3, Laboratoire de Techniques Aéronautiques et Spatiales, Université de Liège, Belgium, 1965.
- R.I.I6. M.J. TURNER, H.C. MARTIN and R.C. WEIKEL, "Further Development and Applications of the Stiffness Method", AGARDograph 72, Pergamon Press, 1965, p. 227-241.
- R.I.I7. S. EGGWERTZ, "Calculation of Stresses in a Swept Multicell Cantilever Box Beam with Ribs Perpendicular to the Spars and Comparison with Test Results". The Aeronautical Research Institute of Sweden, Report 54, Stockholm 1954.
- R.I.I8. S. EGGWERTZ and B. NOTON, "Stress and Deflexion Measurements on a Multicell Cantilever Box Beam with 30° Sweep", Aeronautical Research Institute of Sweden, Report 53, Stockholm, 1954.

2. MODELS LIBRARY.

Most of the elements used in the present report have been described in previous publications. Therefore only the basic assumptions and properties required to set up the stiffness and stress matrices are recalled. Those elements for which there are no previous references, are treated in greater detail.

Matrix notations common to all elements are as follows :

q columnar matrix of generalized displacements

g columnar matrix of generalized loads.

The virtual work is the scalar product $q'g = g'q$ where transposition is indicated by the "prime".

K square stiffness matrix of the element, defined by $g = K q$

T stress matrix, yielding a stress column information on the basis of the product Tq .

2.I- Displacement Models.

2.I.I- Bar elements.

2.I.I.I- Bar with linear displacement field (ref. R.2.I).

It is assumed that the bar element represented in Figure F.2.I undergoes only uniaxial strain and, for simplicity of calculation, the reference axis Ox is taken parallel to the element. If the panels, to which the bar is supposed to be joined, are analyzed on the basis of a linear displacement field, interface compatibility requires that the axial displacement of the bar be also a linear function :

$$u = \alpha_1 + \alpha_2 x$$

The end displacements u_1 and u_2 are chosen as generalized coordinates, so that :

$$u = u_1 \frac{x - x_2}{x_1 - x_2} + u_2 \frac{x_1 - x}{x_1 - x_2}$$

If the loads on the bar segment consist of end loads X_1 and X_2 and a shear flow $q_{12}(x)$, the potential energy can be written as

$$-P = \int_{x_2}^{x_1} q_{12}(x) u(x) dx + X_1 u_1 + X_2 u_2$$

or alternatively, in terms of generalized displacements and associated forces

$$-P = u_1 Q_1 + u_2 Q_2 = q'g$$

so that the generalized loads conjugate to u_1 and u_2 turn out to be

$$Q_1 = X_1 + \int_{x_2}^{x_1} q_{12}(x) \frac{x - x_2}{x_1 - x_2} dx$$

$$Q_2 = X_2 + \int_{x_2}^{x_1} q_{12}(x) \frac{x_1 - x}{x_1 - x_2} dx$$

The strain in the element is

$$\epsilon_x = \frac{\partial u}{\partial x} = \frac{u_1 - u_2}{x_1 - x_2} = \frac{1}{x_1 - x_2} (-1 \ 1) q$$

while the only stress component is :

$$\sigma_x = \frac{E}{x_1 - x_2} (-1 \quad 1) q = T q$$

where T is the stress matrix.

If $S(x)$ is the cross sectional area of the bar, the strain energy can be written as

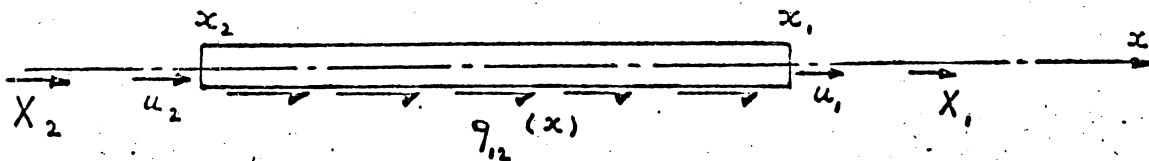
$$U = \frac{1}{2} \int_{x_1}^{x_2} \epsilon_x \sigma_x S(x) dx = \frac{1}{2} q' K q$$

and the stiffness matrix turns out to be :

$$K = \frac{\int_{x_2}^{x_1} E S(x) dx}{(x_1 - x_2)^2} \begin{vmatrix} 1 & -1 \\ -1 & 1 \end{vmatrix} = \frac{E S_m}{x_1 - x_2} \begin{vmatrix} 1 & -1 \\ -1 & 1 \end{vmatrix}$$

where S_m is the average cross sectional area.

Figure F.2.I : Bar with linear displacement field.



Assumption : $u(x) = \alpha_1 + \alpha_2 x$

The stiffness matrix can be written as

$$K = \int_{-a}^{+a} E S(x) N'N dx$$

For a constant cross section S_m there follows

$$K = \frac{E S_m}{6 a} \begin{vmatrix} 7 & -8 & 1 \\ -8 & 16 & -8 \\ 1 & -8 & 7 \end{vmatrix}$$

For a linearly varying cross section such as

$$S(x) = S_m + S_d \frac{x}{a} \quad \text{with} \quad S_m = \frac{S_1 + S_3}{2}$$

$$S_d = \frac{S_1 - S_3}{2}$$

the stiffness matrix becomes :

$$K = \frac{E S_m}{3 l} \begin{vmatrix} 7 & -8 & 1 \\ -8 & 16 & -8 \\ 1 & -8 & 7 \end{vmatrix} + \frac{4 E S_d}{3 l} \begin{vmatrix} 1 & -1 & 0 \\ -1 & 0 & 1 \\ 0 & 1 & -1 \end{vmatrix}$$

The axial stress being linear, the stress matrix should give stress values at two points in order to describe completely the stress field.

The two ends of the bar are the convenient places to express these stresses.

Therefore the stress matrix, defined by :

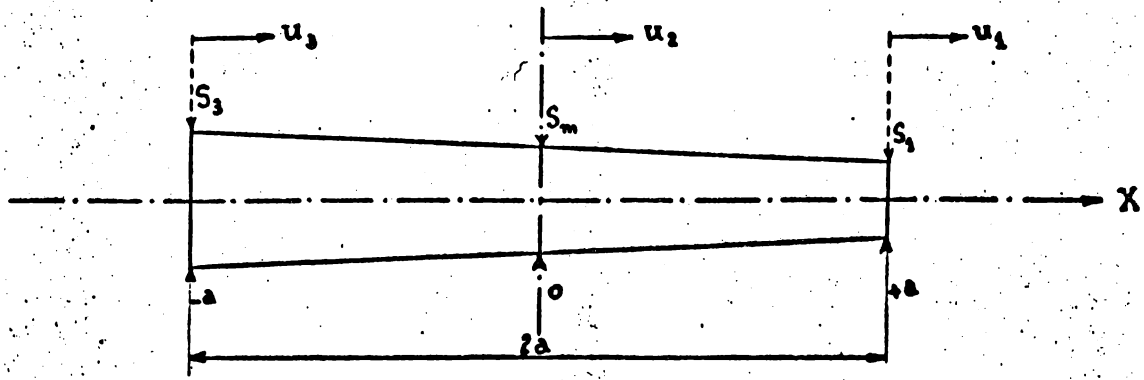
$$\sigma_1 = \sum_1 T_{1,1} q_1$$

$$\sigma_3 = \sum_1 T_{2,1} q_1$$

is given by

$$T = \frac{E}{2 a} \begin{vmatrix} 3 & -4 & 1 \\ -1 & 4 & -3 \end{vmatrix}$$

Figure F.2.2 : Bar with quadratic displacement field.



Assumption : $u(x) = a_1 + a_2 x + a_3 x^2$

2.I.2- Skin elements.

2.I.2.I- Turner triangle (linear displacement field) (ref. R.2.I).

A linear displacement field is assumed, so that

$$u = \alpha_1 + \alpha_2 x + \alpha_3 y$$

$$v = \alpha_4 + \alpha_5 x + \alpha_6 y$$

in the triangle represented in local axes in Figure F.2.3.

If the displacements sequence is

$$q' = (u_1, u_2, u_3, v_1, v_2, v_3)$$

the stiffness matrix, in local axes, takes the well known form reproduced in Figure F.2.4.

Where t_m denotes either the constant thickness or the average

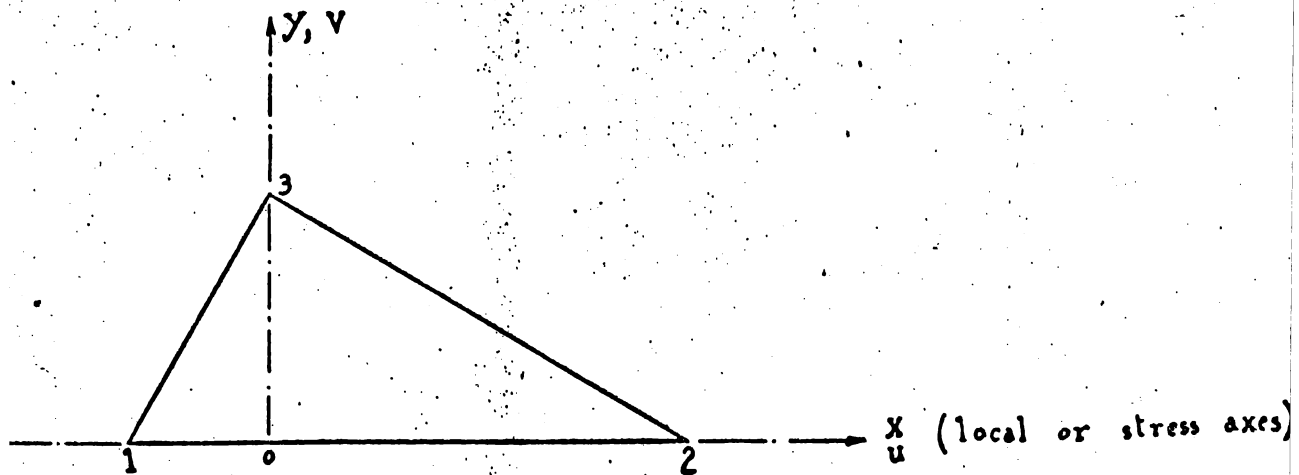
$t_m = \frac{1}{3} (t_1 + t_2 + t_3)$ in the case of a linearly varying thickness such as $t(x) = A + Bx + Cy$.

The stress matrix giving the local stress components in the sequence

$\sigma_x, \sigma_y, \tau_{xy}$ is found to be

$$T = \frac{E}{(1-\nu^2)x_{21}y_3} \begin{vmatrix} -y_3 & y_3 & 0 & -\nu x_2 & \nu x_1 & \nu x_{21} \\ -\nu y_3 & \nu y_3 & 0 & -x_2 & x_1 & x_{21} \\ -\lambda_1 x_2 & \lambda_1 x_1 & \lambda_1 x_{21} & -\lambda_1 y_3 & \lambda_1 y_3 & 0 \end{vmatrix}$$

Figure F.2.3 : The Turner triangle with linear displacement field.



Assumption : $u = \alpha_1 + \alpha_2 x + \alpha_3 y$

$v = \alpha_4 + \alpha_5 x + \alpha_6 y$

2.I.2.2- Triangle using the quadratic displacement field (ref. R.2.2).

The quadratic displacement field

$$u = \alpha_1 + \alpha_2 x + \alpha_3 y + \alpha_4 x^2 + \alpha_5 xy + \alpha_6 y^2$$

$$v = \alpha_7 + \alpha_8 x + \alpha_9 y + \alpha_{10} x^2 + \alpha_{11} xy + \alpha_{12} y^2$$

is assumed for the triangle represented in Figure F.2.4-bis in local axes. Using the corner and mid edge displacements as generalized coordinates, the relation between the 6 u_i displacements and the 6 first field coefficients is easily inverted in the local axes of Figure F.2.4-bis and becomes

$$c_{1,6} = A q_u$$

where

$$c'_{1,6} = (\alpha_1 \ \alpha_2 \ \alpha_3 \ \alpha_4 \ \alpha_5 \ \alpha_6)$$

$$q'_u = (u_1 \ u_2 \ u_3 \ u_4 \ u_5 \ u_6)$$

and the matrix A is displayed on Figure F.2.6.

The same matrix A is applicable to inversion of the relation between the v_i displacements and the last six field coefficients

$$c_{7,12} = A q_v$$

$$c'_{7,12} = (a_7 \ a_8 \ a_9 \ a_{10} \ a_{11} \ a_{12})$$

$$q'_v = (v_1 \ v_2 \ v_3 \ v_4 \ v_5 \ v_6)$$

The strain components are now expressed as

$$\epsilon = \begin{vmatrix} \epsilon_x \\ \epsilon_y \\ \gamma_{xy} \end{vmatrix} = (N_0 + N_x x + N_y y) q$$

where q is now the complete displacements vector

$$q' = (u_1 \ u_2 \ u_3 \ u_4 \ u_5 \ u_6 \ v_1 \ v_2 \ v_3 \ v_4 \ v_5 \ v_6)$$

and where the N matrices are given in Figure F.2.5.

If the strain energy is written as :

$$U = \frac{1}{2} \iint_{\Delta} \epsilon' M \epsilon \ dx dy$$

with

$$M = \frac{E t(x,y)}{1 - \nu^2} \begin{vmatrix} 1 & \nu & 0 \\ \nu & 1 & 0 \\ 0 & 0 & \frac{1 - \nu}{2} \end{vmatrix}$$

the stiffness matrix turns out to be composed of the 9 products

$$K = (N'_0 M_0 N_0 + N'_0 M_x N_x + N'_0 M_y N_y \\ + N'_x M_x N_0 + N'_x M_{xx} N_x + N'_x M_{xy} N_y \\ + N'_y M_y N_0 + N'_y M_{xy} N_x + N'_y M_{yy} N_y)$$

which are to be calculated numerically. The matrices

$$M_0 = \iint_{\Delta} M \, dx dy$$

$$M_x = \iint_{\Delta} M x \, dx dy$$

. . . and so on.

are easily evaluated for the case of constant thickness t :

$$M_0 = \frac{a b}{2} M$$

$$M_x = \frac{(a + d) a b}{6} M$$

$$M_y = \frac{a b^2}{6} M$$

$$M_{xx} = \frac{a b (d^2 + a d + a^2)}{12} M$$

$$M_{xy} = \frac{a b^2 (a + 2 d)}{24} M$$

$$M_{yy} = \frac{a b^3}{12} M$$

The stresses are given, in local axes, by :

$$\sigma = M \epsilon = (M N_0 + M N_x x + M N_y y) q$$

Since the stresses have linear variations, enough stress information is generated by the knowledge of the stress elements at the three vertices. We therefore introduce

$$N_0 \quad N_1 = N_0 + a N_x \quad N_2 = N_0 + d N_x + b N_y$$

and the (9×12) stress matrix will be given by

$$T = \begin{vmatrix} M N_0 \\ M N_1 \\ M N_2 \end{vmatrix}$$

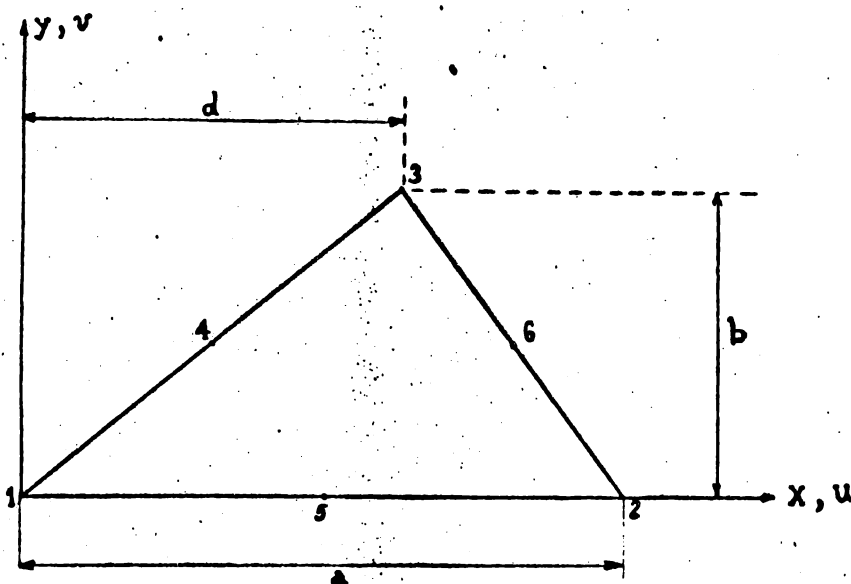
Other types of local reference frames could be used and would present some advantages but also some drawbacks.

For instance oblique coordinates along two edges of the triangle, or areal coordinates. In general it is felt that the attending simplicity in the formulation of the stiffness and stress matrices in local axes is more than counter balanced by the necessity to revert to the global cartesian frame for connecting the elements together.

We can nevertheless observe that a more compact formulation of the stiffness matrix is possible in the present set of axes by using directly the matrices N_0 , N_1 and N_2 which generate the stresses at the vertices

$$K = \frac{ab}{24} \{ (N_0 + N_1 + N_2)' M (N_0 + N_1 + N_2) + N_0' M N_0 + N_1' M N_1 + N_2' M N_2 \}$$

Figure F.2.4-bis : Triangle using the quadratic displacement field.



Local axes

Assumption : $u = a_1 + a_2 x + a_3 y + a_4 x^2 + a_5 xy + a_6 y^2$

$$v = a_7 + a_8 x + a_9 y + a_{10} x^2 + a_{11} xy + a_{12} y^2$$

2.I.3- Spar elements.

2.I.3.I- Spar element for linear displacement field (ref. R.2.4).

This spar element is to be used with skin elements undergoing a linear displacement field, at least along the spar cap interface. Therefore, in order to satisfy interface compatibility, the longitudinal displacement in the spar has to be linear in x (see Figure F.2.6-bis). The other basic assumptions are that the cross section remains plane after deformation and the vertical fibers inextensible ($\epsilon_z = 0$). Consequently, the axial displacement $u(x, z)$ is of the form

$$u = z (\alpha_1 + \alpha_2 x)$$

The cross sectional rotation is therefore

$$\rho(x) = \frac{u(x, z)}{z} = \alpha_1 + \alpha_2 x$$

The vertical displacement will be a function of x only and the connections with adjacent spar elements (in $x = \pm a$) must be conforming.

A cubic function will give the required degrees of freedom

$$w(x) = \alpha_3 + \alpha_4 x + \alpha_5 x^2 + \alpha_6 x^3$$

The 6 generalized coordinates giving a full description of the displacement field coefficients are :

$$u_1 = u(+a, +h)$$

$$u_2 = u(-a, +h)$$

$$w_1 = w(+a)$$

$$w_2 = w(-a)$$

$$\phi_1 = \left(\frac{\partial w}{\partial x} \right)_{+a}$$

$$\phi_2 = \left(\frac{\partial w}{\partial x} \right)_{-a}$$

The six field parameters α_i are easily expressed in terms of the generalized displacements and the displacement field can be placed in the form

$$u(x, z) = \frac{1}{2} \frac{z}{h} \left(u_1 + u_2 + (u_1 - u_2) \frac{x}{a} \right) = z \rho(x)$$

$$w(x) = \frac{1}{2} (w_1 + w_2) - \frac{a}{4} (\phi_1 - \phi_2) + \frac{1}{4} \left(3(w_1 - w_2) - a(\phi_1 + \phi_2) \right) \frac{x}{a} + \frac{a}{4} (\phi_1 - \phi_2) \left(\frac{x}{a} \right)^2 + \frac{1}{4} \left(w_2 - w_1 + a(\phi_1 + \phi_2) \right) \left(\frac{x}{a} \right)^3$$

The normal load in the upper flange of constant cross section S is

$$N = E S h \rho'(x)$$

If one assumes a constant value for the web thickness t , the bending moment and the transverse shear turn out to be :

$$M(x) = 2 N h + \int_{-h}^{+h} \sigma_x z dz = E I \rho'(x)$$

with an effective moment of inertia $I = \frac{2 t h^3}{3(1-\nu^2)} + 2 S h^2$

$$T(x) = t \int_{-h}^{+h} \tau_{xz} dz = 2 G t h (\rho + w')$$

The strain energy is therefore

$$U = \frac{1}{2} \int_{-a}^{+a} \left(\frac{M^2}{EI} + \frac{T^2}{2 G t h} \right) dx = \frac{1}{2} \left(E I \int_{-a}^{+a} (\rho'(x))^2 dx + 2 G t h \int_{-a}^{+a} (\rho'(x) + w'(x))^2 dx \right)$$

From this, the stiffness matrix is easily derived and displayed in Figure F.2.7.

For a displacement sequence

$$q' = (u_1 \ u_2 \ w_1 \ w_2 \ \phi_1 \ \phi_2)$$

The corresponding generalized forces are

$$g' = (2 U_1 \ 2 U_2 \ W_1 \ W_2 \ \phi_1 \ \phi_2)$$

From virtual work consideration, and for the loading described in Figure F.2.8 they turn out to be

$$U_1 = -\frac{M_1}{2h} + \frac{1}{2} \int_{-a}^{+a} \left(1 + \frac{x}{a}\right) q(x) dx$$

$$U_2 = -\frac{M_2}{2h} + \frac{1}{2} \int_{-a}^{+a} \left(1 - \frac{x}{a}\right) q(x) dx$$

$$W_1 = T_1 + \frac{1}{4} \int_{-a}^{+a} \left(2 - \frac{x}{a}\right) \left(1 + \frac{x}{a}\right)^2 p(x) dx$$

$$W_2 = T_2 + \frac{1}{4} \int_{-a}^{+a} \left(2 + \frac{x}{a}\right) \left(1 - \frac{x}{a}\right)^2 p(x) dx$$

$$\phi_1 = -\frac{a}{4} \int_{-a}^{+a} \left(1 - \frac{x}{a}\right) \left(1 + \frac{x}{a}\right)^2 p(x) dx$$

$$\phi_2 = +\frac{a}{4} \int_{-a}^{+a} \left(1 + \frac{x}{a}\right) \left(1 - \frac{x}{a}\right)^2 p(x) dx$$

The stresses have now to be expressed :

$$\sigma_x = E^0 z \rho'(x)$$

$$\sigma_z = E^0 v z \rho'(x) \quad E^0 = \frac{E}{1 - \nu^2}$$

$$\tau_{xz} = G (\rho(x) + w'(x))$$

σ_x and σ_z are constant with respect to x , while τ_{xz} is quadratic and is therefore determined by three local values along the length of the spar.

The stress matrix has therefore to contain the following components:

$$\sigma_x (+h) = E^0 \frac{1}{2a} (u_1 - u_2)$$

$$\sigma_z (+h) = E^0 \frac{\nu}{2a} (u_1 - u_2)$$

$$\tau_{xz} (+a) = E^0 \frac{1-\nu}{2} \left(\frac{u_1}{h} + \phi_1\right)$$

$$\tau_{xz} (0) = E^0 \frac{1-\nu}{8} \left(2\frac{u_1}{h} + 3\frac{w_1}{a} - \phi_1 + 2\frac{u_2}{h} - 3\frac{w_2}{a} - \phi_2\right)$$

$$\tau_{xz} (-a) = E^0 \frac{1-\nu}{2} \left(\frac{u_2}{h} + \phi_2\right)$$

or, in matrix notation, using the same displacement sequence as defined above $\sigma = T q$ with

$$T = \frac{E}{1 - \nu^2}$$

$\frac{1}{2a}$	$-\frac{1}{2a}$				
$\frac{\nu}{2a}$	$-\frac{\nu}{2a}$				
$\frac{1-\nu}{2h}$				$\frac{1-\nu}{2}$	
$\frac{1-\nu}{4h}$	$\frac{1-\nu}{4h}$	$\frac{3(1-\nu)}{8a}$	$-\frac{3(1-\nu)}{8a}$	$\frac{\nu-1}{8}$	$\frac{\nu-1}{8}$
	$\frac{1-\nu}{2h}$				$\frac{1-\nu}{2}$

Two points of theory need to be recalled for this spar element.

The first one is that conformity only requires identification of the edge rotations represented by u_1 and u_2 and of the tip deflections w_1 and w_2 at the interfaces between adjacent spar elements. The tip slopes ϕ_1 and ϕ_2 do not have to be identical at an interface and follow the discontinuities of shearing strain associated with a possible discontinuity of the shear load. Identification of these slopes has usually no significant influence on the displacements but changes completely the shear stress picture in the spar. Therefore the slopes are generalized displacements internal to each element which could be eliminated at the element level. However it is usually more convenient to achieve all condensations at the structure level. The stiffness matrix of the spar element is therefore retained in the form where an internal left-hand slope and an internal right-hand slope are present.

The second point concerns the $\epsilon_z = 0$ assumption which avoids a more detailed specification of the manner in which the transverse distributed load $p(x)$ and the interface shear loads are actually applied but also makes the web stiffer by a factor $\frac{1}{1 - \nu^2}$ as mentioned in the reference papers.

This means that a comparison of structures using displacement spar models or equilibrium spar models will exhibit convergence towards two different "exact" solutions.

This can be avoided by deliberately replacing in the displacement model the previous moment of inertia by the one

$$I = \frac{2}{3} th^3 + 2 Sh^2$$

of classical beam theory (a result of the stress assumption $\sigma_z = 0$). While this modified model, which now implies a stress assumption, is no more a rigorous displacement model and cannot pretend to exhibit lower bound characteristics with respect to the exact solution of elasticity theory, it nevertheless remains a displacement model with lower bound characteristics within a theory which considers classical beam theory as the ideal reference standard.

Figure F.2.6-bis : Spar element for linear displacement field.

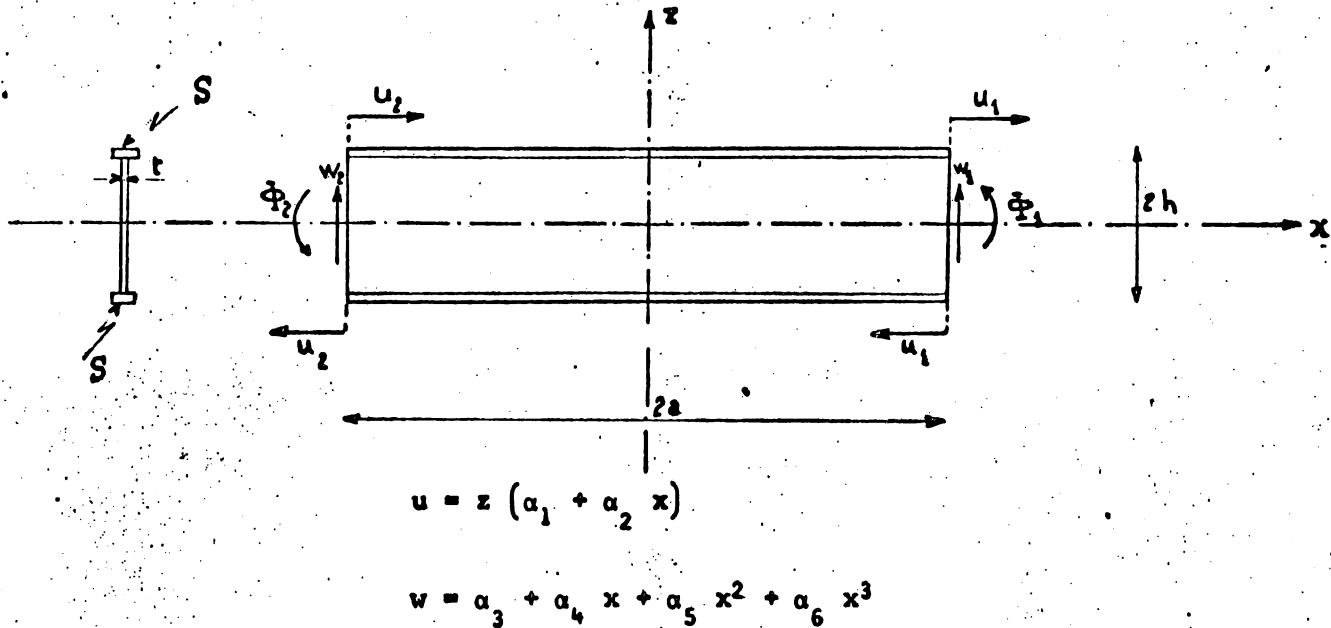
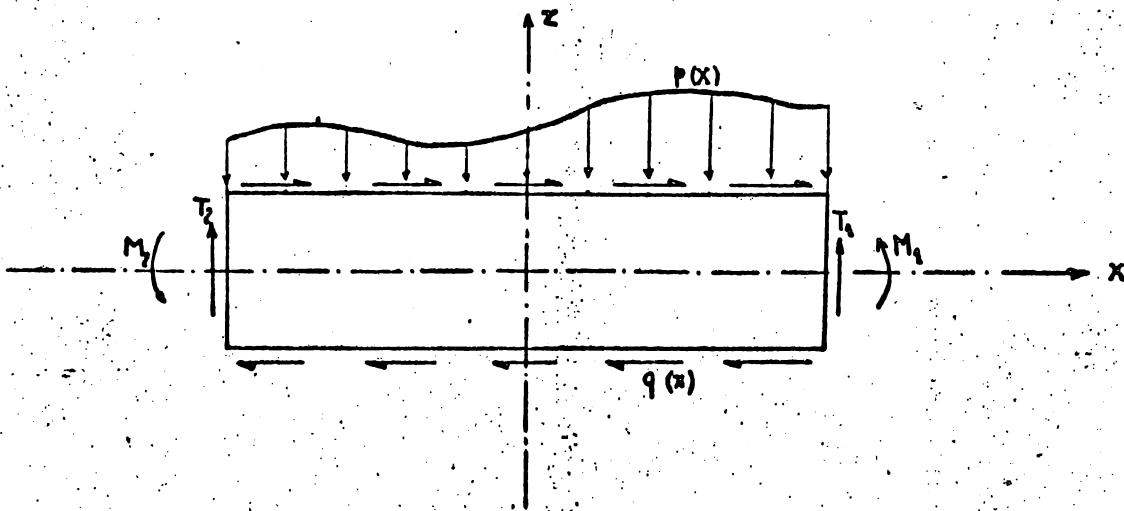


Figure F.2.8 : Loading for a linear spar element.



2.I.3.2- Spar element for quadratic displacement field (ref. R.2.2 and R.2.4).

In this approach, the skin elements to which the spar is attached are supposed to deform according to the quadratic displacement field described in section 2.I.2.2. By simple extension of the previous considerations, the now displacement functions will be

$$u(x, z) = z (\alpha_1 + \alpha_2 x + \alpha_3 x^2) = z \rho(x)$$

$$w(x) = \alpha_4 + \alpha_5 x + \alpha_6 x^2 + \alpha_7 x^3$$

where $\rho(x)$ is again the cross sectional rotation.

It is worth noting that, in this approach, the above assumptions allow an exact representation of the loading cases associated with a constant shearing force and linearly increasing bending moment. The solutions are only weakened by the stiffening assumption of inextensibility of the vertical fibers $\epsilon_z = 0$, which again can be avoided by using the moment of inertia of classical beam theory.

The seven generalized coordinates chosen to describe the displacement field are indicated in Figure F.2.9 :

$$u_1 = u(+a, +h) \quad u_3 = u(0, +h) \quad u_2 = u(-a, +h)$$

$$w_1 = w(+a) \quad w_2 = w(-a)$$

$$\phi_1 = (\partial w / \partial x)_a \quad \phi_2 = (\partial w / \partial x)_{-a}$$

In terms of those generalized coordinates, the displacement functions take the following form

$$u = \frac{z}{h} \left(u_3 + \frac{1}{2} (u_1 - u_2) \frac{x}{a} + \frac{1}{2} (u_1 + u_2 - 2u_3) \left(\frac{x}{a}\right)^2 \right) = z \rho(x)$$

$$w = \frac{1}{2} (w_1 + w_2) - \frac{a}{4} (\phi_1 - \phi_2) + \frac{1}{4} \left(3(w_1 - w_2) - a(\phi_1 + \phi_2) \right) \left(\frac{x}{a}\right) + \frac{a}{4} (\phi_1 - \phi_2) \left(\frac{x}{a}\right)^2 + \frac{1}{4} (w_2 - w_1 + a(\phi_1 + \phi_2)) \left(\frac{x}{a}\right)^3$$

while the strain energy remains as before

$$U = \frac{1}{2} \int_{-a}^{+a} \left(\frac{M^2}{EI} + \frac{T^2}{2Gth} \right) dx$$

$$= \frac{1}{2} \left\{ EI \int_{-a}^{+a} (\rho'(x))^2 dx + 2Gth \int_{-a}^{+a} (\rho(x) + w'(x))^2 dx \right.$$

with

$$I = \frac{2 \text{th}}{3(1-\nu^2)} + 2 \text{Sh}^2$$

Substituting in the strain energy the relations of $\rho(x)$ and $w(x)$ given above and denoting by

$$q' = (u_1 \ u_3 \ u_2 \ w_1 \ w_2 \ \phi_1 \ \phi_2)$$

$$g' = (2 U_1 \ 2 U_3 \ 2 U_2 \ W_1 \ W_2 \ \phi_1 \ \phi_2)$$

the transposed columns of generalized displacements and forces, the stiffness matrix is easily derived and appears in Figure F.2.10.

Using the same external loading as in the linear spar element (Figure F.2.8), the virtual work equation yields the significance of the generalized forces

$$U_1 = -\frac{1}{2} \frac{M_1}{h} + \frac{1}{2} \int_{-a}^{+a} \left(\frac{x}{a} \left(\frac{x}{a} + 1 \right) \right) q(x) dx$$

$$U_3 = \int_{-a}^{+a} \left(1 - \left(\frac{x}{a} \right)^2 \right) q(x) dx$$

$$U_2 = -\frac{1}{2} \frac{M_2}{h} + \frac{1}{2} \int_{-a}^{+a} \left(\frac{x}{a} \left(\frac{x}{a} - 1 \right) \right) q(x) dx$$

The forces $W_1 \ W_2 \ \phi_1 \ \phi_2$ are the same as in the linear approach.

The slopes ϕ_1 and ϕ_2 are again independent of interface requirements and can be eliminated at the structural level. The interface connections between spar elements are the same as before. The newly introduced displacement u_3 must be identified with a corresponding one of a skin panel.

Turning now to the stress calculations, it turns out that

$$\epsilon_x = \frac{\partial u}{\partial x} = z (\alpha_2 + 2 \alpha_3 x)$$

$$\epsilon_z = 0$$

$$\gamma_{xz} = \frac{\partial u}{\partial z} + \frac{\partial w}{\partial x} = \alpha_1 + \alpha_5 + (\alpha_2 + 2 \alpha_6) x + (\alpha_3 + 3 \alpha_7) x^2$$

and from Hooke's law :

$$\sigma_x = \frac{E}{1-\nu^2} z (\alpha_2 + 2 \alpha_3 x)$$

$$\sigma_z = \frac{\nu E}{1-\nu^2} z (\alpha_2 + 2 \alpha_3 x)$$

$$\tau_{xz} = G (\alpha_1 + \alpha_5 + (\alpha_2 + 2 \alpha_6) x + (\alpha_3 + 3 \alpha_7) x^2)$$

To allow easy interpretation of the stress output, the following local stress values are required.

$$\sigma' = \{ \sigma_x (+a, +h), \sigma_z (+a, +h), \tau_{xz} (+a, +h), \sigma_x (-a, +h), \\ \sigma_z (-a, +h), \tau_{xz} (-a, +h), \tau_{xz} (0, +h) \}$$

They are calculated by

$$\sigma = T q$$

with the stress matrix T given in Figure F.2.II.

A special property of the quadratic spar element is worth mentioning.

Suppose we accept the assumptions of plane cross-sections and vertical web fiber inextensibility, implicit in

$$u(x, z) = z \rho(x) \quad w(x, z) = W(x)$$

and derive, from the variational principle of displacements, the corresponding differential equations of beam theory :

$$M = E I \rho'(x)$$

$$T = 2 G h (\rho + W')$$

$$M' = T - 2 h q(x)$$

$$T' = - p(x)$$

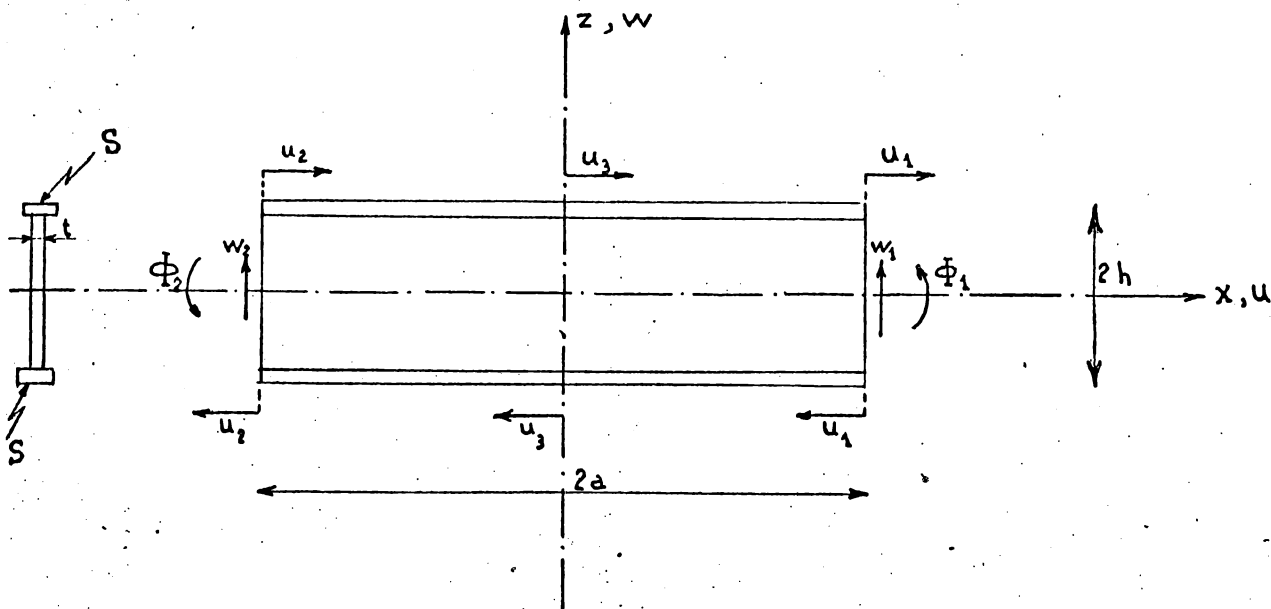
then, the further assumptions on $\rho(x)$ and $W(x)$ contained in the quadratic spar element give an exact solution of those differential equations for the case $q(x) = 0$ and $p(x) = 0$:

Those assumptions were in fact purposely fitted to an exact solution under constant shear load T and linearly varying bending moment M . Hence, if the left-hand side is built-in, all deflections and rotations under tip loads are exact within the contemplated beam theory. Applying the reciprocity principle it follows that the tip deflection and rotation will remain exact under any contemplated loading. The beneficial effect of a subdivision of the spar in more and more elements will only apply to the convergence of intermediate deflections and rotations to their correct values.

The same remarks will hold for the engineering beam theory by the previously commented modification of the moment of inertia.

A special property arises in the quadratic spar element which is worth mentioning. Due to the coherent assumptions formulated for the rotations $\alpha(x)$ and the deflections $w(x)$ the model gives under tip loads or tip moments, deflections and slopes identical to the classical engineering beam theory when the overestimated moment of inertia is used. As the loading by a distributed load $p(x)$ is achieved on the basis of the equality of virtual works for the actual load and for the tip forces representing that load in the model, it follows that the tip deflections and slopes obtained by that procedure are also the ones given by the engineering beam theory. This property can also be stated as follows : the tip deflections and slopes of that spar element are always those of the engineering beam theory for any distribution of transverse force $p(x)$ provided the correct loading functions are used. The deflections and slopes are therefore independant of the number of elements into which the spar is divided.

Figure F.2.9 : Spar element for quadratic displacement field.



Assumption : $u = z (\alpha_1 + \alpha_2 x + \alpha_3 x^2)$

$$w = \alpha_4 + \alpha_5 x + \alpha_6 x^2 + \alpha_7 x^3$$

2.1.4- Plate bending element.

2.1.4.I- The quadrangular plate in oblique coordinates (ref. R.2.5).

A conforming element of quadrilateral shape has been obtained from a combination of cubic displacement fields in the four triangular regions delimited by the edges of the quadrilateral and its diagonals, as represented in Figure F.2.12. Assuming that the complete cubic deflection field

$$w = \alpha_1 + \alpha_2 x + \alpha_3 y + \alpha_4 x^2 + 2 \alpha_5 xy + \alpha_6 y^2 + 4 (\alpha_7 x^3 + \alpha_8 x^2 y + \alpha_9 xy^2 + \alpha_{10} y^3)$$

is valid in the triangle OI2, the 10 coefficients can be determined in terms of the generalized displacements selected to insure the compatibility of deflections and slopes with an adjacent element. These are the local deflections w_0, w_1, w_2 , the local $\frac{\partial w}{\partial x}$ slopes ϕ_0, ϕ_1, ϕ_2 , the local $\frac{\partial w}{\partial y}$ slopes ψ_0, ψ_1, ψ_2 at points O, I and 2 and the $\frac{\partial w}{\partial x}$ slope ϕ_{12} at mid distance along the edge I2. These generalized coordinates are sequenced as follows

$$q_I' = (w_0, \phi_0, \psi_0, w_1, \phi_1, \psi_1, w_2, \phi_2, \psi_2, \phi_{12})$$

The curvatures can be expressed as

$$w_{xx} = 2 \alpha_4 + 24 x \alpha_7 + 8 y \alpha_8$$

$$w_{xy} = 2 \alpha_5 + 8 x \alpha_8 + 8 y \alpha_9$$

$$w_{yy} = 2 \alpha_6 + 8 x \alpha_9 + 24 y \alpha_{10}$$

The coefficients required to express the curvatures in terms of generalized coordinates are easily found

$$\alpha_4 = \frac{1}{a^2} (-3 w_0 - 2 a \phi_0 + 3 w_1 - a \phi_1)$$

$$\alpha_5 = \frac{1}{2 ab} (-6 w_0 - 2 a \phi_0 - 2 b \psi_0 + 6 w_1 - a \phi_1 + 2 b \psi_1 + a \phi_2 - 4 a \phi_{12})$$

$$\alpha_6 = \frac{1}{b^2} (-3 w_0 - 2 b \psi_0 + 3 w_2 - b \psi_2)$$

$$\alpha_7 = \frac{1}{4 a^3} (2 w_0 + a \phi_0 - 2 w_1 + a \phi_1)$$

$$\alpha_8 = \frac{1}{4 a^2 b} (6 w_0 + 2 a \phi_0 + 6 \psi_0 - 6 w_1 + a \phi_1 - b \psi_1 - a \phi_2 + 4 a \phi_{12})$$

$$\alpha_9 = \frac{1}{4 a b^2} (6 w_0 + a \phi_0 + 2 b \psi_0 - 6 w_1 + a \phi_1 - 2 b \psi_1 + 4 a \phi_{12})$$

$$\alpha_{10} = \frac{1}{4 b^3} (2 w_0 + b \psi_0 - 2 w_2 + b \psi_2)$$

Figure F.2.I2 : The quadrangular plate bending element.

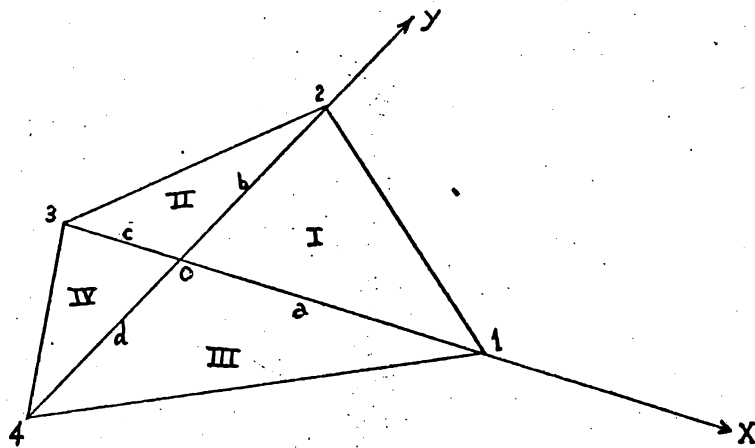
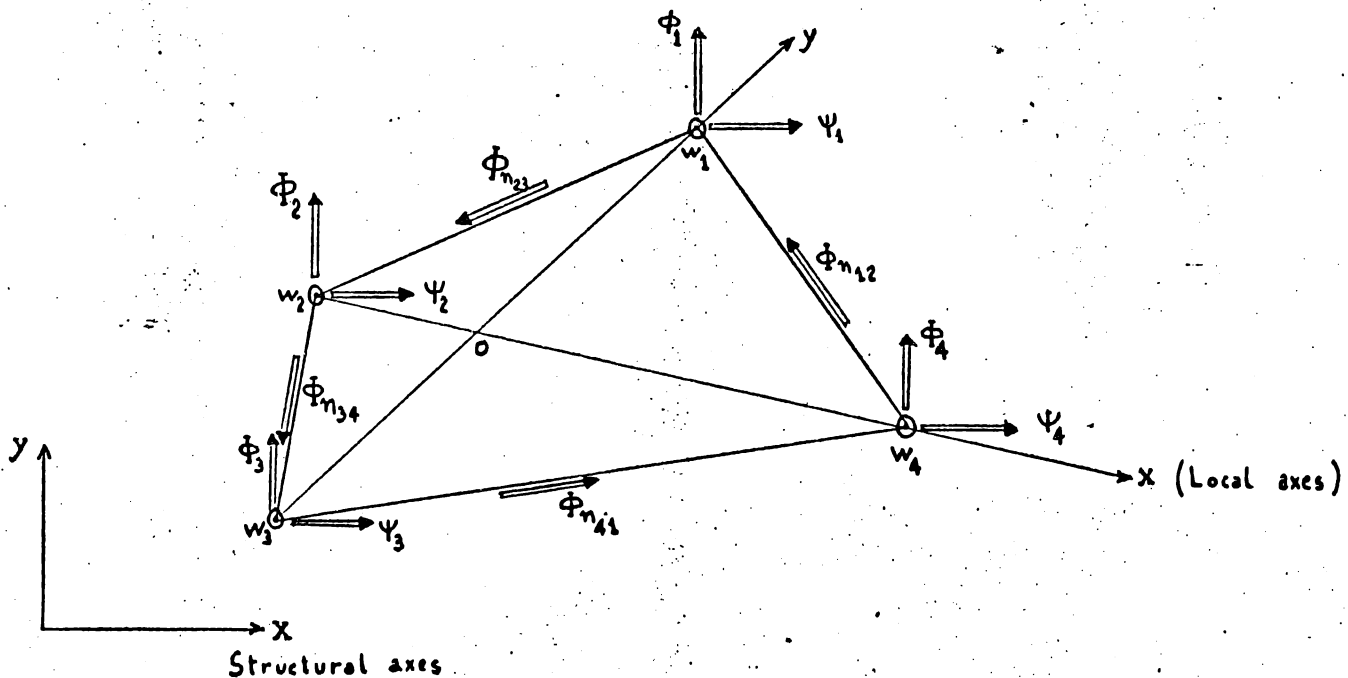


Figure F.2.I4 : The quadrangular plate bending element.

The 16 generalized displacements.



The curvatures can then be expressed in matrix form :

$$\gamma = \begin{pmatrix} w_{xx} \\ w_{xy} \\ w_{yy} \end{pmatrix} = \left(\frac{1}{a^2 b^2} W + \frac{2x}{a^3 b^2} W_x + \frac{2y}{a^2 b^3} W_y \right) q_I$$

where the matrices W , W_x , W_y are built from the above coefficients.
The bending strain energy in the oblique coordinates (x, y) is

$$U_1 = \frac{1}{2 \sin \alpha} \iint_I D \left\{ \left(\frac{w_{xx} + w_{yy} - 2 w_{xy} \cos \alpha}{\sin \alpha} \right)^2 - 2(1-\nu)(w_{xx} w_{yy} - w_{xy}^2) \right\} dx dy$$

or, in matrix form,

$$U_1 = \frac{1}{2} \iint_I D \gamma' H \gamma \, dx dy$$

where

$$H = \frac{1}{\sin^3 \alpha} \begin{vmatrix} 1 & -2 \cos \alpha & \cos^2 \alpha + \nu \sin^2 \alpha \\ -2 \cos \alpha & 4 \cos^2 \alpha + 2(1-\nu) \sin^2 \alpha & -2 \cos \alpha \\ \cos^2 \alpha + \nu \sin^2 \alpha & -2 \cos \alpha & 1 \end{vmatrix}$$

Substituting the curvature expressions into the strain energy and noting that, for a constant bending rigidity D ,

$$\iint_I D \, dx dy = \frac{ab}{2} D$$

$$\iint_I D x \, dx dy = \frac{a^2 b}{6} D$$

$$\iint_I D y \, dx dy = \frac{ab^2}{6} D$$

$$\iint_I D xy \, dx dy = \frac{a^2 b^2}{24} D$$

$$\iint_I D x^2 \, dx dy = \frac{a^3 b}{12} D$$

$$\iint_I D y^2 \, dx dy = \frac{ab^3}{12} D$$

the strain energy turns out in the form

$$U_1 = \frac{1}{2} q_1' K_1 q_1$$

where the stiffness matrix K_1 of the first triangle can be evaluated from :

$$K_1 = \frac{D}{6 a^3 b^3} \left\{ 3 W' H W + 2 \left(W'_x H W + W' H W'_x + W' H W'_y + W' H W \right. \right. \\ \left. \left. + W'_x H W'_x + W' H W'_y \right) + W'_x H W'_y + W' H W'_x \right\}$$

Closer inspection of this formula reveals that, introducing the combinations

$$A_1 = W + W'_x \quad B_1 = W + W'_y \quad C_1 = W + W'_x + W'_y$$

the number of products is reduced to three

$$K_1 = \frac{D}{6 a^3 b^3} \left\{ A_1' H A_1 + B_1' H B_1 + C_1' H C_1 \right\}$$

Furthermore the matrices A_1 , B_1 and C_1 are simpler than the W matrices and are given in Figure F.2.I3.

The generation of the stiffness matrix for the second triangle follows the same procedure. This time we obtain conformity along the interface $x = 0$ of the deflection w (hence also continuity of $\partial w / \partial y$) and of the slope $\partial w / \partial x$ by retaining the values of the coefficients $\alpha_1, \alpha_2, \alpha_3, \alpha_5, \alpha_6, \alpha_9$ and α_{10} of the first field. New values $\alpha'_4, \alpha'_7, \alpha'_8$ can be adopted for the remaining coefficients. The coefficients of the second field are given by the same formulas as above provided we change

$$a \text{ into } -c, \quad w_1 \text{ into } w_3, \quad \phi_1 \text{ into } \phi_3, \quad \psi_1 \text{ into } \psi_3$$

$$\text{and } \phi_{12} \text{ into } \phi_{23}.$$

The generalized coordinates for the second field are thus

$$q_2' = (w_0 \phi_0 \psi_0 w_3 \phi_3 \psi_3 w_2 \phi_2 \psi_2 \phi_{23})$$

The stiffness matrix is then obtained as

$$K_2 = \frac{D}{6 c^3 b^3} \left\{ A_2' H A_2 + B_2' H B_2 + C_2' H C_2 \right\}$$

where A_2, B_2, C_2 are obtained from A_1, B_1, C_1 by changing a into $-c$

For triangle number 3, deflections and slopes at the interface $y = 0$ are identical with those of field 1 if the coefficients $\alpha_1 \alpha_2 \alpha_3 \alpha_4 \alpha_5 \alpha_7$ and α_8 are retained. The new coefficients are $\alpha'_6 \alpha'_9$ and α'_{10} . To determine the coefficients in terms of the generalized displacements

$$q'_3 = (w_0 \phi_0 \psi_0 w_1 \phi_1 \psi_1 w_4 \phi_4 \psi_4 \phi_{41})$$

we can also use the formulas of field 1 changing b into $-d$, w_2 into w_4 , ϕ_2 into ϕ_4 , ψ_2 into ψ_4 and ϕ_{12} into ϕ_{41} . The stiffness matrix K_3 is given by

$$K_3 = \frac{D}{6 a^3 d^3} \{ A'_3 H A_3 + B'_3 H B_3 + C'_3 H C_3 \}$$

where A_3, B_3, C_3 derive from A_1, B_1, C_1 by changing b into $-d$. Finally the fourth field conforms with fields 2 and 3 at the interfaces, if its coefficients are

$$\alpha_1 \alpha_2 \alpha_3 \alpha'_4 \alpha_5 \alpha'_6 \alpha'_7 \alpha'_8 \alpha'_9 \alpha'_{10}$$

In terms of the generalized coordinates

$$q'_4 = (w_0 \phi_0 \psi_0 w_3 \phi_3 \psi_3 w_4 \phi_4 \psi_4 \phi_{34})$$

The coefficients derive from those of field 1 by the combined modifications :

a into $-c$, b into $-d$, $w_1 \phi_1 \psi_1$ respectively into $w_3 \phi_3 \psi_3$, $w_2 \phi_2 \psi_2$ respectively into $w_4 \phi_4 \psi_4$ and ϕ_{12} into ϕ_{34} .

The stiffness matrix is again of the form

$$K_4 = \frac{D}{6 c^3 d^3} \{ A'_4 H A_4 + B'_4 H B_4 + C'_4 H C_4 \}$$

and the matrices A_4, B_4, C_4 are obtained from A_1, B_1, C_1 by the double change of a into $-c$ and b into $-d$.

The four partial stiffness matrices are then combined into a 19×19 matrix J defined by energy addition

$$\sum_1^4 q'_i K_i q'_i = p' J p$$

where

$$p' = (w_0 \phi_0 \psi_0 w_1 \phi_1 \psi_1 w_2 \phi_2 \psi_2 w_3 \phi_3 \psi_3 w_4 \phi_4 \psi_4 \phi_{12} \phi_{23} \phi_{34} \phi_{41})$$

This can be done by addressing correctly the elements of the K_1 matrices in J as they are generated.

But J is not yet a proper stiffness matrix since the 19 coordinates of p are not independent. They depend on 16 coefficients

$$\alpha_i \quad (i = 1, 2, 3 \dots 10) \quad \text{and} \quad \alpha'_i \quad (i = 4, 6, 7, 8, 9, 10)$$

It is interesting to observe that $\alpha_1, \alpha_2, \alpha_3$ which represent the rigid body modes and α_5 which represents a torsional deformation mode, are the only coefficients valid throughout the four fields. Equating the four different field expressions obtained for the α_5 coefficient, we obtain a system of three equations that can easily be solved for the deflection and slopes at the internal node :

$$w_0 = \frac{c}{a+c} w_1 + \frac{a}{a+c} w_3 - \frac{ac}{6(a+c)} \phi_1 + \frac{ac}{6(a+c)} \phi_3 + \frac{2ac}{3(a+c)(b+d)} (-d\phi_{12} + d\phi_{23} + b\phi_{34} - b\phi_{41})$$

$$\phi_0 = \frac{3}{a+c} (w_1 - w_3) - \frac{a}{2(a+c)} \phi_1 - \frac{c}{2(a+c)} \phi_3 + \frac{d}{2(b+d)} \phi_2 + \frac{b}{2(b+d)} \phi_4 - \frac{2}{(a+c)(b+d)} (ad\phi_{12} + cd\phi_{23} + bc\phi_{34} + ab\phi_{41})$$

$$\psi_0 = \frac{c}{a+c} \psi_1 + \frac{a}{a+c} \psi_3 + \frac{2ac}{(a+c)(b+d)} (-\phi_{12} + \phi_{23} - \phi_{34} + \phi_{41})$$

If these relations are put into matrix form

$$\begin{pmatrix} w_0 \\ \phi_0 \\ \psi_0 \end{pmatrix} = M q$$

with $q' = (w_1 \phi_1 \psi_1 w_2 \phi_2 \psi_2 w_3 \phi_3 \psi_3 w_4 \phi_4 \psi_4 \phi_{12} \phi_{23} \phi_{34} \phi_{41})$

a condensation matrix is defined by

$$N = \begin{pmatrix} M \\ E \end{pmatrix}$$

where E is a 16×16 identity matrix so that

$$p = N q$$

The total energy becomes

$$U = \frac{1}{2} q' K q$$

with the (proper) stiffness matrix

$$K = N' J N$$

The next transformation for that matrix is a reference coordinates transformation. The best policy is to refer the slopes at nodal points to global structural axes and transform the mid edge slopes to normal slopes. In fact the displacements known along an edge are just sufficient to express the normal slope anywhere along that edge. In doing this, a sign has to be affected to the normal and the outward normal was selected.

From that choice follows that an identification of normal slopes at mid distance of an interface implies a change of sign of one of the two normal slopes. This is incorporated into the program of element connection. The final set of the 16 generalized displacements is indicated in Figure F.2.I4. Turning now to the stress matrix generation (which here is rather a matrix of bending and twisting moments) it is recalled that, in each triangle, the curvatures are given by a relation which, for the first triangle, is

$$\gamma_1 = \left(\frac{1}{a^2 b^2} W + \frac{2x}{a^3 b^2} W_x + \frac{2y}{a^2 b^3} W_y \right) q_1$$

It follows that the moments expressed in local oblique coordinates are

$$m = \begin{bmatrix} M_x \\ M_{xy} \\ M_y \end{bmatrix}_1 = D H \gamma_1 = D \left(\frac{1}{a^2 b^2} H W + \frac{2x}{a^3 b^2} H W_x + \frac{2y}{a^2 b^3} H W_y \right) q_1$$

These moments being linear in x and y are determined by their values in three points of each triangle and it is convenient to select the three vertices. Therefore the moments generated in the first triangle are

$$m = \begin{vmatrix} m(o, o) \\ m(a, o) \\ m(o, b) \end{vmatrix} = \frac{D}{a^2 b^2} \begin{vmatrix} H W \\ H W + 2 H W_x \\ H W + 2 H W_y \end{vmatrix} \quad q_1 = R_1 q_1$$

The moments matrix can first be expressed in terms of the augmented set of generalized displacements p .

This entails merely an operation involving a localizing matrix L_1

$$q_1 = L_1 p$$

whence

$$m = R_1 L_1 p$$

The second operation is a condensation expressing the moments in terms of the 16 independent displacements. Since

$$p = N q$$

we have $m_1 = T_1 q$ with $T_1 = R_1 L_1 N$

T_1 is the final moments matrix for a triangle.

It is noted that the R_1 matrix is generated from the field coefficients given at the beginning of this section simultaneously with the matrices A , B and C .

Then the localization and condensation processes are applied simultaneously to the stiffness and moment matrices in the final version of the program. The moment matrices for the other triangles are generated using the same changes in R_1 as in the A , B , C matrices. The moments so computed are given in the oblique axes and interpretation is not always easy when passing from one element to the next one. This is a counterpart of the advantages of using oblique coordinates. When general reference stress axes can be defined, an additional change of coordinates can be applied to the m_i matrices.

2.I.5- Rigid jointed frame element (ref. R.2.8).

This element is assumed to obey the classical engineering beam theory. It consists of an axially loaded bar as described in section 2.I.1 to which torsional and bending stiffness have been added.

The behaviour of such an element can be split into 4 modes of deformation : the first one is axial tension, the second is torsion and the last two are bending in orthogonal planes.

The four modes yield independent stiffness matrices which are assembled at the end of the process.

The beam is represented in Figure F.2.15 with sign conventions and local axes location.

Axial deformation mode.

From 2.I.2 follows that, if

$$u = \alpha_1 + \alpha_2 x$$

the stiffness matrix corresponding to the generalized displacements

$q_1' = (u_1, u_2)$ is

$$K_1 = \frac{EA}{L} \begin{vmatrix} 1 & -1 \\ -1 & 1 \end{vmatrix}$$

Torsion mode.

Assuming that

$$\phi_x = \alpha_3 + \alpha_4 x$$

the engineering beam theory furnishes

$$K_2 = \frac{GJ}{L} \begin{vmatrix} 1 & -1 \\ -1 & 1 \end{vmatrix}$$

for a displacement row $q_2' = (\phi_{x1}, \phi_{x2})$

and where GJ is the torsional stiffness.

Bending in the yx plane.

Assuming that the y-wise deflections are given by a cubic such as

$$v = \alpha_5 + \alpha_6 x + \alpha_7 x^2 + \alpha_8 x^3$$

and taking $v_1, v_2, \phi_{z1} = (\partial v / \partial x)_1$ and $\phi_{z2} = (\partial v / \partial x)_2$ as generalized coordinates, the bending moment in the beam

$$M = E I_y \frac{\partial^2 v}{\partial x^2} = 2 E I_y (\alpha_7 + 3 \alpha_8 x)$$

can be placed in the form

$$M = 2 E I_y \left\{ \frac{1}{4a} (\phi_{z1} - \phi_{z2}) + \frac{3x}{4a^2} (\phi_{z1} + \phi_{z2} - \frac{v_1 - v_2}{a}) \right\}$$

The bending energy being

$$U_b = \frac{1}{2} \int_{-a}^{+a} \frac{M^2}{EI_y} dx$$

The stiffness matrix associated to the row matrix $q_3^i = (v_1, \phi_{z1}, v_2, \phi_{z2})$ turns out as

$$K = \frac{EI_y}{L^3} \begin{vmatrix} I2 & -6L & -I2 & -6L \\ -6L & 4L^2 & 6L & 2L^2 \\ -I2 & 6L & I2 & 6L \\ -6L & 2L^2 & 6L & 4L^2 \end{vmatrix}$$

Bending in the zx plane yields a similar relation, where I_y is changed into I_z and ϕ_z into $-\phi_y$, according to the sign conventions of Figure F.2.15.

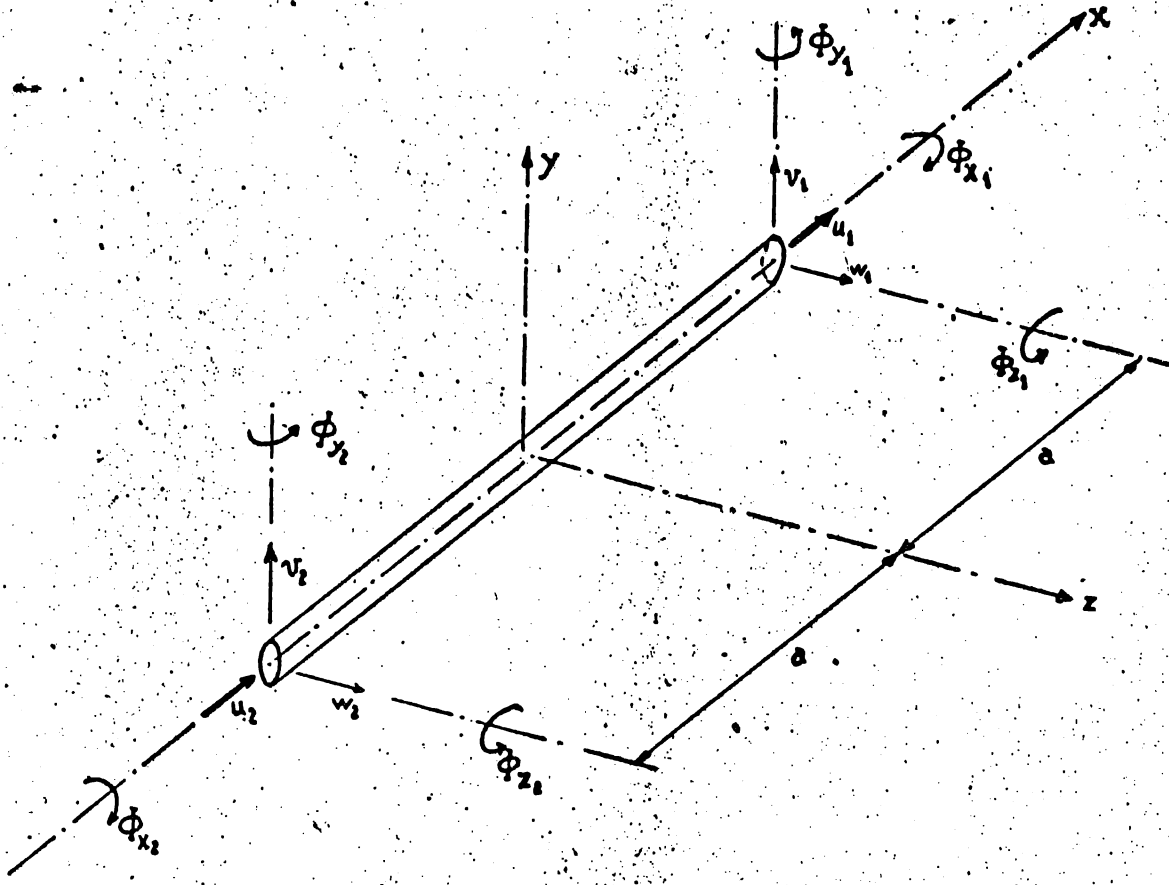
Assembling these matrices with the displacements sequence

$$q^i = (u_1, v_1, w_1, \phi_{x1}, \phi_{y1}, \phi_{z1}, u_2, v_2, w_2, \phi_{x2}, \phi_{y2}, \phi_{z2})$$

yields the complete stiffness matrix of Figure F.2.16.

For stress computation, as no information need be given about intermediate sections of the beam, only the tip forces and moments are printed out so that the so called stress matrix becomes identical to the stiffness matrix.

Figure F.2.15 : Rigid jointed frame element.



cross section	area : A
	moments of inertia : I_y, I_z
	torsional rigidity : J

2.2- Equilibrium Models.

2.2.I- Bar element under constant shear (ref. R.2.3 and R.2.2).

The equilibrium equation governing the axial load $N(x)$ in the bar represented in Figure F.2.I7 is :

$$\frac{dN}{dx} = - \tau \quad (\text{the shear flow})$$

In order to connect this bar with skin panels analyzed under a constant shear assumption, this equilibrium equation can be integrated for constant τ , giving

$$N = \beta - \tau x$$

Two generalized forces are defined at the end points to transmit the axial load to adjacent bar elements. The third is defined as the total axial load transmitted by the constant shear flow :

$$Q_1 = N(+a) = \beta - \tau a$$

$$Q_2 = -N(-a) = -(\beta + \tau a)$$

$$Q_3 = \int_{-a}^{+a} \tau dx = 2 a \tau$$

The overall equilibrium condition $Q_1 + Q_2 + Q_3 = 0$ is of course satisfied. The three equations express the generalized loads in terms of two stress parameters; in matrix form

$$g = C b$$

with

$$g' = (Q_1 \quad Q_3 \quad Q_2)$$

$$b' = (\beta, \tau)$$

$$C = \begin{vmatrix} 1 & -a \\ 0 & 2a \\ -1 & -a \end{vmatrix}$$

is known as the loads connection matrix.

The complementary strain energy of the bar can be written as

$$U = \frac{1}{2} \int_{-a}^{+a} \frac{N^2}{ES} dx$$

$$= \frac{1}{2} b' F b$$

where F , the flexibility matrix, turns out to be :

$$F = \frac{1}{E} \begin{vmatrix} \int_{-a}^{+a} \frac{dx}{S} & - \int_{-a}^{+a} \frac{xdx}{S} \\ - \int_{-a}^{+a} \frac{xdx}{S} & \int_{-a}^{+a} \frac{x^2 dx}{S} \end{vmatrix}$$

The complementary strain energy principle is then written as

$$\left(\frac{1}{2} b' F b - g' q \right) \text{ minimum (in which } g' = b' C').$$

By differentiation with respect to the elements of b (the stress parameters the minimum conditions are found to be

$$F b = C' q$$

Then

$$b = F^{-1} C' q$$

and finally

$$g = C b = K q$$

with a stiffness matrix $K = C F^{-1} C'$.

For a constant cross section S , the stiffness matrix is found to be

$$K = \frac{ES}{a^3} \begin{vmatrix} 2 & -3 & 1 \\ -3 & 6 & -3 \\ 1 & -3 & 2 \end{vmatrix}$$

The axial stress is given by

$$\sigma_x = \frac{N}{S} = \frac{1}{S} (B - \tau x)$$

Being linear it is determined by its end values. Hence we generate

$$\sigma = \begin{bmatrix} \sigma_{x1} \\ \sigma_{x2} \end{bmatrix} = \frac{E}{a} \begin{bmatrix} 2 & -3 & 1 \\ 1 & -3 & 2 \end{bmatrix} q = T q$$

where T is the so called stress matrix.

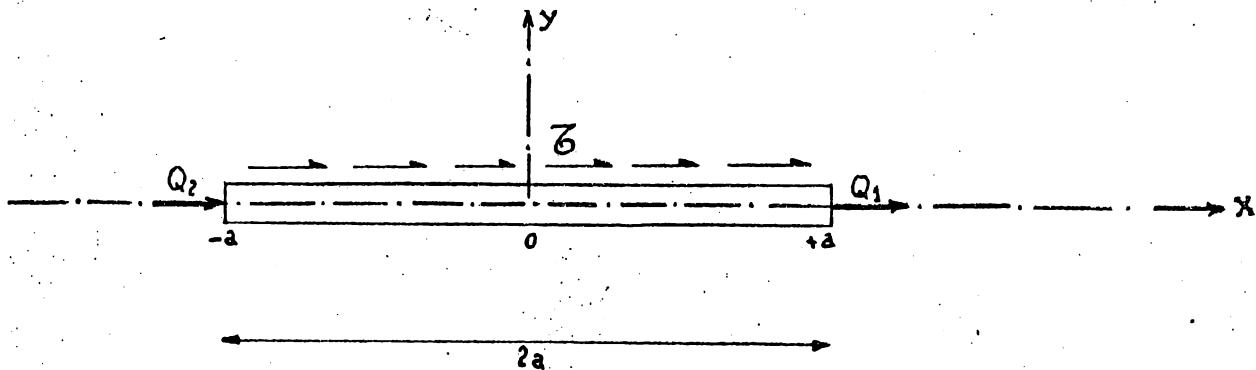
The significance of the generalized displacements is deduced from the virtual work equation which gives

$$q_1 = u(+a)$$

$$q_2 = u(-a)$$

$$q_3 = \frac{1}{2a} \int_{-a}^{+a} u(x) dx$$

Figure F.2.17 : Constant shear bar.



Assumption : $\tau = \text{constant.}$

2.2.2- Skin element. Constant stress quadrangle.

The first skin element to be developed as an equilibrium model for upper bound analysis is the constant stress triangle reported in reference R.2.3 or R.2.2. It is sketched on Figure F.2.18.

The generalized loads are defined to be the stress resultants along each edge. It was shown that, for constant thickness, the corresponding stiffness matrix is directly deducible from that of the linear displacement field triangle of section 2.1.2.1 by taking as reference area the so-called skeleton triangle (hatched in Figure F.2.18); that is dividing the area of the physical triangle by a factor 4.

However, direct manipulation of the stiffness matrices of individual elements of this type can lead to computational difficulties, because kinematical deformation modes arise each time four elements are grouped to form a quadrilateral piece of skin. This situation is depicted on Figure F.2.19.

Mathematically, the complete stress field contains 12 independent parameters : the three stress components of each triangle, while 16 generalized loads are involved in the stress transmission mechanism. The $16 - 12 = 4$ dependency relations between the loads contain the 3 overall equilibrium conditions (corresponding to zero virtual work in a rigid body motion of the quadrilateral) and one further condition that must correspond to zero virtual work in a kinematical mode of freedom. This mode is fairly easy to visualize if one observes that (at least for the constant thickness case) the generalized displacements can be taken to be the local displacements at mid distance of each edge of a triangle. This is equivalent to having the four skeleton triangles pin jointed at their vertices. Then, if one is considered fixed, the other three can deform as a three bar linkage.

In references R.2.2 and R.2.3 it was proved that, provided the 4 internal nodes are not subjected to external loads, this kinematical freedom does not restrict the loads on the 4 external nodes when the subdivision into triangles is through the diagonals of the quadrilateral. In this case the kinematical deformation is such that each skeleton triangle can pivot about its external vertex; whatever the external loads on those vertices, they do not produce any virtual work. As a consequence it must be possible to set up directly a stiffness matrix for such a quadrilateral and one operational procedure is now described.

The local axes of the quadrilateral element, as shown on Figure F.2.20, are orthogonal, their origin is at the intersection of the diagonals and the x axis cuts the edge I2 in equal segments.

Although some simplification would result from the use of the diagonals themselves as a natural set of oblique axes, the necessity of a back transformation to global cartesian axes will perhaps offset the advantages.

A basic stress field (the term stress really denotes here loads per unit length) is first defined in the whole quadrilateral

$$\sigma_x = \beta_1 \quad \sigma_y = \beta_2 \quad \tau_{xy} = \beta_3$$

A first additional field is then defined inside the area 234 by the condition that, along the interface 24 with the basic field, no stresses be transmitted. This is expressed in the local axes $x' y'$ of Figure F.2.20 by

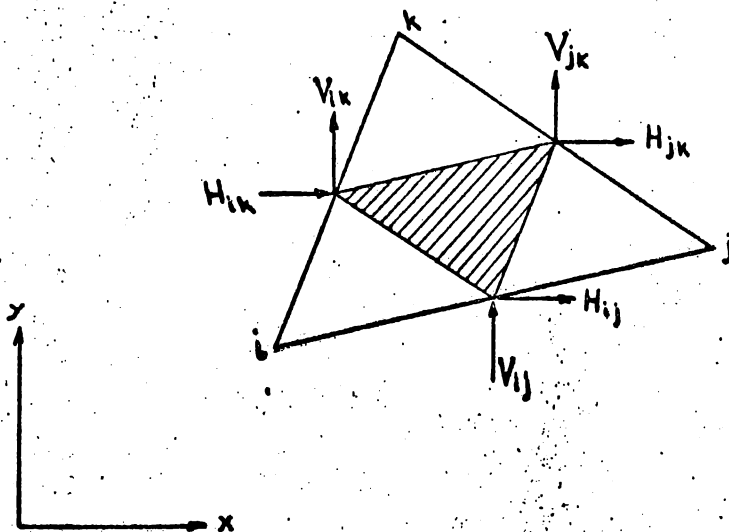
$$\sigma_{y'} = 0 \quad \tau_{x' y'} = 0 \quad \sigma_{x'} = \beta_4$$

Hence, there is one additional parameter applicable to the area 234. Reverting to the axes of the basic field, the additional field is

$$\sigma_x = \beta_4 \cos^2 \theta_1 \quad \sigma_y = \beta_4 \sin^2 \theta_1 \quad \tau_{xy} = \beta_4 \sin \theta_1 \cos \theta_1$$

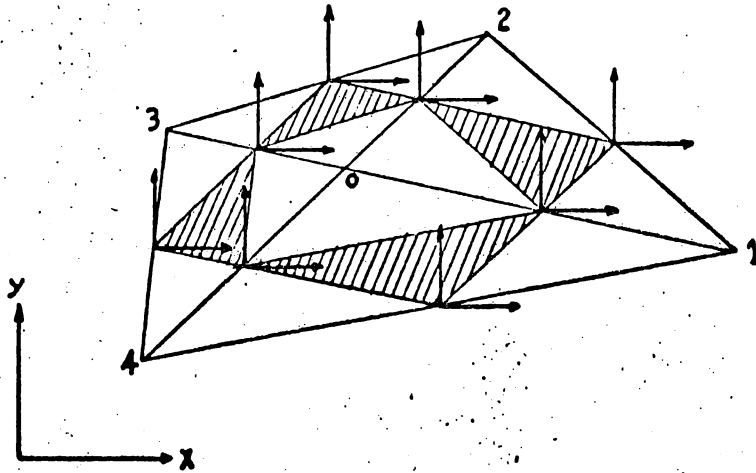
A second additional field can be injected into the area I23.

Figure F.2.18 : The constant stress triangle.



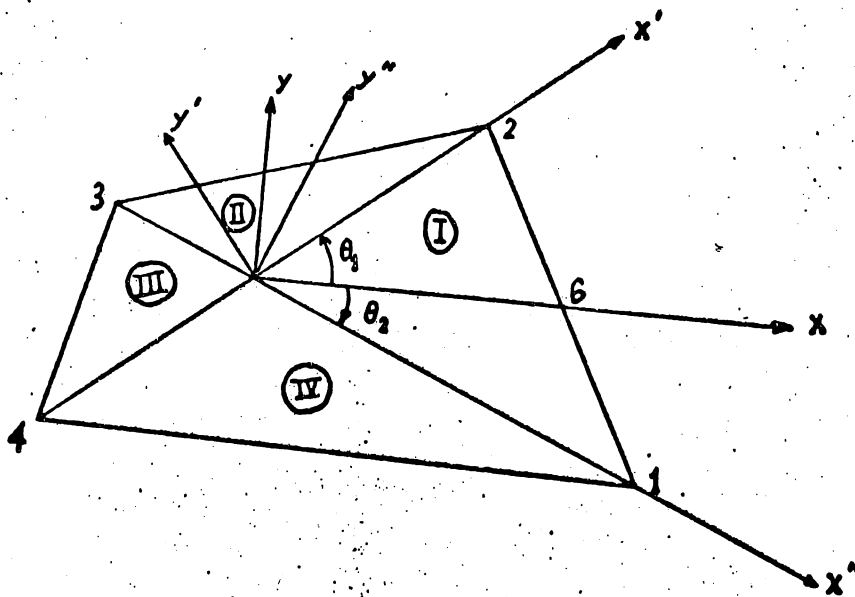
Assumption : $\sigma_x = \beta_1$
 $\sigma_y = \beta_2$
 $\tau_{xy} = \beta_3$

Figure F.2.19 : The quadrangle composed of 4 independent triangles.



Assumption : $\sigma_x = \beta_1$
 $\sigma_y = \beta_2$
 $\tau_{xy} = \beta_3$ in each triangle O_{ij} .

Figure F.2.20 : The quadrangle subdivided by the diagonals.



Note : $\theta_2 < 0$
 $k_{26} = k_{16}$

$$\sigma_y'' \equiv 0 \quad \tau_{x''y''} \equiv 0 \quad \sigma_{x''} = \beta_5$$

Or (the angle θ_2 being considered as negative on Figure F.2.20)

$$\sigma_x = \beta_5 \cos^2 \theta_2 \quad \sigma_y = \beta_5 \sin^2 \theta_2 \quad \tau_{xy} = \beta_5 \sin \theta_2 \cos \theta_2$$

It satisfies the conditions of zero stress transmission across the interface 24. Hence, considering the diagonals as interfaces of stress transmission between the four triangular subareas, we obtain by superposition a 5 parameter field in equilibrium without body forces. The generalized forces or stress resultants along the external boundaries of the quadrilateral are

$$H_{12} = \sigma_x y_{21} + \tau_{xy} x_{12}$$

$$H_{23} = \sigma_x y_{32} + \tau_{xy} x_{23}$$

$$V_{12} = \sigma_y x_{12} + \tau_{xy} y_{21}$$

$$V_{23} = \sigma_y x_{23} + \tau_{xy} y_{32}$$

$$H_{34} = \sigma_x y_{43} + \tau_{xy} x_{34}$$

$$H_{41} = \sigma_x y_{14} + \tau_{xy} x_{41}$$

$$V_{34} = \sigma_y x_{34} + \tau_{xy} y_{43}$$

$$V_{41} = \sigma_y x_{41} + \tau_{xy} y_{14}$$

where x_{ij} and y_{ij} stand for $x_i - x_j$ and $y_i - y_j$ respectively.

The stresses involved in those formulas are those effective in each triangular subarea bordered by the edge under consideration. This is summarized in Figure F.2.2I.

The connection matrix C involved in the relation

$$g = C b$$

with
$$g' = (H_{12} \quad V_{12} \quad H_{23} \quad V_{23} \quad H_{34} \quad V_{34} \quad H_{41} \quad V_{14})$$

$$b' = (\beta_1 \quad \beta_2 \quad \beta_3 \quad \beta_4 \quad \beta_5)$$

follows from this and is given by Figure F.2.22. Again, from the stress table of Figure F.2.2I follow the S_i matrices defined by

$$\sigma_i = \begin{vmatrix} \sigma_x \\ \sigma_y \\ \tau_{xy} \end{vmatrix}_i = S_i b \quad i = I, II, III, IV.$$

and the flexibility matrices

$$F_i = \frac{\Omega_i}{Et_i} (S_i' M^{-1} S_i)$$

expressing the energy content

$$U_i = \frac{1}{2} b' F_i b$$

of each triangle. Ω_i denotes each subarea, t_i the constant thickness of the skin and

$$M^{-1} = \begin{vmatrix} 1 & -\nu & 0 \\ -\nu & 1 & 0 \\ 0 & 0 & 2(1+\nu) \end{vmatrix}$$

The total flexibility matrix is $F = \sum F_i$ and is described in Figure F.2.23 for the case $t_i = t$ a common constant thickness. This matrix is inverted numerically to produce the stiffness matrix of the quadrilateral

$$K = C F^{-1} C'$$

The stresses in each subarea can be computed from

$$\sigma_i = S_i (F^{-1} C') q$$

(the true stresses follow by division by the thickness).

From virtual work the generalized displacements are found to be

$$u_{ij} = \int_i^j u \, ds \quad \text{associated to} \quad H_{ij}$$

$$v_{ij} = \int_i^j v \, ds \quad \text{associated to} \quad V_{ij}$$

If the thickness is constant, the real stresses and then also the strains are constant in each subarea. A linear displacement field is obtained by integration and the generalized displacements can be interpreted as the local values of this displacement field at the middle of the edge ij .

2.2.3- Spar element. (Web only. Spar caps are assembled as bar elements).

2.2.3.I- Upper bound version (ref. R.2.2).

In this approach the skin elements adjacent to the spar cap are supposed to be of the constant stress type. This means that the shear flow feeding the spar cap is constant.

Along a transverse cross section of the web the distribution of shear has to be symmetrical with respect to the longitudinal axis, the distribution of σ_x stresses antisymmetrical. Therefore the following stress field is assumed in the web represented in Figure F.2.24.

$$\sigma_x = \frac{6z}{h^2} (\beta_1 + \beta_2 x)$$

$$\sigma_z = 0$$

Here again stresses mean loads per unit length.

$$\tau_{xz} = \beta_3 - 3 \frac{z^2}{h^2} \beta_2$$

It satisfies the inner equilibrium equations without body forces.

It is worth noting that the assumption $\sigma_z = 0$ implies that the external vertical loading has to take place through end loads in sections $x = \pm a$.

An extension of the model is required to take care of distributed loading. To characterize the continuous stress transmission to neighboring elements, the following generalized forces were selected

$$Q_3 = \int_{-a}^{+a} (\tau_{xz})_{z=h} dx = -6 a \beta_2 + 2 a \beta_3$$

$$M_1 = \int_{-h}^{+h} (\sigma_x)_{x=+a} z dz = 4 h (\beta_1 + a \beta_2)$$

$$M_2 = \int_{-h}^{+h} (\sigma_x)_{x=-a} z dz = 4 h (-\beta_1 + a \beta_2)$$

$$T_1 = \int_{-h}^{+h} (\tau_{xz})_{x=+a} dz = 2 h (-\beta_2 + \beta_3)$$

$$T_2 = \int_{-h}^{+h} (\tau_{xz})_{x=-a} dz = 2 h (\beta_2 - \beta_3)$$

$$V_1 = \int_{-h}^{+h} \left(1 - 3 \frac{z^2}{h^2}\right) (\tau_{xz})_{x=+a} dz = \frac{8}{5} h \beta_2$$

$$V_2 = \int_{-h}^{+h} \left(1 - 3 \frac{z^2}{h^2}\right) (\tau_{xz})_{x=-a} dz = -\frac{8}{5} h \beta_2$$

Two generalized forces T and V are required to characterize the parabolic shear distribution across a vertical web cross section. T represents the total transverse shear load, V measures the parabolic distortion; it would vanish were the shear distribution constant.

The connection matrix follows from those relations :

$$g = C b$$

with $g' = (T_1 \ V_1 \ M_1 \ T_2 \ V_2 \ M_2 \ 2Q_3)$

and $b' = (\beta_1 \ \beta_2 \ \beta_3)$ if

$$C' = \begin{vmatrix} 0 & 0 & 4h & 0 & 0 & -4h & 0 \\ -2h & \frac{8}{5}h & 4ah & 2h & -\frac{8}{5}h & 4ah & -12a \\ 2h & 0 & 0 & -2h & 0 & 0 & 4a \end{vmatrix}$$

A matrix form of the stress field assumptions is

$$\sigma = S b$$

with $S = \begin{vmatrix} \frac{6z}{h^2} & \frac{6zx}{h^2} & 0 \\ 0 & 0 & 0 \\ 0 & -\frac{3z^2}{h^2} & 1 \end{vmatrix}$

and $\sigma' = (\sigma_x \ \sigma_z \ \tau_{xz})$

The complementary strain energy can then be expressed as :

$$\frac{1}{2} \iint \sigma' M^{-1} \sigma \, dx dz = \frac{1}{2} b' F b$$

with the flexibility matrix

$$F = \iint S' M^{-1} S \, dx dz$$

For a constant web thickness t , F is easily obtained as

$$F = \begin{vmatrix} \frac{48 a}{Eth} & 0 & 0 \\ 0 & \left(\frac{16 a^3}{Eth} + \frac{36 ah}{5 Gt} \right) & -4 \frac{ah}{Gt} \\ 0 & -4 \frac{ah}{Gt} & 4 \frac{ah}{Gt} \end{vmatrix}$$

It would be difficult to make use of the corresponding stiffness matrix $K = C F^{-1} C'$, because of the spurious kinematical deformation modes involved. Indeed, the homogeneous system

$$C' z = 0$$

has four independent non trivial solutions, which are of course also solution of the system

$$K z = 0$$

This was to be expected, since seven generalized forces had to be introduced for a stress field having only three parameters. Therefore four relations exist between the seven forces. In their simplest form they are

$$T_1 + T_2 = 0$$

$$a (T_1 - T_2) + M_1 + M_2 + 2 h Q_3 = 0$$

$$V_1 + V_2 = 0$$

$$M_1 + M_2 + 5 a V_1 = 0$$

The first two relations can be recognized as overall equilibrium conditions of the web. By virtual work they correspond to the two rigid body modes

$$z_1 = (1 \ 0 \ 0 \ 1 \ 0 \ 0 \ 0) \quad \text{a vertical translation}$$

$$z_2 = (a \ 0 \ 1 \ -a \ 0 \ 1 \ h) \quad \text{a rotation.}$$

(The third rigid body mode, horizontal translation, is accounted for by the symmetry in the field assumptions).

The last two relations correspond to deformation modes

$$z_3 = (0 \ 1 \ 0 \ 0 \ 1 \ 0 \ 0)$$

$$z_4 = (0 \ 5a \ 1 \ 0 \ 0 \ 1 \ 0)$$

which leave the model unstressed.

They are of the same nature as the deformation modes encountered in building up a quadrilateral skin panel from constant stress triangles (see section 2.2.2). It is not possible here to resort to a special geometry and restricted loading to eliminate excitation of the spurious modes. Instead, a slight relaxation of the condition of continuous stress transmission will be adopted. By a judicious utilisation of the principle of minimum complementary energy it will be even possible, in some cases, to preserve the upper bound property. The procedure is described in reference R.2.2 and can be summarized as follows :

The principle of minimum complementary energy is written in the form

$$\begin{aligned} \delta \left\{ \frac{1}{2} b' F b - g' q \right\} \\ = \delta \left\{ \frac{1}{2} b' F b - (w_1 T_1 + w_2 T_2 + \phi_1 M_1 + \phi_2 M_2 + 2 u_3 Q_3) - (v_1 V_1 + v_2 V_2) \right\} \\ = 0 \end{aligned}$$

It turns out that, for a web of constant thickness, the deformation field is integrable so that v_1 and v_2 can be expressed in terms of the stress parameters. It is then possible to express the unwanted part of the potential energy entirely in terms of the stress parameters; here

$$v_1 V_1 + v_2 V_2 = \frac{1}{2} \left(\frac{32}{5} \nu \frac{ah}{Et} \right) \beta_2^2$$

This term is then grouped with the strain energy, leaving the minimum principle in the form :

$$\delta \left\{ \frac{1}{2} b' H b - (w_1 T_1 + w_2 T_2 + \phi_1 M_1 + \phi_2 M_2 + 2 u_3 Q_3) \right\} = 0$$

where H is a modified flexibility matrix

$$H = F - \frac{32 v ah}{5 Et} \begin{vmatrix} 0 & 0 & 0 \\ 0 & 1 & 0 \\ 0 & 0 & 0 \end{vmatrix} = \begin{vmatrix} \frac{48 a}{Eth} & 0 & 0 \\ 0 & \left(\frac{16a^3}{Eth} + \frac{72ah}{5 Et} + \frac{8 v ah}{Et} \right) & - \frac{4 ah}{Et} \\ 0 & - \frac{4 ah}{Et} & \frac{4 ah}{Et} \end{vmatrix}$$

The generalized loads are reduced to five by the elimination of V_1 and V_2 so that the modified connection matrix is a portion of the old :

$$C'_0 = \begin{vmatrix} 0 & 4 h & 0 & - 4 h & 0 \\ - 2 h & 4 ah & 2 h & 4 ah & - 12 a \\ 2 h & 0 & - 2 h & 0 & 4 a \end{vmatrix}$$

For a force sequence given by

$$g' = (T_1 \quad M_1 \quad T_2 \quad M_2 \quad 2 Q_3)$$

The stiffness matrix without kinematical modes is then :

$$K = C_0 H^{-1} C'_0$$

This can be worked out analytically. The result is given in Figure F.2.25.

The elimination of the kinematical modes being made through the principle of minimum complementary energy, the guarantee of an upper bound to the direct influence coefficients still holds, despite the possibility of local violations in the transmission of shear stresses at the $x = \pm a$ boundaries. The connection loads V_1 and V_2 having disappeared, only the average of the shearing stresses is transmitted through T_1 and T_2 , while the amplitudes of parabolic shearing distribution $(1 - 3 z^2/h^2)$ can now suffer a discontinuity at an interface. However, if we consider the difference as absorbed by an externally applied linear distribution the fact that it is statically equivalent to zero indicates, by an appeal to the de Saint Venant's principle, that its effect must be local.

Turning now to the generalized displacements associated to the loads, the virtual work equations yield the interpretations :

$$u_3 = \frac{1}{2a} \int_{-a}^{+a} (u)_{z=h} dx$$

$$\phi_1 = \frac{3}{2h^3} \int_{-h}^{+h} (u)_{x=a} z dz$$

$$\phi_2 = \frac{3}{2h^3} \int_{-h}^{+h} (u)_{x=-a} z dz$$

$$w_1 = \frac{1}{2h} \int_{-h}^{+h} (w)_{x=a} dz$$

$$w_2 = \frac{1}{2h} \int_{-h}^{+h} (w)_{x=-a} dz$$

The stress matrix has now to be expressed.

Substituting in the previous expression for the stresses :

$$\sigma = S b$$

the value of the stress parameters given by

$$b = H^{-1} C'_0 q$$

there comes $\sigma = T q$

with a stress matrix $T = S H^{-1} C'_0$

whose analytical expression appears in Figure F.2.26.

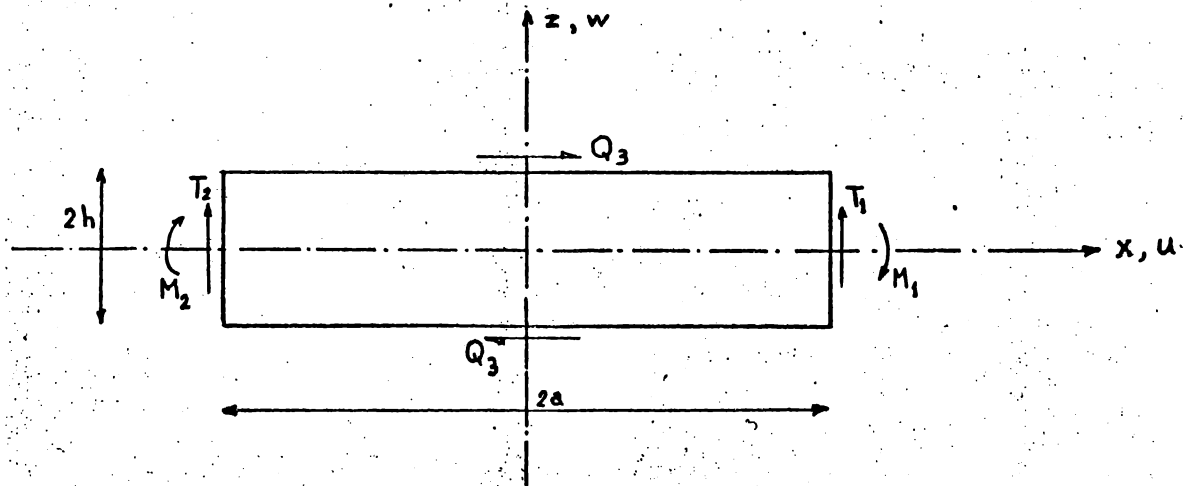
To obtain complete informations on stresses, this matrix is computed at three points and furnishes

$$\sigma_1 = \sigma (+a, +h)$$

$$\sigma_2 = \sigma (-a, +h)$$

$$\sigma_3 = \sigma (0, 0)$$

Figure F.2.24 : The equilibrium spar element (web only).



Assumptions : $\sigma_x = \frac{6z}{h^2} (\beta_1 + \beta_2 x)$

$$\sigma_z = 0$$

$$\tau_{xz} = \beta_3 - 3 \frac{z^2}{h^2} \beta_2$$

2.2.3.2- Direct formulation (ref. R.2.4).

The assumptions for the stress field are exactly the same as for the preceding element :

$$\sigma_x = \frac{6z}{h^2} (\beta_1 + \beta_2 x)$$

$$\sigma_z = 0$$

$$\tau_{xz} = \beta_3 - 3 \frac{z^2}{h^2} \beta_2$$

However now only the 5 generalized forces $(T_1, T_2, M_1, M_2, Q_3)$ are used to characterize the field. Three of them are independent, while the other two are determined by the two overall equilibrium conditions.

In this way the shear distribution at the end cross sections is only related to the forces T_1 and T_2 . Therefore the same type of violation of the shearing stress transmission has to be considered as an "a priori" assumption. The model is no longer an exact equilibrium model but has the advantage of freedom from spurious kinematical modes.

By comparison with other formulations it can give a more precise idea of the shear stress discontinuity effect.

From the above assumptions the connection matrix is the reduced one C_0 , while the flexibility matrix is the original F instead of the modified H . Therefore the stiffness matrix is

$$K = C_0 F^{-1} C_0'$$

and is displayed in analytical form in Figure F.2.27.

One can observe that the differences between the two stiffness matrices affect the terms $k_{22}, k_{42}, k_{44}, k_{52}, k_{54}$ and k_{55} . In the first five terms the factor μ becomes μ^* , whereas the term $\frac{2}{5} h^2$ is now multiplied by $(1 + \nu)$. The differences in these terms are given for some values of the ratio $\frac{a}{h}$ in the following table.

$\frac{a}{h}$	$\frac{\mu}{\mu^*}$	$\frac{k_{55}}{k_{55}^*}$
1	.921053	.948684
2	.973451	.990139
5	.995298	.999563
10	.998806	.999964

It can be seen that the differences decrease with growing ratios $\frac{a}{h}$ and are usually rather small. The models numerically tested, using both formulations, showed no significant differences in the results. It can therefore be concluded that the small and local discontinuities in the stress transmission occurring in these models will not have significant effects when the ratio $\frac{a}{h}$ is normally large, as it can be expected from the de Saint Venant's principle.

2.2.4- Plate elements.

2.2.4.I- The triangular plate in bending (ref. R.2.6).

In the triangle represented in Figure F.2.28 a moments distribution satisfying equilibrium with no shear loads can be written as

$$M_x = \int_t \sigma_x z dz = \alpha_1 + \alpha_2 x + \alpha_3 y$$

$$M_y = \int_t \sigma_y z dz = \alpha_4 + \alpha_5 x + \alpha_6 y$$

$$M_{xy} = \int_t \tau_{xy} z dz = \alpha_7 - \alpha_6 x - \alpha_2 y$$

It involves 7 parameters.

In addition a constant shearing force distribution

$$Q_x = \int_t \tau_{xz} dz = \alpha_8$$

$$Q_y = \int_t \tau_{yz} dz = \alpha_9$$

is taken with an associated solution of the equilibrium equations

$$\frac{\partial M_x}{\partial x} + \frac{\partial M_{xy}}{\partial y} = Q_x = \alpha_8$$

$$\frac{\partial M_y}{\partial y} + \frac{\partial M_{xy}}{\partial x} = Q_y = \alpha_9$$

Such a particular solution can be

$$M_{xy} = x \alpha_9 + y \alpha_8$$

The complete distribution becomes therefore

$$M_x = \alpha_1 + \alpha_2 x + \alpha_3 y$$

$$M_y = \alpha_4 + \alpha_5 x + \alpha_6 y \quad (I)$$

$$M_{xy} = \alpha_7 + (\alpha_9 - \alpha_6)x + (\alpha_8 - \alpha_2)y$$

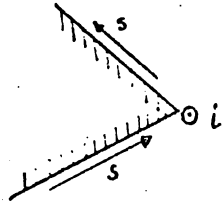
$$Q_x = \alpha_8$$

$$Q_y = \alpha_9$$

Adopting the Kirchhoff-Love theory of plate bending, the continuity of stress transmission reduces to the continuity along each interface segment of : the normal moment M_n

$$\text{the equivalent transverse shear distribution } V_n = Q_n + \frac{\partial M_{sn}}{\partial s}$$

At a corner point i , where several elements meet together, the corner loads



$$Z_i = (M_{sn})_{i+0} - (M_{sn})_{i-0}$$

must add up to balance the external transverse nodal load.

In the triangle, using the linear moments distribution, this is automatically achieved by taking as generalized loads the normal moments $M_{n_{ij}}$ at each vertex and for each edge, the 3 corner forces Z_i and the 3 equivalent and constant transverse shears V_{ij} along each edge. These loads are taken in the order

$$g' = (M_{n_{12}} \quad M_{n_{13}} \quad Z_1 \quad M_{n_{21}} \quad M_{n_{23}} \quad Z_2 \quad M_{n_{31}} \quad M_{n_{32}} \quad Z_3 \quad V_{12} \quad V_{23} \quad V_{31})$$

$M_{n_{ij}}$ stands for a normal moment expressed at i along the edge ij according to an anticlockwise numbering of the vertices.

If l_{ij} , m_{ij} are the direction cosines of the outward normal to the edge ij , the moments and transverse shears along that edge are given by

$$M_{n_{ij}} = l_{ij}^2 M_x + m_{ij}^2 M_y + 2 l_{ij} m_{ij} M_{xy}$$

$$M_{sn_{ij}} = (l_{ij}^2 - m_{ij}^2) M_{xy} - l_{ij} m_{ij} (M_x - M_y)$$

$$Q_{n_{ij}} = l_{ij} Q_x + m_{ij} Q_y$$

while
$$\left(\frac{\partial M_{sn}}{\partial s}\right)_{ij} = l_{ij} \left(\frac{\partial M_{sn}}{\partial y}\right)_{ij} - m_{ij} \left(\frac{\partial M_{sn}}{\partial x}\right)_{ij}$$

Hence forth the generalized loads can be written in terms of the stress field parameters

$$g = C b$$

where C is the connection matrix which, in local axes, appears on Figure F.2.29, and where b is the column of the stress field coefficients taken in the order

$$b' = (\alpha_3 \quad \alpha_6 \quad \alpha_7 \quad \alpha_1 \quad \alpha_4 \quad \alpha_5 \quad \alpha_2 \quad \alpha_8 \quad \alpha_9)$$

In the local axes represented in Figure F.2.28 the direction cosines can be computed from the formulas

$$\begin{aligned} l_{12} &= 0 & m_{12} &= -1 \\ l_{23} &= \frac{y_3 - y_2}{c_{23}} & m_{23} &= \frac{x_2 - x_3}{c_{23}} \\ l_{31} &= \frac{y_1 - y_3}{c_{31}} & m_{31} &= \frac{x_3 - x_1}{c_{31}} \end{aligned}$$

with $c_{ij} = \sqrt{(x_i - x_j)^2 + (y_i - y_j)^2}$ the length of an edge.

The complementary strain energy of the plate, including already the assumption $\sigma_z = 0$, is

$$\phi = \frac{1}{2} \frac{1}{E} \int_{Vol} (\sigma_x^2 + \sigma_y^2 - 2\nu \sigma_x \sigma_y + 2(1+\nu)(\tau_{xy}^2 + \tau_{xz}^2 + \tau_{yz}^2)) dv$$

After integration over the thickness with the additional assumptions of linear distributions in z for σ_x , σ_y and τ_{xy} , and parabolic distributions for τ_{xz} and τ_{yz}

$$\begin{aligned} \phi = \frac{1}{2} \frac{1}{D} \{ \int_s (M_x^2 + M_y^2 - 2\nu M_x M_y + 2(1+\nu) M_{xy}^2) dx dy \\ + 2(1+\nu) \frac{t^2}{10} \int_s (Q_x^2 + Q_y^2) dx dy \} \end{aligned}$$

where $D = \frac{Et^3}{12}$ is the flexural rigidity.

This expression is conveniently split in two parts

$$\phi_1 = \frac{1}{2D} \int_s (M_x^2 + M_y^2 - 2\nu M_x M_y + 2(1+\nu) M_{xy}^2) dx dy$$

and

$$\phi_2 = \frac{1}{2D} 2(1+\nu) \frac{t^2}{10} \int_s (Q_x^2 + Q_y^2) dx dy$$

ϕ_1 is the Kirchhoff energy which neglects the shearing deformations and produces upper bounds to local influence coefficients within the framework of this theory. Inclusion of ϕ_2 is only logical if the boundary conditions and stress transmission conditions are suitably extended, producing thereby convergence towards a more correct solution of the plate bending problem.

As only the equivalent Kirchhoff transverse shears are used in the stress transmission capability of the model, the inclusion of the second part of the energy corresponds to local violations of equilibrium conditions.

It is an imperfect equilibrium model of a more correct plate bending theory. The increased flexibility it gives will nevertheless give some idea of the importance of shearing deformations.

Substitution of expressions (I) for the moments into the complementary strain energy formula leads to

$$\phi = \frac{1}{2D} \left\{ b' F_1 b + 2(1+\nu) \frac{t^2}{10} b' F_2 b \right\}$$

where F_1 is the Kirchhoff flexibility matrix and F_2 an additional flexibility matrix due to shearing deformation.

The integrations leading to these matrices were performed in the local axes of Figure F.2.28 and the results are summarized in Figure F.2.30.

The stiffness matrix is easily obtained after numerical inversion of the flexibility matrix :

$$K_I = C (F_1)^{-1} C'$$

for the Kirchhoff stiffness,

$$K_{II} = C (F_1 + F_2)^{-1} C'$$

for the model including transverse shear effects.

Turning now to the generation of stress information it appears convenient and sufficient to compute the following 14 components

M_{x_i} , M_{y_i} , M_{xy_i} at each vertex

Q_x , Q_y constant in the plate

V_{ij} along the three edges.

These moments and transverse forces expressed in terms of stress field coefficients are written in matrix form as

$$\sigma = S b$$

with $\sigma' = (M_{x1} \ M_{y1} \ M_{xy1} \ M_{x2} \ M_{y2} \ M_{xy2} \ M_{x3} \ M_{y3} \ M_{xy3} \ V_{12} \ V_{23} \ V_{31} \ Q_x \ Q_y)$

and S given by Figure F.2.3I.

Expressed in terms of the generalized displacements :

$$\sigma_I = S F_1^{-1} C' q = T_I q$$

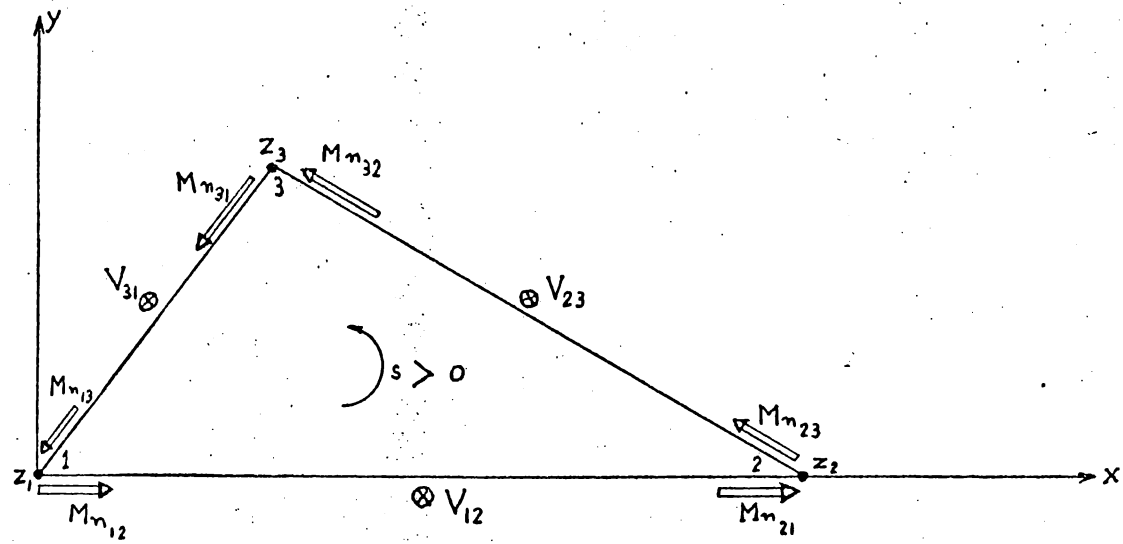
for the Kirchhoff model, and

$$\sigma_{II} = S (F_1 + F_2)^{-1} C' q = T_{II} q$$

for the model including transverse shear energy.

It is recalled that the numerical operation producing $F^{-1} C$ is already necessary to build the stiffness matrix. Therefore the stress matrix computation takes place in the program just after that step.

Figure F.2.28 : The triangular plate in bending.



Assumptions : $M_x = \alpha_1 + \alpha_2 x + \alpha_3 y$

$$M_y = \alpha_4 + \alpha_5 x + \alpha_6 y$$

$$M_{xy} = \alpha_7 + (\alpha_5 - \alpha_6)x + (\alpha_8 - \alpha_2)y$$

$$Q_x = \alpha_8 \quad Q_y = \alpha_9$$

References of Section 2.

- R.2.1. M.J. TURNER, R.W. CLOUGH, H.C. MARTIN and L.J. TOPP, "Stiffness and Deflection Analysis of Complex Structures", J.A.S. 23-9, Sept. 1956.
- R.2.2. B.M. FRAEIJIS de VEUBEKE, "Displacement and Equilibrium Models in the Finite Element Method", "Stress Analysis", ed. by O.C. Zienkiewicz and G.S. Holister, John Wiley and Sons, 1965.
- R.2.3. B.M. FRAEIJIS de VEUBEKE, "Upper and Lower Bounds in Matrix Structural Analysis", AGARDograph 72, Pergamon Press, 1964.
- R.2.4. G. SANDER, "Upper and Lower Bounds in Spar Matrix Analysis", Report SA-3, Laboratoire de Techniques Aéronautiques et Spatiales, Université de Liège, Belgium, 1965.
- R.2.5. B.M. FRAEIJIS de VEUBEKE, "A Conforming Finite Element for Plate Bending", Report SA-5, Laboratoire de Techniques Aéronautiques et Spatiales, Université de Liège, Belgium, 1966.
- R.2.6. G. SANDER, "Bornes Supérieures et Inférieures dans l'Analyse Matricielle des Plaques en Flexion-Torsion", Bull. Soc. R. Sciences de Liège, 33-7 et 8, 1964.
- R.2.7. B.M. FRAEIJIS de VEUBEKE, "Bending and Stretching of Plates - Special Models for Upper and Lower Bounds", Proc. of the Conf. on Matrix Methods in Structural Mechanics, A.F. Flight Dynamics Laboratory - Dayton, OHIO, Oct. 1965.
- R.2.8. P.K. LIVESLEY, "Matrix Methods of Structural Analysis", Pergamon Press, 1964.

$$K = \frac{E t_m}{(1-\nu^2) 2 x_{21} y_3}$$

Sym.

$\lambda_1 x_2^2 + y_3^2$					
$-\lambda_1 x_2 x_1 - y_3^2$	$\lambda_1 x_1^2 + y_3^2$				
$-\lambda_1 x_{21} x_2$	$\lambda_1 x_{21} x_1$	$\lambda_1 x_{21}^2$			
$\lambda_2 x_2 y_3$	$-\lambda_1 x_1 y_3 - \nu x_2 y_3$	$-\lambda_1 x_{21} y_3$	$x_2^2 + \lambda_1 y_3^2$		
$-\lambda_1 x_2 y_3 - \nu x_1 y_3$	$\lambda_2 x_1 y_3$	$\lambda_1 x_{21} y_3$	$-x_2 x_1 - \lambda_1 y_3^2$	$x_1^2 + \lambda_1 y_3^2$	
$\nu x_{21} y_3$	$\nu x_{21} y_3$	0	$-x_{21} x_2$	$x_{21} x_1$	x_{21}^2

$$N_o = \frac{1}{ab}$$

$-3b$	$-b$	o	o	o	o	o	o	o	o	o	o	o
o	o	o	o	o	o	o	$3(d-a)$	d	$-a$	$4a$	$-4d$	o
$3(d-a)$	d	$-a$	$4a$	$-4d$	o	$-3b$	$-b$	o	o	o	$4b$	o

$$N_x = \frac{4}{a^2b}$$

b	b	o	o	o	o	o	o	o	o	o	o	o
o	o	o	o	o	o	o	o	$-d$	o	$-a$	$(2d-a)$	o
$(a-d)$	$-d$	o	$-a$	$(2d-a)$	a	b	b	b	o	o	$-2b$	o

$$N_y = \frac{4}{a^2b^2}$$

$b(a-d)$	$-db$	o	$-ab$	$b(2d-a)$	ab	o	o	o	o	o	o	o
o	o	o	o	o	o	o	o	d^2	a^2	$2a(d-a)$	$2d(a-d)$	$-2da$
$(a-d)^2$	d^2	a^2	$2a(d-a)$	$2d(a-d)$	$-2da$	$b(a-d)$	$-db$	$-d$	o	$-ab$	$b(2d-a)$	ab

1	0	0	0	0	0	0
$-\frac{3}{a}$	$-\frac{1}{a}$	0	0	0	$\frac{4}{a}$	0
$-\frac{3}{b} \left(1 - \frac{d}{a}\right)$	$\frac{d}{ab}$	$-\frac{1}{b}$	$\frac{4}{b}$	0	$-\frac{4d}{ab}$	0
$\frac{2}{a^2}$	$\frac{2}{a^2}$	0	0	0	$-\frac{4}{a^2}$	0
$\frac{4}{ab} \left(1 - \frac{d}{a}\right)$	$-\frac{4d}{a^2b}$	0	$-\frac{4}{ab}$	0	$-\frac{4}{ab} \left(1 - 2\frac{d}{a}\right)$	$\frac{4}{ab}$
$\frac{2}{b^2} \left(1 - \frac{d}{a}\right)^2$	$\frac{2d^2}{a^2b^2}$	$\frac{2}{b^2}$	$-\frac{4}{b^2} \left(1 - \frac{d}{a}\right)$	0	$\frac{4d}{ab^2} \left(1 - \frac{d}{a}\right)$	$-\frac{4d}{ab^2}$

A =

SYM.

$\frac{1}{3h^2} + \frac{1}{I2a^2\lambda} + \mu$					
$\frac{1}{6h^2} - \frac{1}{I2a^2\lambda} - \mu$	$\frac{1}{3h^2} + \frac{1}{I2a^2\lambda} + \mu$				
$\frac{1}{4 ah}$	$\frac{1}{4 ah}$	$\frac{3}{I0a^2}$			
$-\frac{1}{4 ah}$	$-\frac{1}{4 ah}$	$-\frac{3}{I0a^2}$	$\frac{3}{I0a^2}$		
$\frac{1}{I2 h}$	$-\frac{1}{I2 h}$	$-\frac{1}{20 a}$	$\frac{1}{20 a}$	$\frac{2}{I5}$	
$-\frac{1}{I2 h}$	$\frac{1}{I2 h}$	$-\frac{1}{20 a}$	$\frac{1}{20 a}$	$-\frac{1}{30}$	$\frac{2}{I5}$

K = 4 Gtah

$\frac{2}{15h^2} + \frac{7}{36\lambda a^2} + \frac{7}{3} \mu$						
$\frac{1}{15h^2} - \frac{2}{9\lambda a^2} - \frac{8}{3} \mu$	$\frac{8}{15h^2} + \frac{4}{9\lambda a^2} + \frac{16}{3} \mu$					
$-\frac{1}{30h^2} + \frac{1}{36\lambda a^2} + \frac{1}{3} \mu$	$\frac{1}{15h^2} - \frac{2}{9\lambda a^2} - \frac{8}{3} \mu$	$\frac{2}{15h^2} + \frac{7}{36\lambda a^2} + \frac{7}{3} \mu$				
$\frac{1}{20 \text{ ah}}$	$\frac{2}{5 \text{ ah}}$	$\frac{1}{20 \text{ ah}}$	$\frac{3}{10 a^2}$			
$-\frac{1}{20 \text{ ah}}$	$-\frac{2}{5 \text{ ah}}$	$-\frac{1}{20 \text{ ah}}$	$-\frac{3}{10 a^2}$	$\frac{3}{10 a^2}$		
$\frac{7}{60 \text{ h}}$	$-\frac{1}{15 \text{ h}}$	$-\frac{1}{20 \text{ h}}$	$-\frac{1}{20 a}$	$\frac{1}{20 a}$	$\frac{2}{15}$	
$-\frac{1}{20 \text{ h}}$	$-\frac{1}{15 \text{ h}}$	$+\frac{7}{60 \text{ h}}$	$-\frac{1}{20 a}$	$\frac{1}{20 a}$	$-\frac{1}{30}$	$\frac{2}{15}$

SYM.

K = 4 Gtah

$$T = \frac{E}{1 - v^2}$$

$\frac{3}{2a}$	$-\frac{2}{a}$	$\frac{1}{2a}$	\circ	\circ	\circ	\circ	\circ
$\frac{3v}{2a}$	$-\frac{2v}{a}$	$\frac{v}{2a}$	\circ	\circ	\circ	\circ	\circ
$\frac{1-v}{h}$	\circ	\circ	\circ	\circ	\circ	$(1-v)$	\circ
$-\frac{1}{2a}$	$\frac{2}{a}$	$-\frac{3}{2a}$	\circ	\circ	\circ	\circ	\circ
$-\frac{v}{2a}$	$\frac{2v}{a}$	$-\frac{3v}{2a}$	\circ	\circ	\circ	\circ	\circ
\circ	\circ	$\frac{1-v}{h}$	\circ	\circ	\circ	\circ	$(1-v)$
\circ	$\frac{1-v}{h}$	\circ	$\frac{3(1-v)}{4a}$	$-\frac{3(1-v)}{4a}$	$-\frac{(1-v)}{4}$	$-\frac{(1-v)}{4}$	$-\frac{(1-v)}{4}$

0	$-a b^2$	0	0	$a b^2$	0	0	0	0	0	0
0	0	$-a b^2$	0	0	$a b^2$	0	0	0	0	0
0	a^3	$-2 a^2 b$	$-6 a^2$	a^3	$-2 a^2 b$	$6 a^2$	0	$-2 a^2 b$	$-2 a^2 b$	$4 a^3$

$$A_1 =$$

0	$-2 a b^2$	b^3	0	$-a b^2$	$-b^3$	0	$-a b^2$	0	$-a b^2$	$4 a b^2$
0	$-a^2 b$	0	0	0	0	0	0	$a^2 b$	0	0
0	0	$-a^2 b$	0	0	0	0	0	0	$a^2 b$	0

$$B_1 =$$

$6 b^2$	$a b^2$	b^3	$-6 b^2$	$2 a b^2$	$-b^3$	0	$-a b^2$	0	$4 a b^2$
$6 a b$	$a^2 b$	$a b^2$	$-6 a b$	$a^2 b$	$-a b^2$	0	0	0	$4 a^2 b$
$6 a^2$	a^3	$a^2 b$	$-6 a^2$	a^3	$-2 a^2 b$	0	0	$a^2 b$	$4 a^3$

$$C_1 =$$

SYM.

EAL^2	$I_2 EI_y$	$I_2 EI_z$	GJL^2	$4 EI_z L^2$	$4 EI_y L^2$	EAL^2	$I_2 EI_y L^3$	$I_2 EI_z$	GJL^2	$4 EI_z L^2$	$4 EI_y L^2$
		$6 EI_z L$									
	$- 6 EI_z L$										
$- EAL^2$											
	$- I_2 EI_y$				$6 EI_y L$						
		$- I_2 EI_z$		$- 6 EI_z L$							
			$- GJL^2$								
		$6 EI_z L$		$2 EI_z L^2$							
	$- 6 EI_y L$				$2 EI_y L^2$		$6 EI_y L$				
								$- 6 EI_z L$			
									GJL^2		
										$4 EI_z L^2$	
											$4 EI_y L^2$

$$K = \frac{1}{L^3}$$

Triangle number :				
	I or I20	II or 230	III or 340	IV or 410
σ_x	$\beta_1 + \beta_5 \cos^2 \theta_2$	$\beta_1 + \beta_4 \cos^2 \theta_1 + \beta_5 \cos^2 \theta_2$	$\beta_1 + \beta_4 \cos^2 \theta_1$	β_1
σ_y	$\beta_2 + \beta_5 \sin^2 \theta_2$	$\beta_2 + \beta_4 \sin^2 \theta_1 + \beta_5 \sin^2 \theta_2$	$\beta_2 + \beta_4 \sin^2 \theta_1$	β_2
τ_{xy}	$\beta_3 + \beta_5 \sin \theta_2 \cos \nu_2$	$\beta_3 + \beta_4 \sin \theta_1 \cos \theta_1 + \beta_5 \sin \theta_2 \cos \theta_2$	$\beta_3 + \beta_4 \sin \theta_1 \cos \theta_1$	β_3

Figure F.2.22.

Y_{21}	0	x_{12}	0	$Y_{21} \cos^2 \theta_2 + x_{12} \sin \theta_2 \cos \theta_2$
0	x_{12}	Y_{21}	0	$x_{12} \sin^2 \theta_2 + Y_{21} \sin \theta_2 \cos \theta_2$
Y_{32}	0	x_{23}	$Y_{32} \cos^2 \theta_1 + x_{23} \sin \theta_1 \cos \theta_1$	$Y_{32} \cos^2 \theta_2 + x_{23} \sin \theta_2 \cos \theta_2$
0	x_{23}	Y_{32}	$x_{23} \sin^2 \theta_1 + Y_{32} \sin \theta_1 \cos \theta_1$	$x_{23} \sin^2 \theta_2 + Y_{32} \sin \theta_2 \cos \theta_2$
Y_{43}	0	x_{34}	$Y_{43} \cos^2 \theta_1 + x_{34} \sin \theta_1 \cos \theta_1$	0
0	x_{34}	Y_{43}	$x_{34} \sin^2 \theta_1 + Y_{43} \sin \theta_1 \cos \theta_1$	0
Y_{14}	0	x_{41}	0	0
0	x_{41}	Y_{14}	0	0

C =

Ω_{1234}	<u>SYM.</u>		
$-\nu \Omega_{1234}$	Ω_{1234}		
o	o	$2(1+\nu)\Omega_{1234}$	
$\Omega_{234} (\cos^2 \theta_1 - \nu \sin^2 \theta_1)$	$\Omega_{234} (\sin^2 \theta_1 - \nu \cos^2 \theta_1)$	$\Omega_{234} 2(1+\nu) \sin \theta_1 \cos \theta_1$	Ω_{234}
$\Omega_{123} (\cos^2 \theta_2 - \nu \sin^2 \theta_2)$	$\Omega_{123} (\sin^2 \theta_2 - \nu \cos^2 \theta_2)$	$\Omega_{123} 2(1+\nu) \sin \theta_2 \cos \theta_2$	$\Omega_{230} (\cos^2(\theta_1 - \theta_2) - \nu \sin^2(\theta_1 - \theta_2))$
			Ω_{123}

$$F = \frac{1}{Et}$$

Figure F.2.25.

$\frac{h}{a} G$	<u>SYM.</u>		
o	$\frac{Eh^3}{a} \left(\frac{1}{3} + \frac{a^2}{\mu} \right)$		
$-\frac{h}{a} G$	o	$\frac{h}{a} G$	
o	$-\frac{Eh^3}{a} \left(\frac{1}{3} - \frac{a^2}{\mu} \right)$	o	$\frac{Eh^3}{a} \left(\frac{1}{3} + \frac{a^2}{\mu} \right)$

$$K = t$$

0	$\frac{3}{2} E \left(\frac{z}{3a} + \frac{zx}{\mu} \right)$	0	$\frac{3}{2} E \left(-\frac{z}{3a} + \frac{zx}{\mu} \right)$	$-3 E \frac{zx}{h\mu}$
0	0	0	0	0
$\frac{C}{2a}$	$\frac{Eh^2}{\mu} \left(1 - 3 \frac{z^2}{h^2} \right)$	$-\frac{C}{2a}$	$\frac{Eh^2}{\mu} \left(1 - 3 \frac{z^2}{h^2} \right)$	$\left\{ \frac{3}{2} E \frac{z^2}{h\mu} + \frac{Ch}{\mu} \left(\frac{a^2}{h^2} - \frac{3}{5} - \nu \right) \right\}$

I =

Figure F.2.27.

$\frac{h}{a} C$				
0	$\frac{Eh^3}{a} \left(\frac{1}{3} + \frac{a^2}{\mu} \right)$			
$-\frac{h}{a} C$	0	$\frac{h}{a} C$		
0	$-\frac{Eh^3}{a} \left(\frac{1}{3} - \frac{a^2}{\mu} \right)$	0	$\frac{Eh^3}{a} \left(\frac{1}{3} + \frac{a^2}{\mu} \right)$	
$2C$	$-\frac{2 E h^2 a}{\mu}$	$-2C$	$-\frac{2 E h^2 a}{\mu}$	$4 \frac{a}{h} C \left(\frac{a^2}{h^2} + \frac{I^2 h^2}{5 \mu} - \nu \right)$

K = t

SYM.

m_{12}^2	$2 \ 1_{12}^m$	1_{12}^2	0	0	0	0	0	0	0
m_{31}^2	$2 \ 1_{31}^m$	1_{31}^2	0	0	0	0	0	0	0
b_1	a_1	$-b_1$	0	0	0	0	0	0	0
m_{12}^2	$2 \ 1_{12}^m$	1_{12}^2	$m_{12}^2 x_2$	$-2 \ 1_{12}^m x_2$	$1_{12}^2 x_2$	0	0	0	$2 \ 1_{12}^m x_2$
m_{23}^2	$2 \ 1_{23}^m$	1_{23}^2	$m_{23}^2 x_2$	$-2 \ 1_{23}^m x_2$	$1_{23}^2 x_2$	0	0	0	$2 \ 1_{23}^m x_2$
b_2	a_2	$-b_2$	$b_2 x_2$	$-a_2 x_2$	$-b_2 x_2$	0	0	0	$a_2 x_2$
m_{31}^2	$2 \ 1_{31}^m$	1_{31}^2	$m_{31}^2 x_3$	$m_{31} (m_{31} y_3 - 2 \ 1_{31} x_3)$	$1_{31} (1_{31} x_3 - 2 \ m_{31} y_3)$	$1_{31}^2 y_3$	$2 \ 1_{31}^m y_3$	$2 \ 1_{31}^m y_3$	$2 \ 1_{31}^m x_3$
m_{23}^2	$2 \ 1_{23}^m$	1_{23}^2	$m_{23}^2 x_3$	$m_{23} (m_{23} y_3 - 2 \ 1_{23} x_3)$	$1_{23} (1_{23} x_3 - 2 \ m_{23} y_3)$	$1_{23}^2 y_3$	$2 \ 1_{23}^m y_3$	$2 \ 1_{23}^m y_3$	$2 \ 1_{23}^m x_3$
b_3	a_3	$-b_3$	$b_3 x_3$	$-a_3 x_3 + b_3 y_3$	$-a_3 y_3 - b_3 x_3$	$-b_3 y_3$	$a_3 y_3$	$a_3 y_3$	$a_3 x_3$
0	0	0	$-1_{12} m_{12}^2$	$m_{12} (2 \ 1_{12}^2 - m_{12}^2)$	$1_{12} (2 \ m_{12}^2 - 1_{12}^2)$	$-1_{12}^2 m_{12}$	$2 \ 1_{12}^3$	$2 \ 1_{12}^3$	$2 \ m_{12}^3$

SYN.

6								
0		I2 μ						
-6 ν		0	6					
2 n		0	-2 νn	m				
2 y_3		-4 μn	-2 νy_3	$\frac{1}{2} y_3 (n+x_3)$	$y_3^2 + 2 \mu m$			
-2 νn		-4 μy_3	2 n	- νm	$\frac{1+\mu}{2} y_3 (n+x_3)$	$2 \mu y_3^2 + m$		
-2 νy_3		0	2 y_3	$-\frac{\nu}{2} y_3 (n+x_3)$	$-\nu y_3^2$	$\frac{1}{2} y_3 (n+x_3)$	y_3^2	
0		4 μy_3	0	0	$-\mu y_3 (n+x_3)$	$-2 \mu y_3^2$	0	$2 \mu y_3^2$
0		4 μn	0	0	$-2 \mu m$	$-\mu y_3 (n+x_3)$	0	$\mu y_3 (n+x_3)$
								2 μm

$$F_1 = \frac{x_2 y_3}{I_2}$$

0	0	1	0	0	0	0	0	0	0	0	0	0	0	0	0	0	0	0	0
1	0	0	0	0	0	0	0	0	0	0	0	0	0	0	0	0	0	0	0
0	1	0	0	0	0	0	0	0	0	0	0	0	0	0	0	0	0	0	0
0	0	1	0	0	0	0	0	0	0	x_2	0	0	0	0	0	0	0	0	0
1	0	0	0	0	0	0	0	0	0	x_2	0	0	0	0	0	0	0	0	0
0	1	0	0	0	0	0	0	0	0	0	0	0	0	0	0	0	0	0	x_2
0	0	1	0	0	0	0	0	0	0	0	0	0	0	x_3	0	0	0	0	0
1	0	0	0	0	0	0	0	0	0	y_3	0	0	0	0	0	0	0	0	0
0	1	0	0	0	0	0	0	0	0	0	0	0	0	0	0	0	0	0	x_3
0	0	0	0	0	0	0	0	0	0	$m_{12}(2 \cdot 12^2 - m_{12}^2)$	$1_{12}(2 \cdot m_{12}^2 - 12^2)$	$-12^2 m_{12}$	$2 \cdot 12^3$	$2 \cdot m_{12}^3$	0	0	0	0	0

S =

3. NUMERICAL RESULTS.

3.I- Spar.

The spar elements were described and evaluated in references R.2.2 and R.2.4 with details. The cantilever beam model illustrated in Figure F.3.I with various cap sections was tested with the different previously described idealizations. A non dimensional cross section of the spar cap was denoted by

$$\zeta = \frac{\text{Spar caps section}}{\text{web section}} = \frac{S}{th}$$

and given the values 0, 0.2, 1, 2 and 10. The model was divided into 1, 2, 4 and 8 elements in order to check the convergence properties. The deflections are given in dimensional form (mm) and in a non dimensional form, the deflection given by the engineering beam theory including shear being taken as unity. The three loading cases are represented in Figure F.3.2. They consist in a vertical concentrated tip load, a uniformly distributed load $p(x) = p_0$ and a distributed load having the form of a Dirac measure located in the middle of the element.

Loading case I : Concentrated tip load.

The tip deflections associated with the load P are given in table I in Figure F.3.3 for the three previously described approaches as well as the engineering beam theory including shear deformation. For both displacement models the results are given for the theoretical web moment of inertia $I = I^* / (1 - \nu^2)$ and for the classical but non consistent moment of inertia $I^* = \frac{2 th^3}{3}$.

This removes the stiffening effect of the assumption $\epsilon_z = 0$ but, violating compatibility, also removes the guaranty of a lower bound.

However the results, using I^* are significantly improved.

As expected from theory, the results for both quadratic displacement and equilibrium models are independent of the number of elements into which the model is divided; they are exact solution in the sense of engineering beam theory for either $\epsilon_z = 0$ or $\epsilon_z \neq 0$ depending on the moment of inertia used.

Loading with distributed loads.

The displacement models can be subjected to any load provided the correct weighting functions are used. These functions insure that the virtual work of the applied forces on the displacements equals the work done by the generalized forces on the generalized displacements describing the behaviour of the model. The expressions of the generalized forces to be used for distributed loads have been given in section 2.

In an equilibrium model the possibilities of loading depend on the assumptions made for the stress field. It is pointed out in the theory that the assumption $\sigma_z = 0$ in the equilibrium spar model implies that the transverse loading can take place only at the tip cross sections through concentrated shear forces. This means that a distributed load is ruled out in a strict application of the principle. However a statically equivalent set of transverse forces can be used provided the results be compared in terms of bounds with those of displacement models under the same statically equivalent representation.

The behaviour of the three models under concentrated forces having been illustrated by loading case number I, the response of the displacement models for a distributed load is now examined and compared with the equilibrium model loaded by an equivalent set of transverse forces keeping in mind that the procedure removes the guaranty of upper bound.

Loading case 2 : Constant distributed load.

Integration of the weighting functions for the displacement models is straightforward for $p(x) = \text{constant}$. It leads to 4 non zero generalized forces for each element $(W_1, W_2, \phi_1, \phi_2)$. In the equilibrium model the load is split into two tip loads for each element.

Figures F.3.4, F.3.5 and F.3.6 give the longitudinal distribution of the bending moment for a subdivision into 1, 2 and 4 elements. The effect of the generalized forces ϕ_1 and ϕ_2 in the quadratic displacement model is well pointed out in the first of these diagrams. They bring moments of opposite sign to the ones produced by W_1 and W_2 , which explains the negative sign for the bending moment at the free end. It is also to be pointed out that, while the approximation for the stresses are excellent for a subdivision in 4 elements in the quadratic displacement model, the linear model gives only a rough stress representation. For the equilibrium model the discrepancies between the actual bending moment distribution and the distribution due to the equivalent loading point to an overestimation of the bending moment between two point loads, decreasing when the subdivision into elements becomes finer. This presents the appearance of an upper bound but should be interpreted as a refinement in the loading representation.

The tabulated deflections are given in table II, Figure F.3.7, while table III in Figure F.3.8, gives the deflections in the middle of the beam. They show how the quadratic model approximates the actual deflections and show also that the tip deflections for that model are again the exact ones in the sense previously understood.

Loading case 3 : Dirac measure for the distributed load.

This type of loading was selected as a severe test for the special property

of the quadratic model. The load is equal to p_0 at mid-span and zero at any other point of the beam idealized with one single element. This can be represented by the Dirac measure

$$p(x) = \delta(a) p_0$$

The generalized loads calculated for that particular load reduce to :

$$W_1 = \frac{1}{2} p_0 \quad \phi_1 = -\frac{a}{4} p_0 \quad W_2 = \frac{1}{2} p_0 \quad \phi_2 = +\frac{a}{4} p_0$$

for both displacement models.

Figure F.3.9 gives the deflections for each method using the I or I^* moment of inertia and for the engineering beam solution.

An equilibrium model cannot be used in this special case with a single element, while the use of two elements produces the engineering beam solution.

Convergence properties.

Figure F.3.10 gives for $\zeta = 0$, and loading case 2 the convergence curves of the tip deflections as function of the number of generalized coordinates.

Remark.

These results pertain to an isolated spar. They allow a clear understanding of the mechanism of spar deformation but do not give a complete picture of its behaviour in a complex box beam structure. This is the subject of the next sections dealing with box beams.

3.2- Box Beam.

In order to evaluate the convergence properties of beam like structures a simple straight cantilever box beam with rectangular, cross section was selected as illustrated in Figure F.3.II. Such a structure is still physically simple enough to allow quite a few different idealization schemes and mesh sizes, while already complex enough to exhibit the characteristics of the various methods and combinations of elements.

The stress distribution in such a structure is still accessible to physical intuition so that the interpretation of the stress output is more fruitful than in a more complex structure.

Two different web thicknesses t_s were used. The first one is the same as the cover thickness $t_c = 3$ mm. The second one is 10 mm. This will show the influence of the different web idealizations, in particular of the two assumptions $\epsilon_z = 0$ of the displacement model, $\sigma_z = 0$ of the equilibrium model.

The two loading cases are sketched in Figure F.3.II. One is a bending case, the other a torsion case, both due to tip loads on the free ends of the two webs. Boundary conditions at the other end of the box beam are those of completely built in cover sheets and webs.

The different idealizations into finite elements are illustrated in Figure F.3.I2. Their choice was directed by two considerations. The first was to allow comparisons between the three available cover models on the basis of the same pattern of elements. For that reason the first five subdivisions are identical for the 3 methods (linear or quadratic displacement field and equilibrium). Comparisons on the basis of number of generalized coordinates are also possible for there are schemes using about 30, 40, 100 and 300 generalized coordinates in each type of analysis. The second idea was to allow some comparison of the influence of the pattern on the results, holding the number of generalized coordinates about the same. This is the reason for investigating idealizations (6) to (8). Finally a few cases were computed using special assumptions, detailed further on, and even a few hybrid models were tried together with an analytical solution using lumped bars and shear panels (idealizations (10)).

Deflection results.

Tip deflections are tabulated in Figure F.3.I3 to F.3.I6 while convergence curves are drawn for the 4 basic configurations (bending and torsion with web thickness equal 10 or 3 mm). They appear in Figures F.3.I7 to F.3.20. They are plotted versus the number of generalized coordinates, which is probably the best comparison criterion between the different approaches.

The deflection results will for some comments :

- The upper and lower bound property is well illustrated by the convergence curves as expected from the theory. However it is obvious that convergence is not directed toward the same "exact" solution. This is of some importance since it shows, that if a displacement model implies a lower bound and an equilibrium model an upper bound, it does not mean that subsequent refinements of the subdivision will necessarily tend to close the gap completely between the two bounds. The difference here comes from the spar idealization which, as already mentioned, includes two different basic assumptions : $\epsilon_z = 0$ for the compatible spar, $\sigma_z = 0$ for the equilibrium spar.

Comparing the gaps for the two web thicknesses shows that, taking the average of the best two bounds as a reference, the gap in the bending case is 3.784 % for the 10 mm thick web while it is of 2.178 % for the 3 mm thick web. This indicates the rate of gap closure with reduction in web thickness. To avoid this basic difference in the convergence limits more refined spar models are necessary. It is of course possible to treat the web as an array of triangular elements of the quadratic displacement type. This could be tried in the future but would increase the number of coordinates.

- The convergence curves of the equilibrium model in torsion require some explanation. In the three simpler idealizations, the width of the cover is taken at places by a single element. As the constant σ_x stress distribution in that element has to be antisymmetrical, the only equilibrium solution for that case is with zero stress in the cover and therefore the loads are taken only by differential bending of the two spars. Seen geometrically, the cover plates, pin jointed at their mid edge points, allow a kinematical deformation mode under that loading. This explains the very poor results of these idealizations. It is of interest to compare them with the corresponding idealization using the linear displacement field where the stresses are also constant across the width of the cover. Their deflections are in fact as poor as for the equilibrium models but on the stiff side. Only the idealizations using the quadratic displacement field exhibit, even for the simplest subdivision, as good a behaviour as for the bending case.

- Comparing now the 3 approaches, it can be stated that equilibrium models converge "grosso modo" as their duals : the linear displacement models. The one uses a constant stress assumption, the other a constant strain in the cover. At closer look, in bending, the equilibrium models give slightly better results than their duals, while the reverse happens in torsion due to the previously mentioned peculiarity of the equilibrium solution. In both loading cases a decent picture of the deflections is obtained for about 100 coordinates. However torsion yields much worse results than bending.

Let us now compare in the quadratic displacement models the improvement coming from the refinement in the idealization. Even the crudest idealization, for both loading cases, is already a good approximation. In terms of number of generalized coordinates the improvement is really significant, since 34 generalized coordinates, using quadratic displacement fields, yield approximately as good results as 125 generalized coordinates using linear displacement fields. This represents, in terms of core memory in a computer, a saving of more than 90 %. The computer time of course is not cut down by the same amount but the improvement is still very valuable. Another interesting characteristic of the idealization with quadratic displacement fields is that it gives results of similar quality for both loading cases. This is not true of the other two approaches.

Finally it seems that the quality of approximation obtained by the best run, using quadratic displacement fields, is out of reach for models using linear displacement fields. Such a large number of coordinates would be required that significant inaccuracies in computation would probably appear.

- Turning to the non standard idealizations, some of them (6 to 8) purport to exhibit the sensitivity of the results to the geometry of the subdivision pattern. Therefore, results of idealization (6) have to be compared to those of idealization (3), while idealization (7) or (8) is to be compared with idealization (2).

These comparisons show that in torsion the differences are more important than in bending and affect more the models analysed with linear displacement fields. Those are, in this sense, less "safe" as they will be more sensitive to an error of judgement in the subdivision pattern for complicated structures, where areas of high stress gradient are not always known a priori.

- An attempt was made to remove the effect of the $\epsilon_z = 0$ assumption for the displacement spar models by adjusting simply Poisson's ratio to zero in the input data. This removes in principle the stiffening effect of the assumption $\epsilon_z = 0$. Unfortunately the organisation of the input data is presently such that the value of the shear modulus is generated by the formula $G = E/2(1+\nu)$ so that modifications in Poisson's ratio also affect this value and consequently the spar shearing deformations.

This explains probably the reason why the results obtained are better than the original ones for the thicker web box beams using and worse for the thinner web ones. The correct way to achieve the test would be to run the same problems with a new version of the spar programs, where the modification affects only the moment of inertia.

- To justify the use of our spar models a computation was performed with rectangular web elements analyzed with the displacement assumptions

$$u = \alpha_1 + \alpha_2 x + \alpha_3 y + \alpha_4 xy$$

$$v = \alpha_5 + \alpha_6 x + \alpha_7 y + \alpha_8 xy$$

This was performed by the program given in reference R.3.1. The idealization bears number (9) and uses 30 rectangular elements for half a spar web; the box beam being reduced by symmetry to 1/4 of the actual structure. 12 elements were used for half a cover sheet. That quarter box beam saturates the capability of the program in question and is equivalent to a 224 generalized coordinates model according to the standard of the other models.

Due to the reduction to one fourth, only bending was investigated. The results are very poor compared to those using our spar elements, although the subdivision of the web is already abnormally high. This indicates that for beam like structures our spar elements are an essential ingredient.

- Idealization number (10) refers to an analytical solution where covers and webs are represented by shear panels and bars to which the normal stress carrying capacity is transferred. Two thirds of the normal stress carrying section of each panel is concentrated in the middle of the panel, while the rest is equally divided along the edges.

(Ref. R.3.2).

That sort of lumping yields usually hybrid models as lumping is equivalent to a displacement type assumption, while the shear panel assumption is of the stress type. That analytical solution gave results slightly more flexible than the best equilibrium model.

Note about Stress representation.

Stress outputs are different for each type of element. For skin elements, stresses are constant inside an element in linear displacement and equilibrium models. The computed stress distribution in a set of these elements is therefore, strictly speaking, represented by a succession of steps.

In general, stress discontinuities occur at interfaces both in equilibrium and displacement models. In the former case this is due to the fact that a continuous stress transmission does not require continuity of the direct stress on a facet normal to the interface.

In skin elements analyzed with the quadratic displacement field, stresses are linear and given at each corner so that the computed stress distribution is composed of a set of linear parts which usually do not fit at an interface due to lack of local equilibrium.

In spar elements, two stresses only are considered, the longitudinal σ_x stress, which, being antisymmetrical across the height, is determined by its maximum in the cap, and the shear stress τ_{xy} .

In spars with a linear u displacement field, σ_x is constant along the length of the element so that cap stresses in the structure are also represented by a step wise curve. Shear stresses are constant across the height, but quadratic along the length; hence they are given in three points along the length.

In spars with a quadratic u displacement field, σ_x is linear along the length but does not usually match at an interface, while the shear stress has the same lengthwise parabolic variation as before.

In both displacement spar elements, a σ_z stress component is generated which is exactly ν times σ_x ; a by product of the $\epsilon_z = 0$ assumption.

In equilibrium spars σ_x is also linear but is continuous between spar elements due to equilibrium requirements, while the shear stress τ_{xy} is now constant along the length but parabolic across the height.

Therefore the longitudinal distribution of shear appears in stepwise form, while the amount of shear transmitted to the cover can be different in each element even in the absence of intermediate shear load application. This arises from the fact that only the average value of the shear stress is transmitted at a joint, while the parabolic distribution may have a different intensity. The shear stress output for that spar element gives the minimum and maximum values of shear stress across the height.

Faced with so many stress representations, a general policy had to be devised to allow interpretation of the output.

For those elements having a constant stress component, that stress is assumed to hold at the centroid of the element, a procedure more or less equivalent to taking the average stress at an interface (Ref. R.3.3). For elements with linear stress variations the average stresses are taken for the stress state at an interface. These procedures work well in regions of low stress gradient, but appear somewhat arbitrary elsewhere. It is then sometimes less confusing to use both interpretations as the following examples will show.

Stress distribution in the box beam.

Stress distribution in the box beam models described above are illustrated by Figures F.3.23 to F.3.65. The stresses are given for the 10 mm web models only. They are expressed in kg/mm^2 for a load P of 1000 kg on each spar. Signs conventions and idealizations are given in Figure F.3.22. A non dimensional length x/L and width y/l are used as references.

Looking first at longitudinal cap stress distribution in the spars, Figures F.3.23 to F.3.25 represent the bending case for the 5 basic idealizations in

the three approaches.

Although the flange area of the spars has been taken to be zero ($\zeta = 0$) the terminology of spar cap is used in the text to denote the line joining spar web and cover sheet.

Figures F.3.26 and F.3.27 represent the cap stresses as computed before smoothing the jumps at the interfaces.

Figure F.3.28 shows the σ_x distribution for the more refined idealization in the three methods. Linear and quadratic displacement models are practically coincident, while the equilibrium models produce lower stresses everywhere except at the built-in section where the three maximum stresses are very near to each other.

Figures F.3.29 to F.3.31 give the same cap stress distribution under torsion. It can be seen that the linear models yield stresses which increase with mesh refinement, while for bending they fall almost on the same curve for all idealizations.

In the equilibrium models the reverse happens : stresses decrease as the number of elements grows. This behaviour is easily understood by reference to the associated behaviour of the deflections. Here, the quadratic displacement models reveal their superiority by giving, for all idealizations, stresses falling close to the final curve.

Figure F.3.32 presents the best stress distribution for each approach.

- Shear stress distribution in the spars is trivial for both displacement models as it is constant and equal to $.5 \text{ kg/mm}^2$ everywhere. For the equilibrium models it is interesting to examine the variations in the transverse parabolic shear distribution along the spar length as illustrated in Figure F.3.33 for bending and in Figure F.3.34 for torsion. The average shear stress remains of course constant, while the τ_{xy} minimum curve gives the amount of shear feeding the cover.

- Turning to the cover stresses, Figures F.3.35 to F.3.37 give the longitudinal σ_x stress distribution along the spar (where $y/l = 0$) in bending. Agreement between the different idealizations is very good and also between the two displacement approaches, but the equilibrium approach does not show the peak of stress at the built-in edge that could be expected from the shear feed from the spar (Figure F.3.33). The difference is rather important as the equilibrium peak stress is only 76 % of the stress given by the displacement models.

The shear lag effect is apparent in the difference between the σ_x stresses along the spar cap line and along the mid cover line ($y/l = 1/2$). The last ones are represented in Figures F.3.38 to F.3.40.

The equilibrium solutions do not show any appreciable shear lag, in fact along the mid cover line they produce ~~again~~ the highest stresses.

The two displacement approaches show convergence to the same stress distribution, slightly below the level of the equilibrium solution. In crude idealizations the linear type produces quite scattered stress points, while the quadratic type immediately furnishes a good approximation.

- The direct stress distributions of the torsion case are represented in Figure F.3.41 to F.3.43. Assuming that the computed stresses in the linear displacement and equilibrium models are representative of the stress state at each centroid, a linear extrapolation, from the torsional axis of symmetry ($y/l = 1/2$) to the spar axis ($y/l = 0$) was made to obtain the σ_x distributions of Figures F.3.44 and F.3.45. The need for such a procedure to find the σ_x along the spar axis does not arise for the quadratic displacement model. The procedure is empirical and, for the linear displacement models, produces in fact slightly higher stresses than those exhibited by the quadratic models. Those of the equilibrium models are much lower, the discrepancies being more pronounced than for the bending case. This again illustrates the difficulty for the spars to feed the cover sheet.

- The σ_x distribution along the mid line of the cover is identically zero in torsion, by reason of symmetry.

- The τ_{xy} shearing stress distribution is given along the cover to spar connection line in Figures F.3.46 to F.3.48 for the bending case.

For equilibrium and linear displacement models the same remark concerning centroids location applies as for the σ_x distribution in torsion, for in first approximation, the transverse τ_{xy} distribution is also antisymmetrical and linear. However if the extrapolation technique can be applied with success to the linear displacement model, this is not so for equilibrium models, where τ_{xy} is fixed by the stress transmission requirement between web and cover. The τ_{xy} distribution obtained for the equilibrium approach is in fact exactly the same as the distribution obtained for the spar cap (Figure F.3.32) but scaled in the ratio of thickness t_s/t_c . This is a case where the concept of stresses effective at the element centroid yields a false interpretation of the stress distribution.

Comparison of quadratic displacement and equilibrium models with corrected linear displacement models shows a very good agreement between the three approaches. However it is observed that the correction applied to linear displacement models, if leading to a good representation for idealizations 4 and 5, does not improve significantly the stresses in idealizations 1, 2 and 3 (they are still almost equal to zero).

- Figures F.3.49 to F.3.51 yield the same stress distribution in torsion. Here the transverse shear stress distribution should be parabolic from physical considerations and therefore correction for centroid location is no longer simple. This explains probably the very different output of the different idealizations.

- Shear stresses are identically zero along $y/l = 1/2$ in bending.

- Figures F.3.52 to F.3.54 show the shear stress distribution along $y/l = 1/2$ under torsion. In contrast with the previous results, no immediate correspondence is evident between the different idealizations, nor between the different approaches.

Closer inspection however reveals that the idealizations yielding the worst scatter are those having a single element across the width of the cover. If idealizations 4 and 5 only are compared, some trends in the stresses can be observed. The fact that equilibrium models yield zero stress for idealizations 1, 2 and 3 corresponds to cases where a single element spans the width of the cover.

Displacement models, which generate stresses in any circumstances, yield, as a rule, rather confusing stresses in this case.

- Figures F.3.55 and F.3.56 represent the distribution of transverse stresses σ_y along the spar for linear and quadratic displacement models in bending. For the equilibrium model σ_y is identically zero as it should be from equilibrium considerations. In displacement models, these stresses are a measure of the lack of satisfaction of equilibrium conditions.

Figure F.3.57 to F.3.59 show the same stress distribution for bending along $y/l = 1/2$.

There, σ_y stresses exist in all models due to Poisson's ratio effect. Good agreement is observed between the finer idealizations of the three approaches.

- Looking finally at stress distributions across the chord, Figures F.3.60 to F.3.62 represent the σ_x distribution in bending at $x/L = 1/12$, close to the built in section.

Examined in conjunction with the longitudinal distributions given in Figures F.3.35 to F.3.40, they confirm what was previously said about σ_x distributions. Shear lag effect is very similar in both displacement models, while it is obvious that stress transmission follows another pattern in equilibrium models.

Figures F.3.63 to F.3.65 represent the same distribution in torsion and justify the corrections made for centroid location in linear displacement models. The distribution in equilibrium models can be seen to be entirely different and shows also why the concept of stresses located at the centroids of elements has to be used with care in such a case.

3.3- Multiwebbed swept back wing.

This section presents the capability of a dual analysis of a real complex structure, using the three types of cover elements described before. Additional comparisons are made with test results and with results generated by the displacement program described in reference R.3.1 and by the Douglas Redundant Force Method.

Description of the structure.

The multi spar 30° swept back wing model to be investigated was tested in Sweden (ref. R.3.4), then analyzed by a force method in reference R.3.5 and by a displacement method in reference R.3.3. The model is described in Figures F.3.66 and F.3.67 reproduced from reference R.3.4. It has five spars and three ribs perpendicular to the spars and is untapered throughout. All elements were made of Swedish 245-T aluminum alloy whose elastic properties are

Components	Compression tests.	Tensile tests.
	Young's modulus E_c (Kg/mm ²)	Young's modulus E_t (Kg/mm ²)
Spar and rib booms	7600	7300
Spar and rib webs	6950	6850
Cover plates	7450	7350

The top and bottom covers are made out of a single sheet and all joints glued. The central part of the wing is filled with a machined aluminum alloy block, detailed in Figure F.3.67 to provide a support consisting of 2 hard steel balls along the axis of symmetry of the wing.

Two loading cases were considered as sketched in Figure F.3.68. Support and loading are such that the semi-span can be considered as a cantilever supported 39 mm out board of the vertical plane of symmetry.

The stresses were recorded by strain gages located on the cover, spar and rib webs as indicated by Figure F.3.69. The description of the test stresses in the cover is good in the neighbourhood of the root but the tip of the wing and the spars were not provided with enough gages to obtain a detailed description of stress flow in these regions.

Numerical checks for equilibrium, included in the test report, indicate that the normal stresses in the covers are affected by errors up to - 4.2 % meaning that the resultant of the measured stresses falls short of the applied forces by 4.2 %. In spars and ribs the shear stresses are affected by much larger errors, as reported in reference R.3.5.

Idealization of the structure.

The physical structure is idealized in such a way that all the matter is concentrated in the mid planes of covers and webs and on axes defined by the intersections of these planes for the spar and rib booms. This is achieved in such a way that the moment of inertia of the wing cross sections is identical to that of the physical structure.

Figure F.3.70 shows the idealization of a cross section perpendicular to the spars. Bending stiffness of the spar and rib booms as well as of the cover plates has been neglected.

Subdivision of this idealized structure leads to the pattern of finite elements.

Using the displacement and equilibrium models, advantage has been taken of the horizontal plane of symmetry of the wing to idealize spar and rib webs by the spar elements used in the preceding sections.

The displacement program of reference R.3.1 and the Douglas redundant force method of reference R.3.6 having no such elements it becomes necessary to idealize the wing without using that symmetry property.

The Force Method output resulted from the work accomplished by the Douglas Aircraft Company under Contract AF 33(615)-2483 sponsored by the United States AF Flight Dynamics Laboratory. These results were made available by FDTR/Mr. J.R. Johnson.

Comparison between the different analyses were conducted on the assumption that the refinement of the idealization is measured by the number of generalized coordinates and not by the number of elements or modes. This gives a more uniform appreciation of the total labour involved especially when comparing the quadratic displacement approach to the others. Hence the fine grid was chosen to represent about 375 generalized coordinates rather than to correspond to a given subdivision into elements.

The number of generalized coordinates counted is that of the so called "effective" coordinates in the ASEP program.

It includes only the displacements for which a non zero diagonal stiffness coefficient is generated in building up the master stiffness matrix of the structure. This concept being peculiar to the stiffness method of resolution does not apply to the redundant force method. In the case of analyses run with a redundant force method, the number of generalized coordinates established for comparison purposes was taken to correspond to the same idealization solved by the direct stiffness method.

Comparison of the respective advantages of stiffness and force methods for the final solution is beyond the scope of the present work.

The fine grid idealization using linear displacement models is represented in Figure F.3.71 and is close to that used by TURNER in reference R.3.3. It involves 378 generalized coordinates and is given the code reference LD-378. Figure F.3.72 shows the fine grid of equilibrium models representing 350 coordinates code reference EQ-350. A local refinement near the rear spar root is indicated in Figure F.3.73. Its code reference is EQ-367 as 367 coordinates are involved. Figure F.3.74 represents the fine grid of quadratic displacement models coded QD-353, involving 353 effective coordinates. Two simplified idealizations were used to show convergence properties.

LD-189 is a linear displacement idealization using the same grid of elements as QD-353 as represented on Figure F.3.75.

EQ-185 is again the same grid for equilibrium models and appears on Figure F.3.76.

All the above idealizations take advantage of the availability of spar elements. In an effort to obtain better agreement with test results, a special case of EQ-350 was run using an idealization of the central block introducing some flexibility to the support.

This special case is coded EQWB-383. The idealization is represented in Figure F.3.77 and will be discussed later.

Figure F.3.78 shows the idealization associated with the displacement program of reference R.3.1 and using only rectangular panels and bars. It required 180 generalized displacements and is coded LD-RECT-180. Finally Figures F.3.79 and F.3.80 show the two subdivisions used with the redundant force method and respectively coded RFM-304 and RFM-569.

As mentioned before, the number of generalized coordinates implied by the code numbers are those that would be required by a direct stiffness resolution.

Deflection results.

The test report does not contain tabulated deflections but only deflection curves of front and rear spars. They are reproduced in Figures F.3.81 and F.3.82 for both loading conditions. The accuracy of the information is not better than approximately 1.5 % of the tip deflection.

The problems of presenting and comparing analytically and experimentally determined displacements or influence coefficients have been considered in numerous past studies (e.g. references R.3.6 - R.3.7).

For comparison purposes two presentations of the test and theoretical results are provided. One is tabular. Figures F.3.83 through F.3.85 present a listing of the deflections at the spar-rib intersection points under both loading conditions. They are given in thousands of mm for 1 Kg load on the tip rib.

For loading condition nbr 2 the deflection is numerically equal to the influence coefficient at the tip end of the rear spar. The second type of presentation is a graphical comparison of a limited number of results taken from tables F.3.83 through F.3.85. These graphs, which take the form of carpet plots of the deflected shape, appear as Figures F.3.86 through F.3.101. Presentation of all derived results would be unwieldy and confusing. For this reason only a limited number are shown. They generally consist of the test data, against one or two computed data.

A global study of these results discloses first the remarkable consistency in the numerical data generated by the various theoretical analyses. Secondly, there appear in some cases relatively important discrepancies with the test data. It seems therefore indicated to compare first the numerical results of the theoretical approaches before aiming at discovering the reasons for discordance with experiments.

Figures F.3.102 and F.3.103 represent large scale graphs of the deflections computed for the tip rib (rib 1) under both loading cases.

As expected from theory the gap between equilibrium solutions and conforming solutions closes more and more as the subdivision is refined. The gap between the best approximations is about 1.5 % of the tip deflections and can be considered as a fairly good enclosure for any practical purpose. The convergence rate of the equilibrium and linear displacement models is about the same when doubling the number of coordinates. The quadratic displacement models give again better results than the linear ones for the same number of generalized coordinates. This was already observed in the box beam case. In fact their results could hardly be matched by linear displacement models even when doubling the number of coordinates. The bars and shear panels idealization of the RFM seems to behave roughly as the equilibrium models, keeping in mind that no spar element is available in that program. In Figures F.3.104 through F.3.107 similar deflection curves are given for ribs 2 and 3. The gap between dual solutions is still of about the same relative importance. However these displacements should not be considered as true brackets for the exact displacements. In fact, if an appeal is made to theory, upper and lower bounds are only provided to direct influence coefficients and not to all the displacement components under any loading. If the direct and cross influence coefficients are respectively noted c_{ii} and c_{ij} ($i \neq j$) and if \bar{c} is an influence coefficient approximated by an equilibrium solution while \underline{c} is the approximation obtained by a conforming solution, then the theory given in reference R.2.3 states that the exact influence coefficients c satisfy the inequalities

$$\bar{c}_{ii} \geq c_{ii} \geq \underline{c}_{ii} \quad (I)$$

and

$$c_{ij} \leq \bar{c}_{ij} + \sqrt{(\bar{c}_{ii} - c_{ii})(\bar{c}_{jj} - c_{jj})} \quad (2)$$

$$c_{ij} \geq \bar{c}_{ij} - \sqrt{(\bar{c}_{ii} - c_{ii})(\bar{c}_{jj} - c_{jj})} \quad (3)$$

$$c_{ij} \leq c_{ij} + \sqrt{(\bar{c}_{ii} - c_{ii})(\bar{c}_{jj} - c_{jj})} \quad (4)$$

$$c_{ij} \geq c_{ij} - \sqrt{(\bar{c}_{ii} - c_{ii})(\bar{c}_{jj} - c_{jj})} \quad (5)$$

Usually $\bar{c}_{ij} > c_{ij}$, which gives an appearance of upper and lower bounds to the cross coefficients.

Coming back to the rib deflection study and affecting the subscript r and f respectively to tip loads or deflections of rear and front spars, it follows that only w_r is bounded for loading case 2. The direct and cross influence coefficients relative to these displacements in the dual analyses LD-I89 and EQ-I85 have been computed as respectively

$$\begin{array}{ll} \underline{c}_{rr} = 12.239774 & \bar{c}_{rr} = 12.837950 \\ \underline{c}_{ff} = 12.896564 & \text{and} \quad \bar{c}_{ff} = 13.541310 \\ \underline{c}_{rf} = 9.848910 & \bar{c}_{rf} = 10.419377 \end{array}$$

Applying inequalities (2) to (5) leads to

$$c_{rf} \leq 11.040401 \quad \text{and} \quad c_{rf} \leq 10.469934$$

$$c_{rf} \geq 9.798352 \quad \text{and} \quad c_{rf} \geq 9.227885$$

Hence the bracket for c_{rf} is

$$9.798352 \leq c_{rf} \leq 10.469934$$

instead of

$$9.848910 \leq c_{rf} \leq 10.419377$$

if the computed cross influence coefficients could be taken as true bounds. The modification in this case is only a .5 % widening of the bracket. However as the enlarging term in (2) to (5) depends on the gap between dual values of two direct influence coefficients, this effect could be more important for two more distant points in the structure. Unfortunately, at the time the results were generated, the output necessary for checks of that nature on other than tip displacements were not printed out. It is thought however that such a correction is not usually required except from a strict academic point of view, since other sources of errors arise in practical structures which are much more important.

Comparison of computed deflections with experimental results is restricted because only front and rear spar deflections are available from the test report. This excludes comparison of rib deformations.

The tip deflections of front and rear spars, recorded in the tests, are not in good agreement in the first loading case; the slope of the end rib is misrepresented. On the contrary the agreement is remarkably good in the second loading case, the test results lying exactly between the theoretical upper and lower bounds for both spars. However, from Figures F.3.83 to F.3.101 it is apparent that the overall correspondance between spar deflections is not so good, the largest discrepancies occuring in the second loading case at the level of the second rib.

As revealed by previous studies (see for instance reference R.3.6) the infinite stiffness assumed for the central supporting block can explain to a large extent the observed differences and some form of idealization of the elastic behaviour of the block was proposed as a cure. Figure F.3.77 shows the idealization as a spar-bar and plate arrangement preserving the moments of inertia of the block. The equivalent wing is now built in in the vertical plane of symmetry instead of in the end plane of the block. The deflections resulting from this modification are presented in Figures F.3.98 and F.3.99. Although improved, the agreement is not yet satisfactory and further refinement would be necessary to represent correct support conditions. Unfortunately the test report does not provide enough information to devise such refinement with hopes of success.

In any case, even if the correct boundary conditions could not be simulated, the convergence and upper-lower bound characteristics of the dual types of analysis were conclusively proven.

Stress results.

A clean presentation of all the stresses computed by different finite element methods is difficult, as discontinuities are present and different idealizations have been considered for the same structure. To avoid confusion, only part of the stress output is presented; enough to understand the trends in

the distributions generated by the different models and idealizations and to qualify the agreement with experimental evidence.

The stresses are given for the loading case number 2, selected as the more severe because it involves more torsion.

Figures F.3.I08 through F.3.II6 show part of the cover between the first outboard rib and the root. The various subdivisions into finite elements are drawn as used in the different idealizations. The stress state reduces practically to a spanwise tensile stress σ_x in all the region under study. The σ_x components are given in each skin element as computed, that is constant inside each element for LD and EQ idealizations or linearly varying for QD idealizations. Also given are the axial stresses in the spanwise oriented spar caps. These stresses are constant in an element in LD idealizations, linear in all others. For those models used in the RFM, the cap stresses are the only longitudinal stress components to be computed. Figure F.3.I08 presents the experimental stresses at the points where measured. They are all tensile and given in kg/mm^2 for an applied load of 1000 kg at the rear spar tip.

Another presentation of the same σ_x stresses is provided by Figures F.3.II7 and F.3.II8 illustrating for the three best idealizations the spanwise variation of σ_x along the intersection of front and rear spars with the cover. In Figure F.3.II7 the stresses computed in the skin elements are plotted, while Figure F.3.II8 presents the stresses computed in the spar cap elements. The test stresses are obviously the same in the two graphs as the physical points are identical.

Remembering that the test report indicates that the experimental stresses are liable to be in error up to 4 %, the computed stresses are in fairly good agreement provided one limits the comparison to the four fine grid idealizations. Each of them however has its own peculiarity. The displacement idealizations LD-378 and QD-353 yield approximately the same skin and cap stresses, while the equilibrium idealization EQ-367, due to its special connection properties, does not furnish the peak stress occurring at the rear spar root in the skin but in the spar cap. In fact the skin stress at that point is about 18 % below the test stress, while the cap stress at the same point differs also by about 22 % from the test stress but on the high side. The same phenomenon appears at the front spar root in reverse as the skin stress is now too high, while the cap stress is too low. This behaviour should be compared with that of the box beam cover of the preceding section as discussed in the paragraph dealing with shear lag effects.

Turning to the RFM-569 fine grid idealization, the stresses in the lumped bars are slightly underestimated (about 10 %) everywhere.

The coarse grid idealizations reveal that the displacement idealization

LD-I89 does not show the peak stress at the rear spar root, although the computed stresses, if plotted as valid at the centroid of the elements, appear to lie on the average curve of Figure F.3.II7.

In the EQ-I85 idealization, the discrepancy between the skin and cap stresses is larger than for the finer grid but the stress concentration at the rear spar root is still evident.

This is not the case in the dual displacement model LD-I89.

The coarse grid of RFM-304 yields approximately the same results as the finer grid but the refinement brought in the idealization does not affect the part of the wing considered here.

Finally, the LD-RECT-I80 idealization shows plainly that such models are not competitive with the preceding ones except when only a rough idea of the stresses is required.

In order to clarify the stress interpretation in linear and quadratic displacement models, three dimensional graphs of the maximum principal stress were drawn for both LD-378 and QD-353 idealizations, based on the computed stresses. For the linear displacement models, the surface representing the stress field in such graphs is composed of a set of constant stress triangular facets, as shown on Figure F.3.II9. For the quadratic displacement models, the stress surface is composed of a set of triangular plane facets, oblique with respect to the axes, and which do not fit exactly at the interfaces, as shown by Figure F.3.I20. From these two "computed" stress surfaces, "interpreted" stress surfaces are to be obtained. Obviously the freedom left to the "interpreter" is less significant in the case of the quadratic displacement models and therefore the stress picture is less subject to errors of interpretation and more rapidly derived from the stress output. Under the common assumptions that the stresses are effective at the centroid of the elements in linear displacement models, while average stresses are taken at nodal points in quadratic displacement models, "interpreted" surfaces are deducted from the previous ones and appear in Figures F.3.I21 and F.3.I22 for both idealization. It can be seen that the smoothed final stress surface is in better agreement with the test stresses in the case of quadratic displacement models.

The next distribution to be examined is that of the shear transmitted between the different spars and ribs. The test results, summarized in Figure F.3.I23, are rather scarce; only a few strain gages were glued to the spars and ribs. The test report claims an accuracy of about 15 %. An equilibrium check at the intersection of the spars with the tip rib gives a resultant of the measured shear stresses in the two webs representing only 69 % of the applied load. This reveals another source of discrepancy between computed and experimental data. In the computation, all shear stresses are supposed to be carried by

the spar and rib webs, while the equilibrium check indicates that, at least near the point of load application, more than 30 % of the shear load is transmitted by the cover and the spar caps.

As regards computed shear force distributions of Figures F.3.I24 and F.3.I25 present the results obtained by the two fine grid analyses using displacement models, respectively LD-378 and QD-353. With these models the shear stresses are constant over the height of the webs. Figures F.3.I26 records the results of the equilibrium fine grid idealization EQ-367 where the vertical distribution of shear is parabolic; minimum and maximum values of the shear stress are given for each element.

The next Figure F.3.I27 presents the average shear stresses derived from the preceding distribution. The last fine grid idealization, RFM-569 yields the values collected in Figure F.3.I28.

Comparison of all the results reveals a very good agreement between the different analyses. The maximum shear stress occurring at the rear spar root presents a variation of only 4.5 % between the 4 approaches. The results, if compared with the test values, fall within the limit of accuracy quoted in the test report.

A point of some interest is perhaps that the rather scattered experimental stresses recorded in the rear spar section, between the root and the first outboard rib, are better explained if compared with the results of the equilibrium approach. Figure F.3.I26 indicates that the parabolic shape of the vertical shear distribution is rather pronounced and that the maximum values computed at mid height of the web correspond better with the experimental stresses recorded at the same point.

Shear distributions obtained from coarse grid idealizations appear in Figures F.3.I29 through F.3.I33. In contrast to the case of direct stresses, they are very close to those obtained from the more refined idealizations. Even the LD-RECT-180 idealization yields a decent picture of the shear distribution. This indicates that the constant shear assumption for the webs, implicit in all these idealizations, is close enough to the actual stress state for these components.

3.4- Plates in bending.

The present evaluation of plate bending elements is chiefly concerned with convergence properties of the displacements. In order to appreciate the relative merits of the two models described in section 2, they are compared with seven other plate bending elements previously studied by R. CLOUGH in reference R.3.8 : three of rectangular and four of triangular shape. They will be referred to under the same code names as in Clough's paper. The basic assumptions underlying these models are as follows :

Rectangular elements.

I.- (ACM) is the code for the rectangular element developed by ADINI, CLOUGH and MELOSH in references R.3.9 and R.3.10.

Its starting assumption is that the displacement field is defined by

$$w = \alpha_1 + \alpha_2 x + \alpha_3 y + \alpha_4 x^2 + \alpha_5 xy + \alpha_6 y^2 + \alpha_7 x^3 \\ + \alpha_8 x^2y + \alpha_9 xy^2 + \alpha_{10} y^3 + \alpha_{11} x^3y + \alpha_{12} xy^3$$

This element, as all the elements studied in Clough's paper, is connected only at the vertices by continuity of slopes and deflection. Therefore continuity of the normal slopes along the boundary is not secured.

2.- (M) refers to an earlier element proposed by MELOSH in reference R.3.II and developed on the basis of physical analogies with beam bending. In bending the plate distorts along the edges with shapes defined by beam displacement functions. These displacement modes vanish linearly towards the opposite edge. In addition a uniform twist mode is provided. Again, the manner in which the element can be connected is such that perfect conformity at the interfaces cannot be secured.

3.- (P) refers to a perfectly compatible model presented by PAPPENFUSS in reference R.3.I2. A set of displacement functions with built-in compatibility are obtained by considering separately the nodal displacements at each corner.

Unfortunately this procedure drops the uniform twist term (xy term) and therefore the element cannot even represent a general uniform state of curvature with resulting loss of convergence.

Triangular elements.

I.- (A) is the symbol used for the element proposed by ADINI in reference R.3.I3. It is based on the following polynomial approximation to the deflection :

$$w = \alpha_1 + \alpha_2 x + \alpha_3 y + \alpha_4 x^2 + \alpha_5 y^2 + \alpha_6 x^3 + \alpha_7 x^2y + \alpha_8 xy^2 + \alpha_9 y^3$$

in which again the constant twist term (xy) is absent.

- 2.- (T) stands for an attempt by TOCHER to improve the preceding element by reintroducing the constant twist term. In order to find the required number of generalized displacements he then adds two third degree terms so that

$$w = \alpha_1 + \alpha_2 x + \alpha_3 y + \alpha_4 x^2 + \alpha_5 xy + \alpha_6 y^2 + \alpha_7 x^3 \\ + \alpha_8 (x^2y + xy^2) + \alpha_9 y^3$$

is the assumed polynomial representation of the deflection.
(reference R.3.I4).

- 3.- (T-IO) is Tocher's second element, obtained by starting with the complete IO terms cubic function for the deflection. These IO terms are then reduced to 9 by a Ritz method (reference R.3.I5). This procedure claims to produce a stiffness matrix invariant with respect to the orientation of the x - y axes. It appears that the element flexibility is greatly increased by the process.

In addition to other weaknesses each of those three elements suffers from lack of conformity due to possible discontinuities in normal slope transmission.

- 4.- (HCT) stands for the high compatibility triangle presented by CLOUGH in the afore mentioned paper. It is obtained by subdivision of the physical triangle into three subtriangles where, in suitable local axes, a cubic function of the deflections can be so chosen that the normal slope becomes linear along the edges of the physical triangle. Therefore the normal slopes are conforming to those of the adjacent elements by simple continuity at the vertices. The assemblage of the three subtriangles is performed in a perfectly compatible way by identification of the normal slopes at mid distance along their interfaces.

The final stiffness matrix is condensed to retain the advantage of being a 9×9 .

Moreover, conformity is secured by identification of deflections and slopes at the nodal points only which, from a programming point of view, is a valuable simplification.

It is unfortunate that, by lack of available numerical results for direct comparison, it was not possible to include the conforming and non

conforming triangular plate elements developed by BAZELEY, CHEUNG, IRONS and ZIENKIEWICZ in reference R.3.I6.

By virtue of the symmetry provided by the ingenious use of areal coordinates they were able to manipulate the complete cubic deflection field in a more scientific manner.

Investigation program.

From the comprehensive testing program presented in Clough's paper, which covers no less than 10 different plate configurations, four cases were retained for the present evaluation. They consist in a comparison of the center deflection of a square and a rectangular plate with either simply supported or clamped edges under a concentrated load applied at the center. The aspect ratio of the rectangular plate is 2. In those four cases the convergence of the center deflection (which is numerically equal to the direct influence coefficient of the applied load) is evaluated by four increasingly fine mesh sizes.

The conforming quadrilateral element presented in section 2 is referred to as (CQ); the equilibrium triangle is called (EQT).

Figure F.3.I34 summarizes the plate geometry and schedule of cases. The analysis can be reduced to that of a quarter plate by virtue of the double symmetry. Typical finite element patterns are shown in Figure F.3.I35; the dashed lines refer to idealizations using triangular elements. The mesh number N is related to the number of rectangles along a quarter edge; the rectangles are eventually composed of two triangles.

The center deflections are presented in two different forms.

The first one is tabular. In Figures F.3.I36 through F.3.I39 the non dimensional deflection coefficient β , defined by

$$w_c = \beta \frac{P a^2}{D}$$

is recorded; w_c is the deflection at the center, P is the applied load, a is the length of one quarter of the physical plate and D is the flexural rigidity.

Also given are the exact deflections according to Timoshenko's theory. However, as the numerical values given in reference R.3.I7 are only two digits accurate, they were recomputed to raise their accuracy to the level required for comparison. The tables also present the scaled non dimensional deflection coefficient μ , defined as

$$\mu = \frac{\beta_{\text{computed}}}{\beta_{\text{exact}}}$$

This coefficient is a direct figure of merit for the computed deflection. Finally the tables contain the number of generalized coordinates used in the various idealizations.

It should be stressed that the tabulated results for the elements analysed in Clough's paper have only 2 or 3 digits accuracy; they were simply measured on the graphs included in that paper.

Another presentation of the same data is furnished by Figures F.3.I40 through F.3.I47 where μ is plotted versus the number of generalized coordinates for the 9 elements. Two figures are used for each case, one with a deflection scale allowing representation of all the results and a larger scale one restricted to the best results.

The graphs are similar to those of Clough except that convergence is measured by μ instead of β and versus the number of generalized coordinates rather than versus nodal points number. This is a uniform rule adopted in this report.

Comparison of the results.

CLOUGH reported that only 3 elements, out of the seven he investigated, behaved accurately enough to be retained. The two rectangles (M) and (AC1) give rather good results and exhibit convergence towards the exact solution in all cases. However, by lack of conformity or equilibrium, they cannot predict to either overestimate or underestimate the plate deflection. Indeed their convergence is sometimes oscillatory. The (HCT) triangle has the advantage of the monotonic convergence characteristic of conforming elements and shows rather good accuracy for fine mesh sizes.

As regards our own two elements, their upper and lower bound behaviour appears very effective and convergence is especially good for the (CQ) element. The gap is reduced to about 1 % for the simply supported cases and 2.5 % for the clamped case. The (EQT) triangle is the only upper bound element available at the present time. Its convergence is similar to that of the (HCT) element but involves a rather large number of generalized coordinates as is usually the case with equilibrium models treated by the direct stiffness method.

The approximation obtained by the compatible (CQ) element is most of the time the best and is equivalent in terms of general accuracy to the (M) rectangle but enjoys two advantages. One is the guaranteed monotonic convergence, the other is its geometrical flexibility as it can assume any quadrilateral shape.

In the (EQT) triangle the orientation of the diagonal dividing the rectangles has an effect on the computed deflections. For the smallest mesh size ($N = 1$) the computation was performed using in turn each diagonal as inter-

face between the two elements. The results appear in Figure F.3.I48. The effect is to increase the deflections when the diagonal is not directed toward the load. This is understandable as the joints allow slipping in displacement transmission in equilibrium models. Obviously the behaviour of a rectangular subunit could be made insensitive to its subdivision pattern if divided into four triangles by the two diagonals. However it was decided to use Clough's pattern to reinforce validity of the comparison ^{with} his results and to keep the number of generalized coordinates to a minimum.

The final investigation concerns the effect of shear deformation. The (EQT) triangle allows, as stated in the theory, to take into account the effect of shearing deformation by including the shear energy ϕ_2 in the complementary strain energy computation. The model is no longer a strict equilibrium model but should yield a first approximation to the effect of shearing deformation on deflections. The computation was performed by a special version of the (EQT) program using the $N = 2$ mesh size in case number I. Nine different thicknesses are defined by their ratio η with the length of the plate

$$\eta = \frac{t}{2a}$$

The deflection coefficients β^* , computed taking into account the shearing deformation, are compared to those using the standard Kirchhoff theory, β . The ratio of the two coefficients is

$$\rho = \frac{\beta^*}{\beta}$$

The results are collected in Figure F.3.I49.

As could be expected the relative influence of shearing deformation on deflections is only significant for very thick plates.

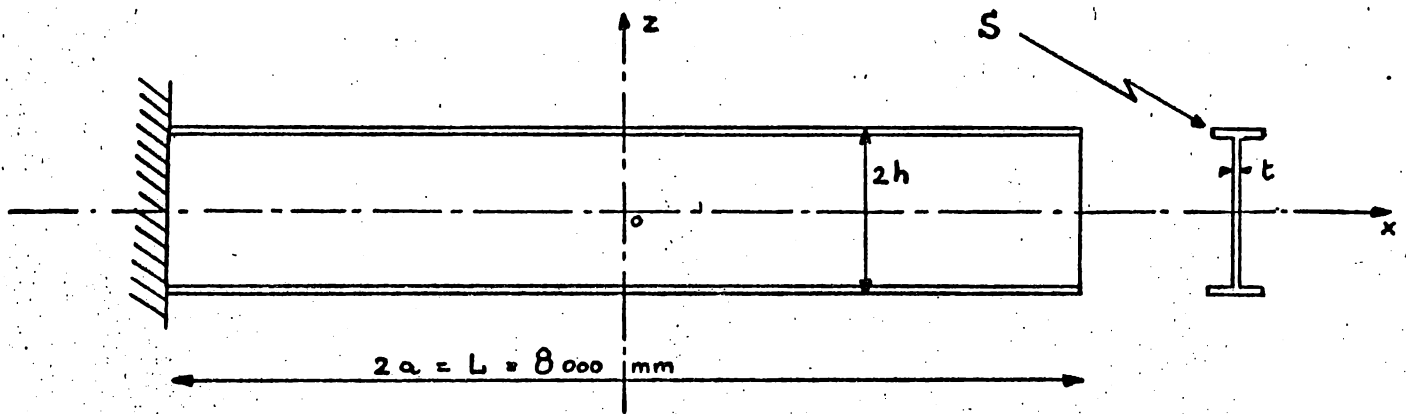
In conclusion it appears from the comparisons that quite accurate computations are possible with plate bending elements and that the enclosure of the deflections by upper and lower bounds is efficient. In the future the (CQ) and (EQT) elements should be evaluated for more complex structures including output and interpretation of the moments distributions.

An important feature of the (CQ) element is the conformity of its deflection field along one edge with the deflection field of our spar displacement elements. Both are complete cubics. This opens the way to analyses where cover sheets are stressed both as a membrane and as a plate. In particular the influence of wing skin bending rigidity, which tends to become significant for thin wings, can now be investigated with an array of finite elements.

References of Section 3.

- R.3.1. J.S. PRZEMIENIECKI and L. BERKE, "Digital Computer Program for the Analysis of Aerospace Structures by Matrix Displacement Method", Technical documentary N° FDL TDR 64-18.
AF. Flight Dynamics Laboratory, WPAFB, OHIO.
- R.3.2. H. EBNER and KOELLER, "Zur Berechnung der Kraft-verlaufes in versteiften Zylinderschalen", Luftfahrtforschung, XIV-12, Dec. 1937.
- R.3.3. M.J. TURNER, H.C. MARTIN and R.C. WEIKEL, "Further Development and Applications of the Stiffness Method", AGARDograph 72 - Pergamon Press, 1964.
- R.3.4. S. EGGWERTZ and B. NORTON, "Stress and Deflection Measurements on a Multicell Cantilever Box Beam with 30° Sweep", The Aeronautical Research Institute of Sweden - FFA - Report 53, 1954, Stockholm.
- R.3.5. S. EGGWERTZ, "Calculation of Stresses in a Swept Multicell Cantilever Box Beam with Ribs Perpendicular to the Spars and Comparison with Test Results", The Aeronautical Research Institute of Sweden - FFA - Report 54, 1954, Stockholm.
- R.3.6. R.H. GALLAGHER, "A Correlation Study of Methods of Matrix Structural Analysis", AGARDograph 69 - Pergamon Press, 1964.
- R.3.7. R.H. GALLAGHER and J. RATTINGER, "The Experimental and Theoretical Determination of the Elastic Characteristics of Modern Air Frames", Paper presented at the AGARD Structures and Material Panel, Aachen, Germany - Sept. 1959.
- R.3.8. R.W. CLOUGH and J.L. TOCHER, "Finite Element Stiffness Matrices for Analysis of Plate Bending", Proc. of the Conf. on Matrix Methods in Structural Mechanics. AF. Flight Dynamics Laboratory, Dayton, OHIO - Oct. 1965.
- R.3.9. A. ADINI and R.W. CLOUGH, "Analysis of Plate Bending by the Finite Element Method", Rpt. submitted to the Nat. Sci. Foundation, Grant G7337 - 1960.
- R.3.10. R.J. MELOSH, "Basis for Derivation of Matrices for the Direct Stiffness Method", J. AIAA, 1, 1631 - 1963.

- R.3.II R.J. MELOSH, "A Stiffness Matrix for the Analysis of thin Plates in Bending", J.A.S. 28, 34 - 1961.
- R.3.I2. S.W. PAPPENFUSS, "Lateral Plate Deflection by Stiffness Matrix Methods with Application to a Marquee", M.S. Thesis - Dpt. of Civil Engineering, Univ. Washington, Seattle - Dec. 1959.
- R.3.I3. A. ADINI, "Analysis of Shell Structures by the Finite Element Method", Ph. D. Thesis - Dpt. of Civil Eng., Univ. of California, Berkeley - 1961.
- R.3.I4. J.L. TOCHER, "Analysis of Plate Bending using Triangular Elements", Ph. D. Dissertation - Univ. of California, Berkeley - 1962.
- R.3.I5. T.H.H. PIAN, "Derivation of Element Stiffness Matrices", J. AIAA, 2-3, March 1962.
- R.3.I6. G.P. BAZELEY, Y.K. CHEUNG, B.M. IRONS and O.C. ZIENKIEWICZ, "Triangular Elements in Plate Bending - Conforming and Non-conforming Solutions", Proc. Conf. Matrix Methods in Structural Mechanics, Dayton, OHIO - 1965.
- R.3.I7. TIMOSHENKO, "Theory of Plates and Shells", Mc. Graw Hill, 1940.



$$2h = 500 \text{ mm}$$

$$t = 2 \text{ mm}$$

$$L/h = 16$$

$$E = 22,000 \text{ Kg/mm}^2$$

$$\nu = .3$$

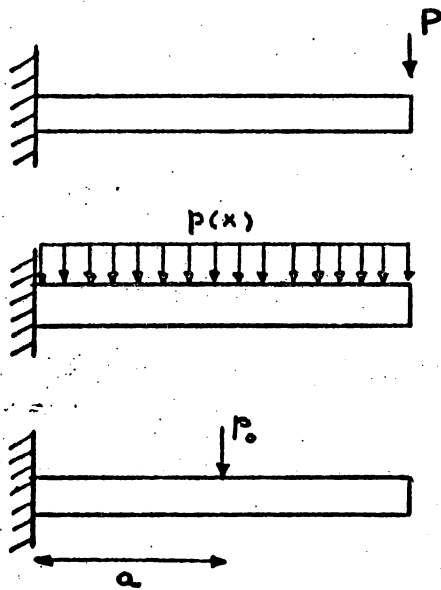
$$\text{Section of the web} = 2th = 10^2 \text{ mm}^2.$$

$$\text{Section of the flanges} = 2S = 0. ; 2 \cdot 10^2 ; 10^3 ; 2 \cdot 10^3 ; 10^4 \text{ mm}^2.$$

$$\zeta = \frac{S}{th} = 0. ; .2 ; 1.0 ; 2.0 ; 10.0$$

Figure F.3.1 The cantilever beam model.

LOADING CASES



1 $P = 10^2 \text{ Kg.}$

2 $p(x) = 2 \cdot 10^{-2} \text{ Kg/mm.}$

3 $p_0 \text{ (at } x = a) = 10^2 \text{ Kg.}$

Figure F.3.2 The 3 loading cases.

TABLE I Tip deflections for load nbr. 1



A.- DEFLECTIONS IN MM. (d)

TYPE OF ANALYSIS	Nbr. of elements	Σ = 0.		Σ = .2		Σ = 1.0		Σ = 2.0		Σ = 10.0	
		I	I*	I	I*	I	I*	I	I*	I	I*
Linear compatible	1	25.510	28.032	16.572	17.559	6.9080	7.0669	4.0286	4.0810	.99256	.9954
	2	31.862	35.013	20.643	21.873	8.6113	8.8090	5.0121	5.0773	1.2170	1.2205
	4	33.453	36.761	21.671	22.962	9.0373	9.2450	5.2580	5.3264	1.2724	1.2761
	8	33.852	37.199	21.934	23.241	9.1440	9.354	5.3197	5.3889	1.2872	1.2909
Quadr. compatible	1 to 8	33.979	37.339	22.012	23.323	9.1790	9.3901	5.3399	5.4842	1.2919	1.2956
Theory of beams	—	33.979	37.331	22.012	23.367	9.1789	9.4035	5.3398	5.4139	1.2918	1.29565
Equilibrium	1 to 8	—	37.239	—	23.374	—	9.4041	—	5.4141	—	1.2957

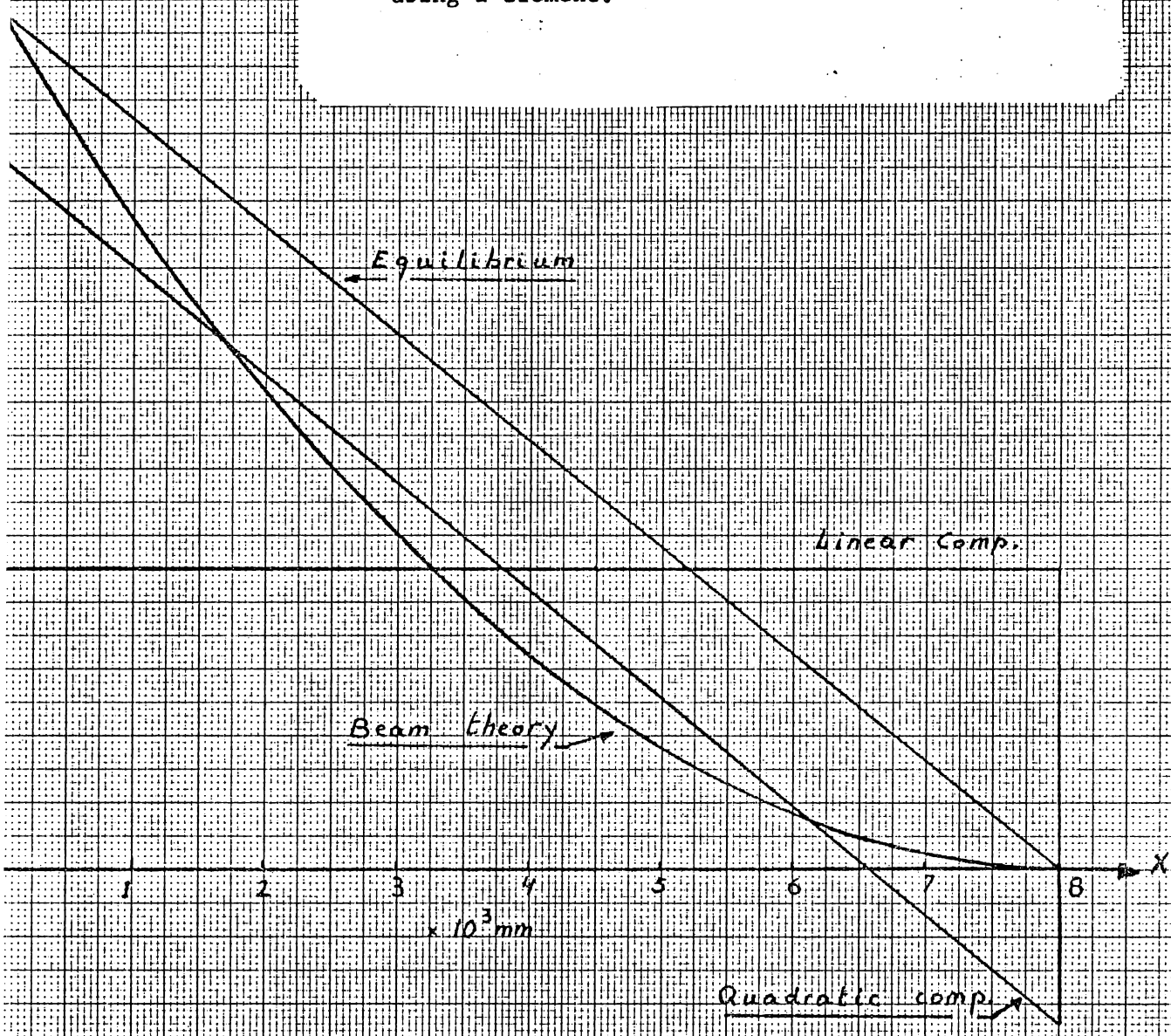
$$d^* = \frac{d}{[PL^3/3EI^* + PL/GA]}$$

B.- NON DIMENSIONAL DEFLECTIONS

TYPE OF ANALYSIS	Nbr. of elements	Σ = 0.		Σ = .2		Σ = 1.0		Σ = 2.0		Σ = 10.0	
		I	I*	I	I*	I	I*	I	I*	I	I*
Linear compatible	1	.6833	.7509	.7092	.7514	.7346	.7515	.7441	.7538	.7661	.7683
	2	.8535	.9379	.8834	.9360	.9157	.9367	.9258	.9378	.9393	.9420
	4	.8961	.9847	.9274	.9827	.9611	.9831	.9712	.9838	.9820	.9849
	8	.9068	.9964	.9387	.9946	.9724	.9947	.9826	.9954	.9935	.9963

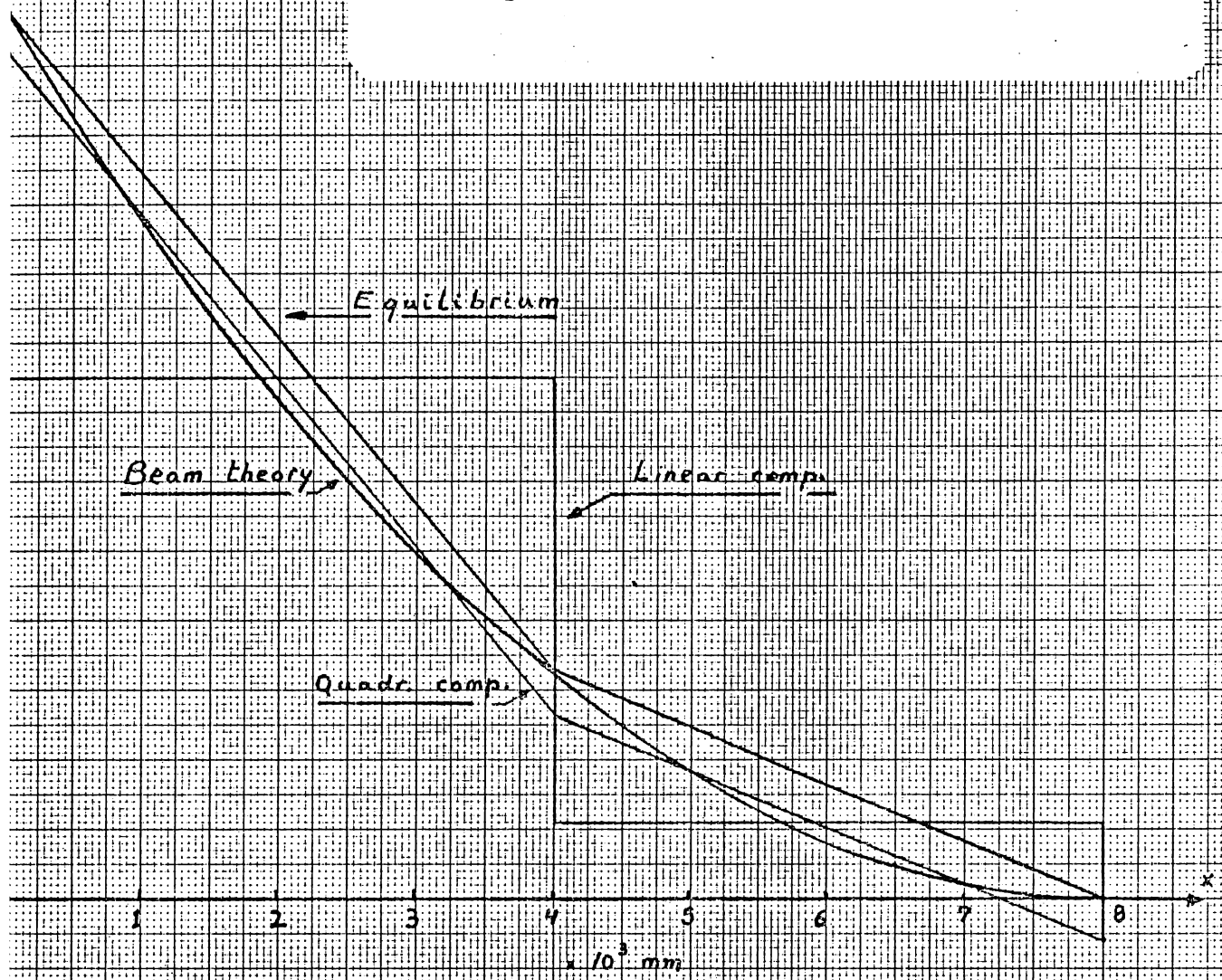
M_x
 $\times 10^4 \text{ Kg} \cdot \text{mm}$

Figure F.3.4
Bending moment distribution for load nbr. 2
using I element.



M_x
 $\times 10^4 \text{ Kg}\cdot\text{mm}$

Figure F.3.5
Bending moment distribution for load nbr. 2
using 2 elements.



$4 \text{ Kg} \cdot \text{mm}$

Figure F.3.6

Bending moment distribution for load nbr. 2
using 4 elements.

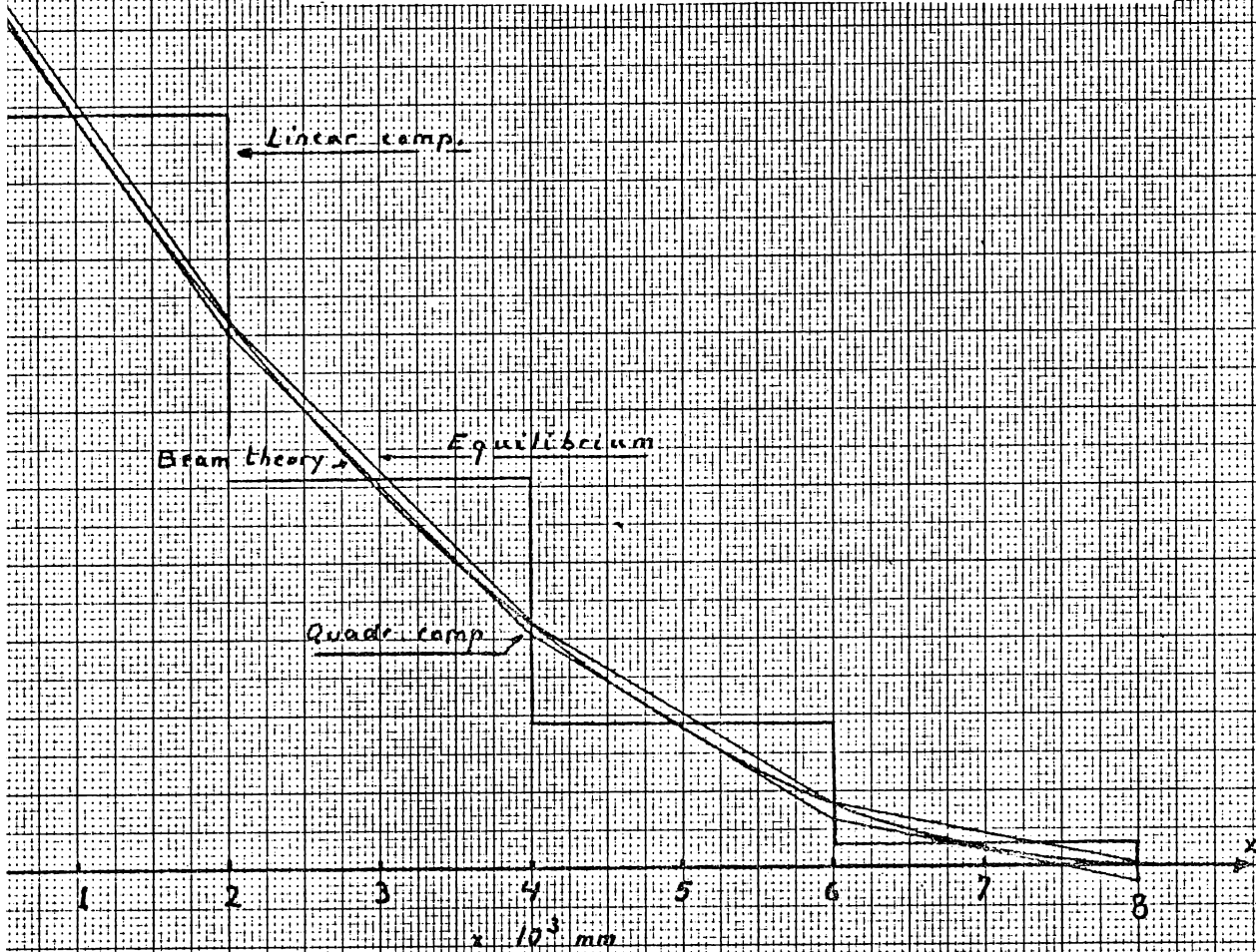


Figure F.3.7.

	$d^* = \left[\frac{PL^3}{8EI^*} + \frac{PL^3}{2GA} \right]$																			
	1	2	4	8	1,2,4 and 8	Theory of beams	1	2	4	8	13.631	14.979	8.843	9.370	3.7096	3.7949	2.1738	2.2021	.55459	.55620
Linear compatible											18.713	20.563	12.310	12.853	5.0722	5.1889	2.9606	2.9991	.73418	.73631
										19.985	21.961	12.953	13.724	5.4129	5.5374	3.1573	3.1984	.77900	.78121	
										20.304	22.312	13.162	13.946	5.4982	5.6247	3.2066	3.2483	.79031	.79260	
										20.407	22.425	13.226	14.014	5.5264	5.6535	3.2229	3.2648	.79406	.79637	
Equilibrium											22.432		14.054		5.6762		3.2824			.81146
											29.791		18.699		7.5238		4.3315			1.0365
											24.222		15.209		6.1275		3.5336			.85641
											22.891		14.336		5.7784		3.3341			.81187
											22.543		14.118		5.6911		3.2842			.80013

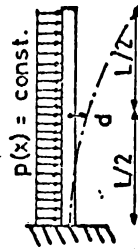
B.- NON DIMENSIONAL DEFLECTIONS

TYPE OF ANALYSIS	Nbr. of elements	$\mathcal{J} = 0.$		$\mathcal{J} = .2$		$\mathcal{J} = 1.0$		$\mathcal{J} = 2.0$		$\mathcal{J} = 10.0$	
		I	I*	I	I*	I	I*	I	I*	I	I*
Linear compatible	1	.60765	.66775	.62921	.66671	.65353	.66856	.66225	.67088	.68344	.68543
	2	.83421	.91668	.87590	.91454	.89359	.91415	.90196	.91369	.90476	.90738
	4	.89091	.97900	.92165	.97651	.95361	.97554	.96188	.97440	.95999	.96272
	8	.90513	.99465	.93653	.99231	.96864	.99092	.97690	.98961	.97393	.97675
Quadr. compatible	1,2,4 and 8	.90973	.99968	.94108	.99715	.97360	.99600	.98187	.99463	.97855	.98140
Theory of beams			1.0000		1.0000		1.0000		1.0000		1.0000

TABLE III Deflections in the middle for load nbr. 2

A.- DEFLECTIONS d IN MM

TYPE OF ANALYSIS	Σ = 0.		Σ = .2		Σ = 1.0		Σ = 2.0		Σ = 10.0	
	I	I*	I	I*	I	I*	I	I*	I	I*
Linear compatible	2	5.986	3.892		1.646		.9746		.2662	
	4	6.940	4.509		1.902		1.122		.2990	
	8	7.179	4.664		1.965		1.159		.3083	
Quadr. compatible	2,4 and 8	7.261	4.715		1.987		1.171		.3116	
Theory of beams	—	7.262	4.731	5.013	2.000	2.046	1.1717	1.187	.31106	.31196
Equilibrium	2			5.297		2.152		1.254		.3270
	4			5.079		2.065		1.204		.3157
	8			5.025		2.043		1.191		.3129



$$d^* = \left[\frac{17 pL^3}{384 EI^*} + \frac{3 pL^2}{8 GA} \right]$$

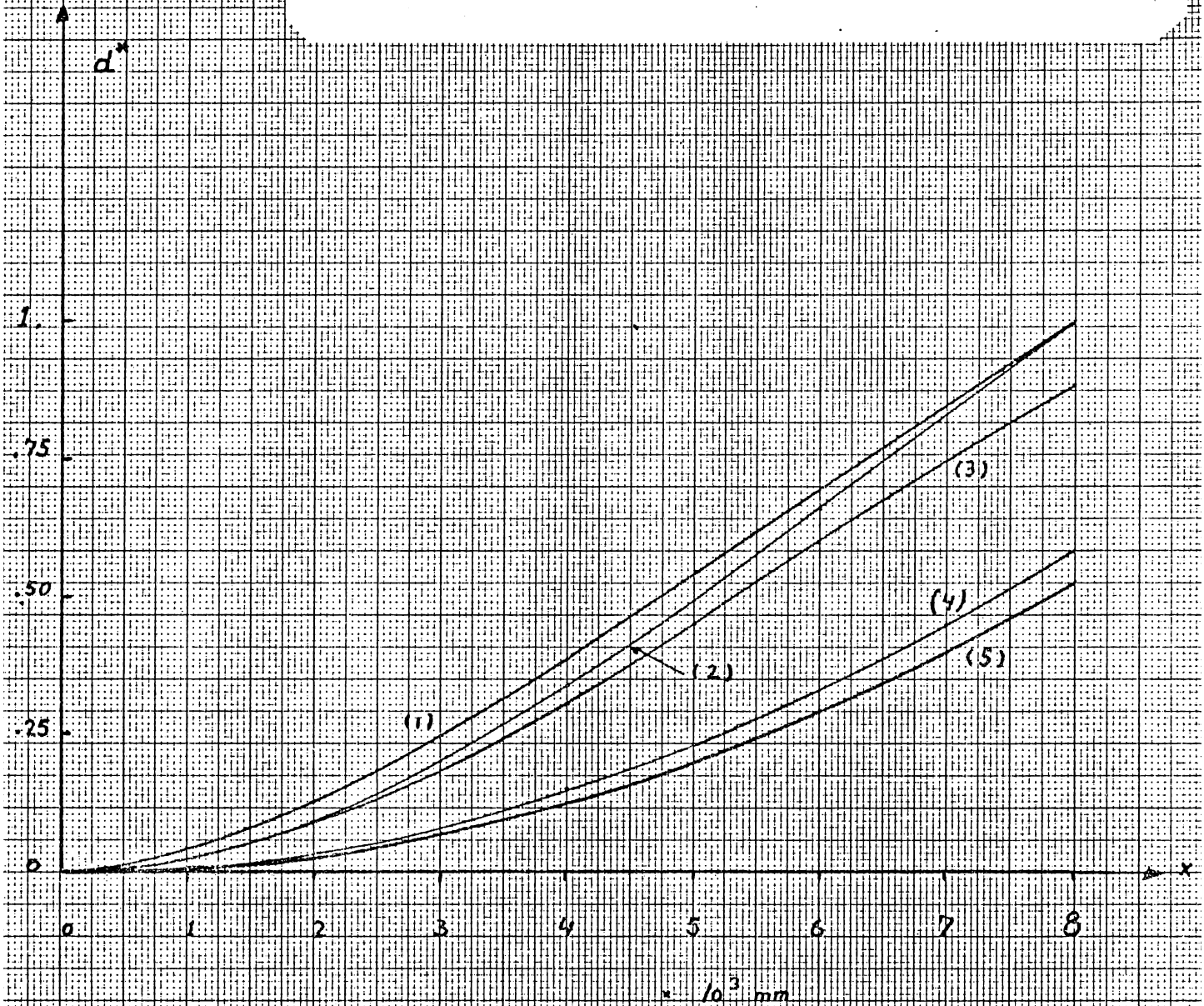
B.- NON DIMENSIONAL DEFLECTIONS

TYPE OF ANALYSIS	Σ = 0.		Σ = .2		Σ = 1.0		Σ = 2.0		Σ = 10.0	
	I	I*	I	I*	I	I*	I	I*	I	I*
Linear compatible	2	.7500	.7763		.8044		.8211		.8533	
	4	.8696	.8994		.9295		.9452		.9584	
	8	.8995	.9303		.9603		.9764		.9883	
Quadr. compatible	2,4 and 8	.9098	.9405		.9713		.9868		.9988	
Theory of beams	—	.9099	.9437	1.0000	.9775	1.0000	.9871	1.0000	.9971	1.0000

Figure F.3.9

Non dimensional deflections for load nbr. 3.

- (1) Beam theory.
- (2) Quadratic displacement model using I^* .
- (3) Quadratic displacement model using I .
- (4) Linear displacement model using I^* .
- (5) Linear displacement model using I .



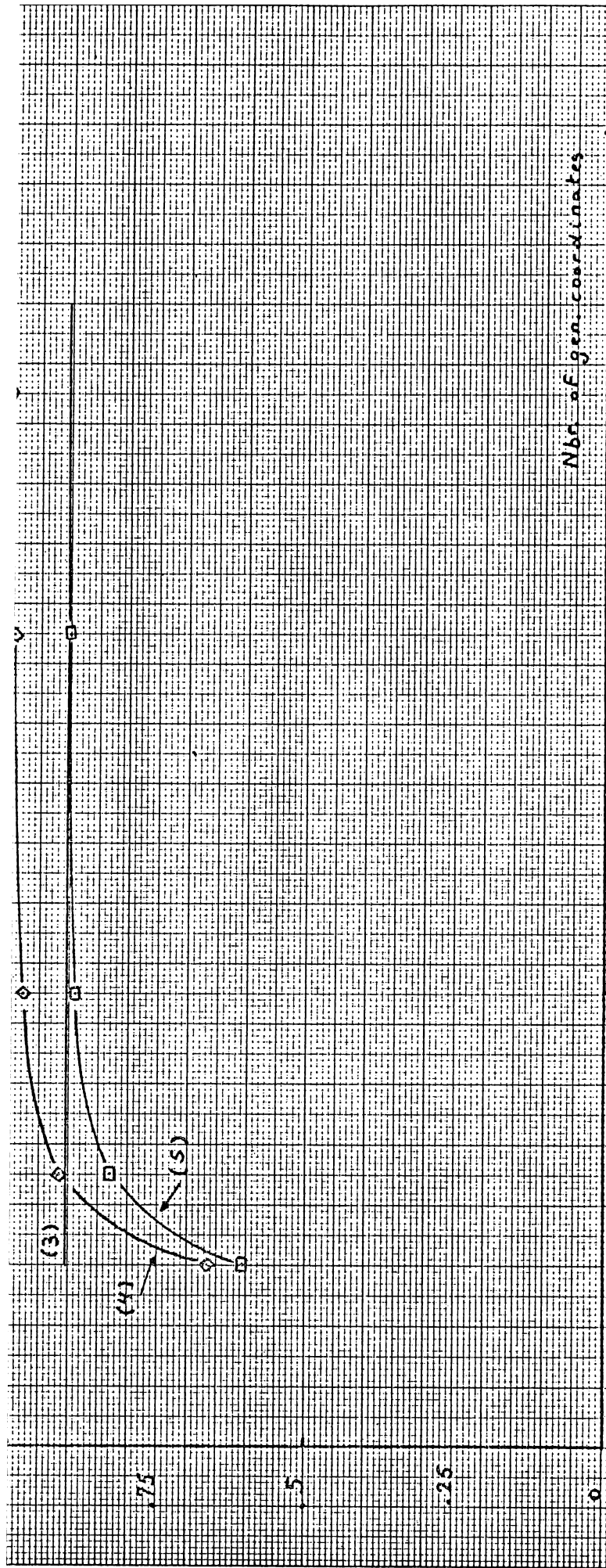
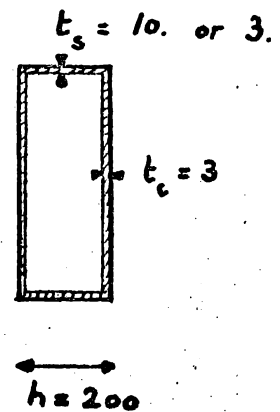
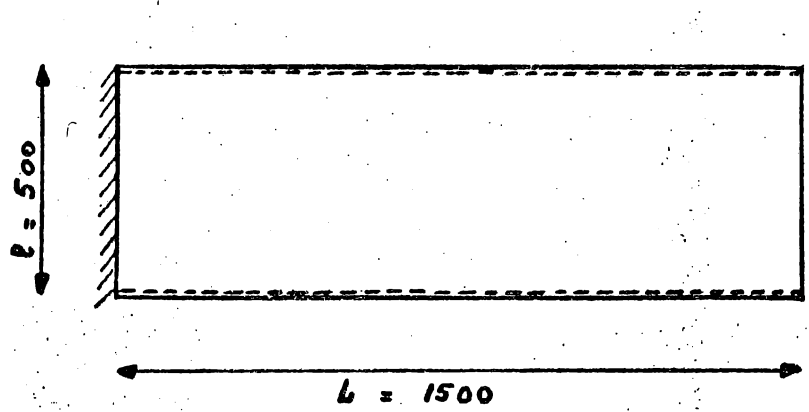
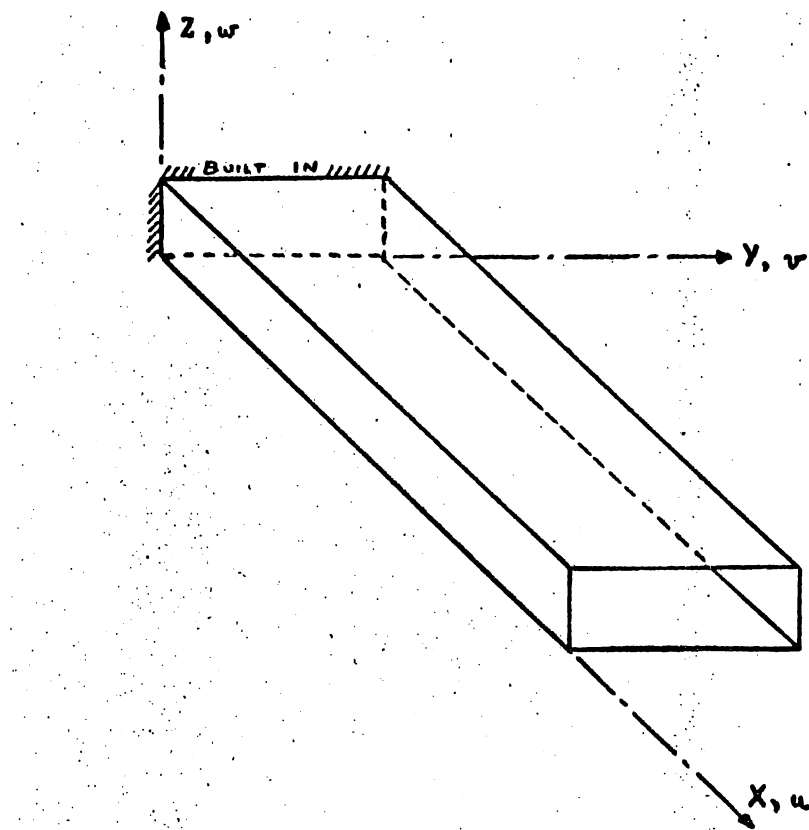
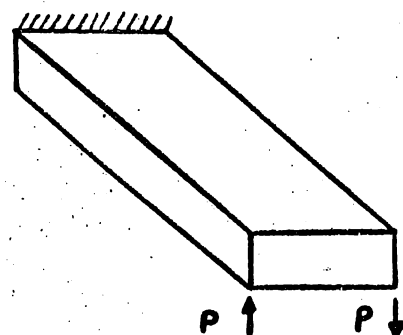
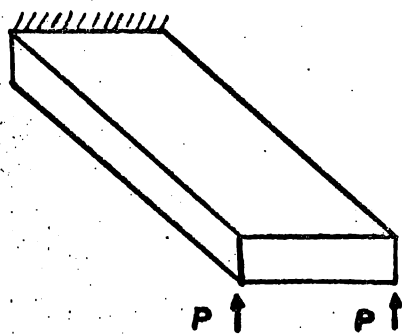
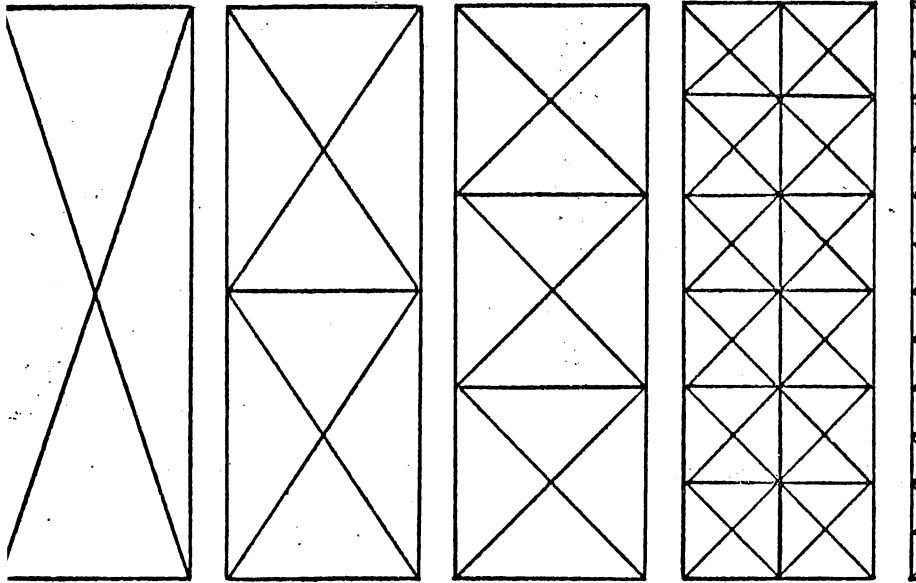


Figure F.3.II
Box Beam Model.

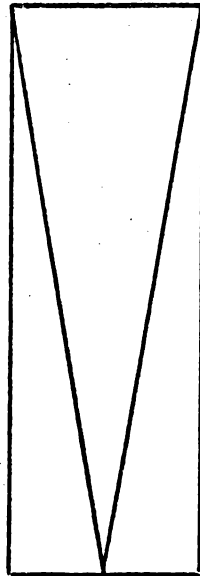
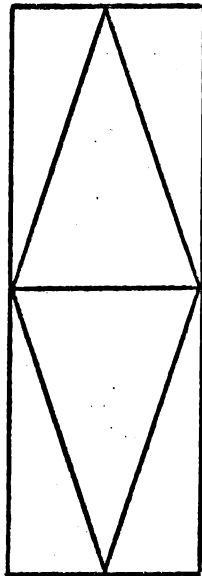
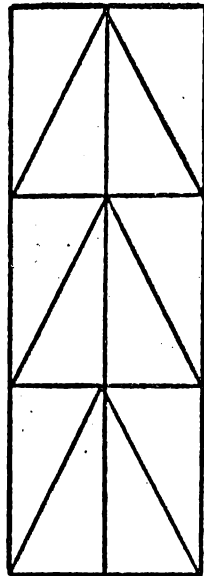


Loading Cases.





(1)	6	18	34	16
(2)	12	30	60	26
(3)	18	42	86	36
(4)	60	104	264	92



Code nbr.	Nbr. of el.	Lin. displ.	Quadr. displ.	Equilibrium
(6)	18	44	90	/
(7)	10	30	56	/
(8)	5	18	32	/

BOX BEAM TIP DEFLECTIONS USING THE LINEAR DISPLACEMENT FIELD

Idealization	Nbr.of Gen.Coord.	Web Thickness mm	Tip Deflections	
			Bending	Torsion
(1)	18	10	5.194	3.206
(2)	30	10	6.379	7.643
(3)	42	10	6.658	9.447
(4)	104	10	7.048	11.480
(5)	300	10	7.166	12.192
(6)	44	10	6.832	7.304
(7)	30	10	6.374	5.219
(8)	18	10	/	/
(9)	224	10	6.170	/
(10)	/	10	/	/
(1)	18	3	7.233	4.271
(2)	30	3	8.746	10.971
(3)	42	3	9.123	14.439
(4)	104	3	9.728	19.151
(5)	300	3	9.920	21.037
(6)	44	3	9.416	10.230
(7)	30	3	8.741	6.922
(8)	18	3	/	/
(9)	224	3	/	/
(10)	/	3	/	/

N.B. Tip deflections are given in millimeters for

$$E = 7.500 \text{ kg/mm}^2 \quad \nu = .3$$

$$P = 1.000 \text{ Kg}$$

Figure F.3.I5

BOX BEAM TIP DEFLECTIONS USING THE QUADRATIC DISPLACEMENT FIELD

Idealization	Nbr.of Gen.Coord.	Web Thickness mm	Tip Deflections	
			Bending	Torsion
(1)	84	10	7.076	11.712
(2)	60	10	7.165	12.349
(3)	86	10	7.185	12.384
(4)	264	10	7.207	12.448
(5)	708	10	/	/
(6)	90	10	7.180	12.385
(7)	56	10	7.130	11.602
(8)	32	10	7.004	10.923
(9)	/	10	/	/
(10)	/	10	/	/
(1)	34	3	9.753	19.872
(2)	60	3	9.908	21.473
(3)	86	3	9.945	21.575
(4)	264	3	9.991	21.762
(5)	708	3	/	/
(6)	90	3	9.937	21.584
(7)	56	3	/	/
(8)	32	3	9.632	18.293
(9)	/	3	/	/
(10)	/	3	/	/

N.B. Tip deflections are given in millimeters for

$E = 7.500 \text{ kg/mm}^2$ $\nu = .3$

$P = 1.000 \text{ Kg}$

BOX BEAM TIP DEFLECTIONS USING THE EQUILIBRIUM STRESS FIELD

Idealization	Nbr.of Gen.Coord.	Web Thickness mm	Tip Deflections	
			Bending	Torsion
(1)	16	10	8.146	22.800
(2)	26	10	7.779	22.800
(3)	36	10	7.793	22.800
(4)	92	10	7.586	14.844
(5)	276	10	7.485	13.574
(6)	/	10	/	/
(7)	/	10	/	/
(8)	/	10	/	/
(9)	/	10	/	/
(10)	/	10	7.570	/
(1)	16	3	11.310	75.999
(2)	26	3	10.696	75.999
(3)	36	3	10.726	75.995
(4)	92	3	10.397	27.534
(5)	276	3	10.211	23.576
(6)	/	3	/	/
(7)	/	3	/	/
(8)	/	3	/	/
(9)	/	3	/	/
(10)	/	3	/	/

N.B. Tip deflections are given in millimeters for

$E = 7.500 \text{ kg/mm}^2$ $\nu = .3$

$P = 1.000 \text{ Kg}$

Figure F.3.I7

BOX BEAM TIP DEFLECTIONS USING SOME HYBRID METHODS

Idealization	Nbr. of Gen. Coord.	Web Thickness mm	Tip Deflections	
			Bending	Torsion
(9)	224	10	7.329	/
(7)	L.D.F. 30	10	6.494	5.278
(5)	L.D.F. 300	10	7.322	12.791
(8)	Q.D.F. 32	10	7.150	11.414
(4)	Q.D.F. 264	10	7.366	13.078
(7)	L.D.F. 30	3	8.630	6.774
(6)	L.D.F. 44	3	9.316	10.150
(4)	L.D.F. 104	3	9.634	19.406
(5)	L.D.F. 300	3	9.831	21.393
(7)	Q.D.F. 32	3	9.534	18.542
(6)	Q.D.F. 90	3	9.847	21.966
(4)	Q.D.F. 264	3	9.902	22.154

N.B. 1.- Tip deflections are given in millimeters for

$$E = 7.500 \text{ kg/mm}^2 \quad \nu = .3 \quad P = 1.000 \text{ Kg.}$$

2.- That run uses the linear stress assumption.

3.- L.D.F. stands for linear displacement Field:

Q.D.F. stands for quadratic displacement Field

(the $\nu = 0$. assumption makes the method hybrid).

Figure F.3.18

B O X B E A M

Bending - $t_s = 10$

Convergence curve of the tip deflections versus the number of generalized coordinates.

TIP DEFLECTION

u_B (mm)

8

7

6

5

11

mean value

- equilibrium models.
- quadratic displacement models.
- ◇ linear displacement models.

Nbr. of gen. coordinates

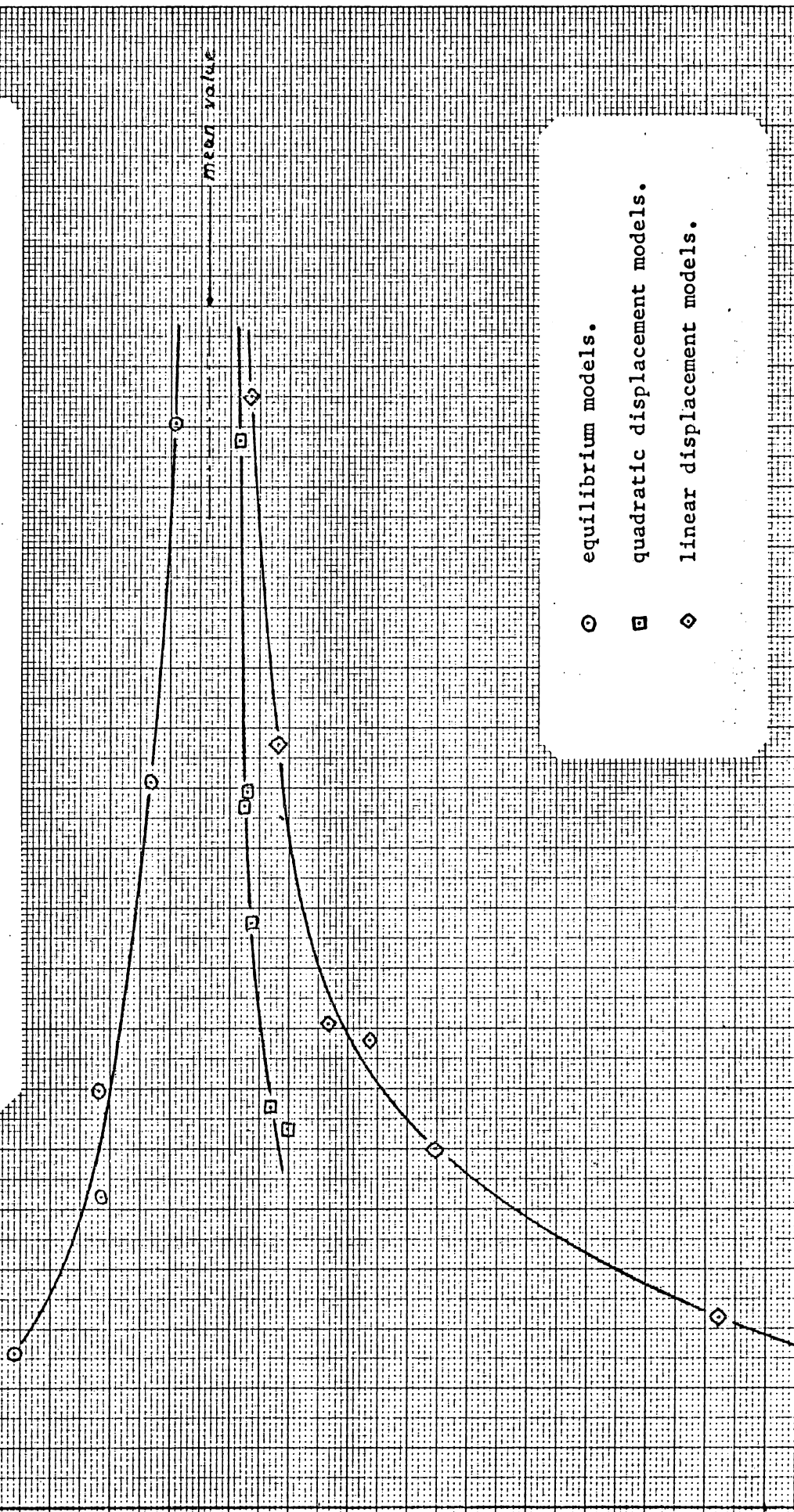


Figure F.3.19

B O X B E A M

Bending - $t_s = 3$

Convergence curve of the tip deflections versus the number of generalized coordinates.

TIP DEFLECTION

w_B (mm)

12

11

10

9

8

7

mean value

- equilibrium models.
- quadratic displacement models.
- ◇ linear displacement models.

Nbr. of gen. coordinates

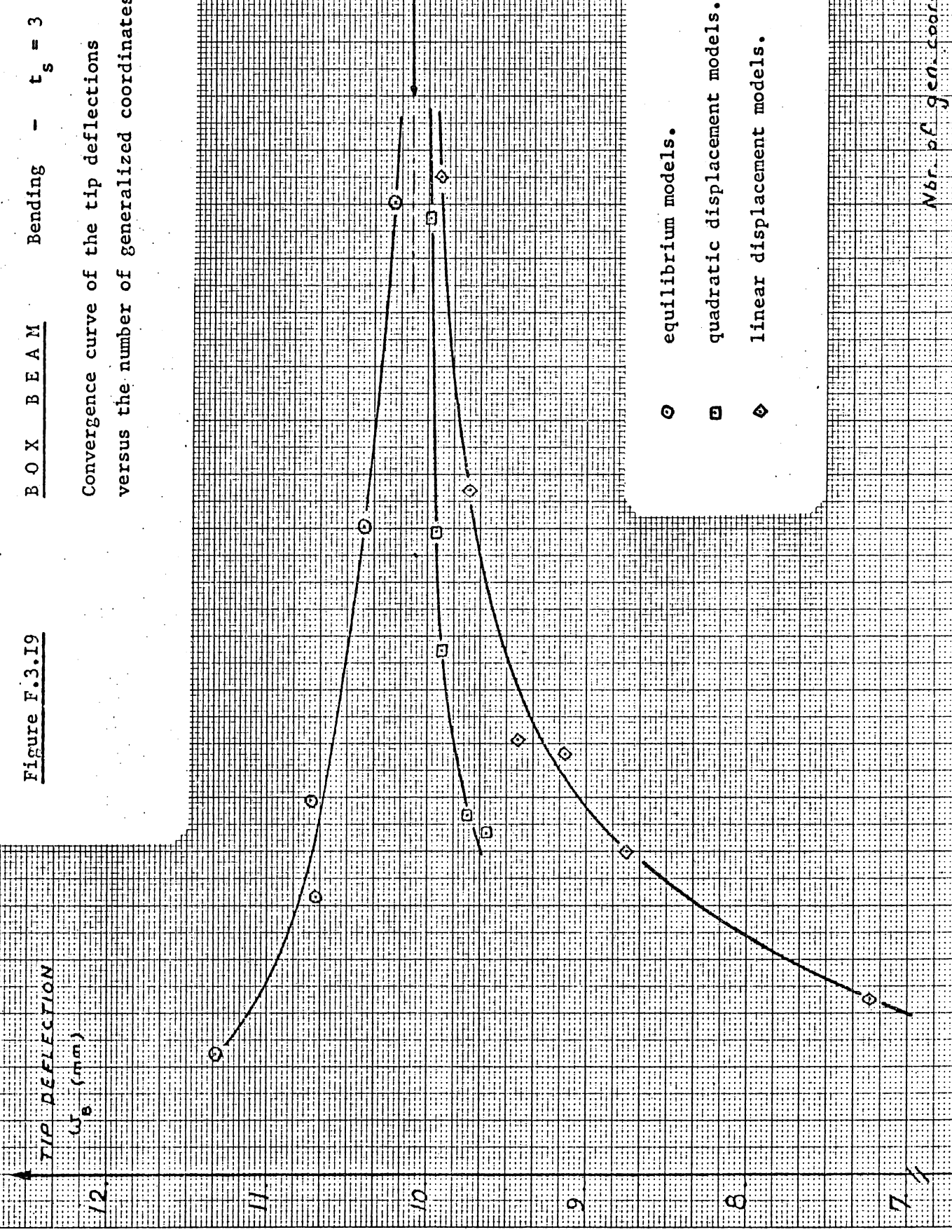


Figure F.3.20

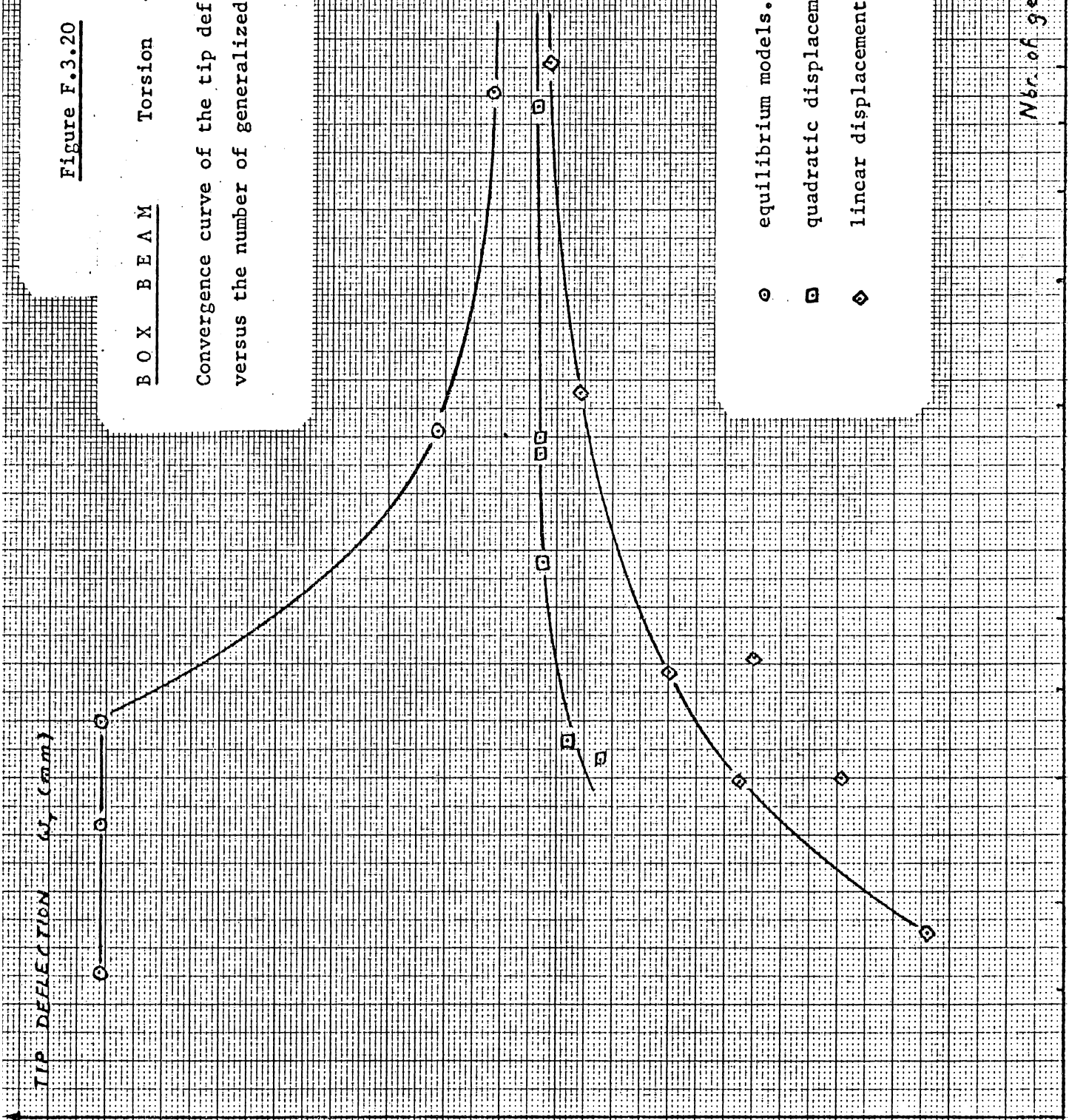
BOX BEAM

Torsion - $t_s = 10$

Convergence curve of the tip deflections versus the number of generalized coordinates.

TIP DEFLECTION (μ, mm)

2.4
2.2
2.0
1.8
1.6
1.4
1.2
1.0
0.8
0.6
0.4
0.2
0



- equilibrium models.
- quadratic displacement models.
- ◇ linear displacement models.

Nbr. of gen. coordinates

Figure F.3.2I

BOX BEAM

Torsion - $t_s = 3$

Convergence curve of the tip deflections
versus the number of generalized coordinates.

TIP DEFLECTION

w_T (mm)

80

70

60

50

40

30

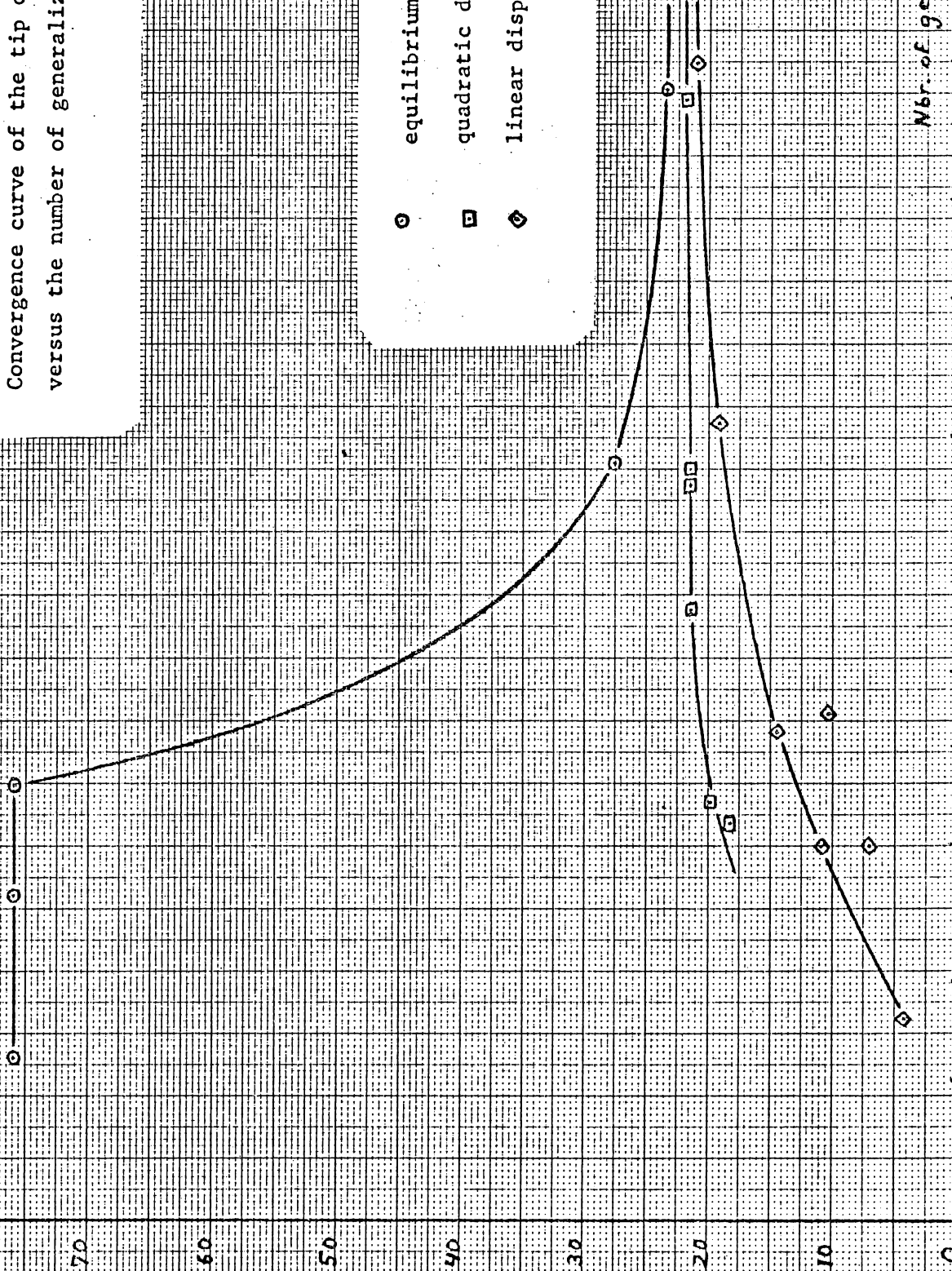
20

10

0

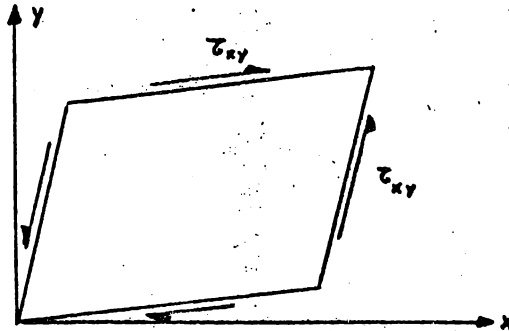
- equilibrium models.
- quadratic displacement models.
- ◇ linear displacement models.

Number of gen. coordinates



Stress representation.

- Stresses are given in the cover sheet where longitudinal stress is traction.
- Traction stresses are positive.
- Positive shear stresses are defined by :



- Stresses computed for :

- idealization (1) are indicated by \diamond ————
- idealization (2) are indicated by \times - - - - -
- idealization (3) are indicated by \square - - - - -
- idealization (4) are indicated by \odot — - - - -
- idealization (5) are indicated by \bullet —————

- For clarity of drawing, when the curves corresponding to the different idealizations are to close from each other, only the curve corresponding to the more refined idealization is drawn.

Figure F.3.22

B O X B E A M Linear displacement Field
 Bending - $t_s = 10$

Longitudinal distribution of σ_x in the spar cap

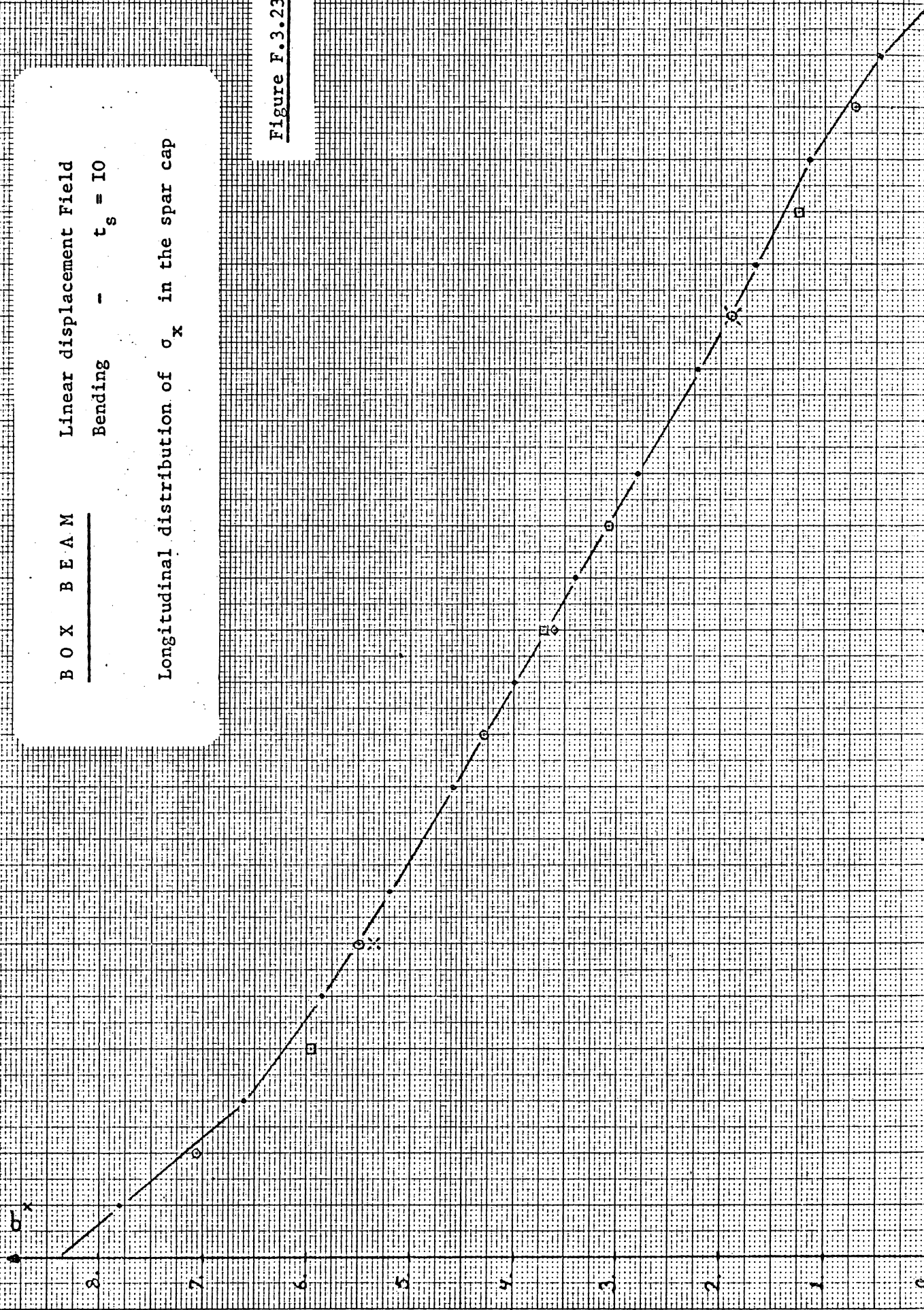


Figure F.3.23

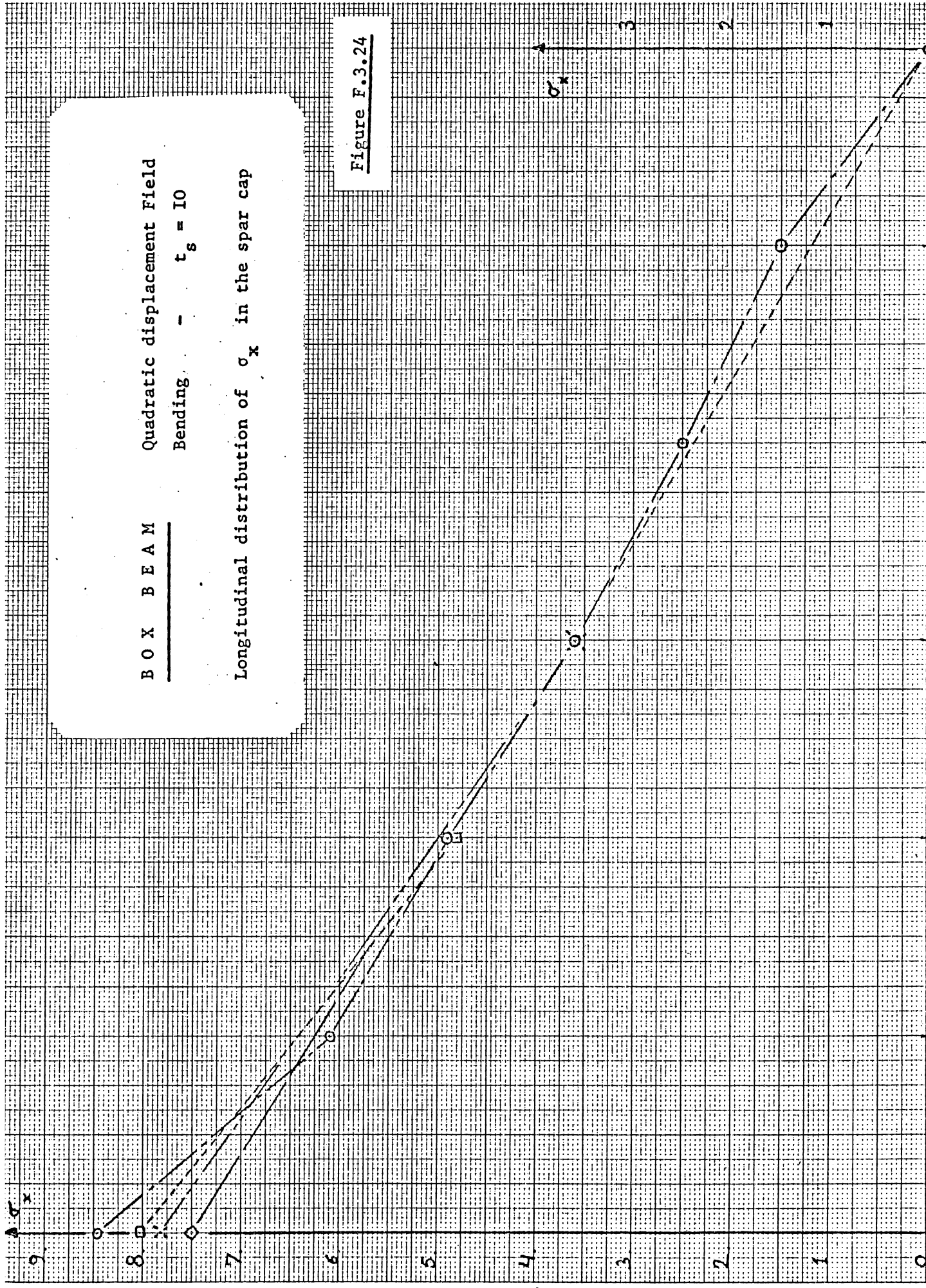


Figure F.3.24

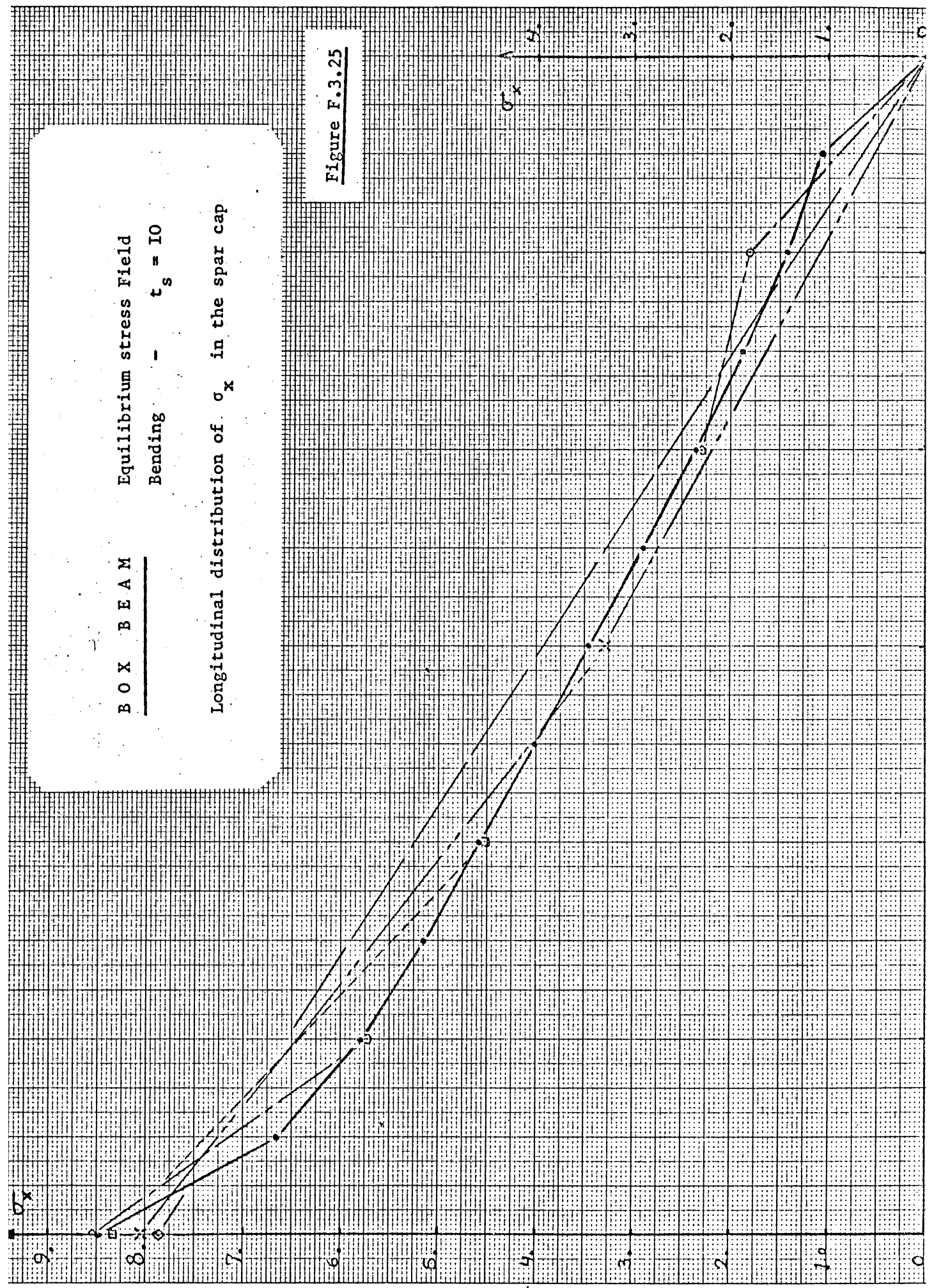
B O X B E A M

Equilibrium stress field

Bending - $t_s = 10$

Longitudinal distribution of σ_x in the spar cap

Figure F.3.25



B O X B E A M

Linear displacement Field

Bending - $t_s = 10$

Longitudinal distribution of σ_x in the spar cap
(unsmoothed)

σ_x

8

7

6

5

4

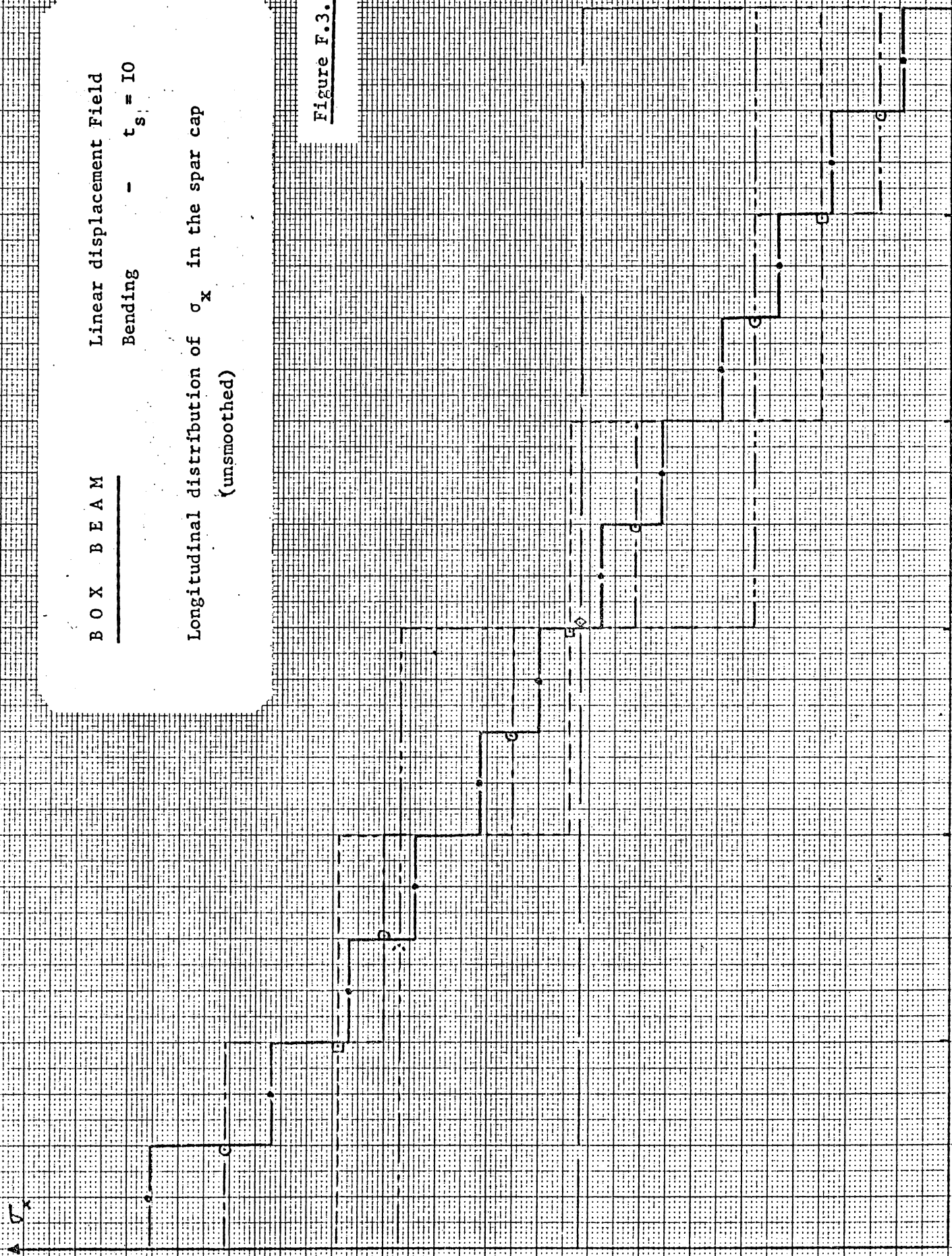
3

2

1

0

Figure F.3.26



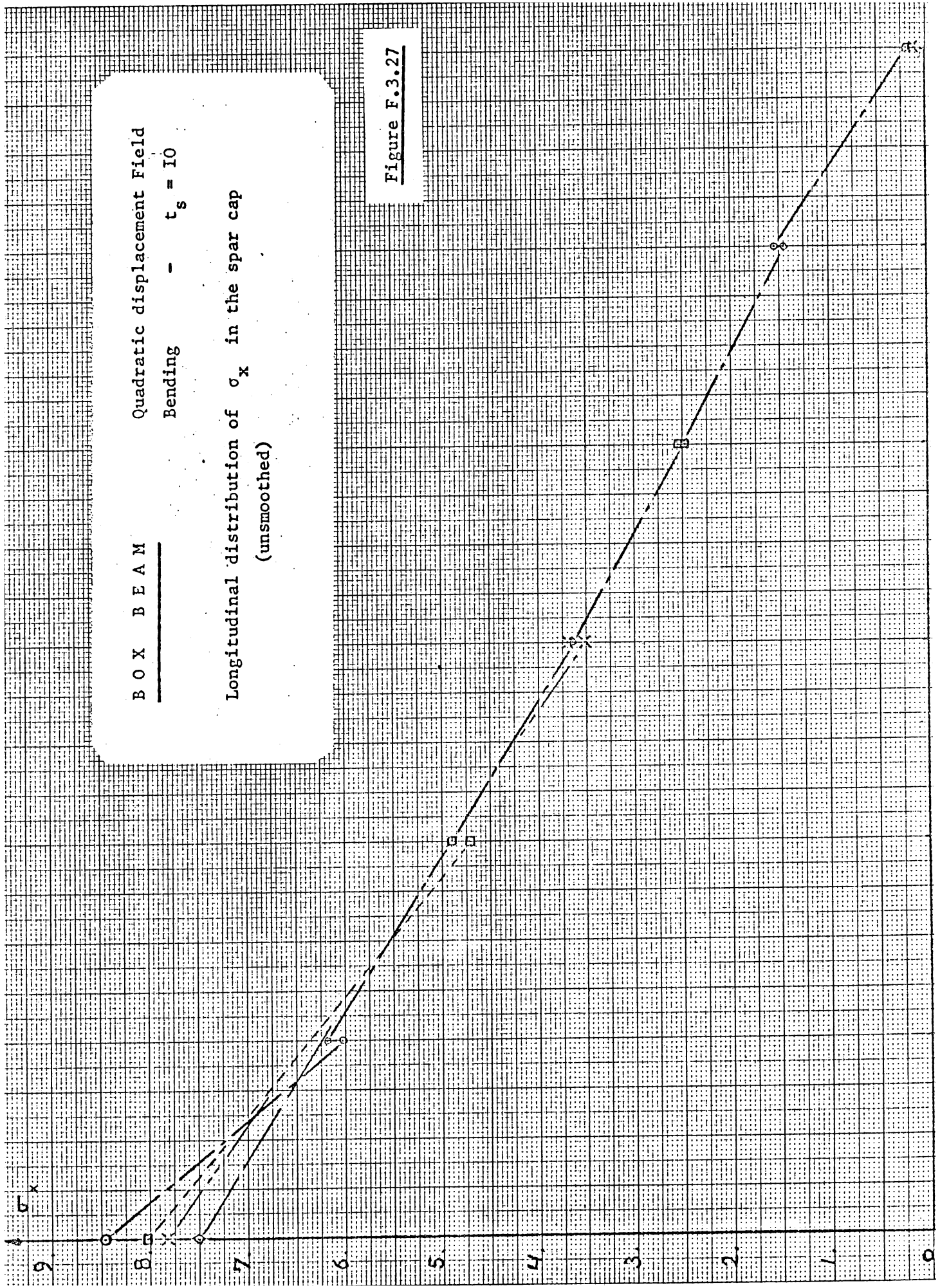


Figure F.3.27

BOX BEAM

Bending - $t_s = 10$

Comparison of spar cap stresses using the three methods

- for linear displacement field
- for quadratic displacement field
- for equilibrium stress field

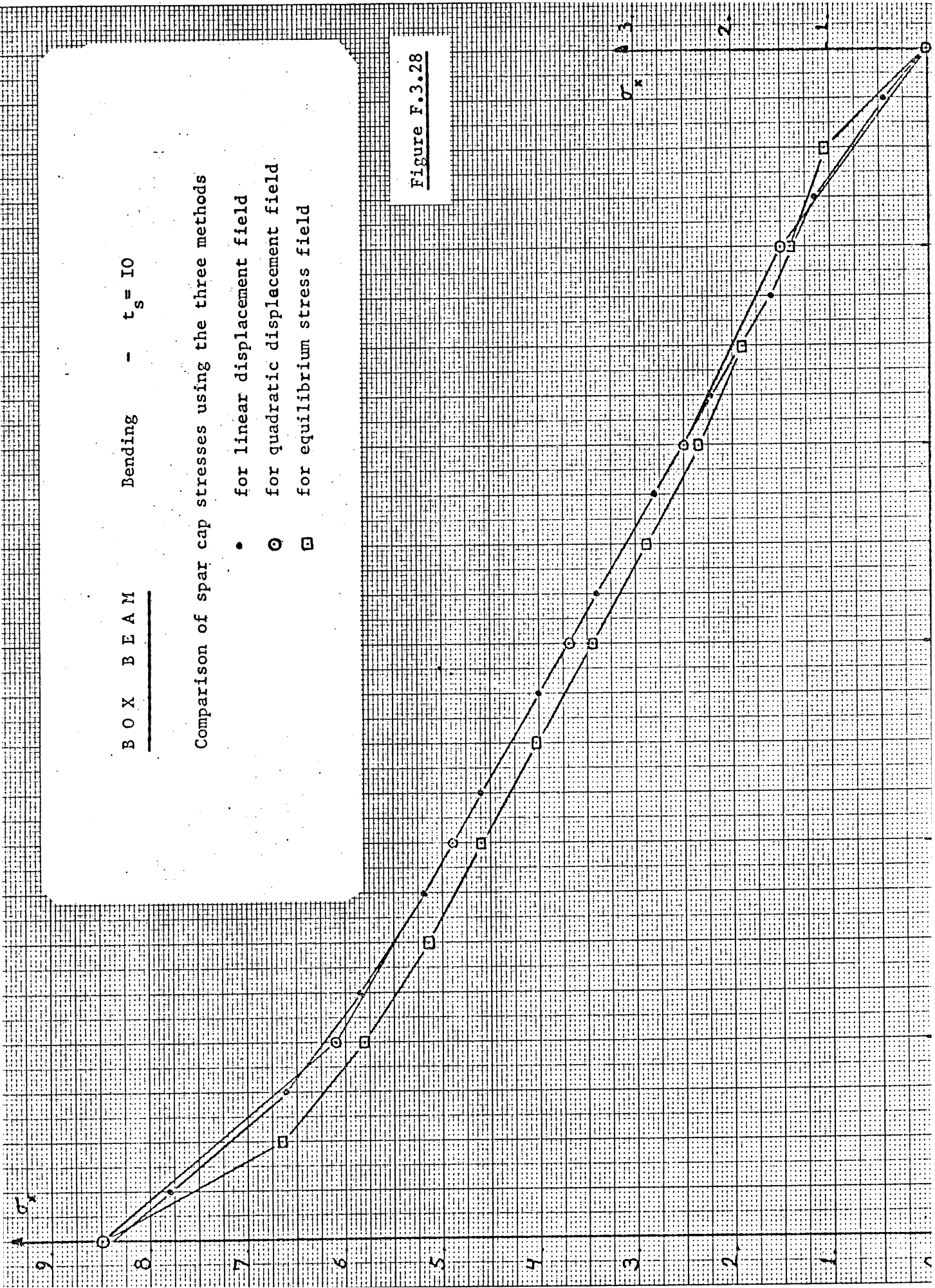


Figure F.3.28

B O X B E A M

Linear displacement Field

Torsion

$t_s = I_0$

Longitudinal distribution of σ_x in the spar cap

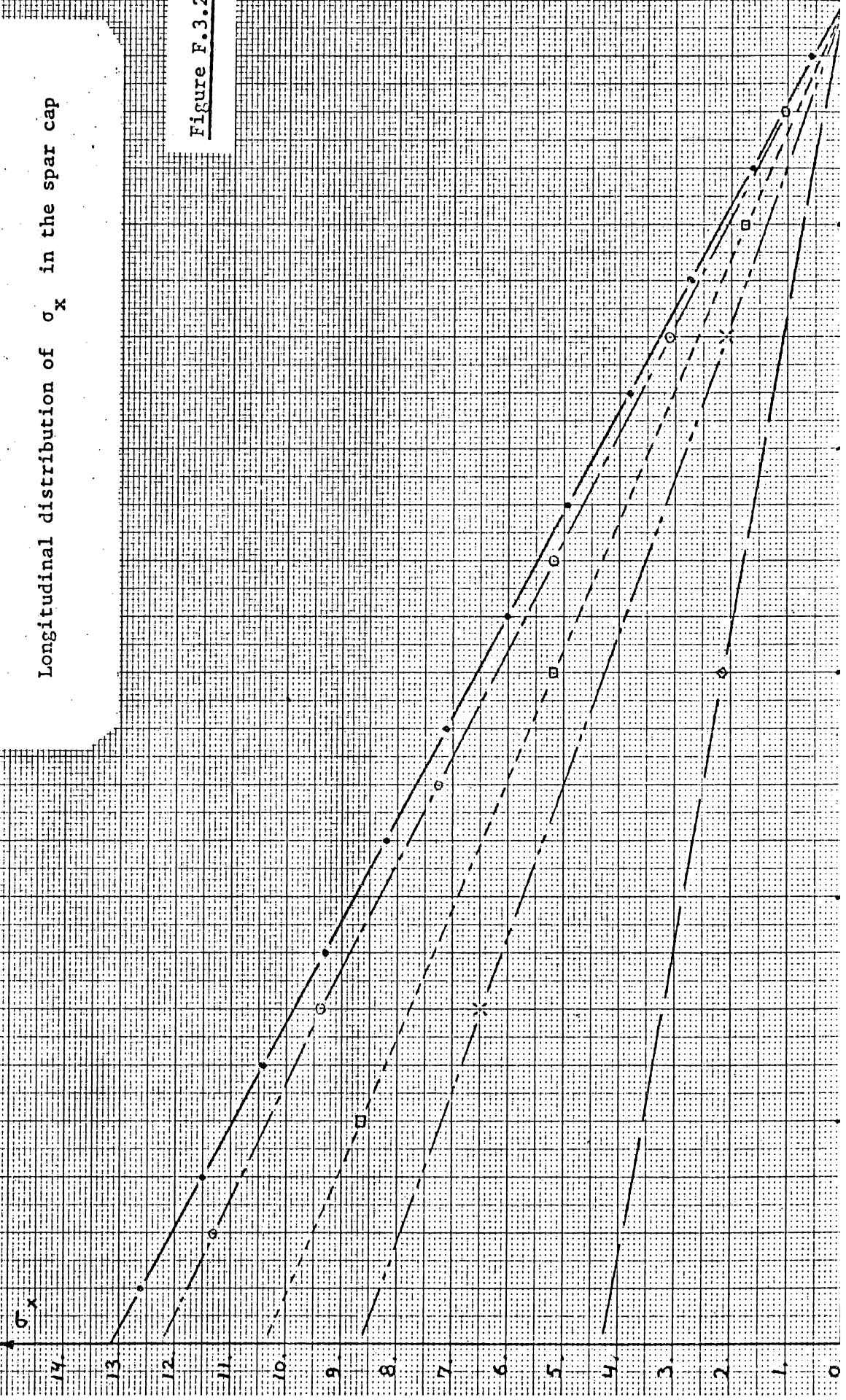


Figure F.3.29

BOX BEAM Quadratic displacement Field

Torsion - $t_s = 10$

Longitudinal distribution of σ_x in the spar cap

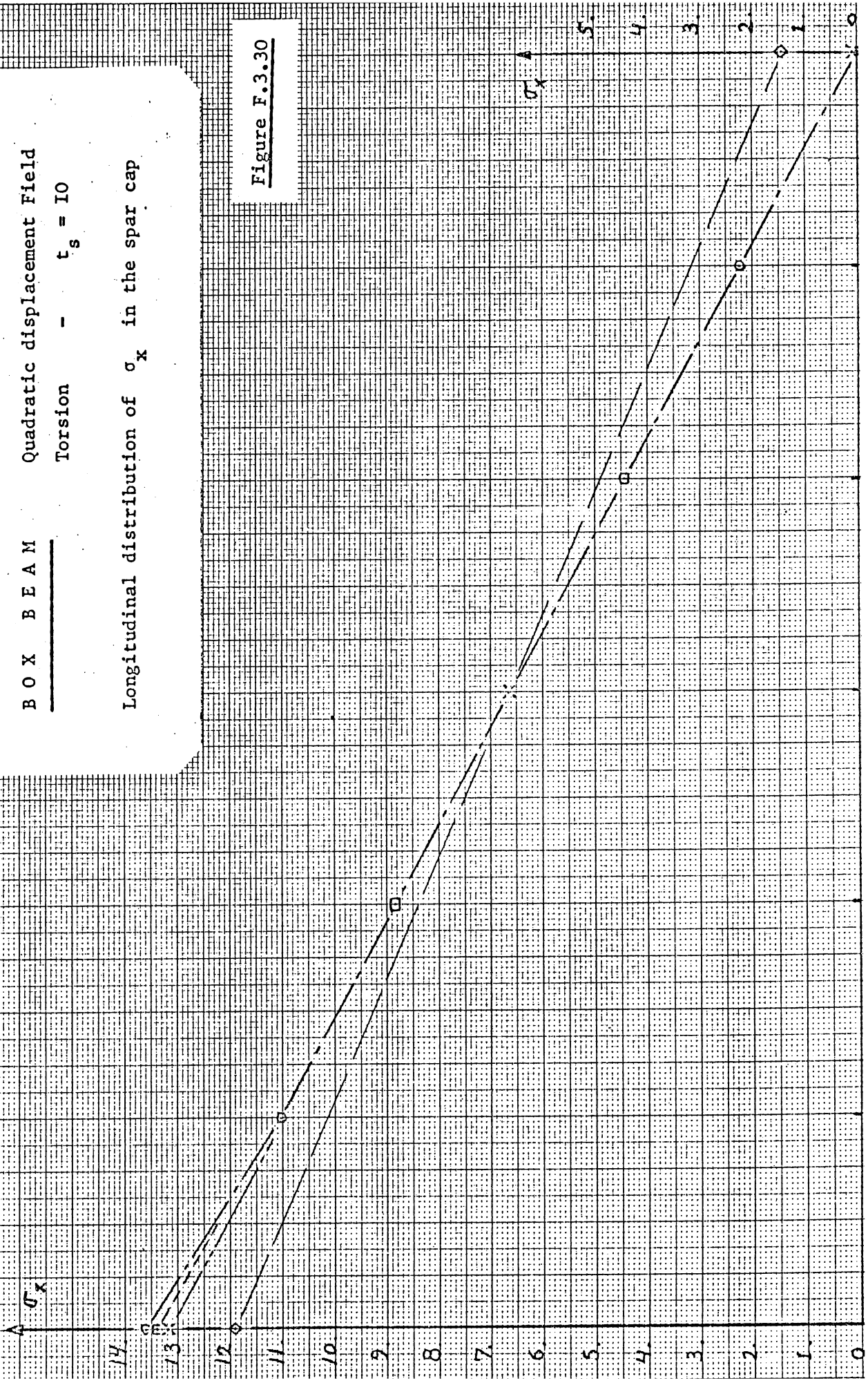


Figure F.3.30

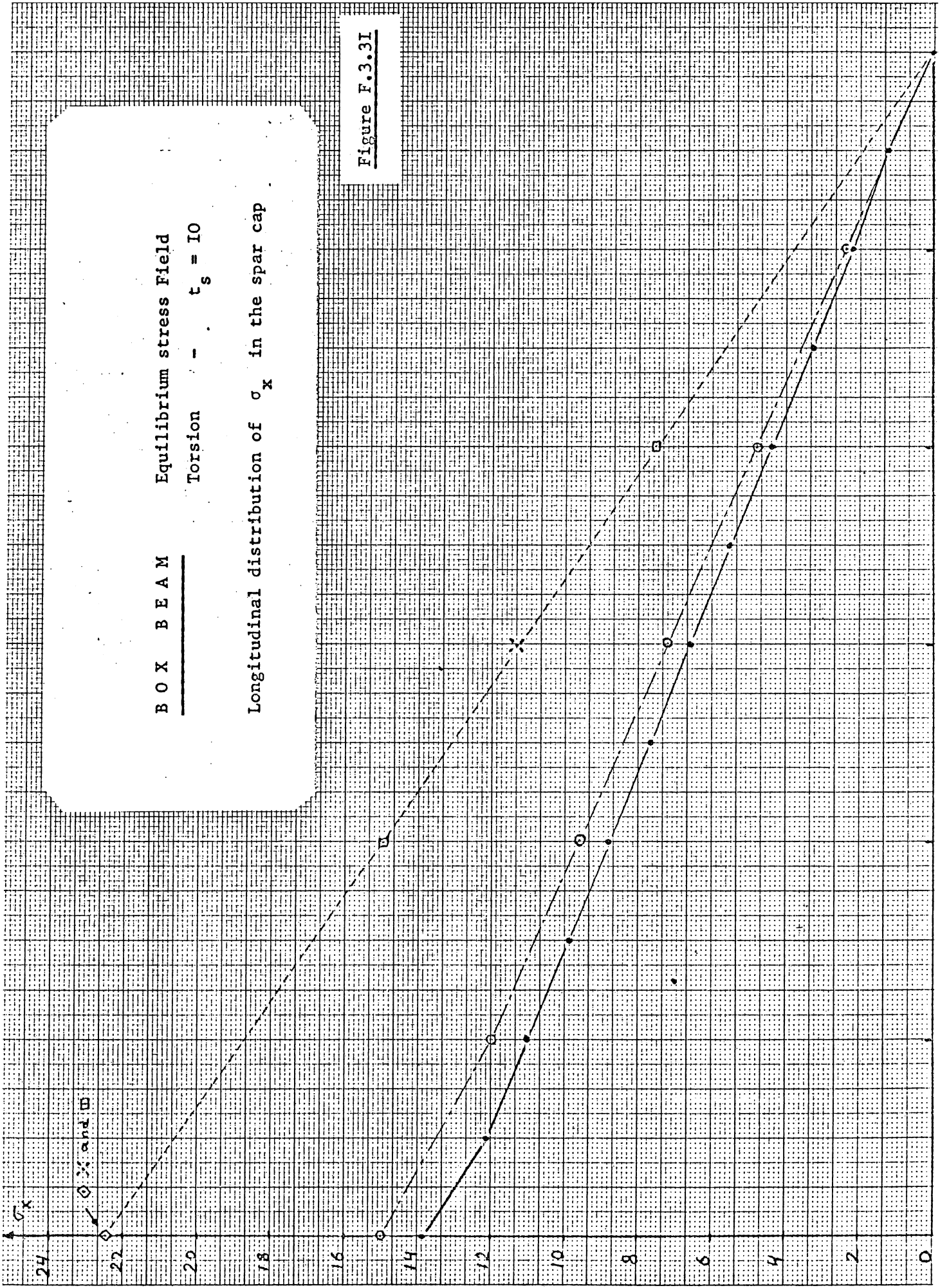


Figure F.3.3I

B O X B E A M

Torsion

- $t_s = 10$

Comparison of spar cap stresses using the three methods
• for linear displacement field
○ for quadratic displacement field
□ for equilibrium stress field

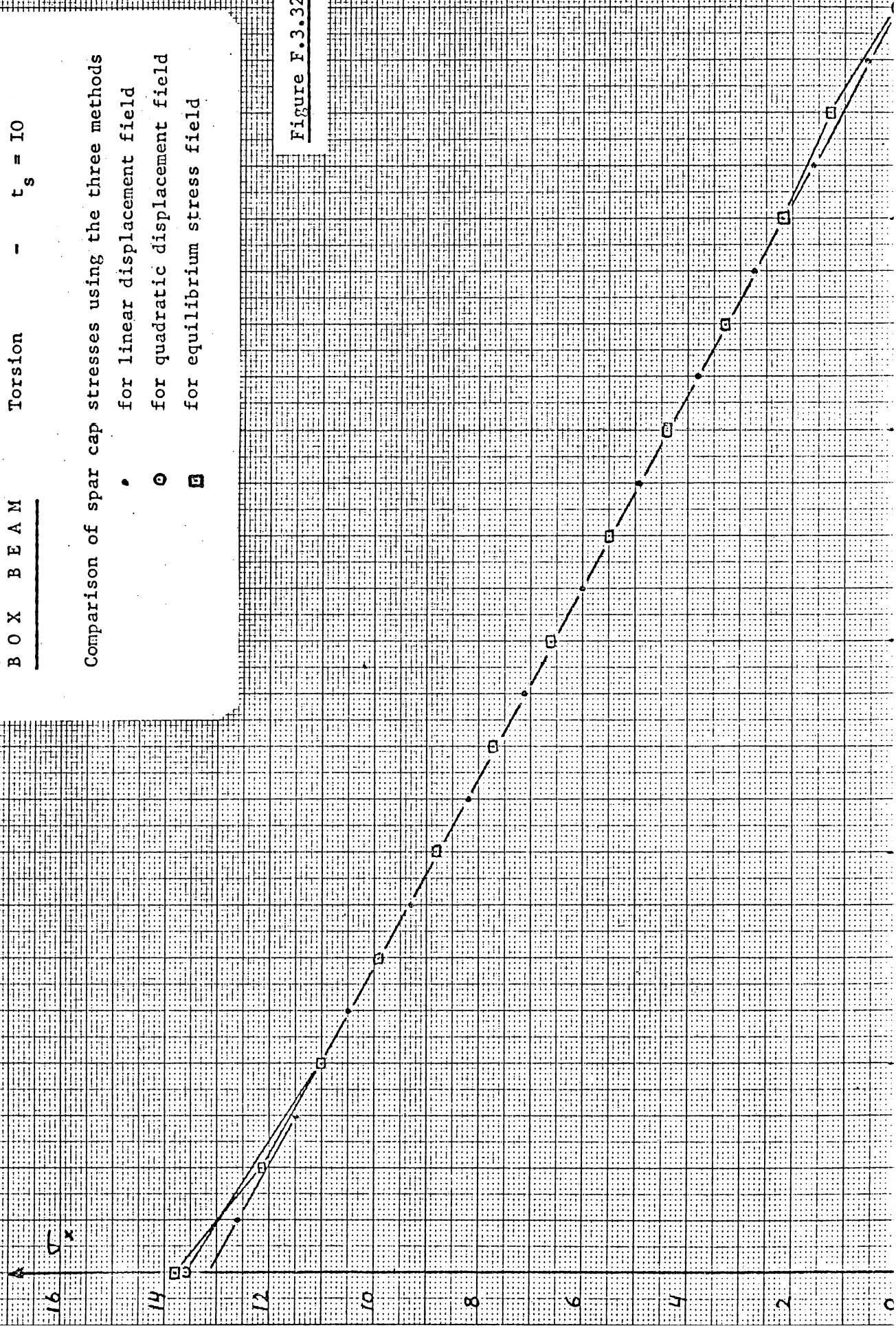
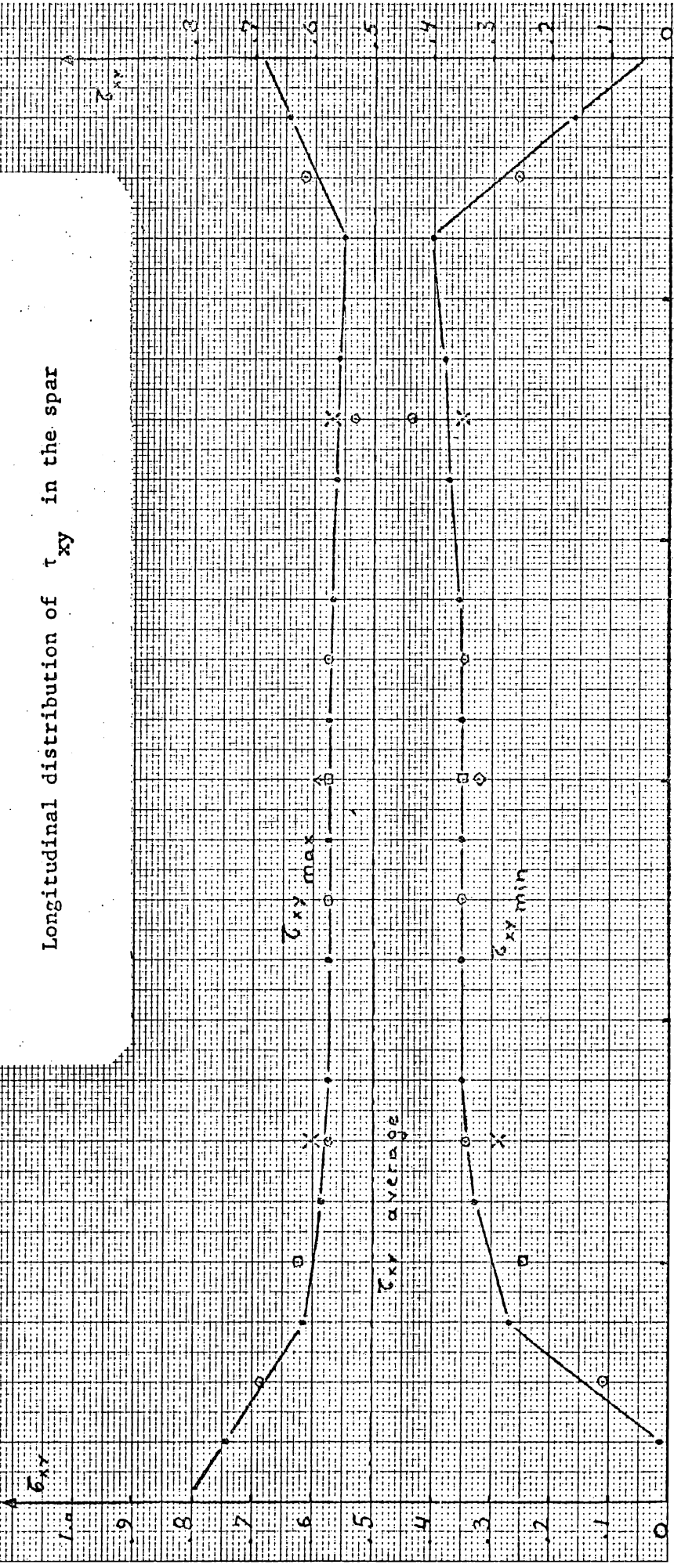


Figure F.3.32

B O X B E A M Equilibrium stress field
 Bending - $t_s = 10$

Longitudinal distribution of τ_{xy} in the spar

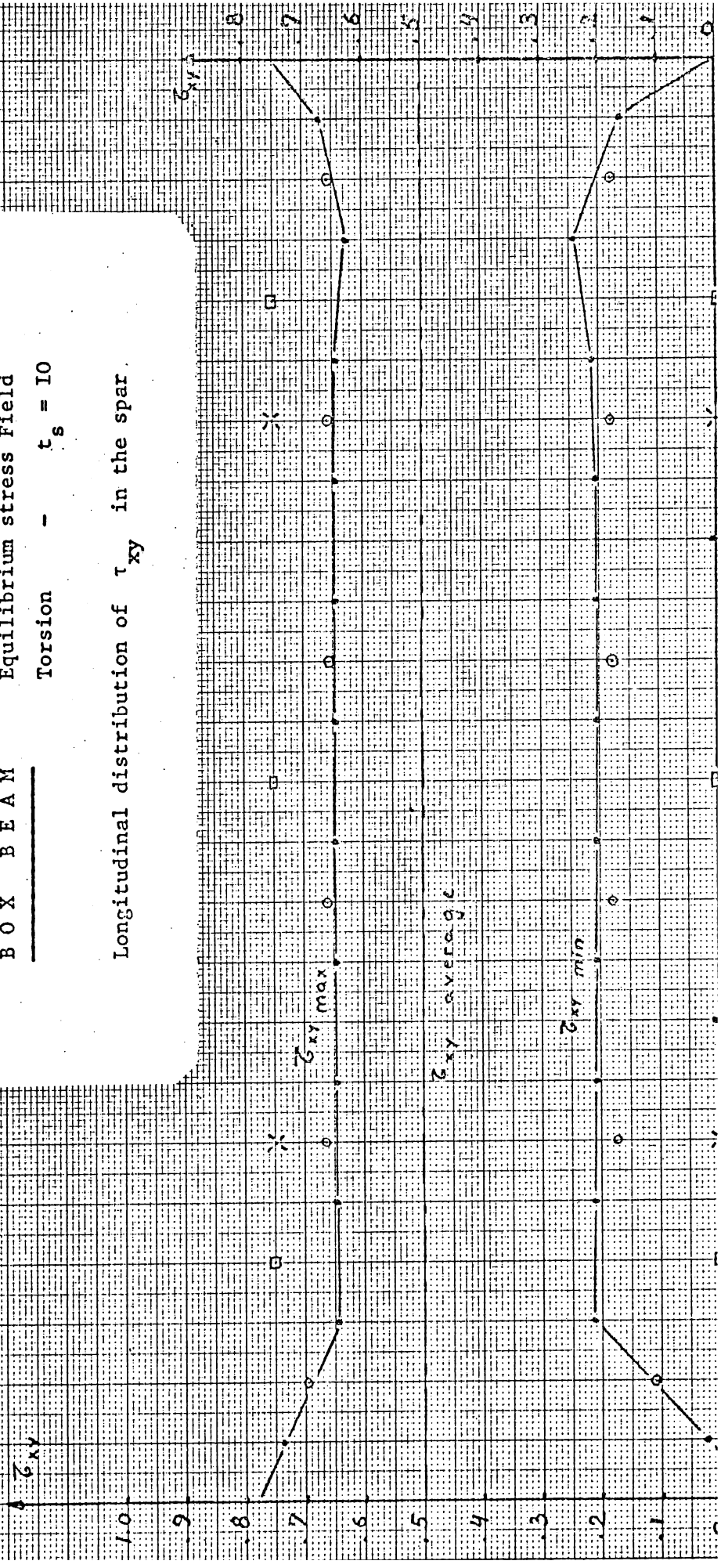


B O X B E A M

Equilibrium stress field

Torsion - $t_s = 10$

Longitudinal distribution of τ_{xy} in the spar.



B O X B E A M

Linear displacement field

Bending - $t_s = I_0$

Longitudinal distribution of σ_x in elements adjacent to $\frac{y}{I} = 0$

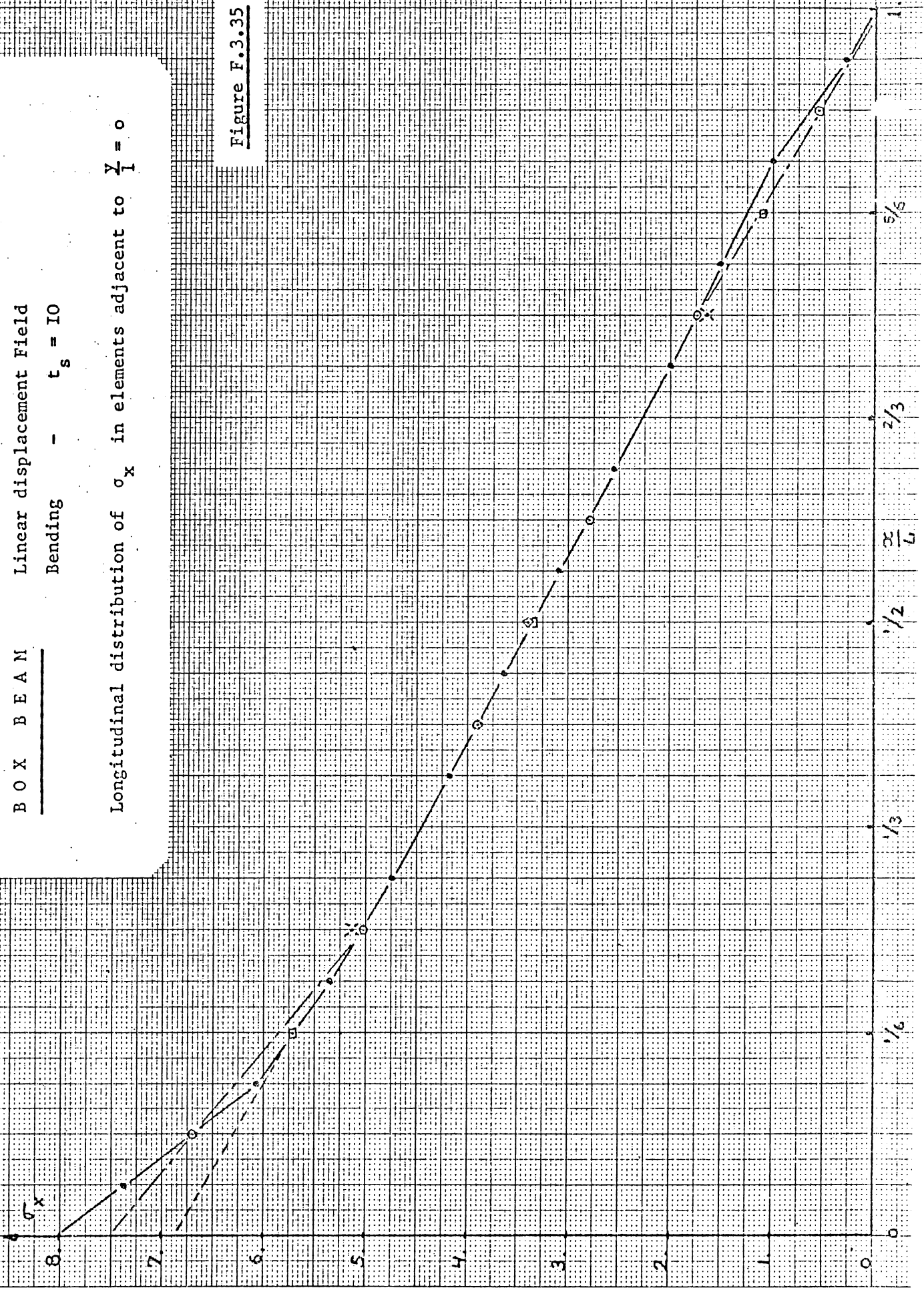


Figure F.3.35

B O X B E A M

Quadratic displacement field

Bending - $t_s = 10$

Longitudinal distribution of σ_x in elements adjacent to $\frac{y}{l} = 0$

σ_x

8

7

6

5

4

3

2

1

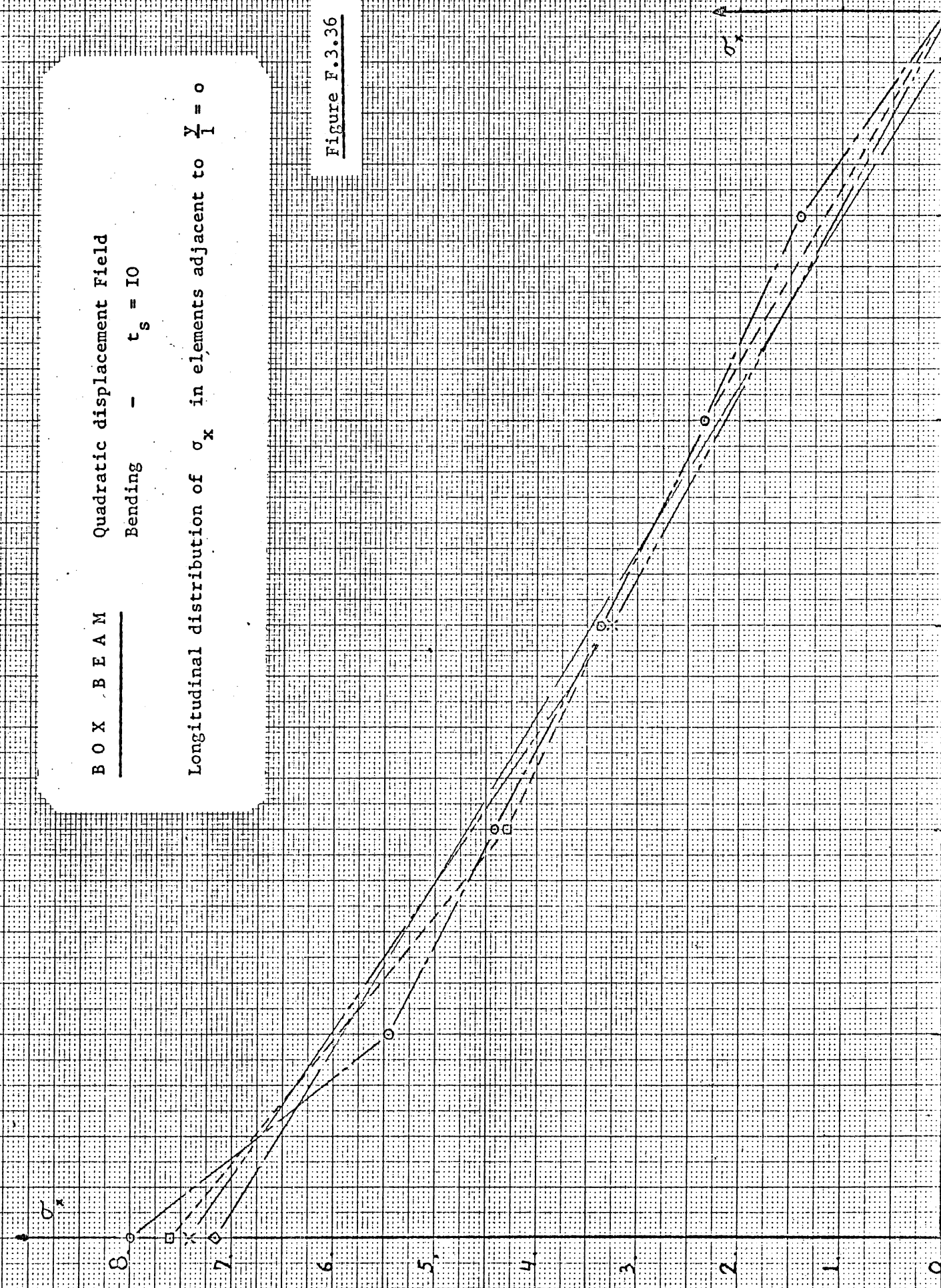
0

σ_x

1

2

Figure F.3.36



B O X B E A M

Equilibrium stress Field

Bending - $t_s = 10$

Longitudinal distribution of σ_x in elements adjacent to $\frac{y}{l} = 0$

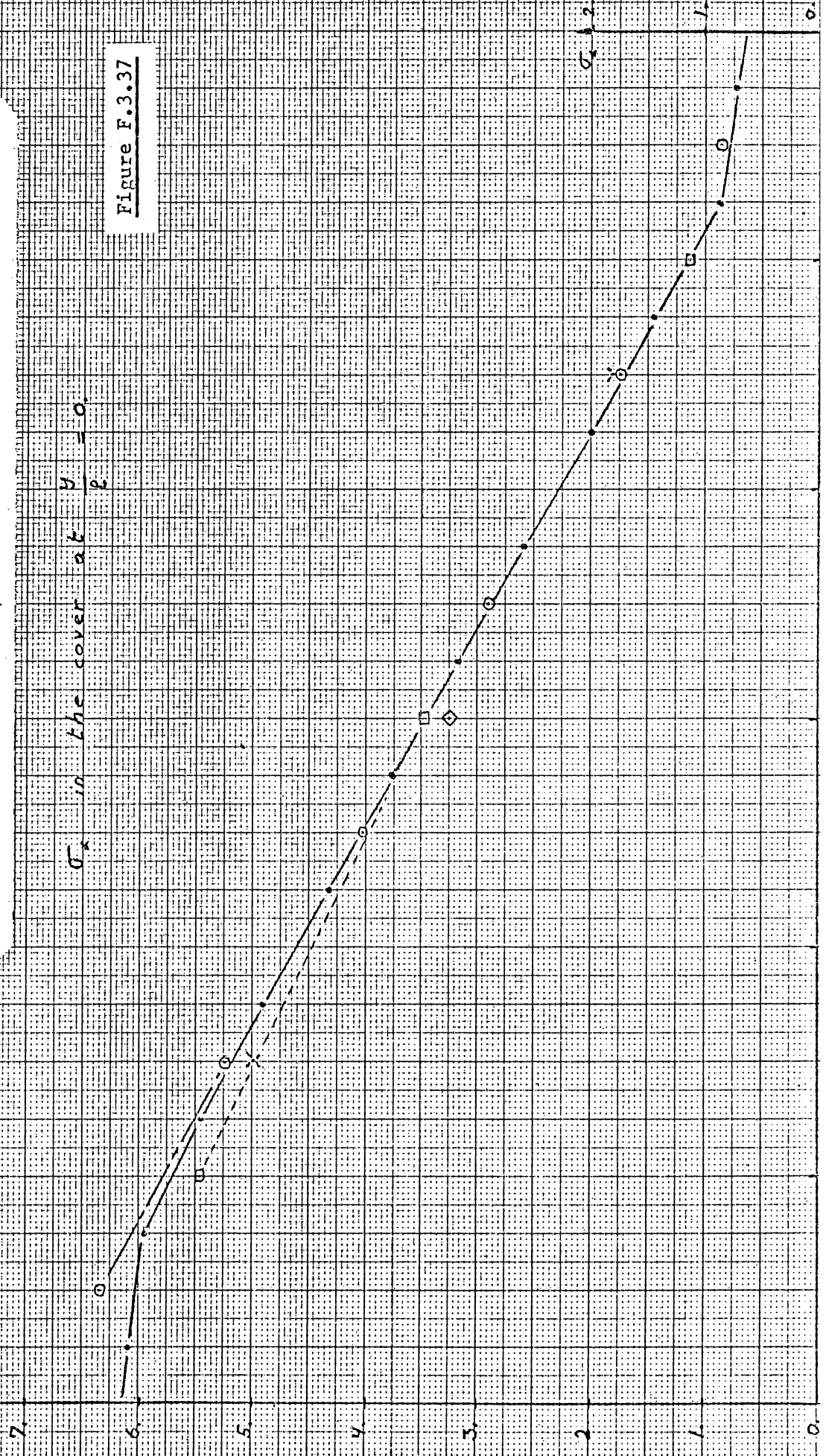


Figure F.3.37

B O X B E A M

Linear displacement Field

Bending - $t_s = 10$

Longitudinal distribution of σ_x in elements adjacent to $\frac{y}{I} = \frac{1}{2}$

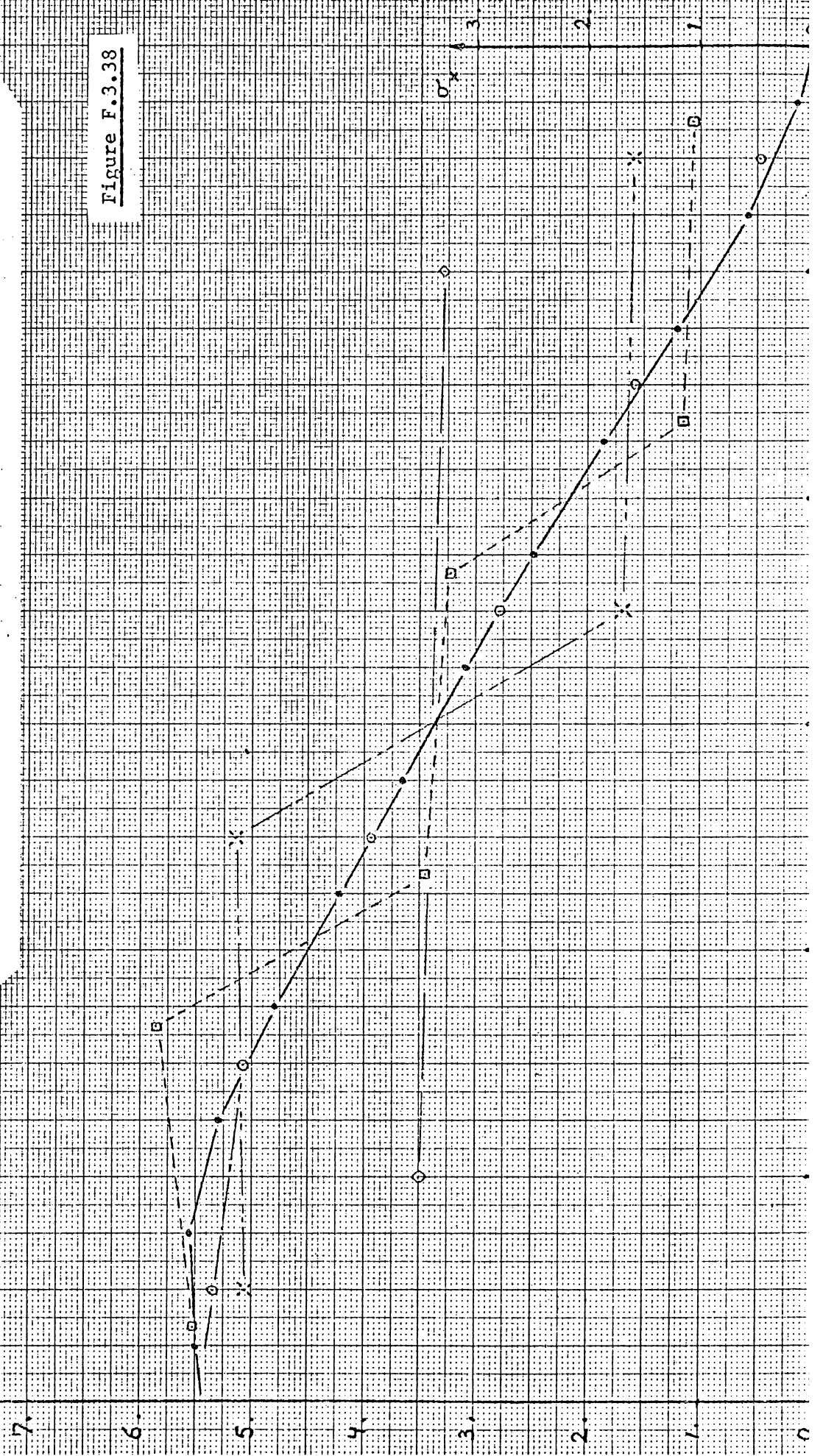
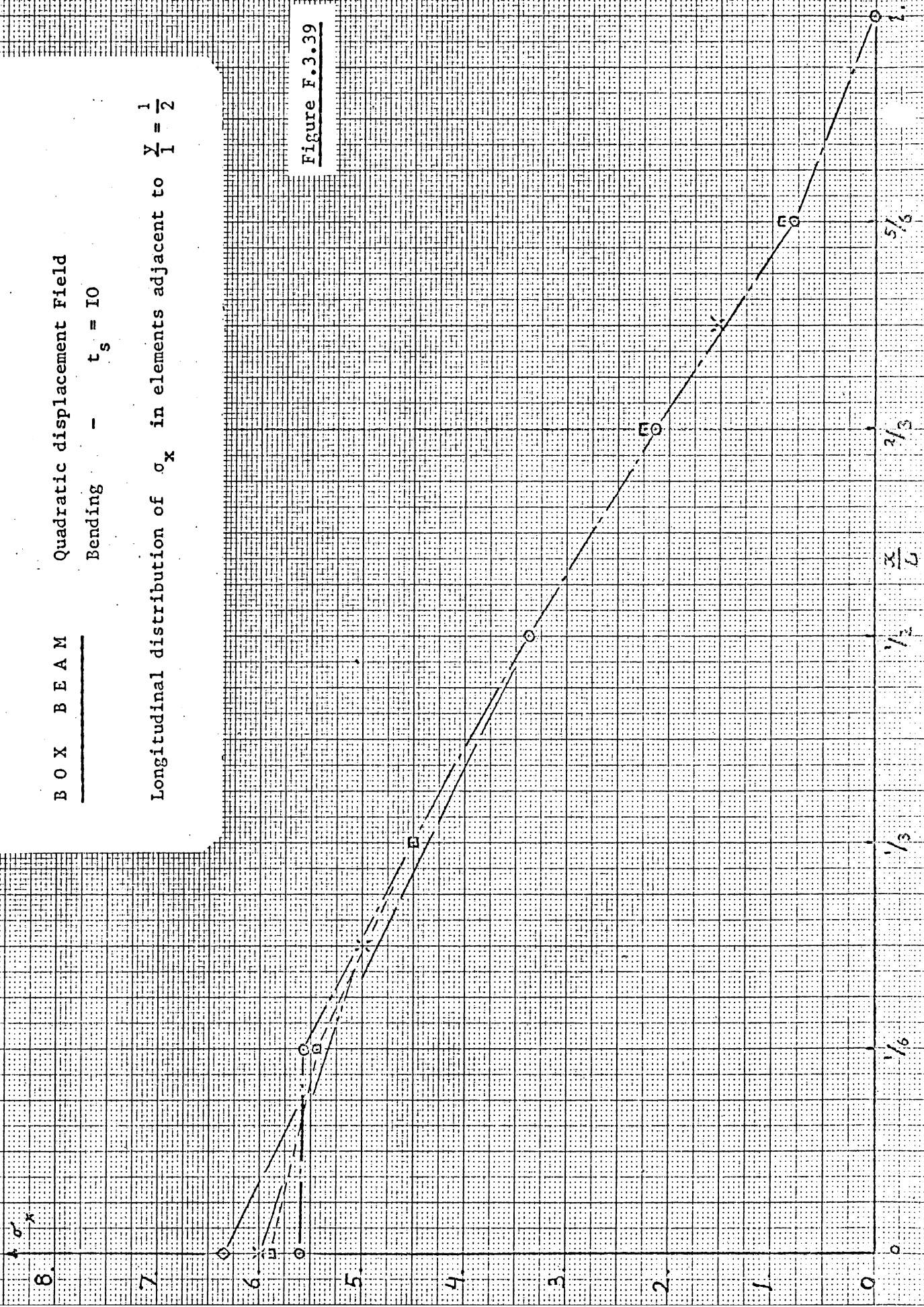


Figure F.3.38

BOX BEAM Quadratic displacement field

Bending - $t_s = 10$

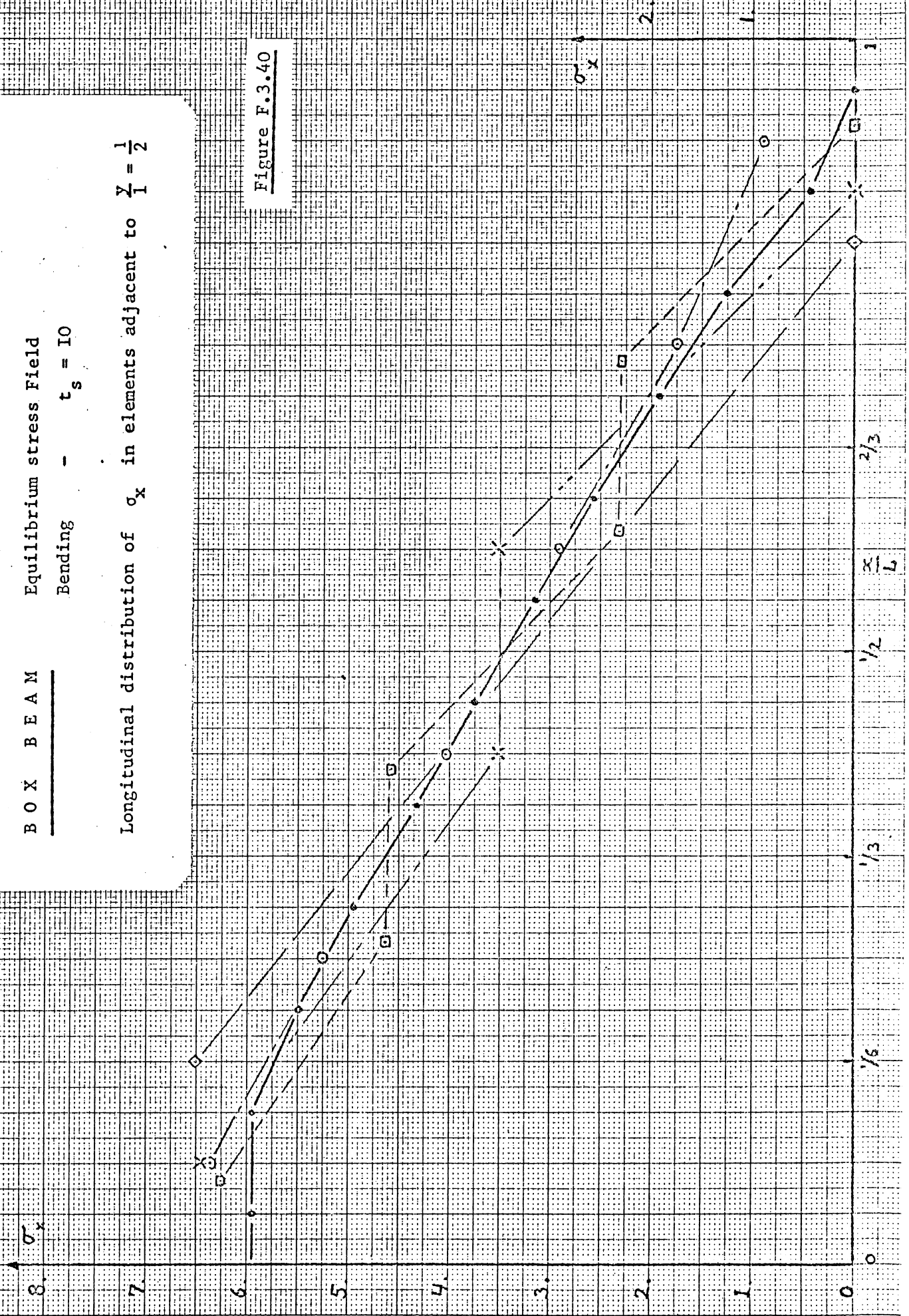
Longitudinal distribution of σ_x in elements adjacent to $\frac{y}{l} = \frac{1}{2}$



B O X B E A M Equilibrium stress field
 Bending - $t_s = 10$

Longitudinal distribution of σ_x in elements adjacent to $\frac{Y}{I} = \frac{1}{2}$

Figure F.3.40



B O X B E A M

Linear displacement field

Torsion - $t_s = 10$

Longitudinal distribution of σ_x in elements adjacent to $\frac{y}{I} = 0$
(without correction)

Figure F.3.4I

σ_x

15

14

13

12

11

10

9

8

7

6

5

4

3

2

1

0

1/6

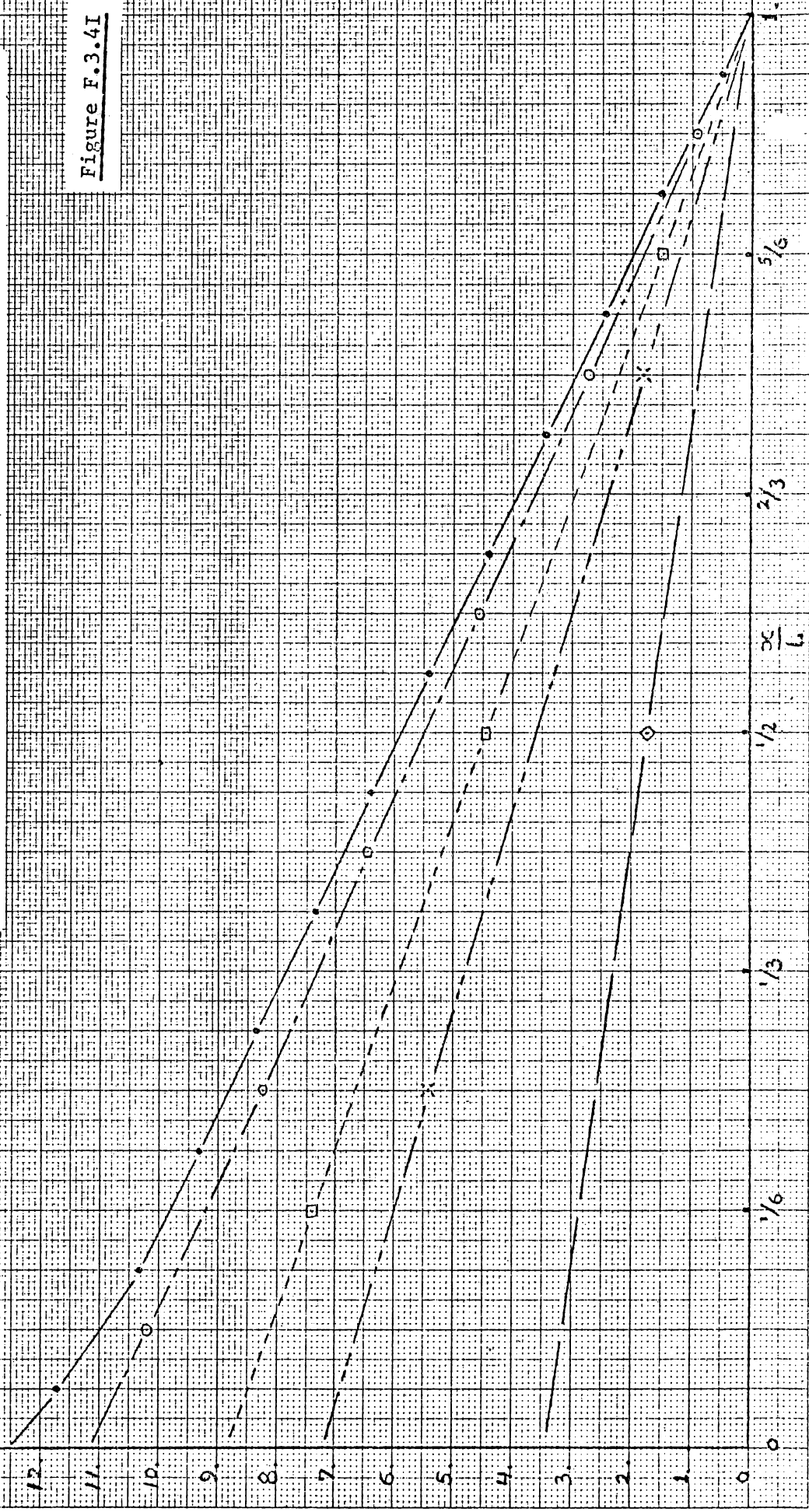
1/3

1/2

2/3

5/6

$\frac{x}{L}$



B O X B E A M

Quadratic displacement field

Torsion - $t_s = 10$

Longitudinal distribution of σ_x in elements adjacent to $\frac{y}{I} = 0$

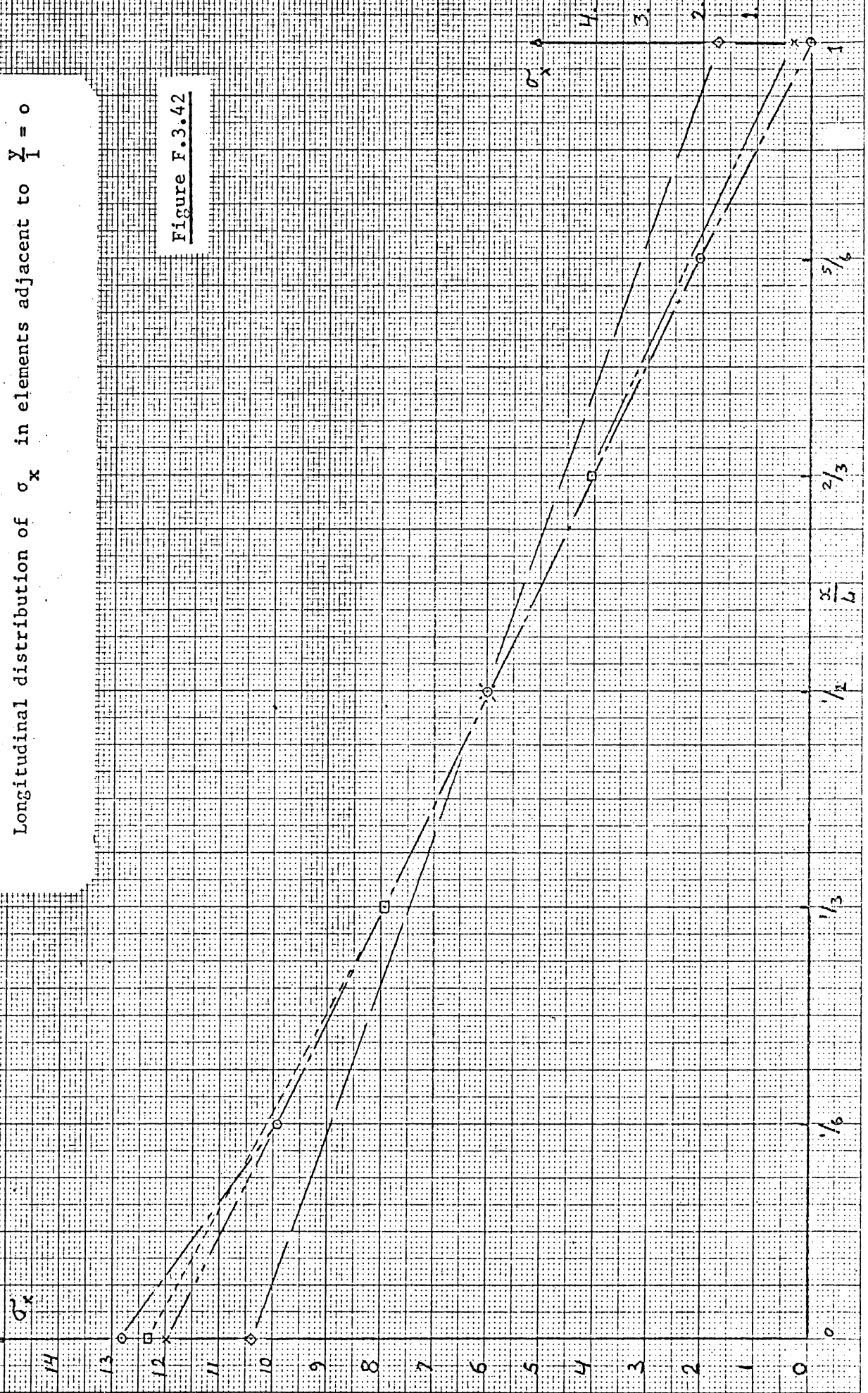


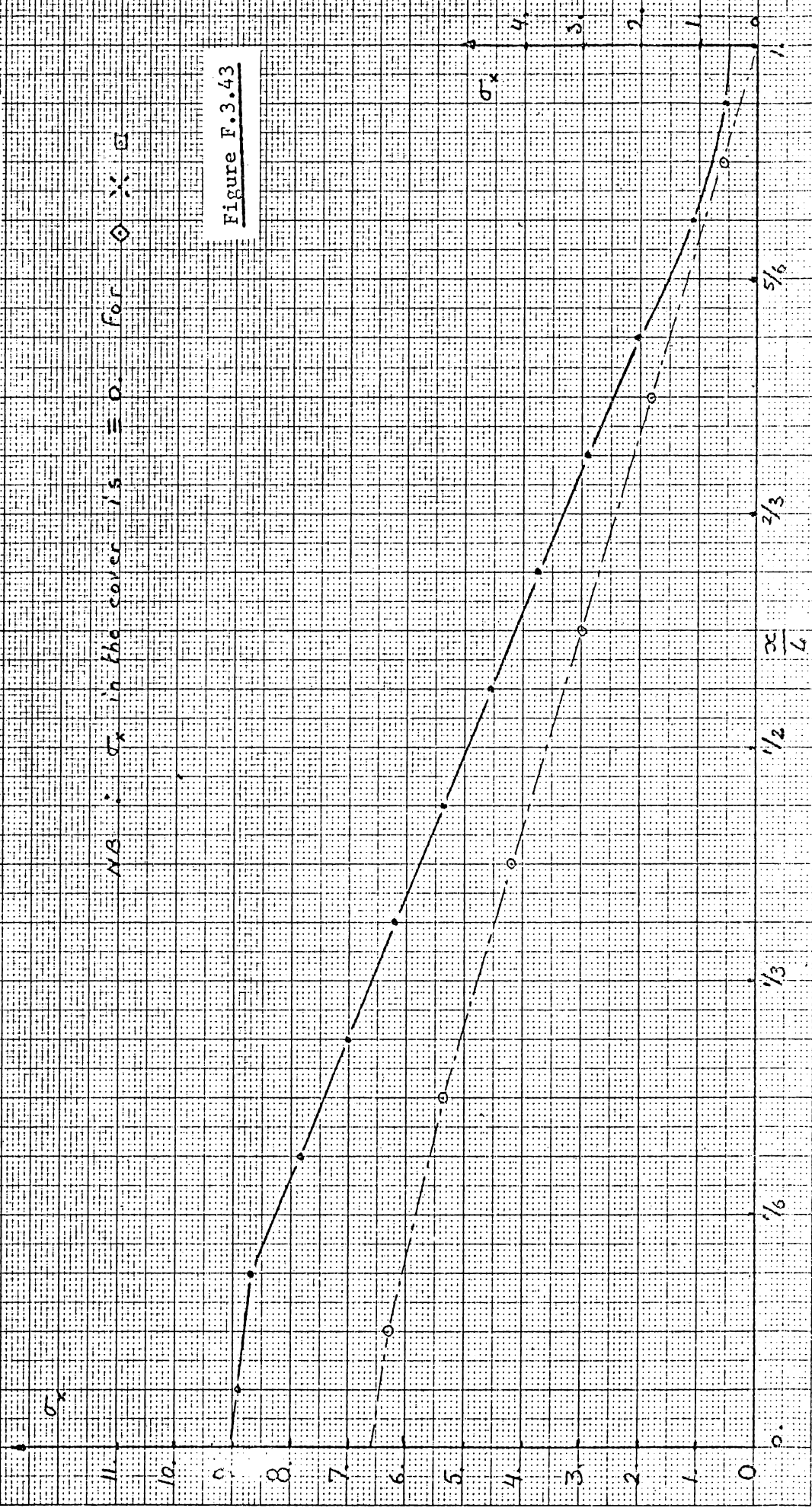
Figure F.3.42

B O X B E A M

Equilibrium stress field

Torsion - $t_s = 10$

Longitudinal distribution of σ_x in elements adjacent to $\frac{y}{I} = 0$
(without correction)



N.B. : σ_x in the cover is 0. For \diamond X \square

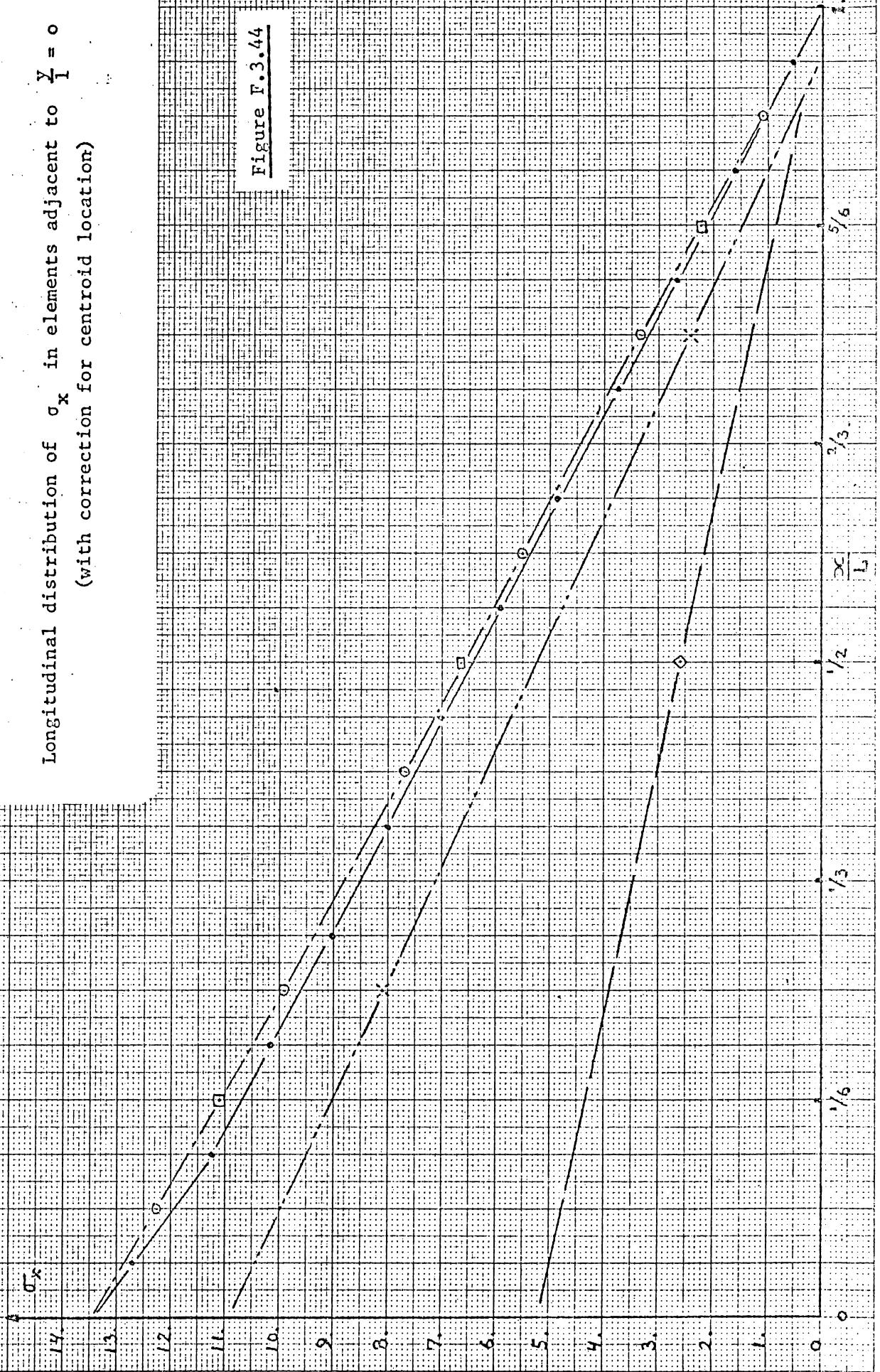
Figure F.3.43

B O X B E A M

Linear displacement field

Torsion - $t_s = 10$

Longitudinal distribution of σ_x in elements adjacent to $\frac{y}{l} = 0$
(with correction for centroid location)



B O X B E A M

Equilibrium stress field

Torsion - $t_s = 10$

Longitudinal distribution of σ_x in elements adjacent to $\bar{Y}_1 = 0$
(with correction for centroid location)

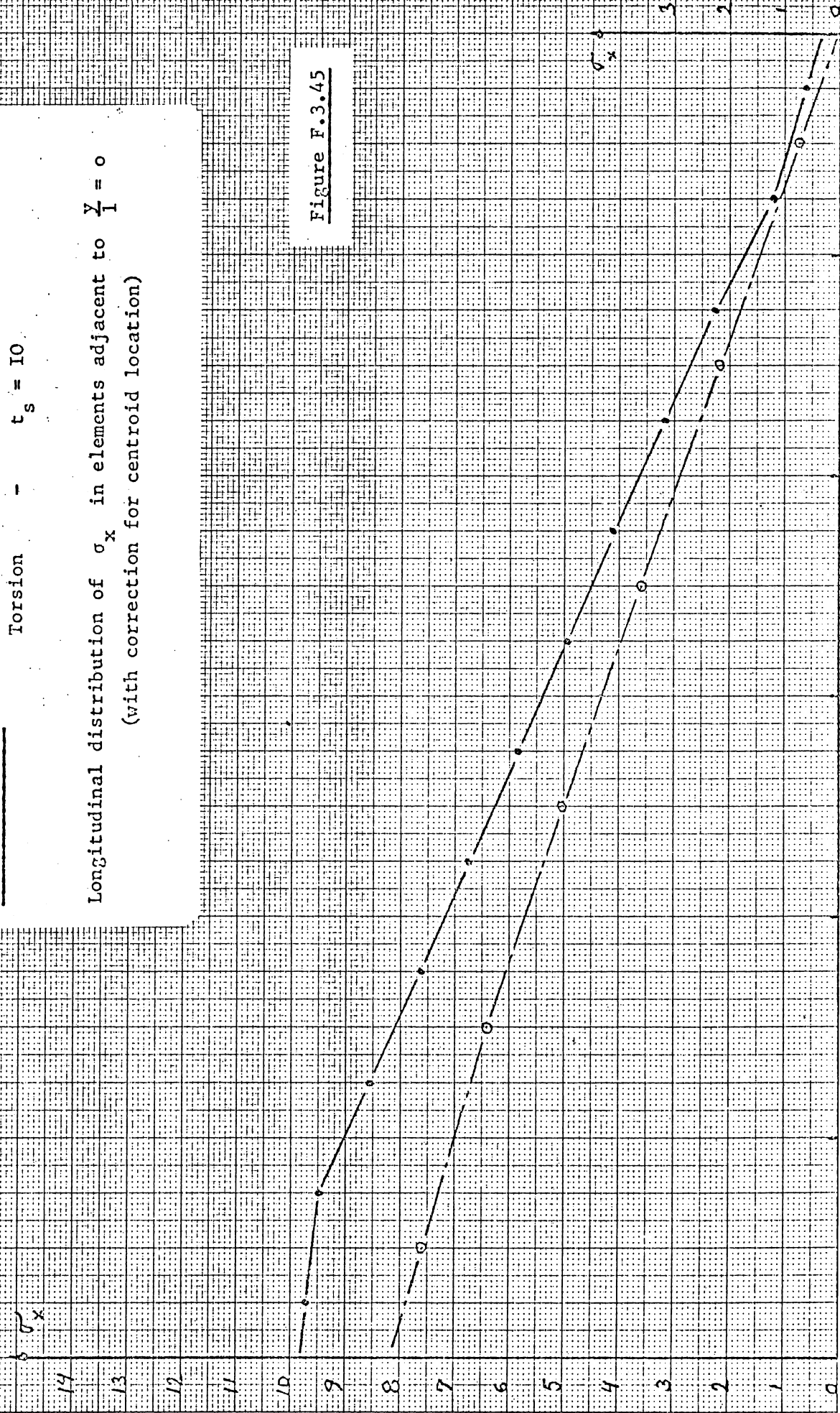


Figure F.3.45

B O X B E A M **Linear displacement Field**

Bending - - $t_s = 10$

Longitudinal distribution of τ_{xy} in elements adjacent to $\frac{y}{l} = 0$

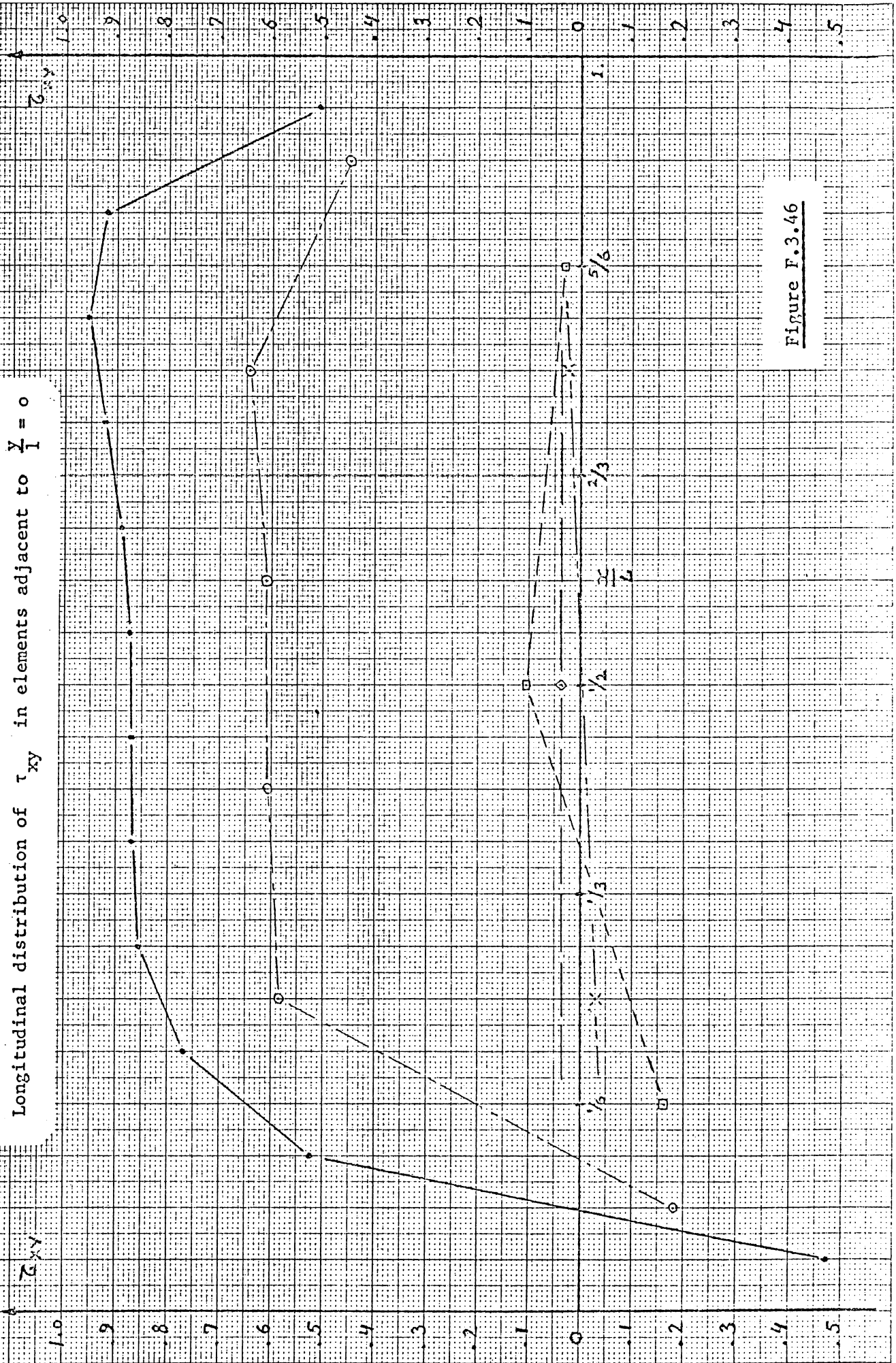


Figure F.3.46

B O X B E A M

Equilibrium stress field

Bending - $t_s = 10$

Longitudinal distribution of τ_{xy} in elements adjacent to $\frac{y}{I} = 0$



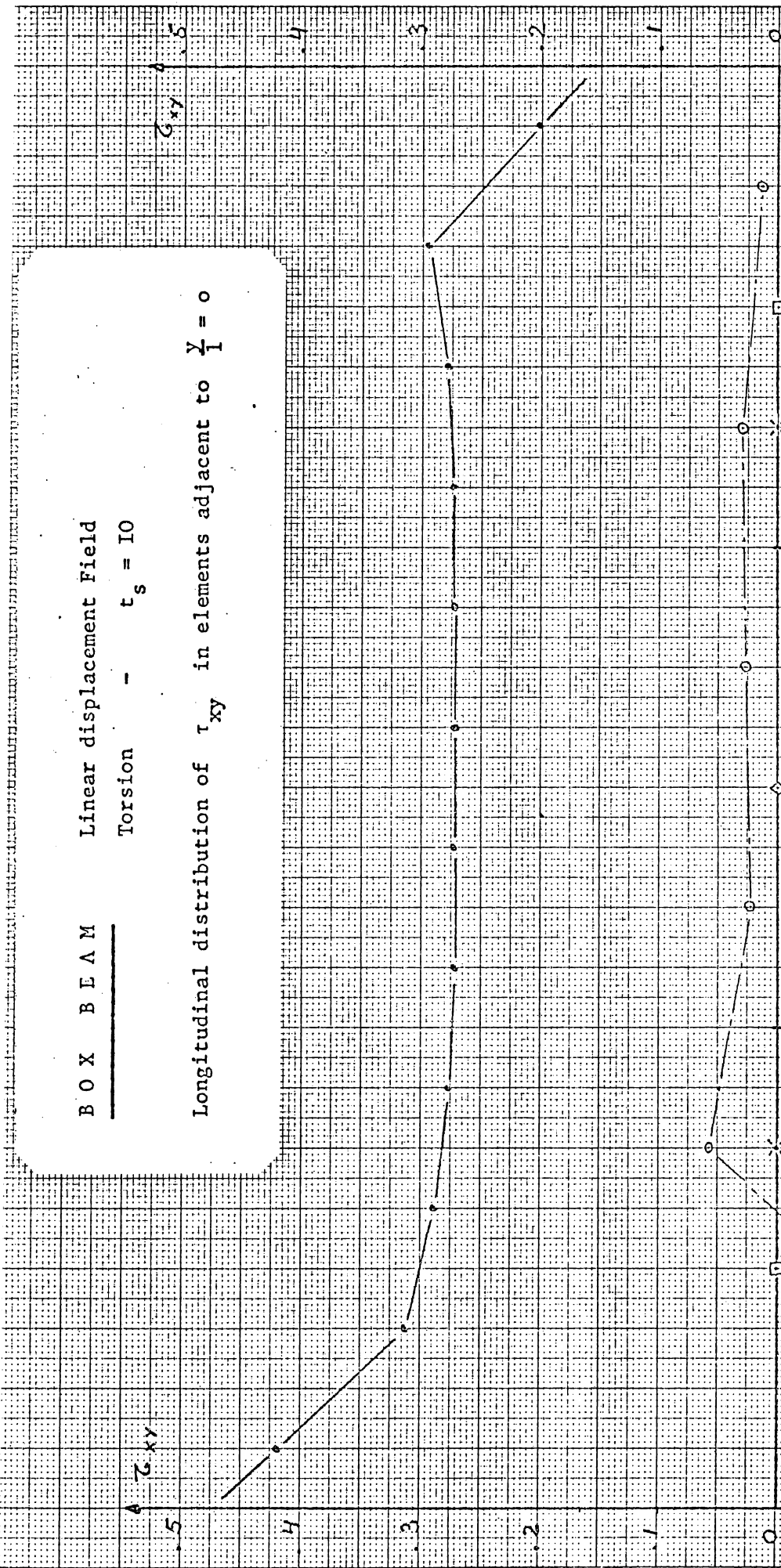
Figure F.3.48

BOX BEAM

Linear displacement Field

Torsion - $t_s = 10$

Longitudinal distribution of τ_{xy} in elements adjacent to $\frac{Y}{I} = 0$



B O X B E A M

Quadratic displacement field

Torsion

- $t_s = 10$

Longitudinal distribution of τ_{xy} in elements adjacent to $\frac{y}{l} = 0$

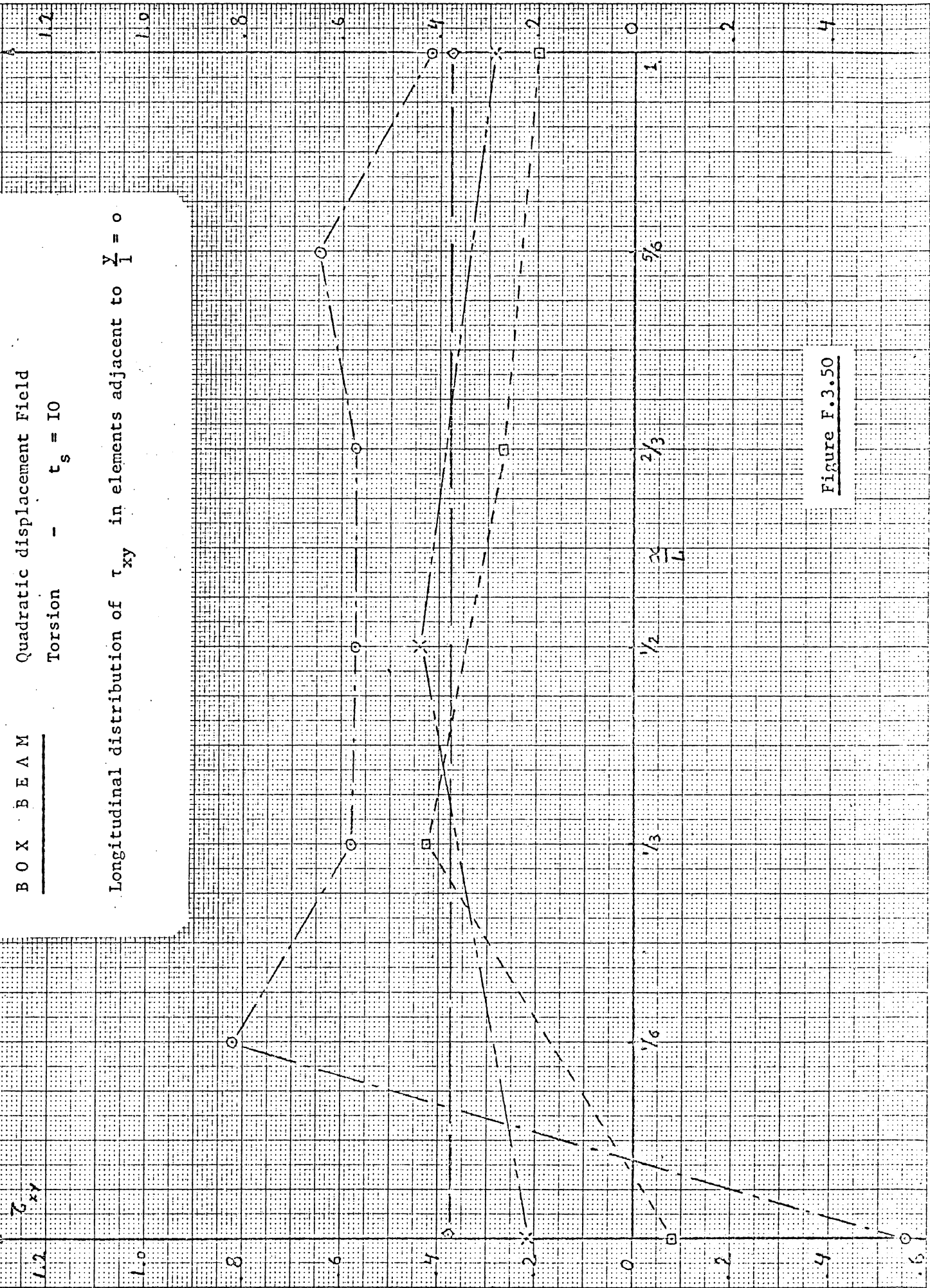


Figure F.3.50

B O X B E A M

Equilibrium stress field

Torsion - $t_s = 10$

Longitudinal distribution of τ_{xy} in elements adjacent to $\frac{Y}{I} = 0$

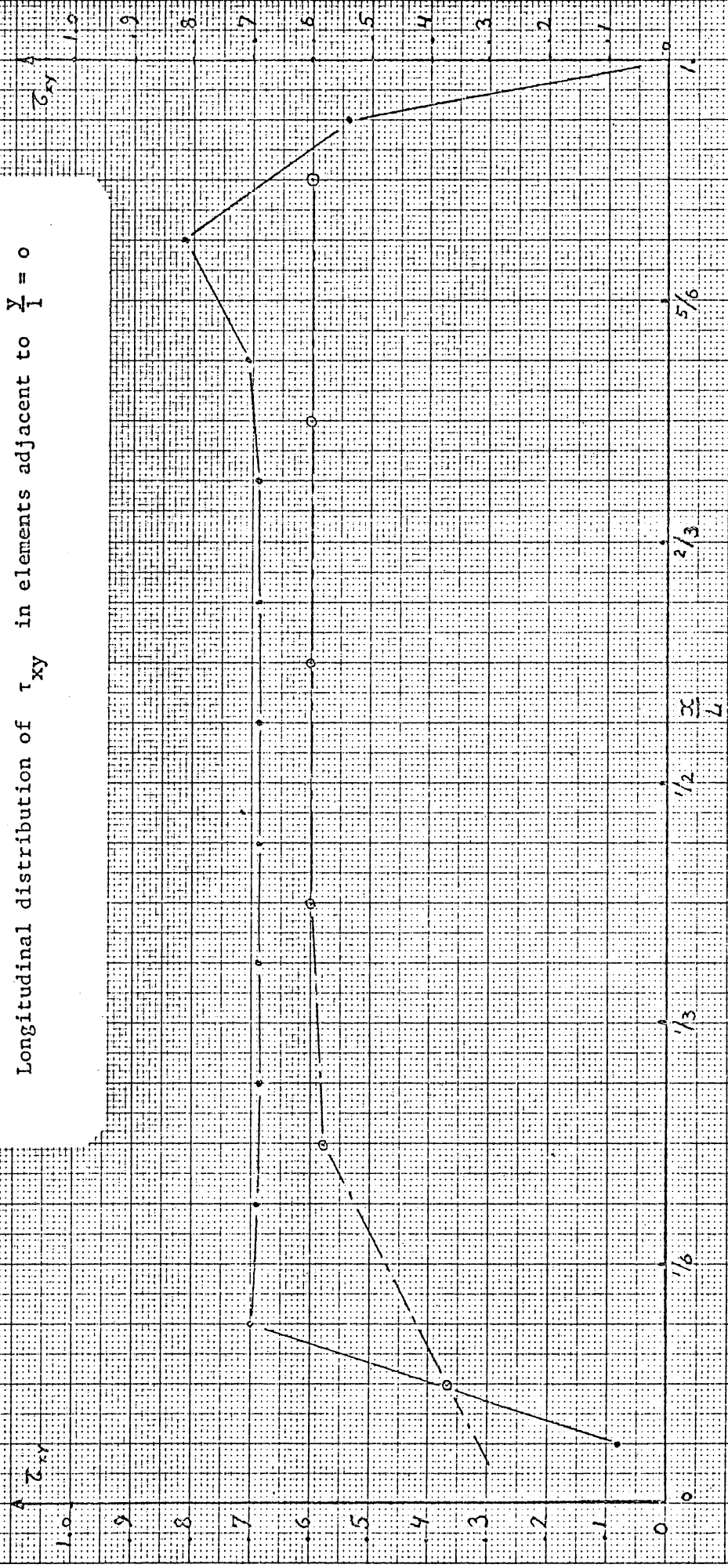


Figure F.3.5I

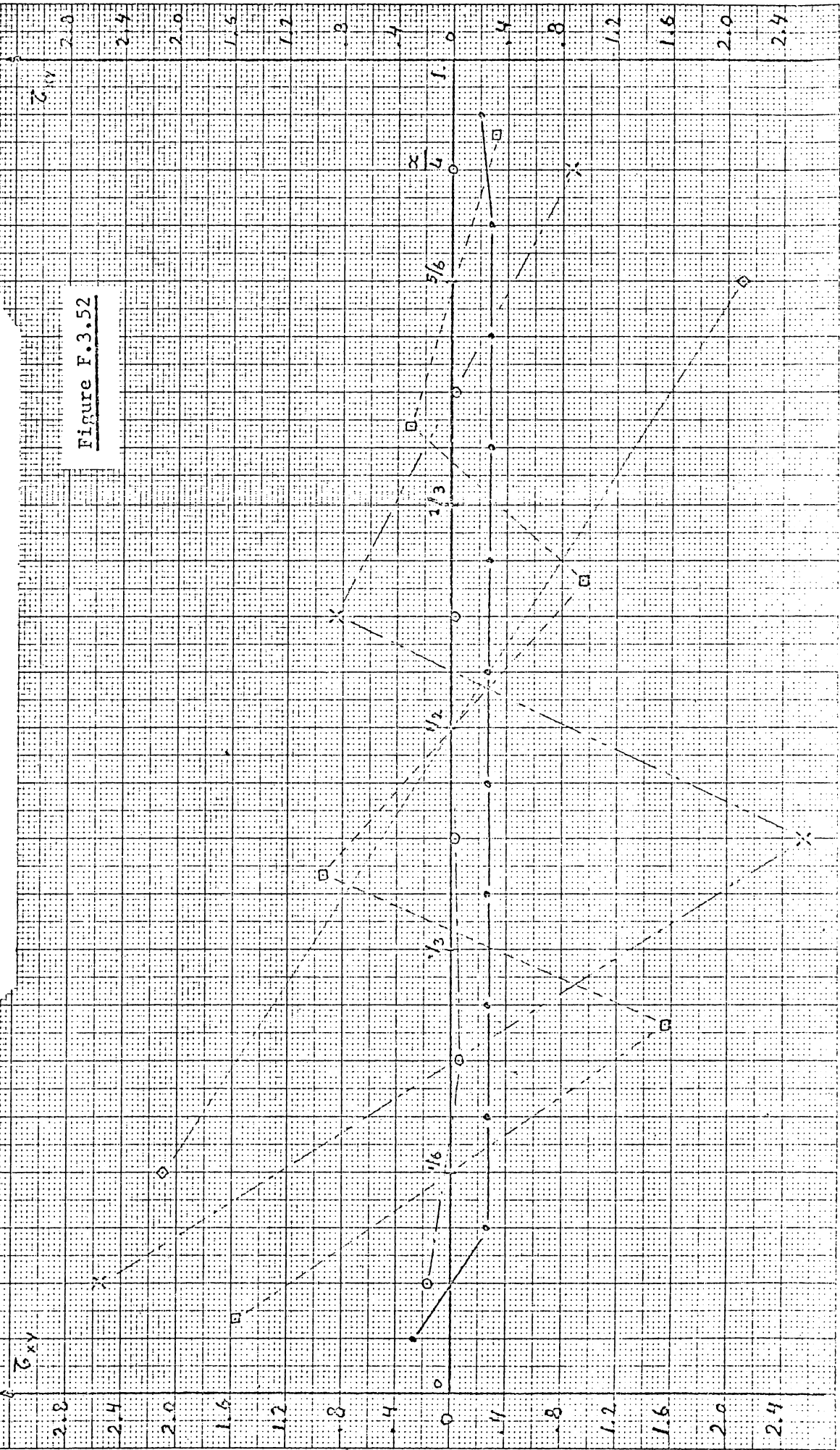
B O X B E A M

Linear displacement Field

Torsion -

$t_s = 10$

Transverse distribution of τ_{xy} at $\frac{x}{L} = \frac{1}{2}$



B O X B E A M

Quadratic displacement field

Torsion - $t_s = 10$

Longitudinal distribution of τ_{xy} in elements adjacent to $\frac{Y}{l} = \frac{1}{2}$

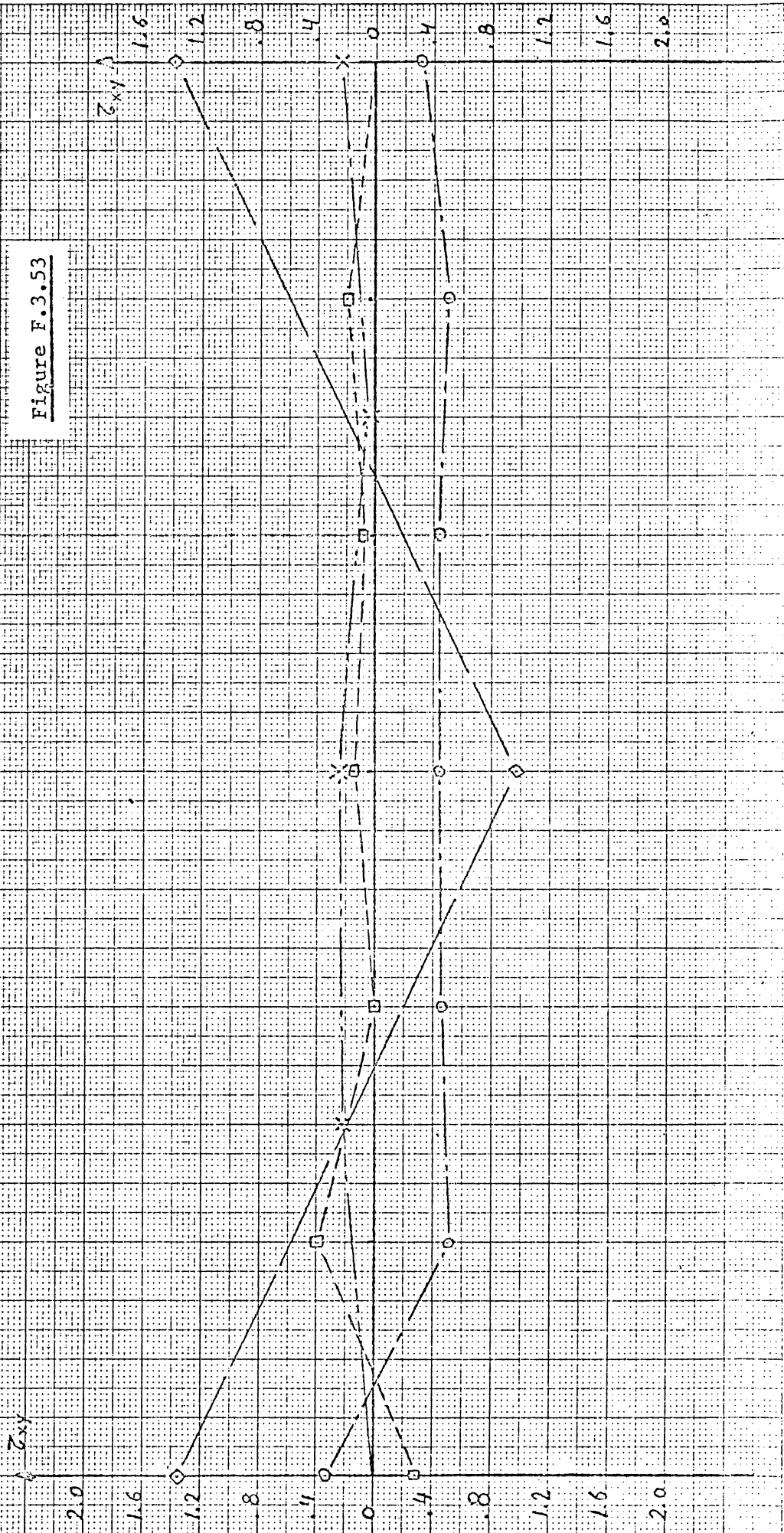


Figure F.3.53

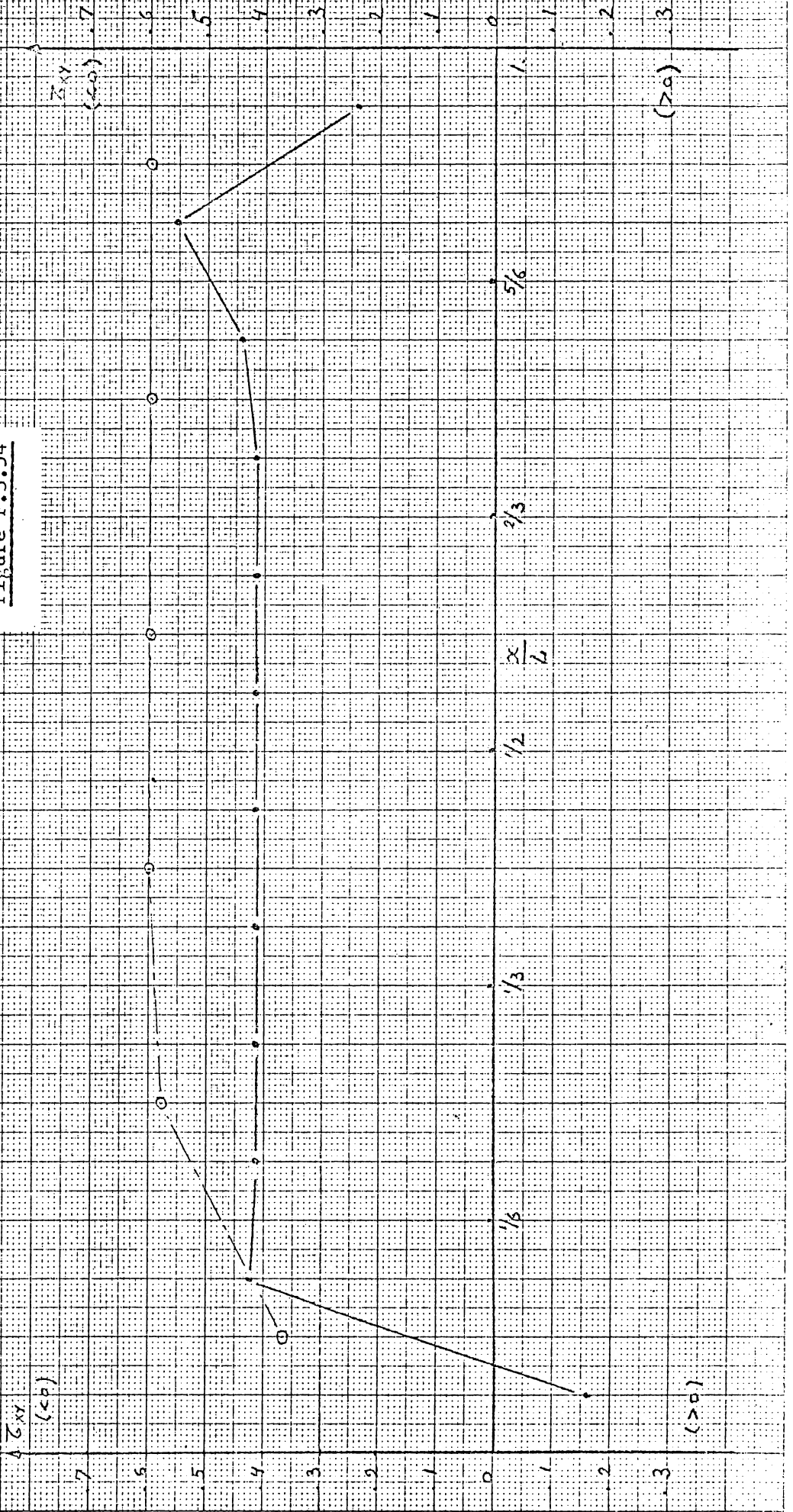
BOX BEAM

Equilibrium stress Field

Torsion - $t_s = 10$

Longitudinal distribution of τ_{xy} in elements adjacent to $\frac{Y}{I} = \frac{1}{2}$.

Figure F.3.54



B O X B E A M

Quadratic displacement field

Bending - $t_s = 10$

Longitudinal distribution of σ_y in elements adjacent to $\frac{Y}{I} = 0$

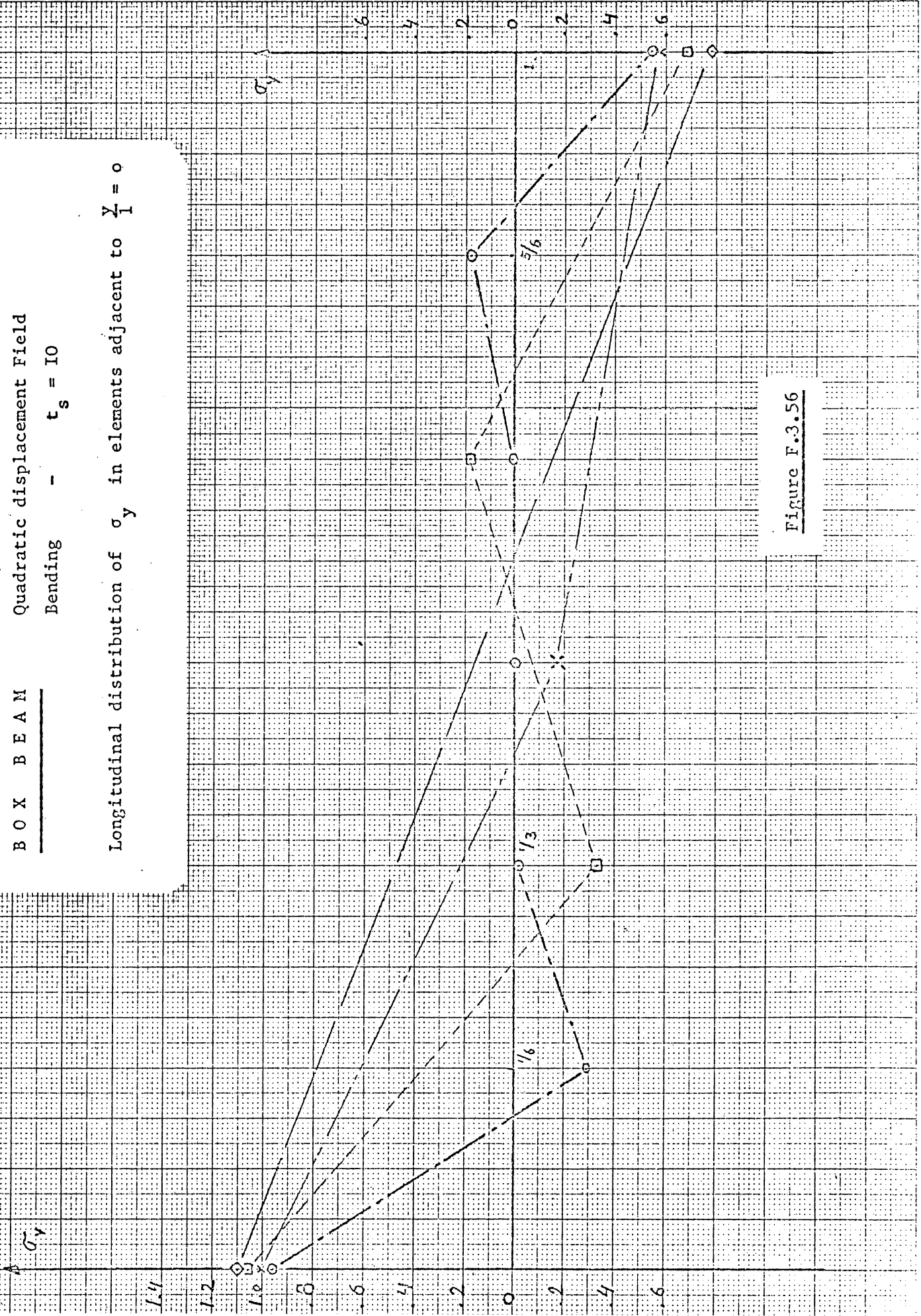


Figure F.3.56

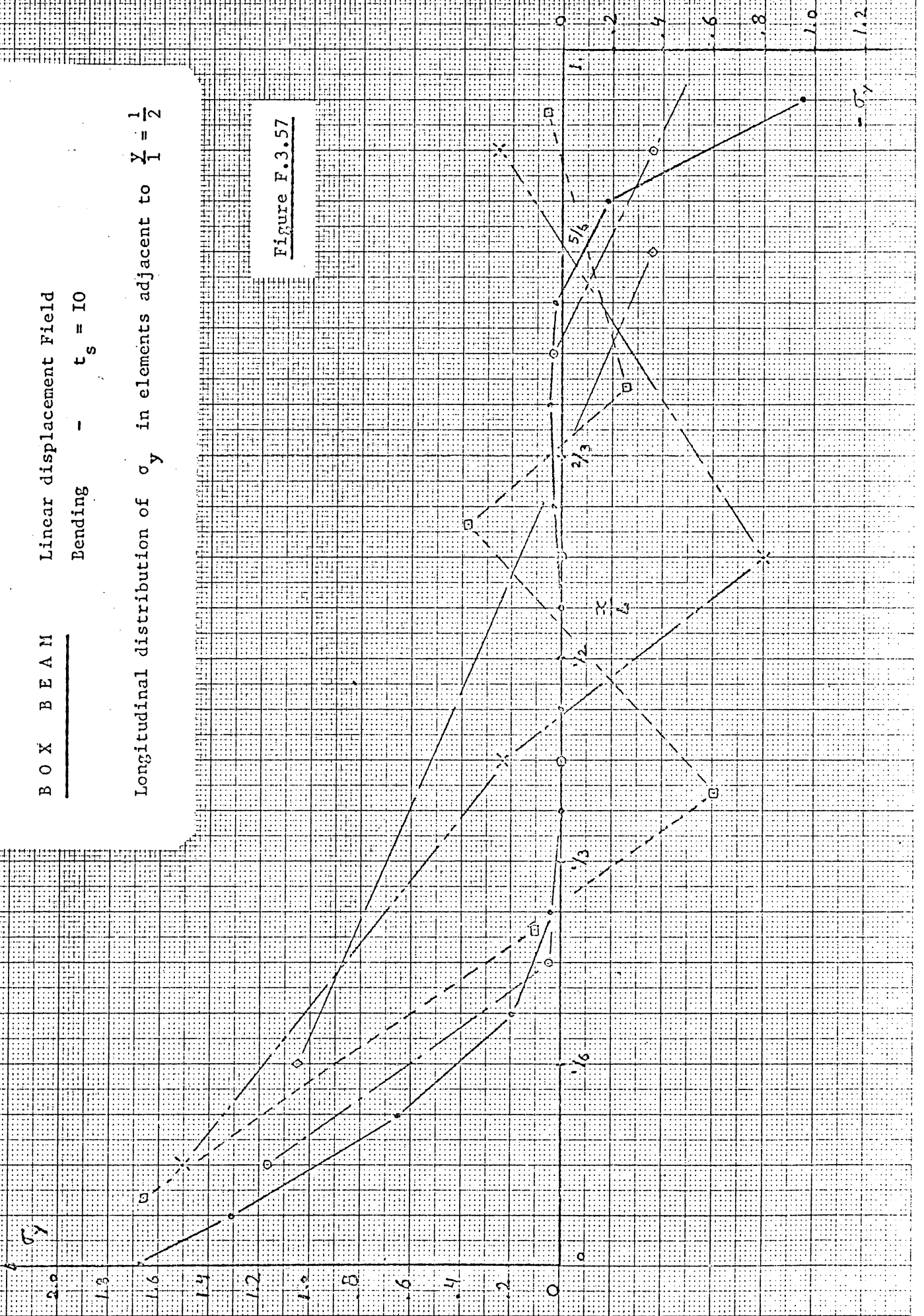
BOX BEAM

Linear displacement field

Bending - $t_s = 10$

Longitudinal distribution of σ_y in elements adjacent to $Y = \frac{1}{2}$

Figure F.3.57

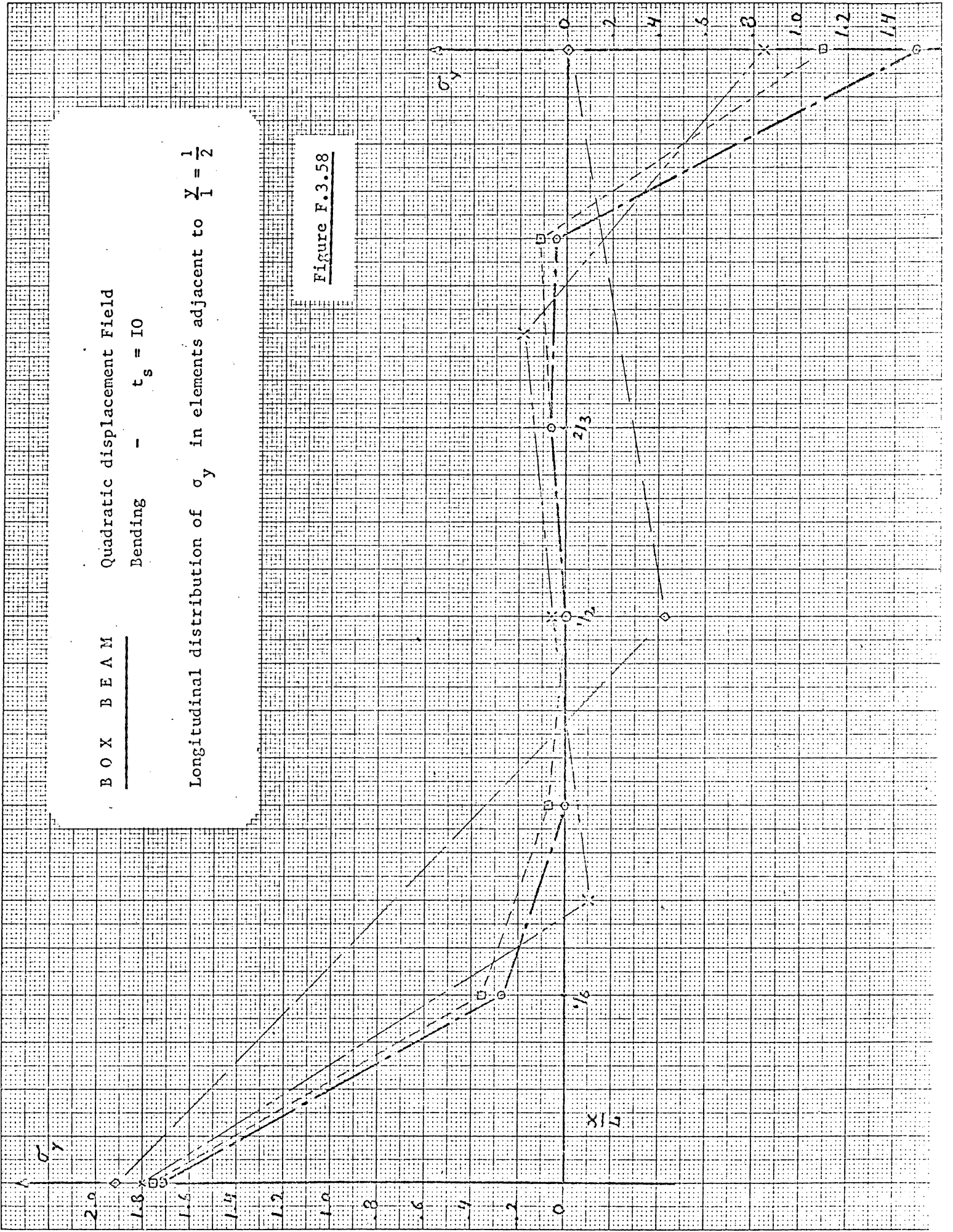


BOX BEAM Quadratic displacement field

Bending - $t_s = 10$

Longitudinal distribution of σ_y in elements adjacent to $\frac{Y}{I} = \frac{1}{2}$

Figure F.3.58



B O X B E A M

Equilibrium stress field

Bending - $t_s = 10$

Longitudinal distribution of σ_y in elements adjacent to $\frac{y}{I} = \frac{1}{2}$

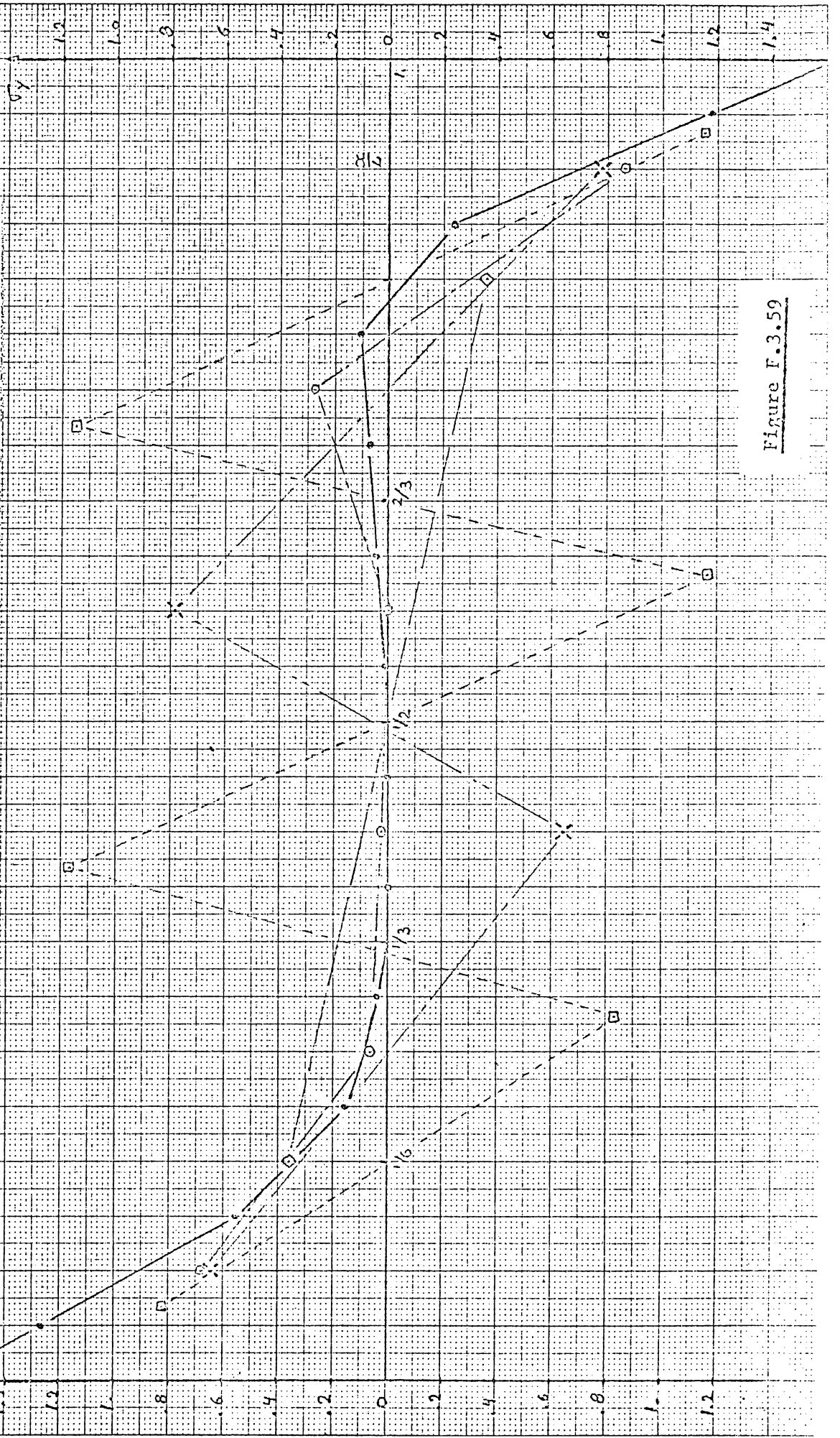


Figure F.3.59

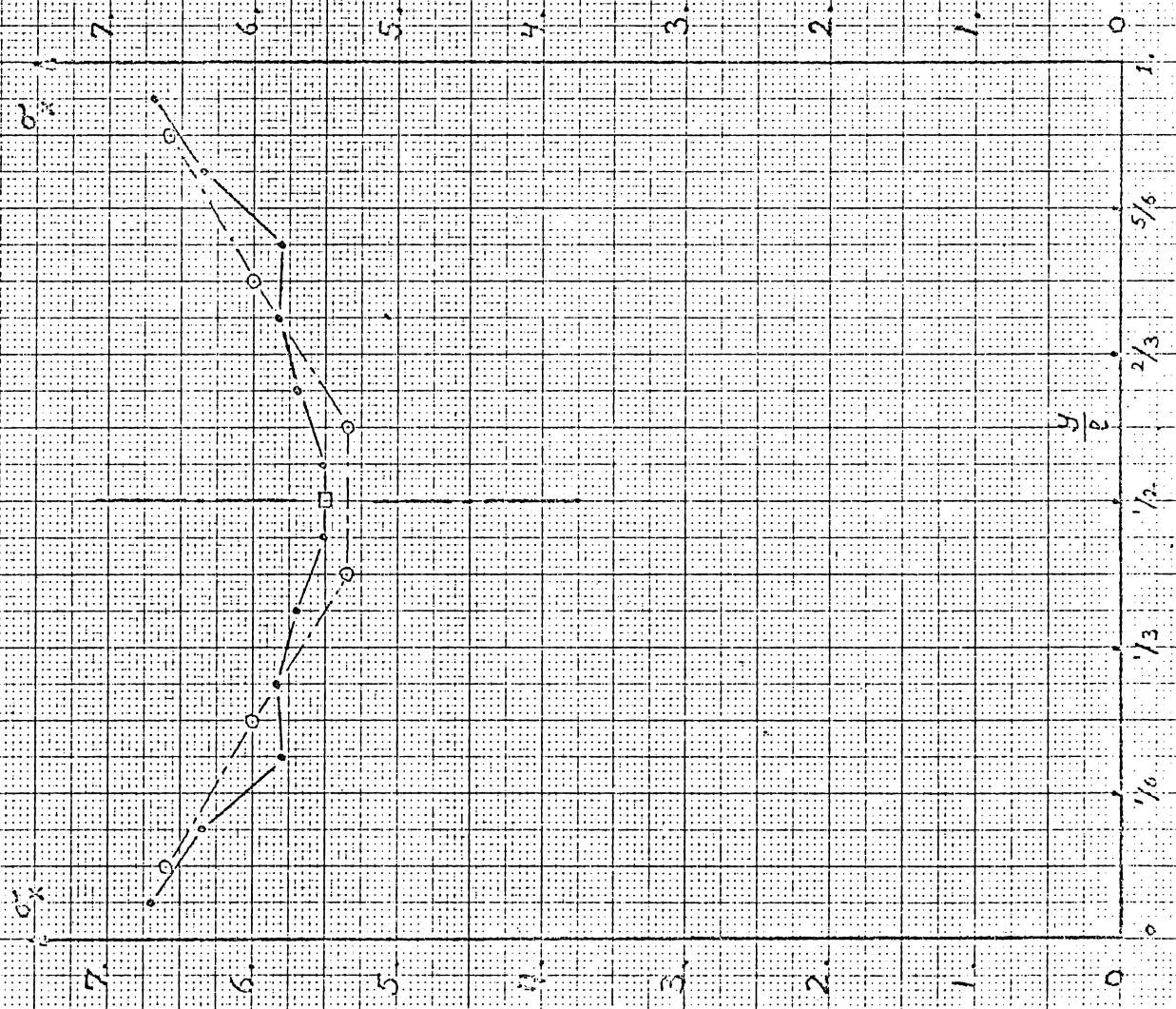
B O X B E A M

Linear displacement Field

Bending - $t_s = 10$

Transverse distribution of σ_x at $\frac{x}{L} = \frac{1}{12}$

Figure F.3.60



BOX BEAM Quadratic displacement field

Bending - $t_s = 10$

Transverse distribution of σ_x at $\frac{x}{L} = \frac{1}{12}$

Figure F.3.6I



B O X B E A M

Equilibrium stress field

Bending - $t_s = 10$

Transverse distribution of σ_x at $\frac{x}{L} = \frac{1}{12}$

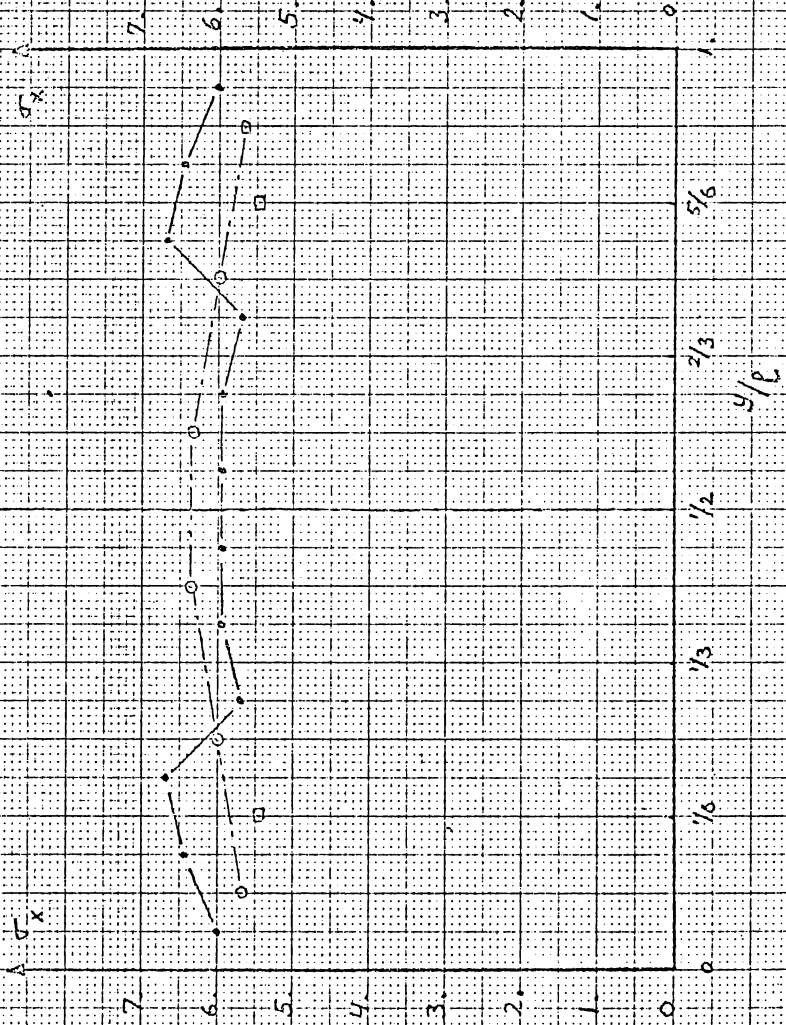


Figure F.3.62

B O X B E A M Linear displacement Field
 Torsion - $t_s = I\theta$

Transverse distribution of σ_x at $\frac{x}{L} = \frac{1}{12}$

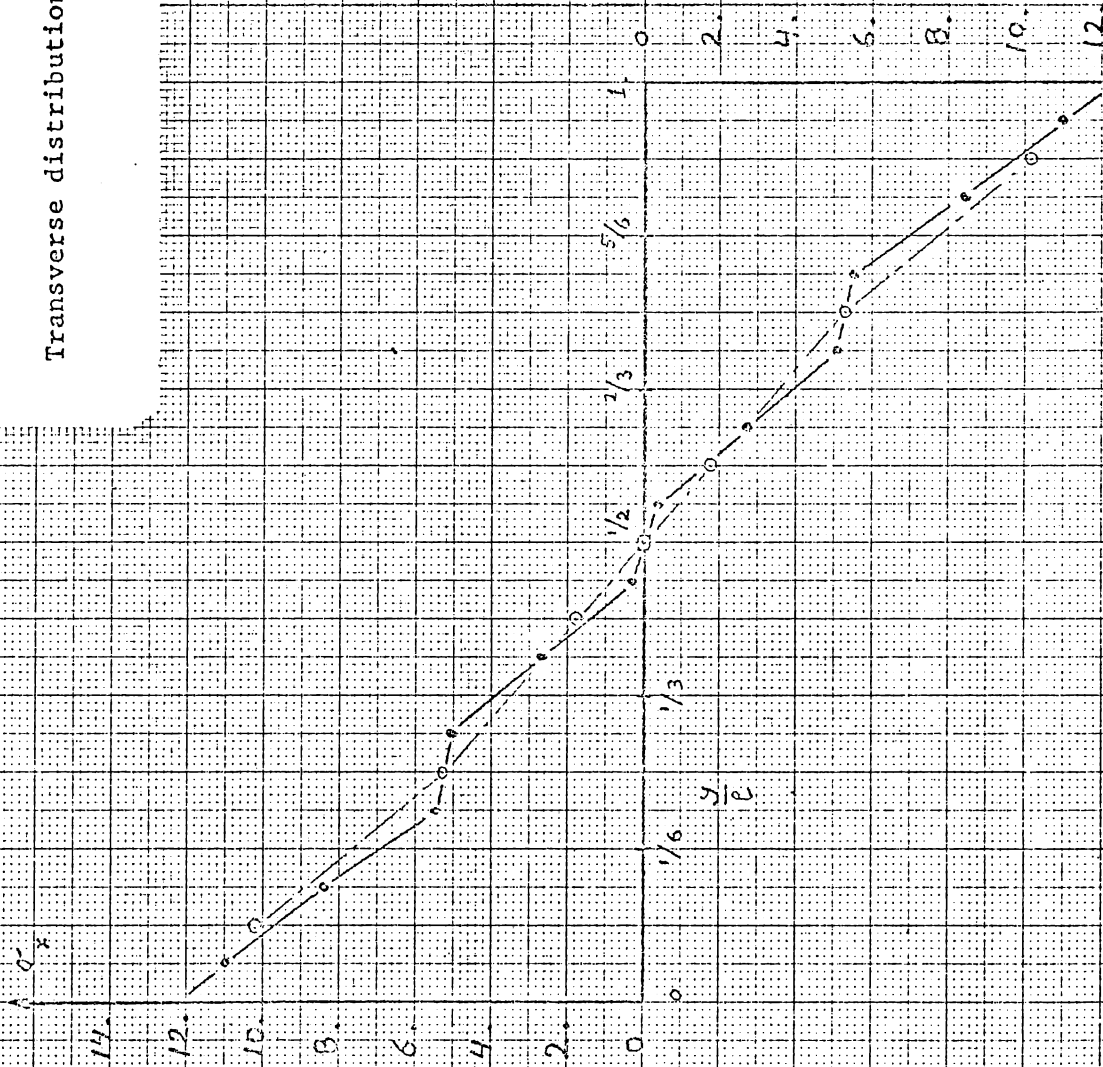


Figure F.3.63

B O X B E A M

Quadratic displacement field

Torsion

$t_s = 10$

Transverse distribution of σ_x at $\frac{x}{L} = \frac{1}{12}$

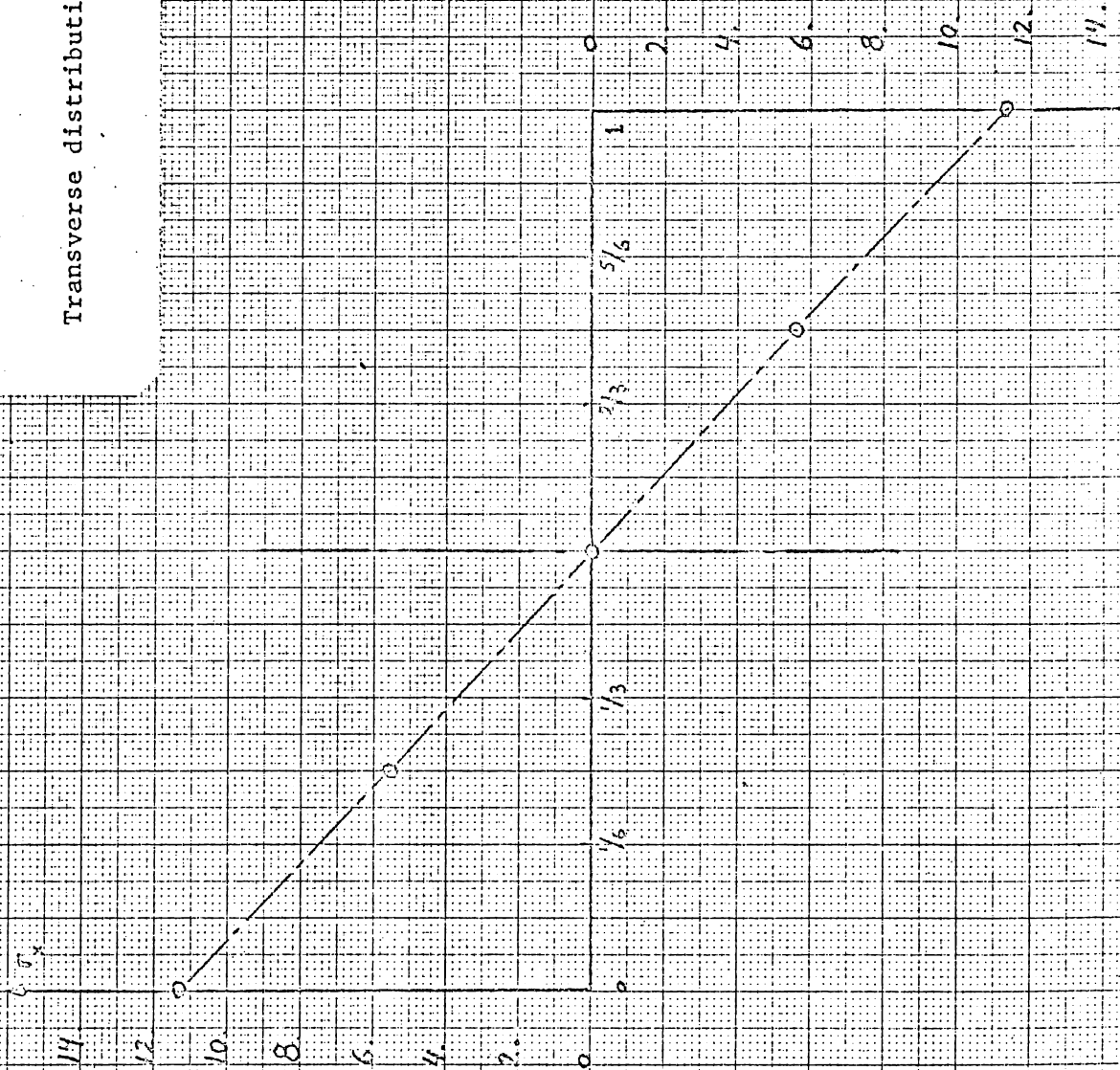


Figure F.3.64

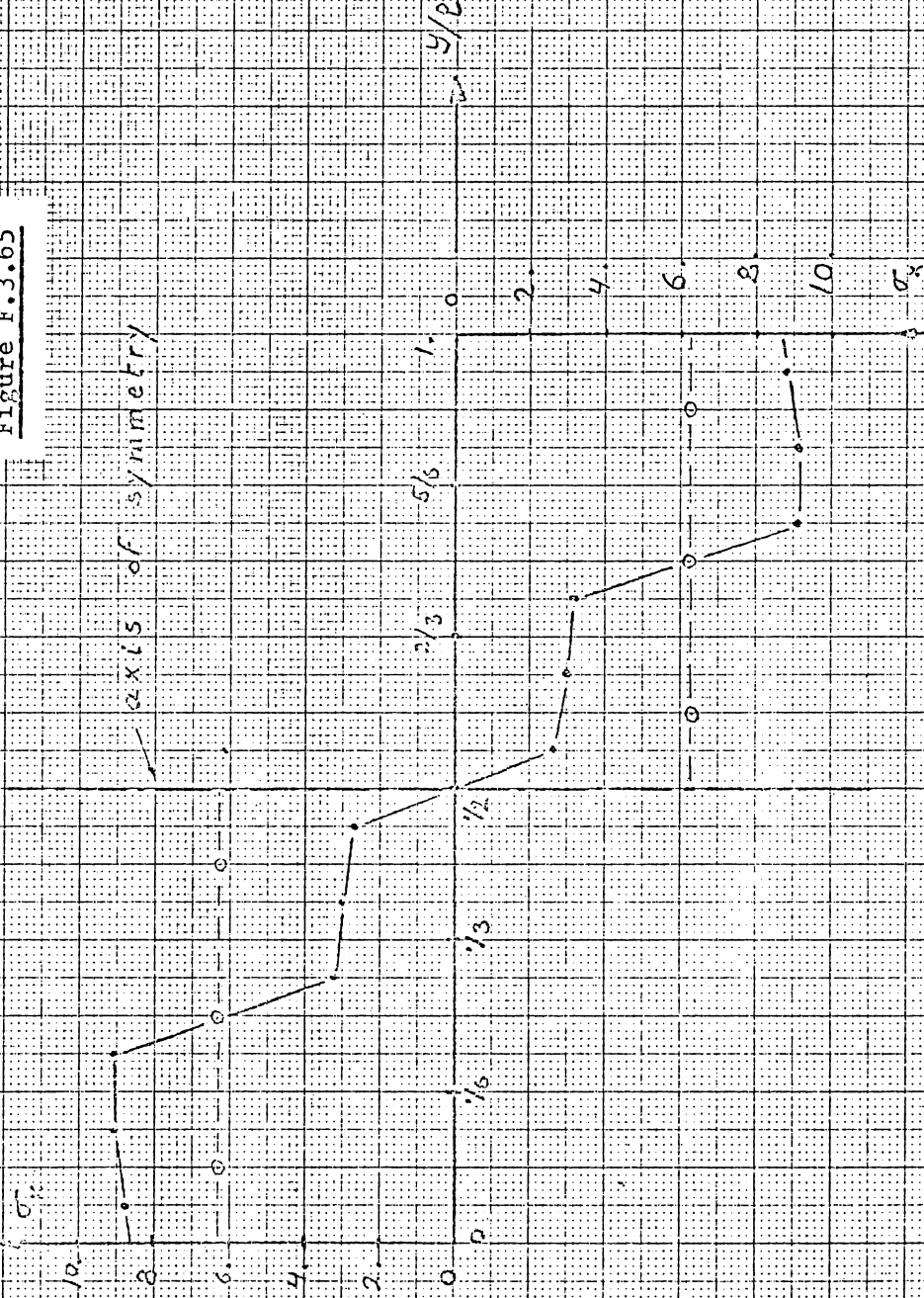
B O X B E A M

Equilibrium stress field

Torsion - $t_s = 10$

Transverse distribution of σ_x at $\frac{x}{L} = \frac{1}{12}$

Figure F.3.65



NB: for $\sigma_x = 0$

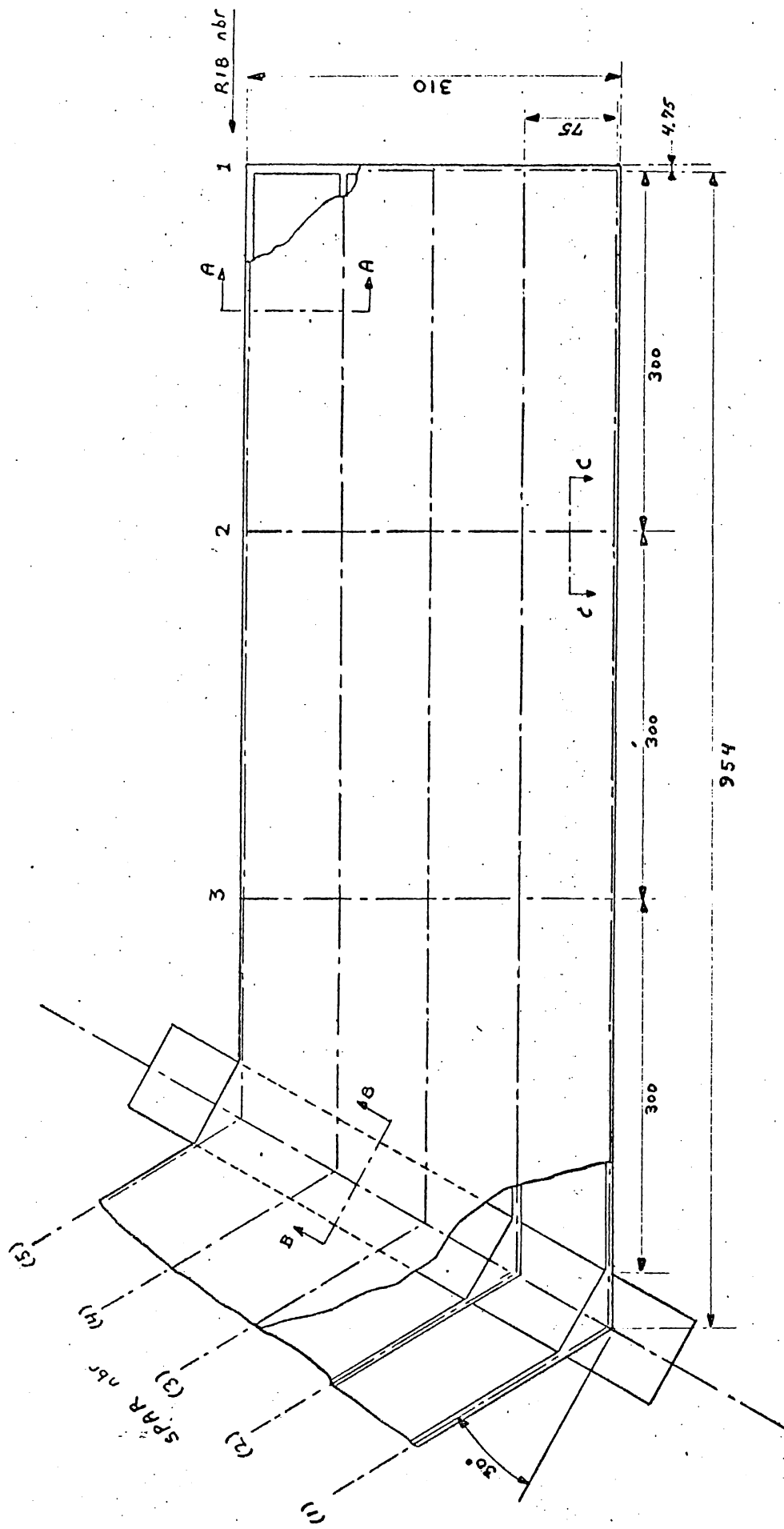
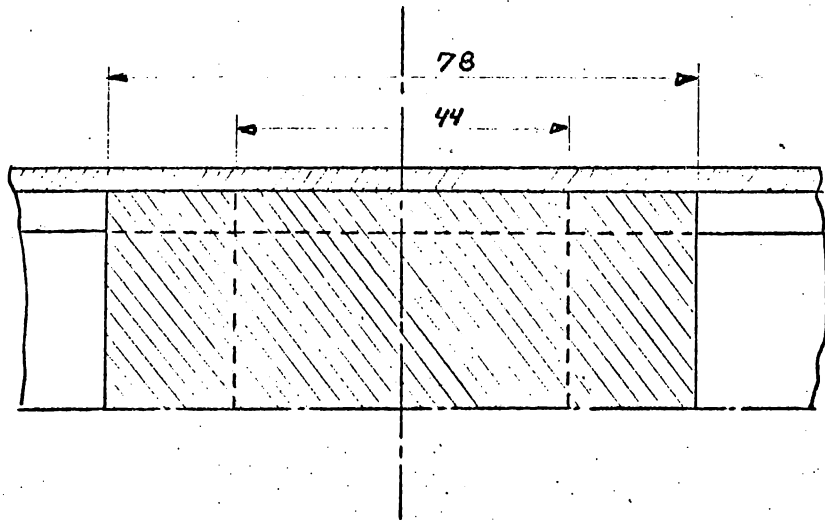
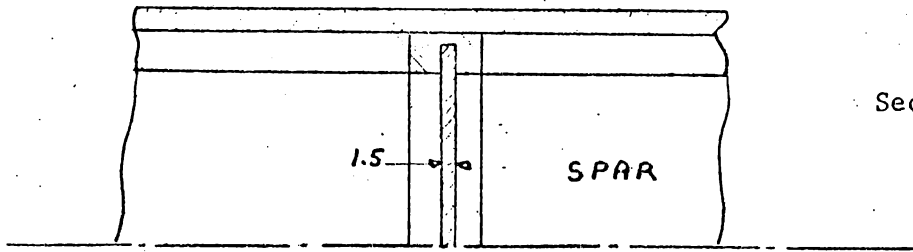
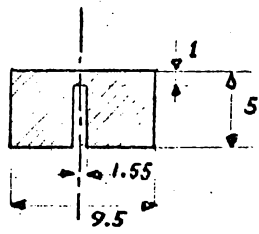
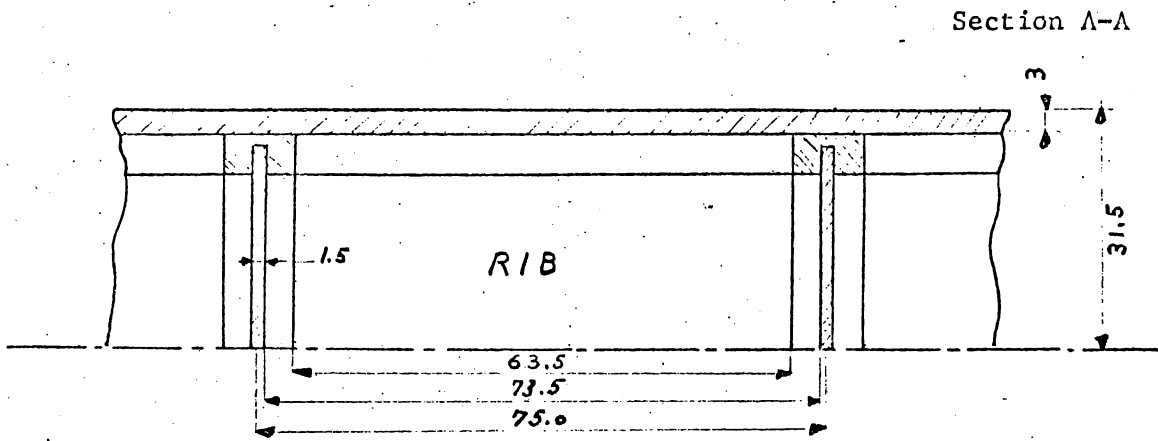


Figure F.3.66. The physical structure of the swept back wing model.

Figure F.3.67.

Details of the structure :



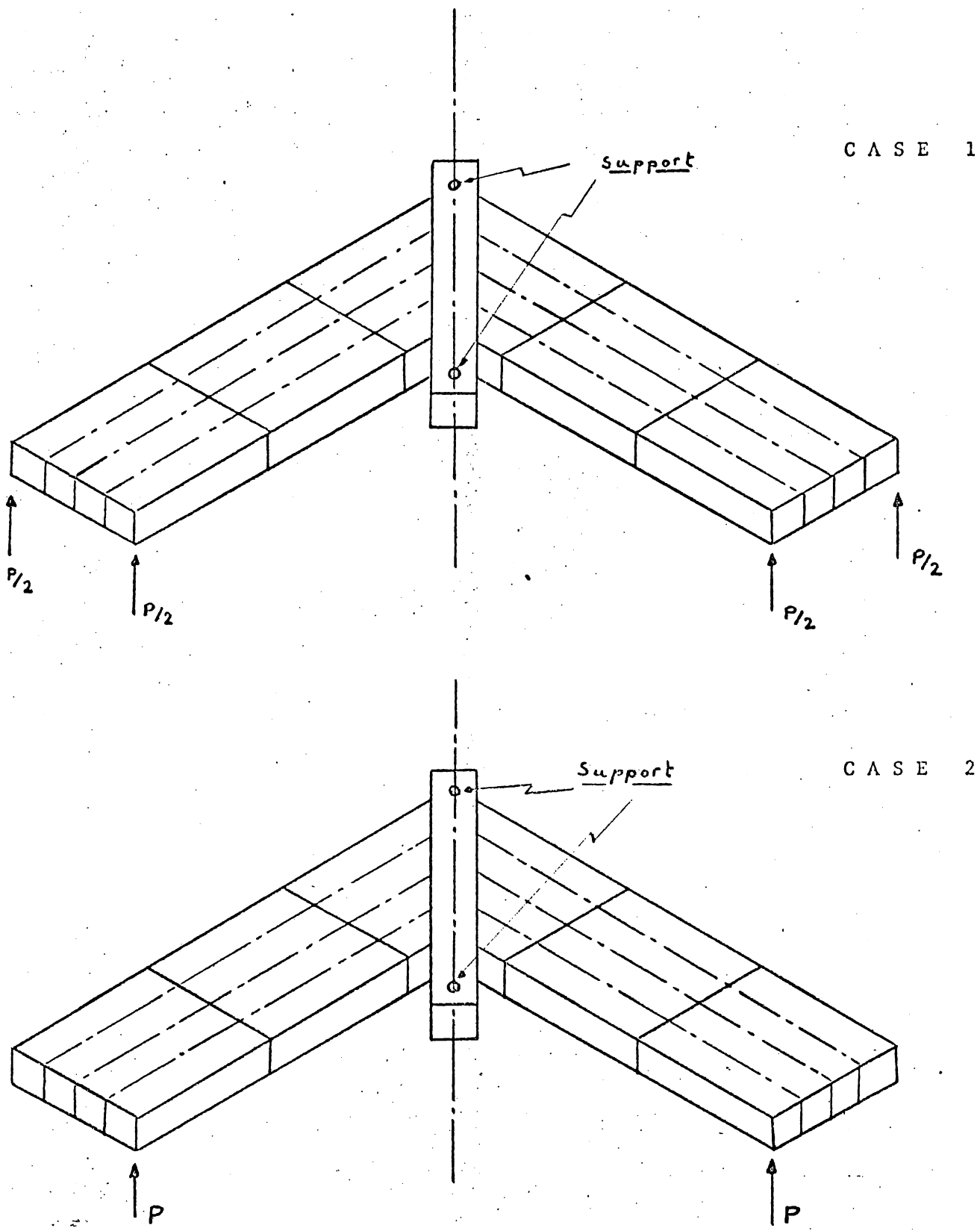


Figure F.3.68. Loading cases.

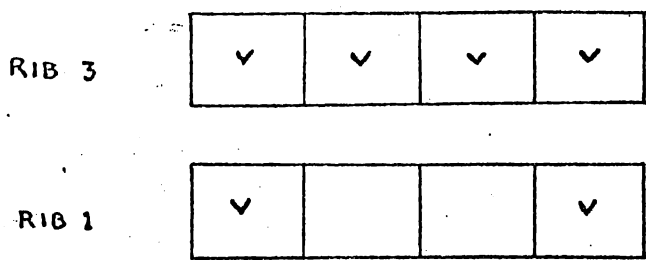
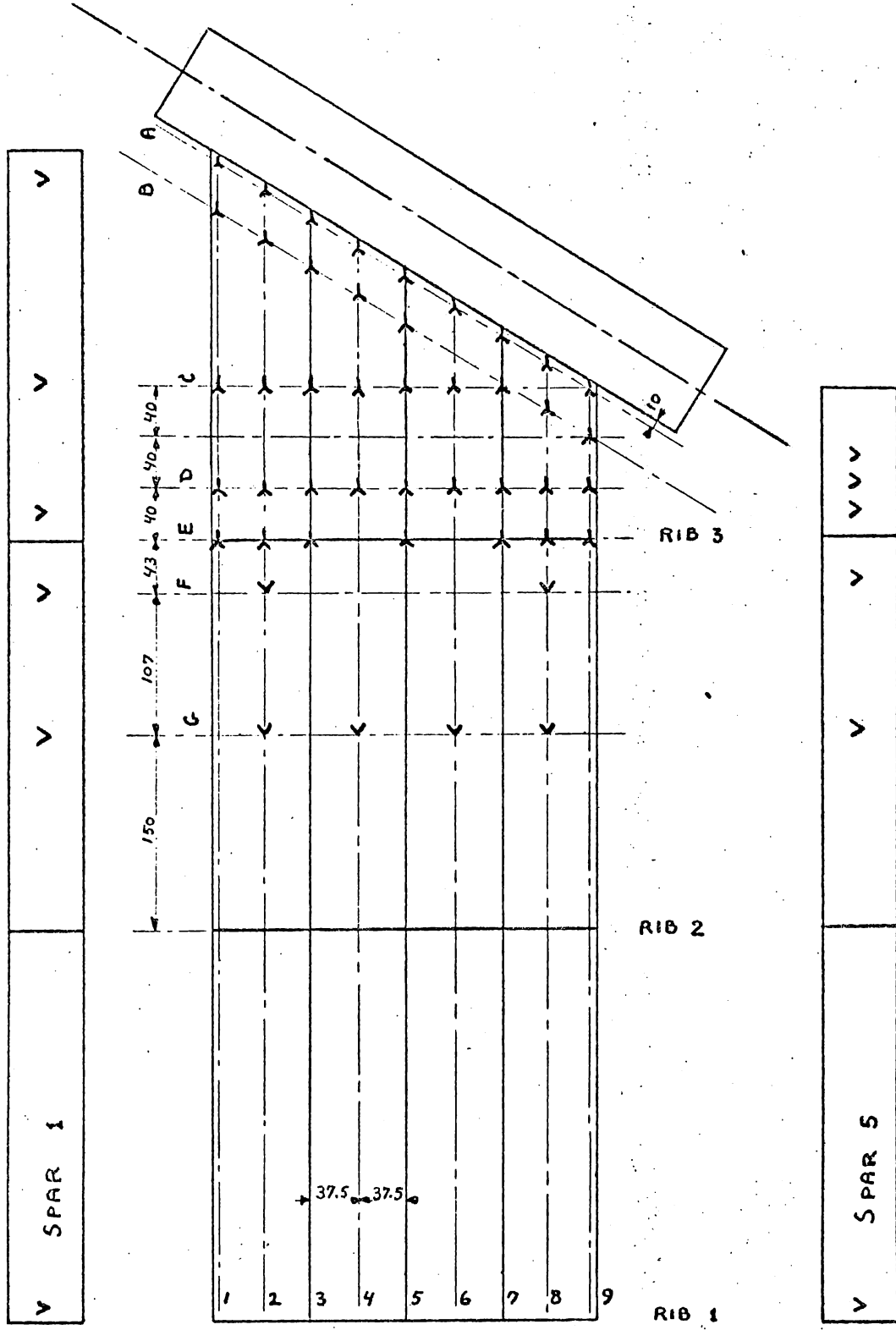


Figure F.3.69. Strain gages distribution. (V or Y = strain gage).

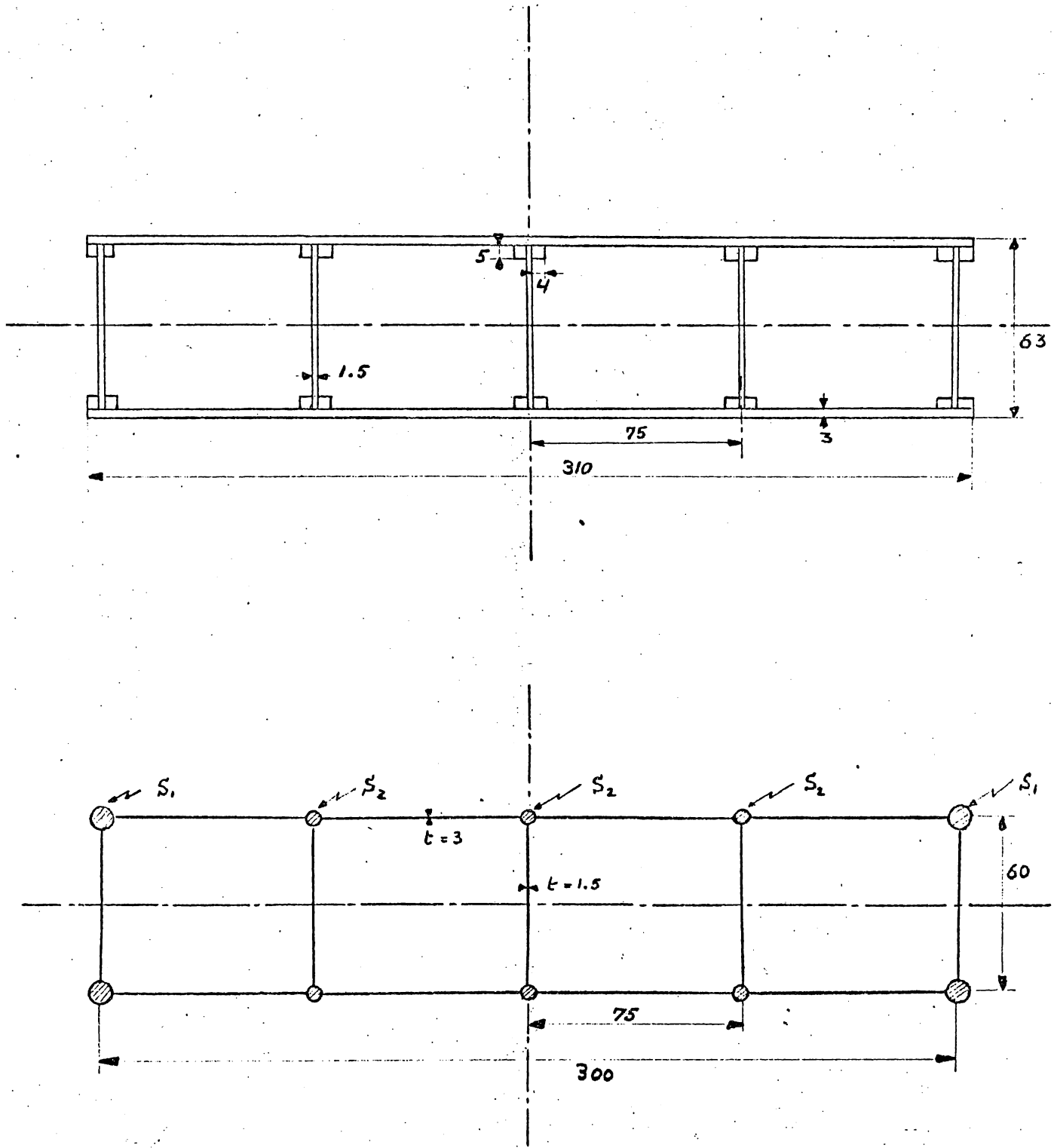


Figure F.3.70. Idealization of a cross section.

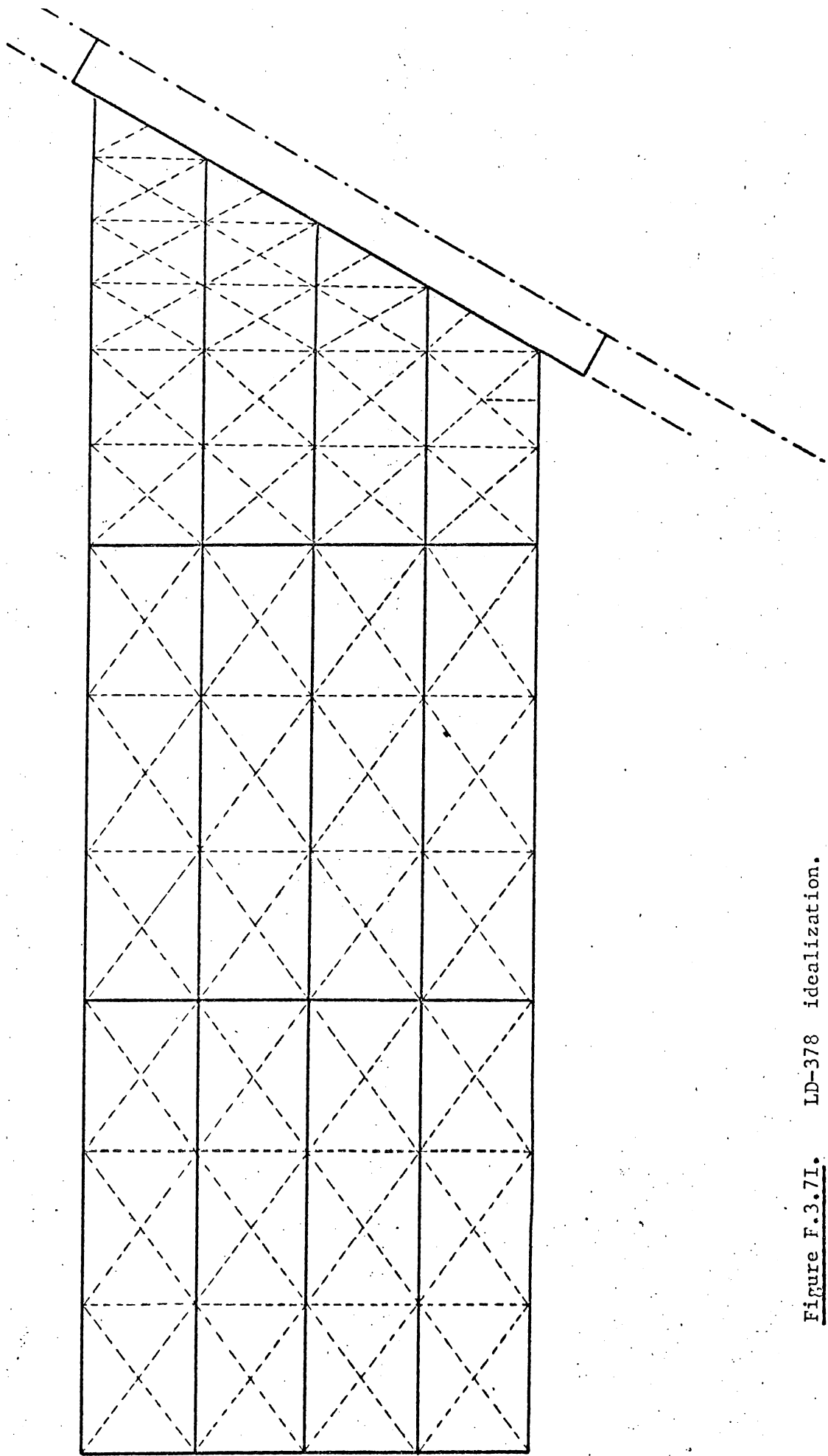


Figure F.3.7I. LD-378 idealization.

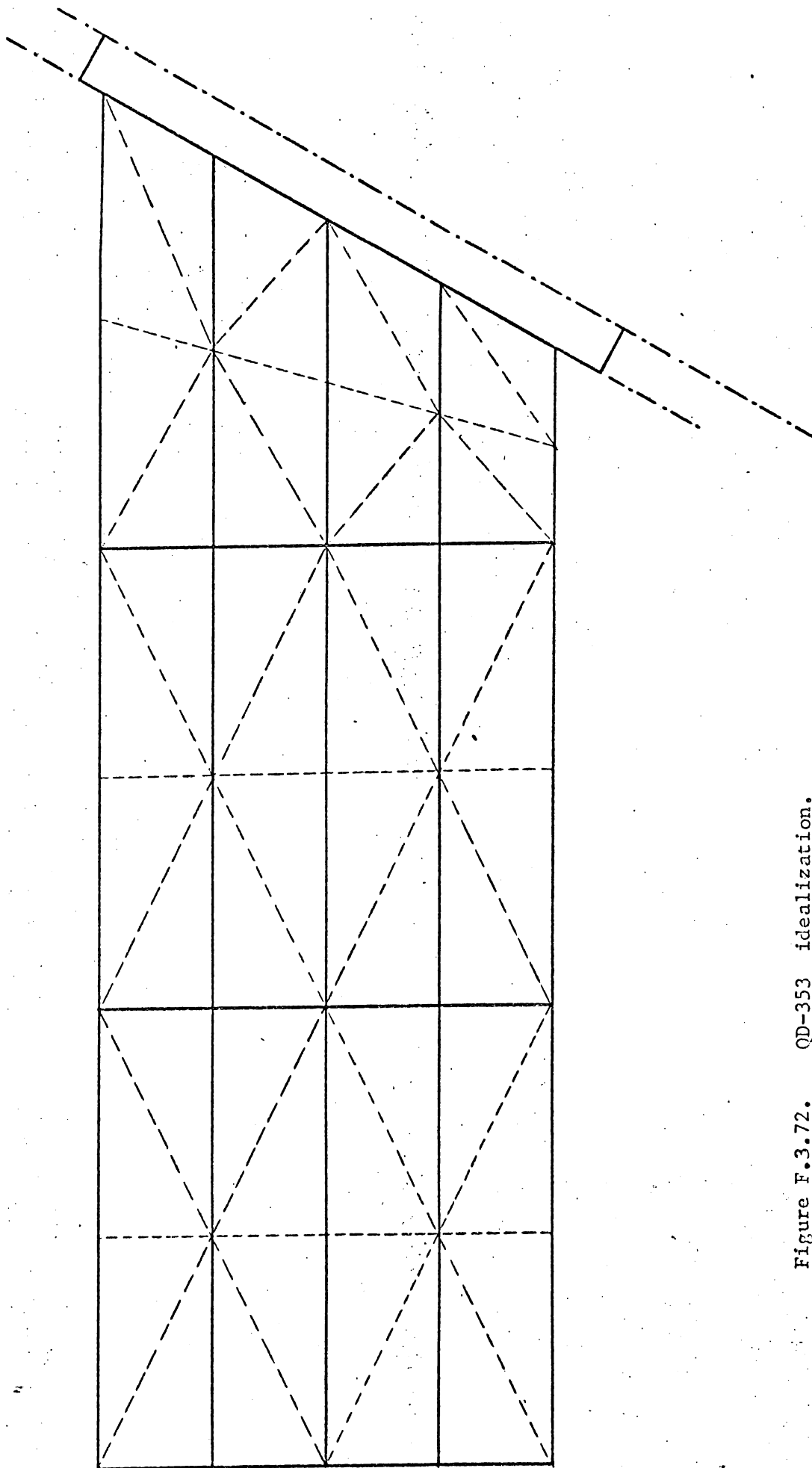


Figure F.3.72. QD-353 idealization.

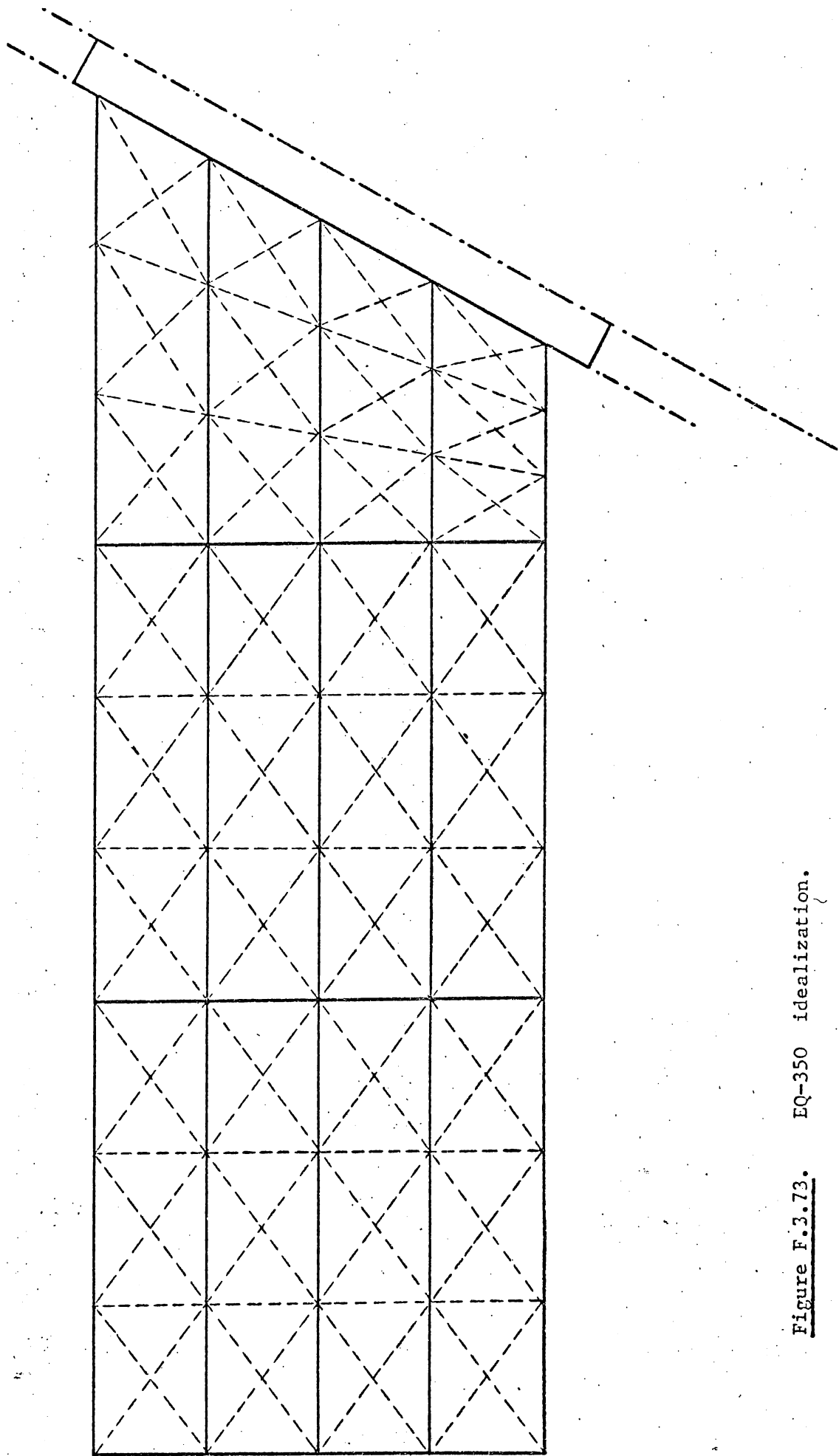


Figure F.3.73. EQ-350 idealization.

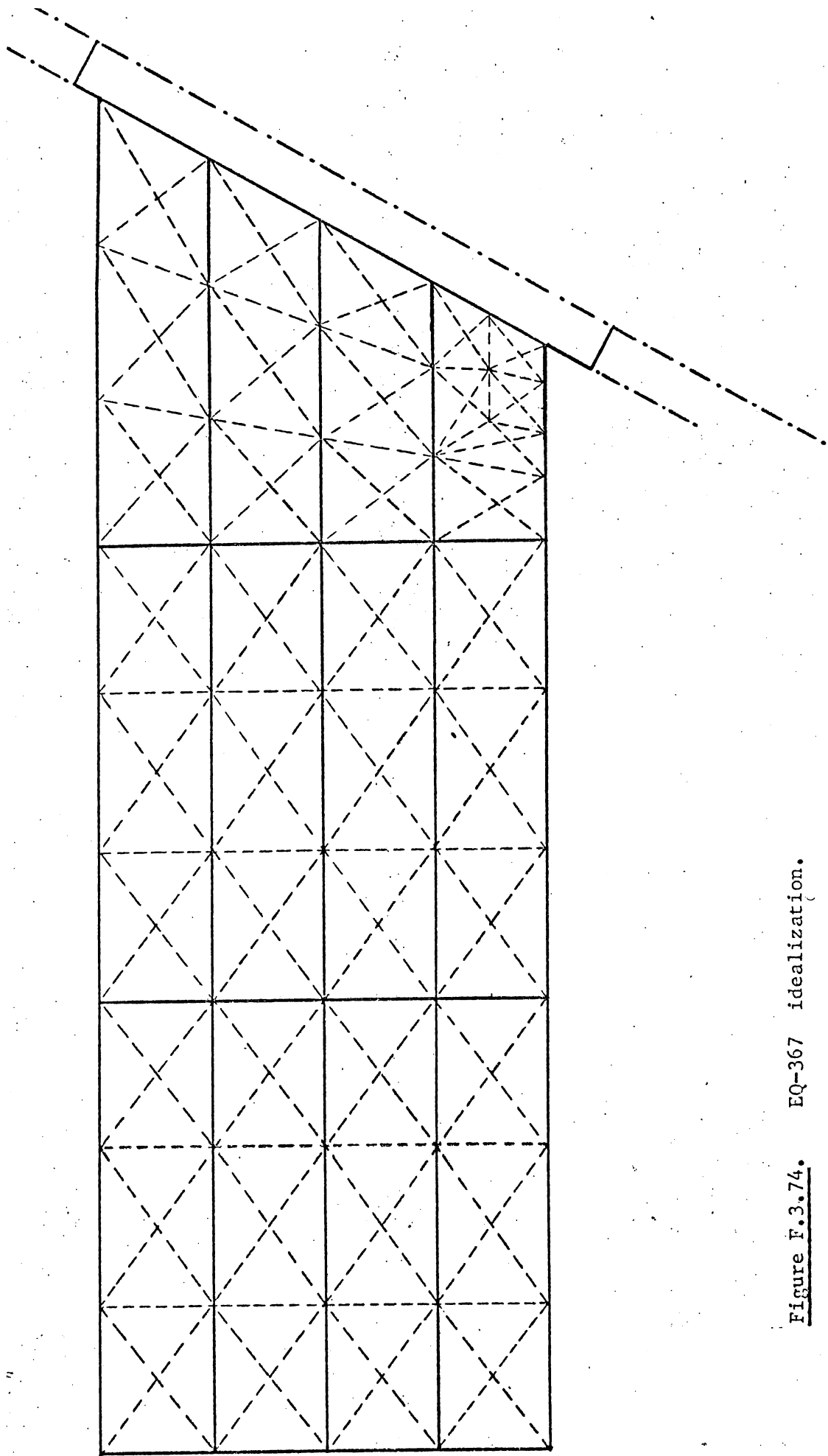


Figure F.3.74. EQ-367 idealization.

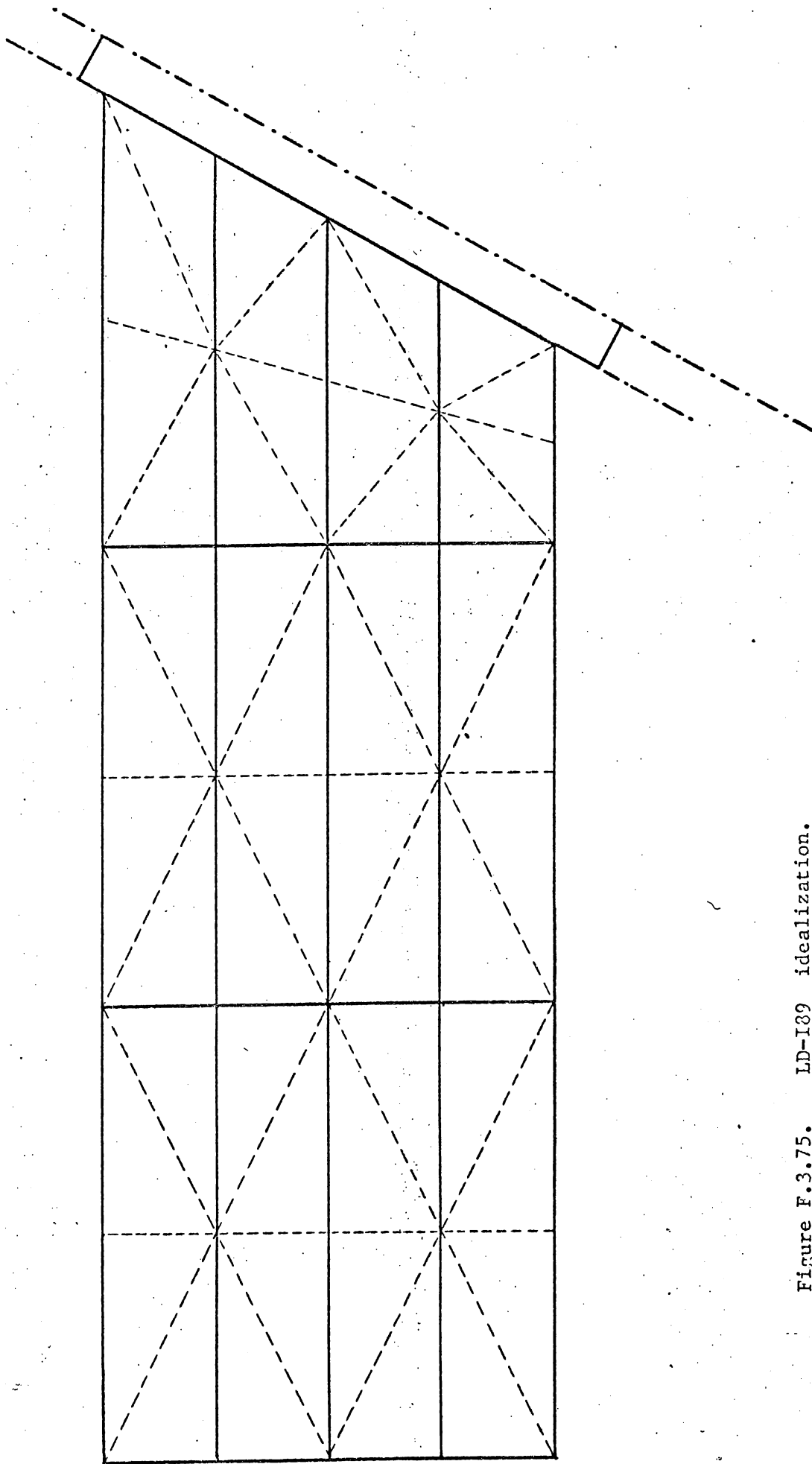


Figure F.3.75. LD-I89 idealization.

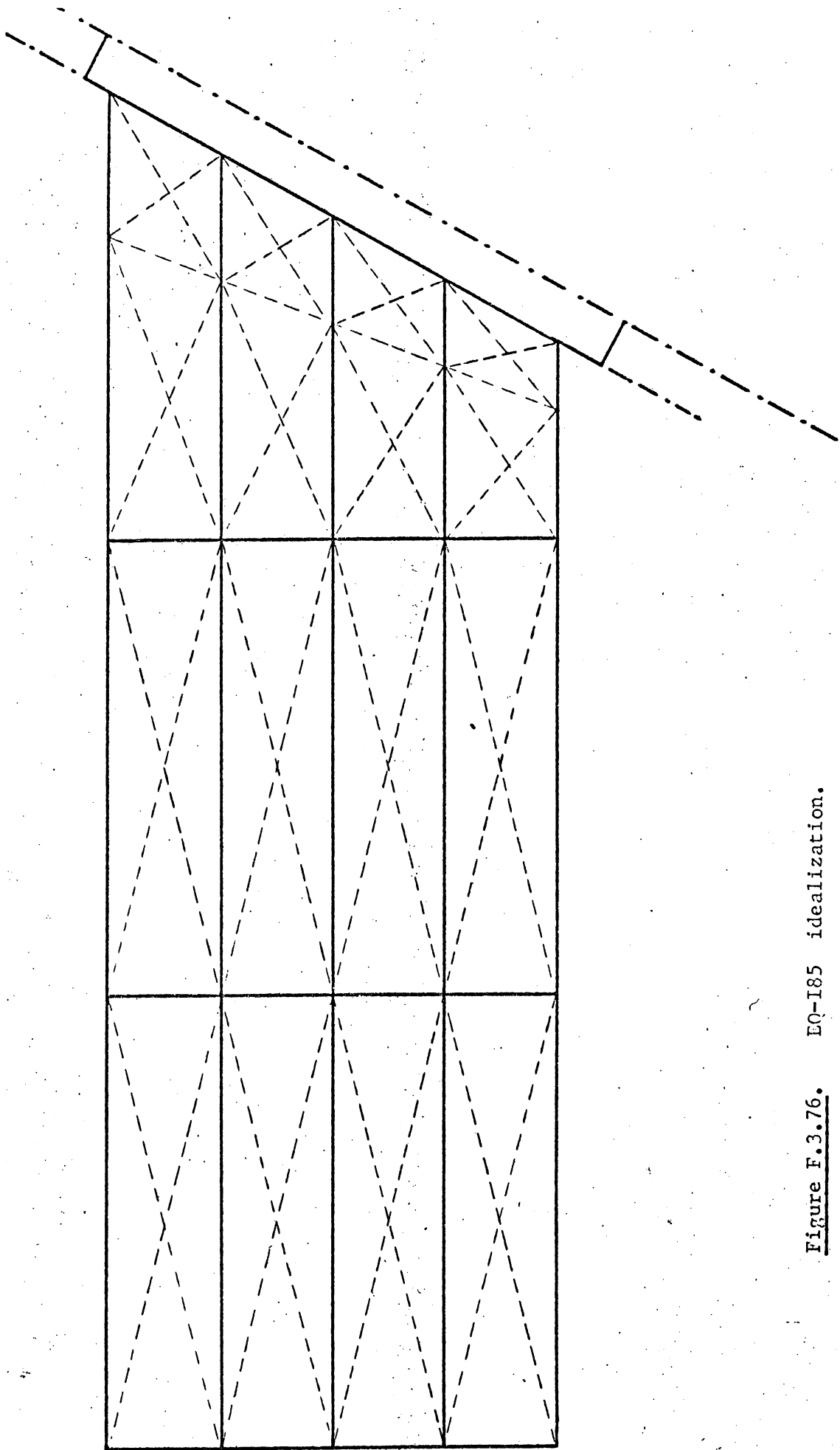


Figure F.3.76. EQ-I85 idealization.

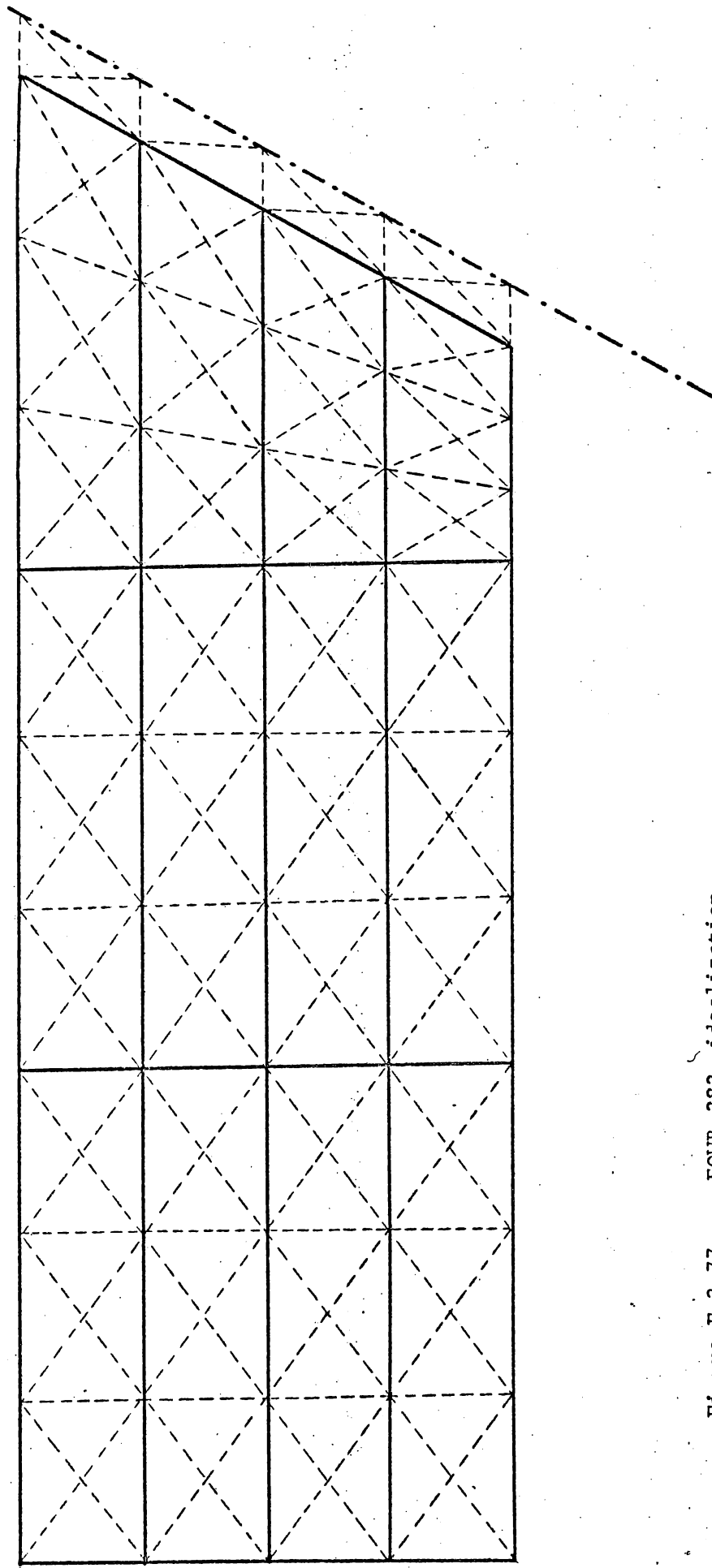


Figure F.3.77. EQNB-383 idealization.

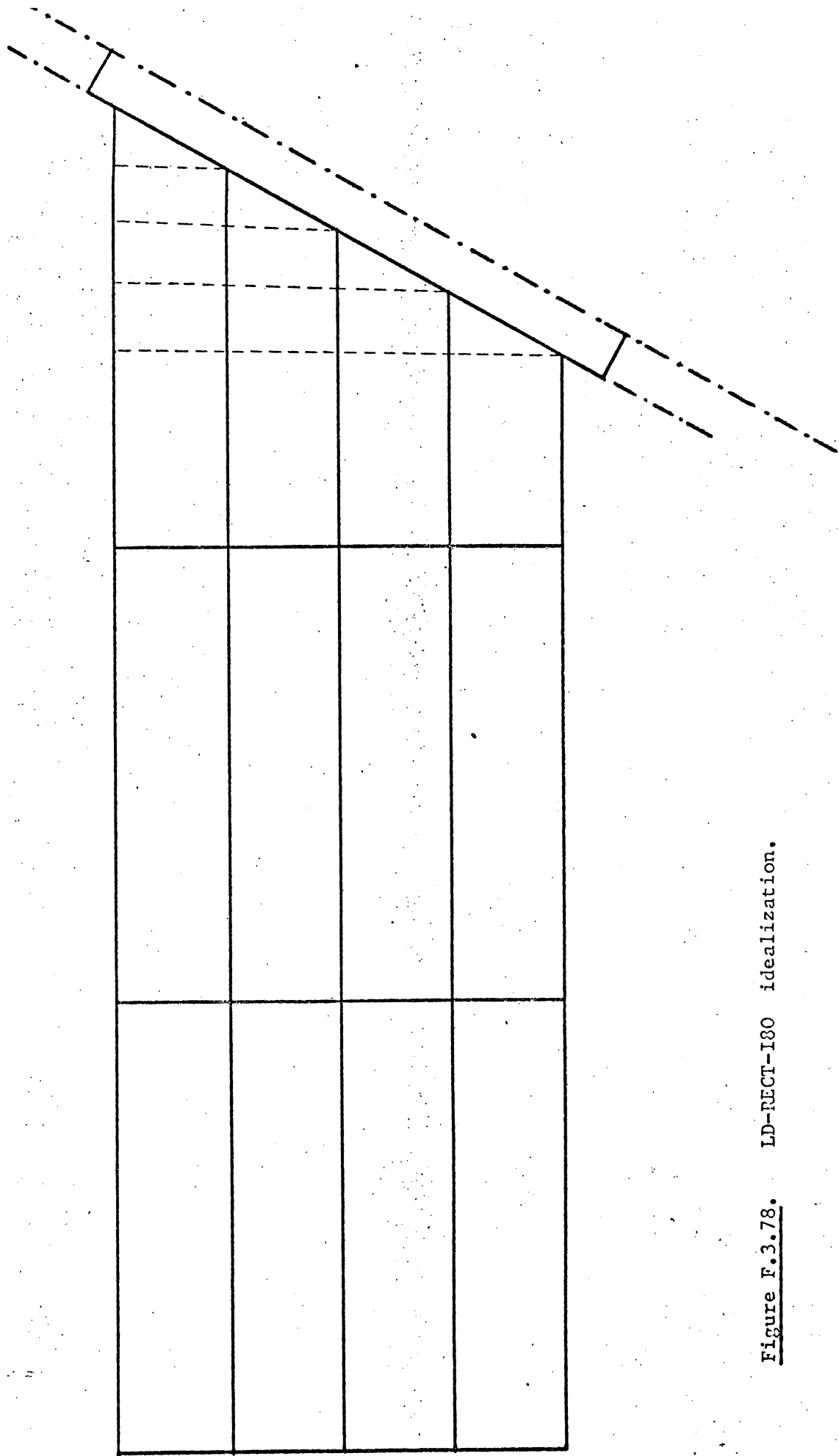


Figure F.3.78. LD-RECT-I80 idealization.

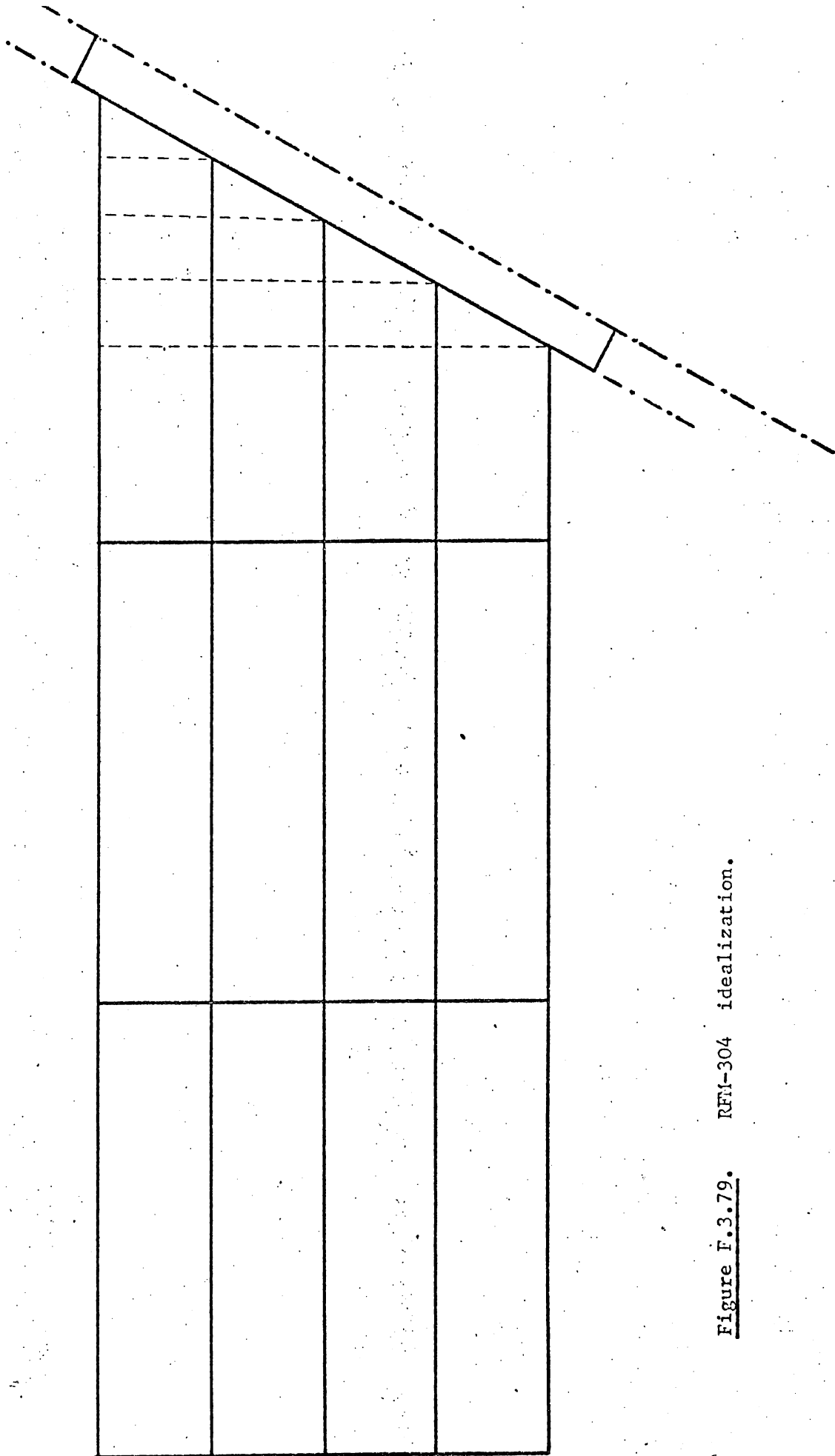


Figure F.3.79. RFM-304 idealization.

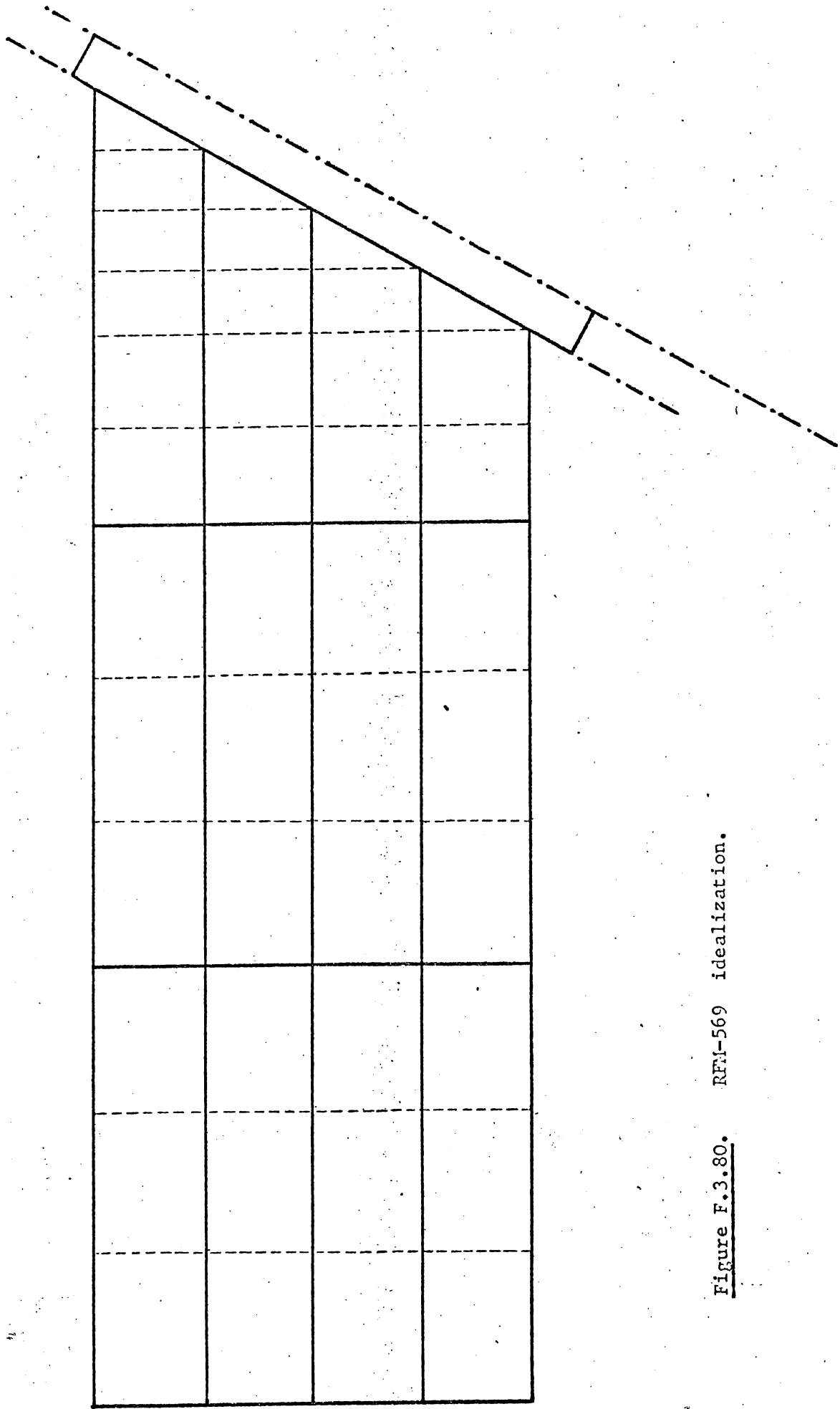


Figure F.3.80. RFM-569 idealization.

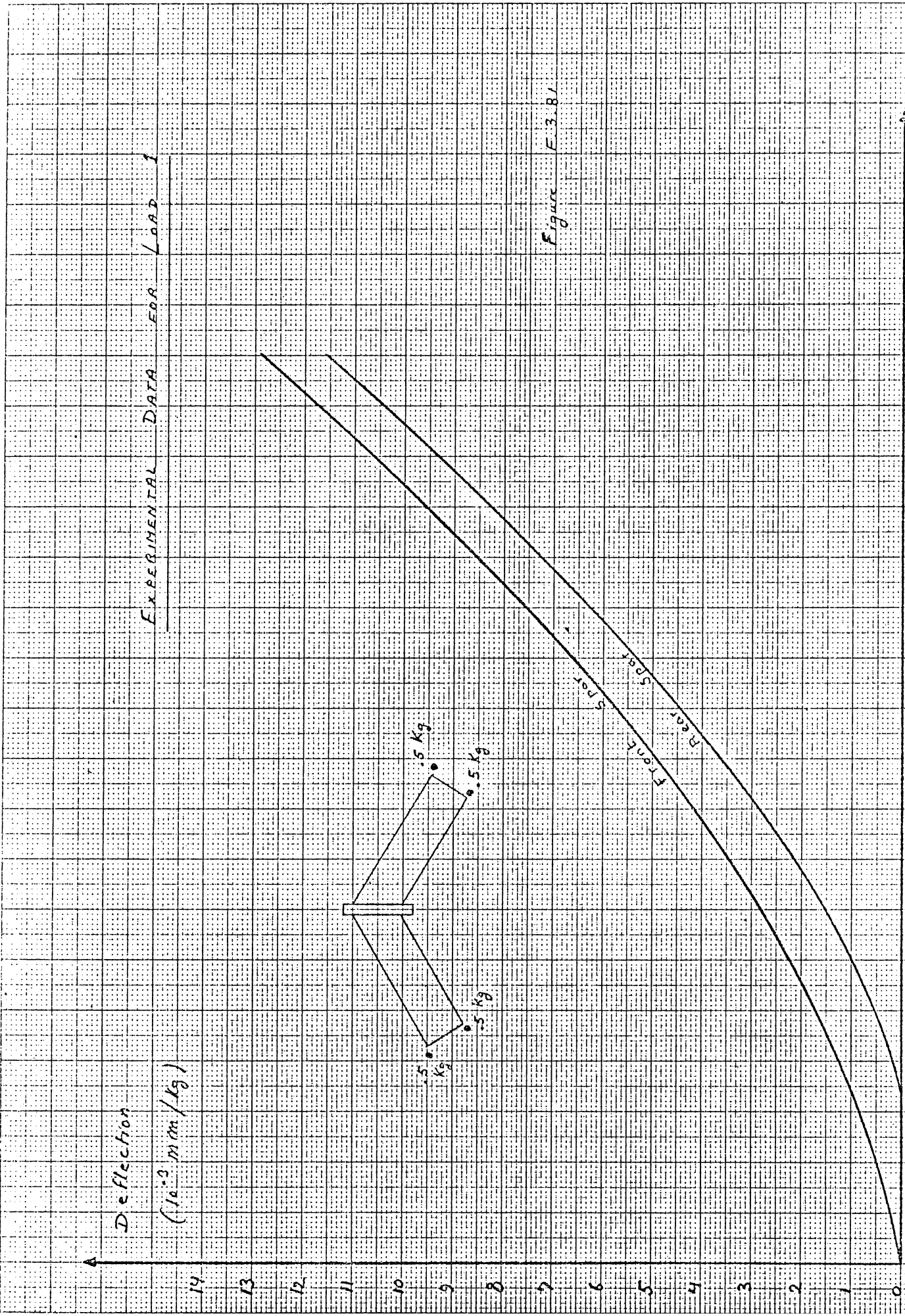


Figure E-3.81

EXPERIMENTAL DATA FOR LOAD 2

Deflection
(10^{-3} mm/kg)

14
13
12
11
10
9
8
7
6
5
4
3
2
1
0

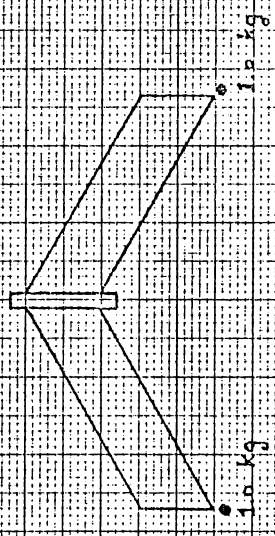


Figure F 3. B4

Front Spar
Rear Spar

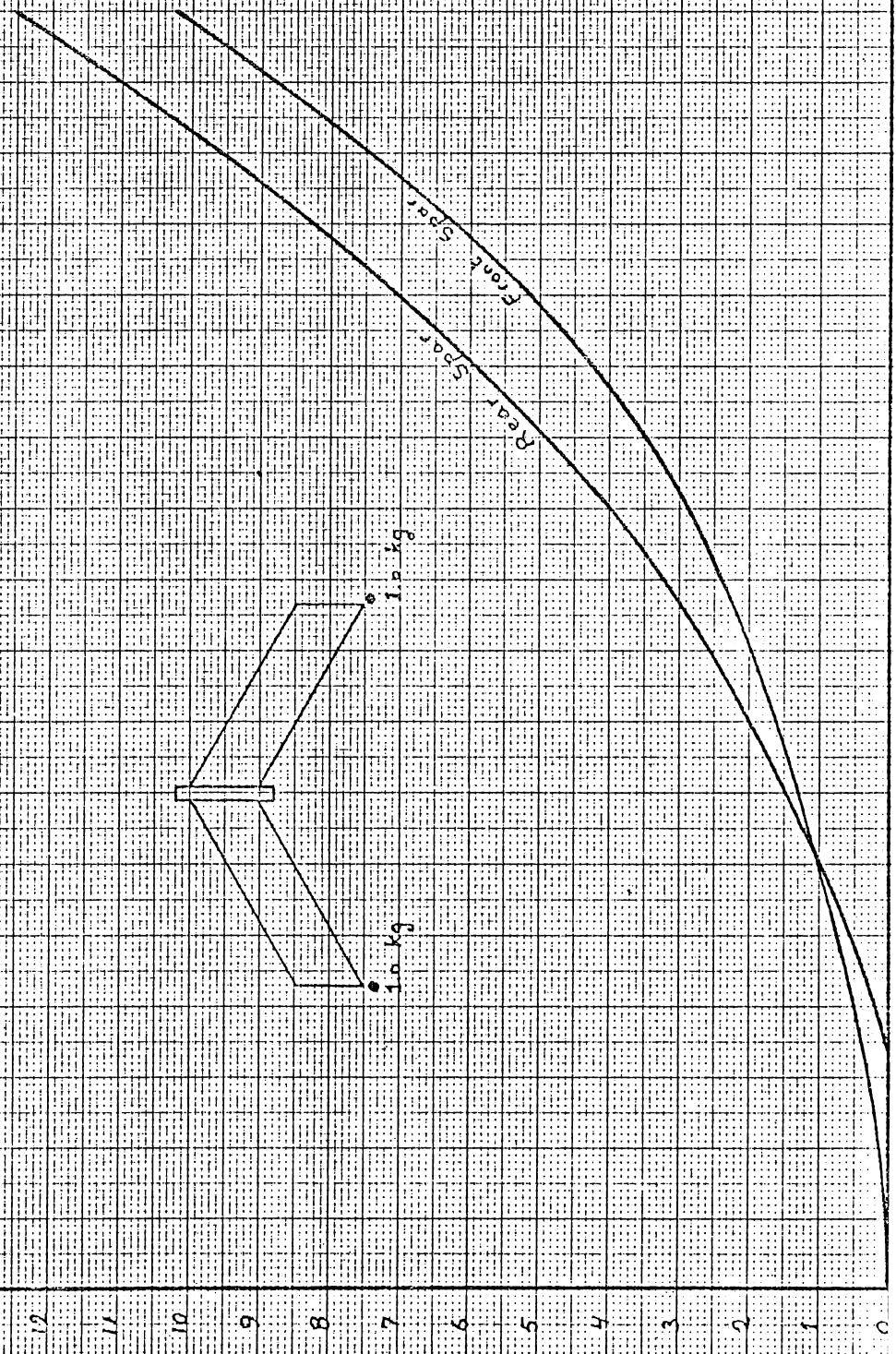


Figure F.3.83.

ANALYSIS	LOAD	X = 900 (RIB 1)				
		y = 0	y = 75	y = 150	y = 225	y = 300
TEST	1	12.85	/	/	/	11.6
TEST	2	10.25	/	/	/	12.55
LD-RECT-180	1	9.205	9.007	8.882	8.822	8.835
LD-RECT-180	2	7.650	8.153	8.695	9.303	10.020
LD-189	1	11.373	11.192	11.077	11.028	11.044
LD-189	2	9.849	10.360	10.913	11.532	12.239
LD-378	1	11.535	11.339	11.216	11.169	11.195
LD-378	2	9.994	10.496	11.047	11.672	12.396
QA-353	1	11.622	11.424	11.303	11.259	11.292
QA-353	2	10.083	10.586	11.138	11.767	12.500
EQ-367	1	11.834	11.622	11.496	11.456	11.502
EQ-367	2	10.286	10.783	11.331	11.964	12.717
EQ-350	1	11.854	11.642	11.516	11.475	11.521
EQ-350	2	10.305	10.802	11.350	11.983	12.737
EQ-185	1	11.980	11.715	11.563	11.539	11.629
EQ-185	2	10.419	10.869	11.393	12.039	12.838
RFM-569	1	11.997	11.724	11.550	11.459	11.474
RFM-569	2	10.329	10.771	11.247	11.879	12.621
RFM-304	1	12.418	12.169	12.000	11.910	11.902
RFM-304	2	10.795	11.244	11.743	12.319	13.010
EQWB-383	1	12.728	12.509	12.375	12.326	12.364
EQWB-383	2	11.135	11.638	12.193	12.832	13.592

Figure F.3.84.

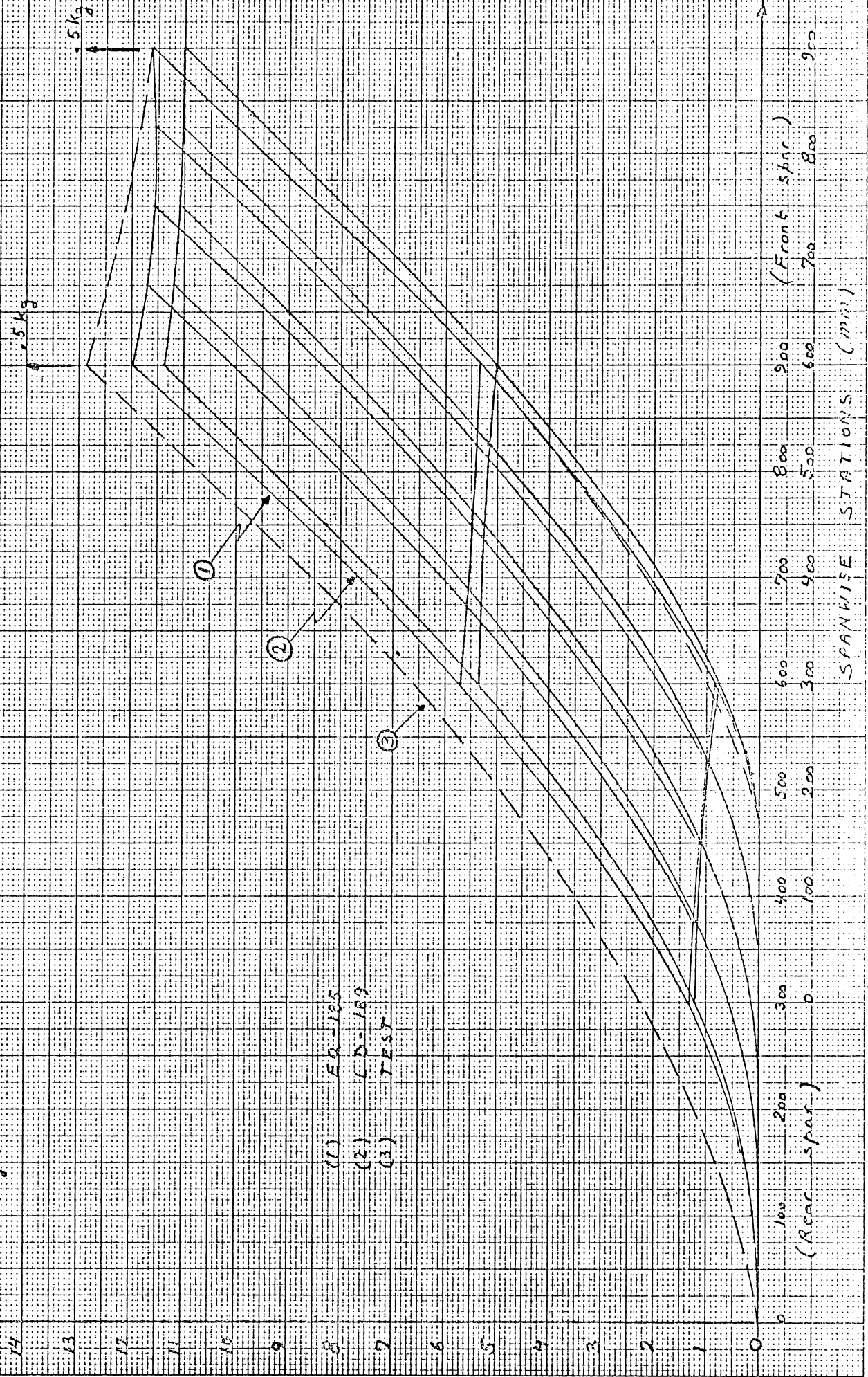
ANALYSIS	LOAD	X = 600 (RIB 2)				
		y = 0	y = 75	y = 150	y = 225	y = 300
TEST	1	6.6	/	/	/	5.3
TEST	2	3.5	/	/	/	4.9
LD-RECT-180	1	4.610	4.532	4.430	4.316	4.198
LD-RECT-180	2	3.682	3.999	4.296	4.577	4.853
LD-189	1	5.382	5.328	5.241	5.136	5.017
LD-189	2	4.474	4.815	5.121	5.406	5.677
LD-378	1	5.472	5.411	5.320	5.216	5.101
LD-378	2	4.550	4.889	5.196	5.486	5.767
QA-353	1	5.518	5.457	5.369	5.268	5.159
QA-353	2	4.595	4.936	5.247	5.542	5.830
EQ-367	1	5.632	5.563	5.474	5.375	5.274
EQ-367	2	4.700	5.039	5.352	5.651	5.950
EQ-350	1	5.645	5.576	5.487	5.388	5.287
EQ-350	2	4.713	5.052	5.364	5.664	5.964
EQ-185	1	5.717	5.599	5.490	5.405	5.341
EQ-185	2	4.776	5.073	5.367	5.679	6.014
RFM-569	1	5.781	5.633	5.481	5.345	5.227
RFM-569	2	4.785	5.041	5.302	5.570	5.857
RFM-304	1	6.001	5.859	5.718	5.588	5.471
RFM-304	2	5.031	5.289	5.543	5.805	6.082
EQWB-383	1	6.199	6.123	6.027	5.922	5.813
EQWB-383	2	5.227	5.573	5.894	6.201	6.508

Figure F.3.85.

ANALYSIS	LOAD	X = 300 (RIB 3)				
		y = 0	y = 75	y = 150	y = 225	y = 300
TEST	1	2.25	/	/	/	1.0
TEST	2	1.0	/	/	/	1.0
LD-RECT-180	1	1.178	1.135	1.030	.886	.725
LD-RECT-180	2	.795	.914	.958	.949	.913
LD-189	1	1.214	1.189	1.092	.944	.778
LD-189	2	.843	.977	1.027	1.010	.965
LD-378	1	1.238	1.213	1.110	.961	.794
LD-378	2	.856	.994	1.043	1.028	.985
QA-353	1	1.245	1.220	1.119	.973	.810
QA-353	2	.859	1.000	1.052	1.042	1.005
EQ-367	1	1.274	1.245	1.147	1.001	.845
EQ-367	2	.879	1.021	1.079	1.072	1.043
EQ-350	1	1.280	1.251	1.152	1.008	.854
EQ-350	2	.884	1.026	1.084	1.079	1.053
EQ-185	1	1.304	1.239	1.128	.991	.854
EQ-185	2	.903	1.015	1.063	1.063	1.051
RFM-569	1	1.395	1.275	1.121	.958	.813
RFM-569	2	.977	1.028	1.035	1.013	1.001
RFM-304	1	1.403	1.282	1.131	.971	.833
RFM-304	2	1.000	1.045	1.047	1.024	1.014
EQWB-383	1	1.520	1.482	1.375	1.221	1.058
EQWB-383	2	1.093	1.239	1.300	1.298	1.276

Figure F.3.85

Deflection
(10^{-3} mm/kg)



(1) $E_0 = 125$
(2) $L D = 189$
(3) TEST

0 100 200 300 400 500 600 700 800 900
(Rear spar) (Front spar)
SPANWISE STATIONS (mm)

Figure F.3.87.

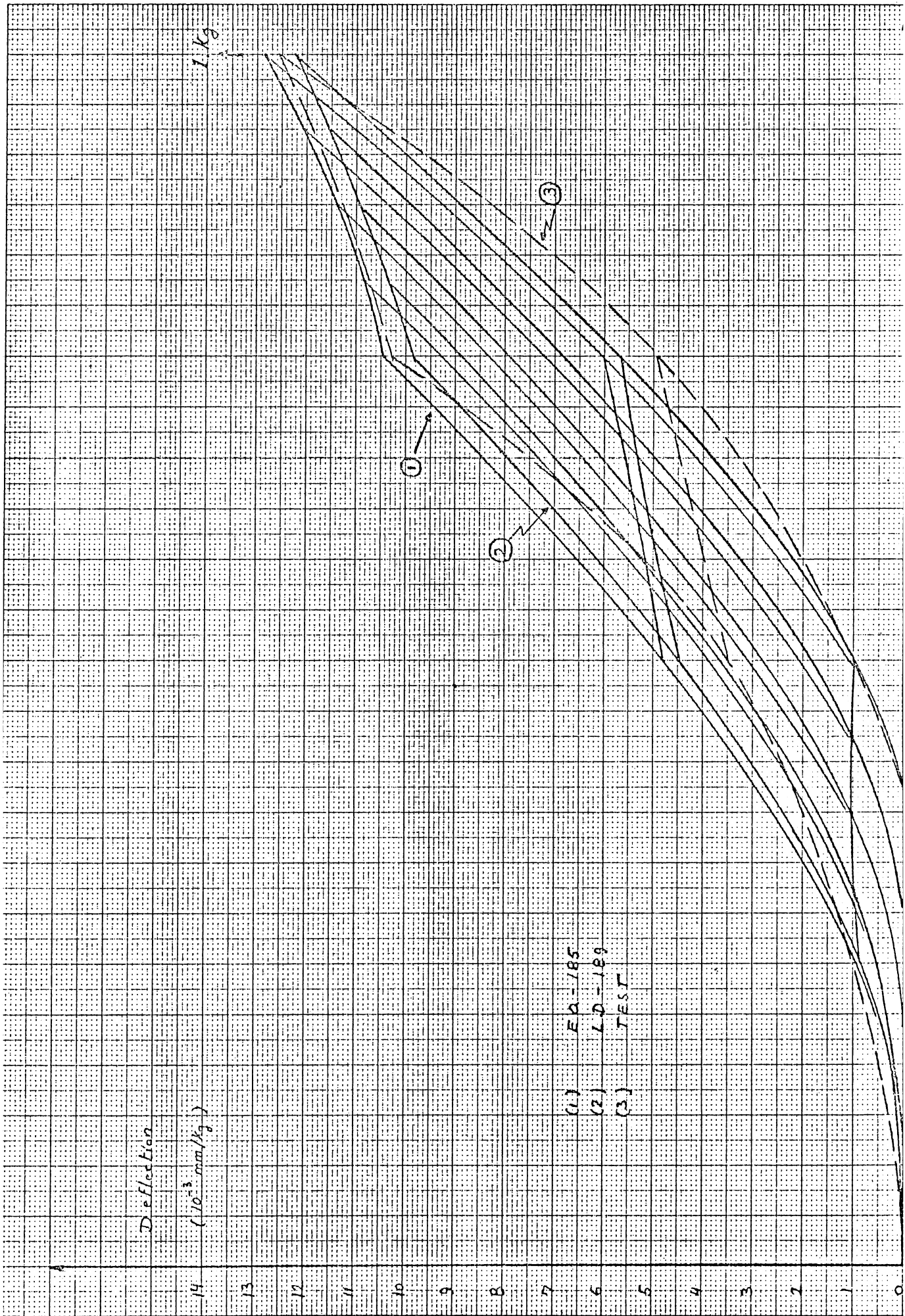


Figure F.3.88.

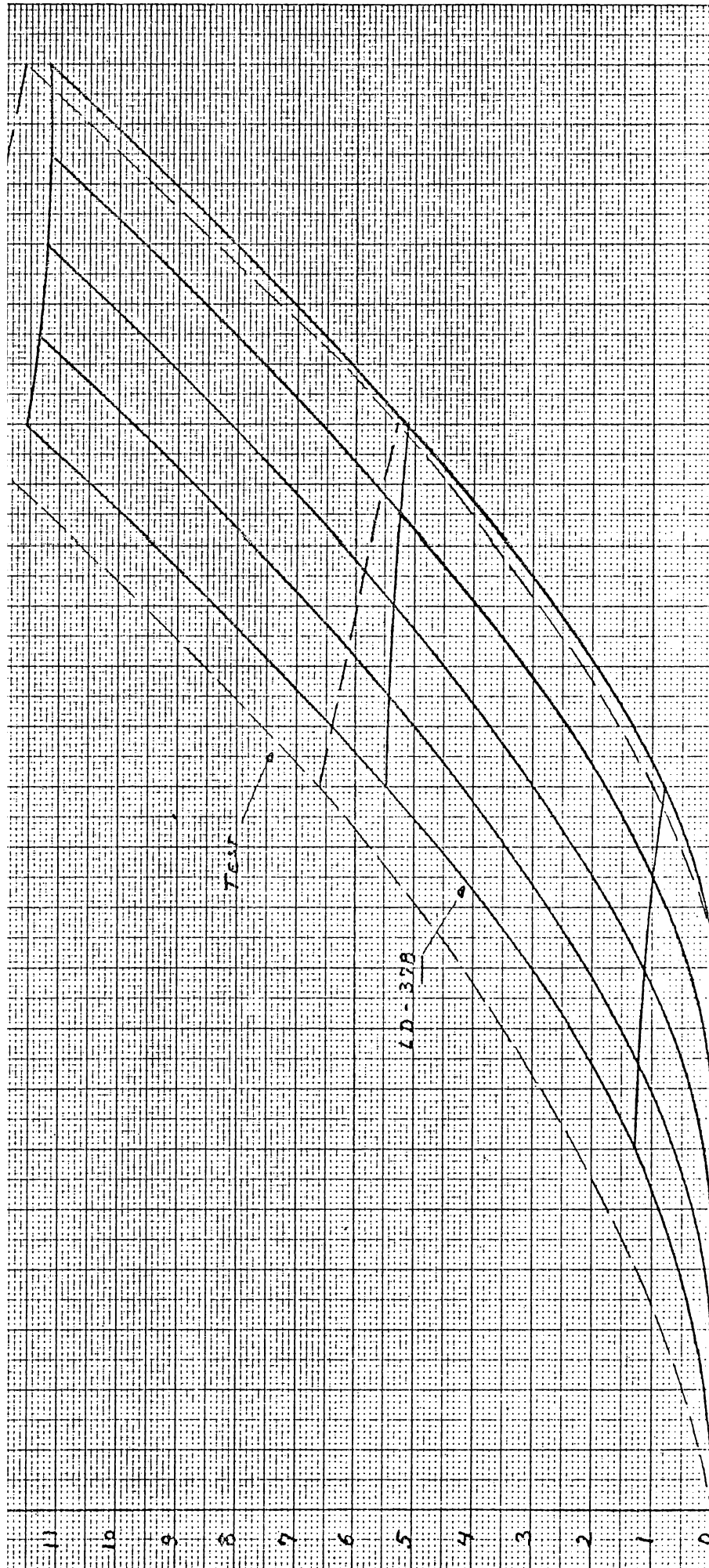


Figure F.3.89.

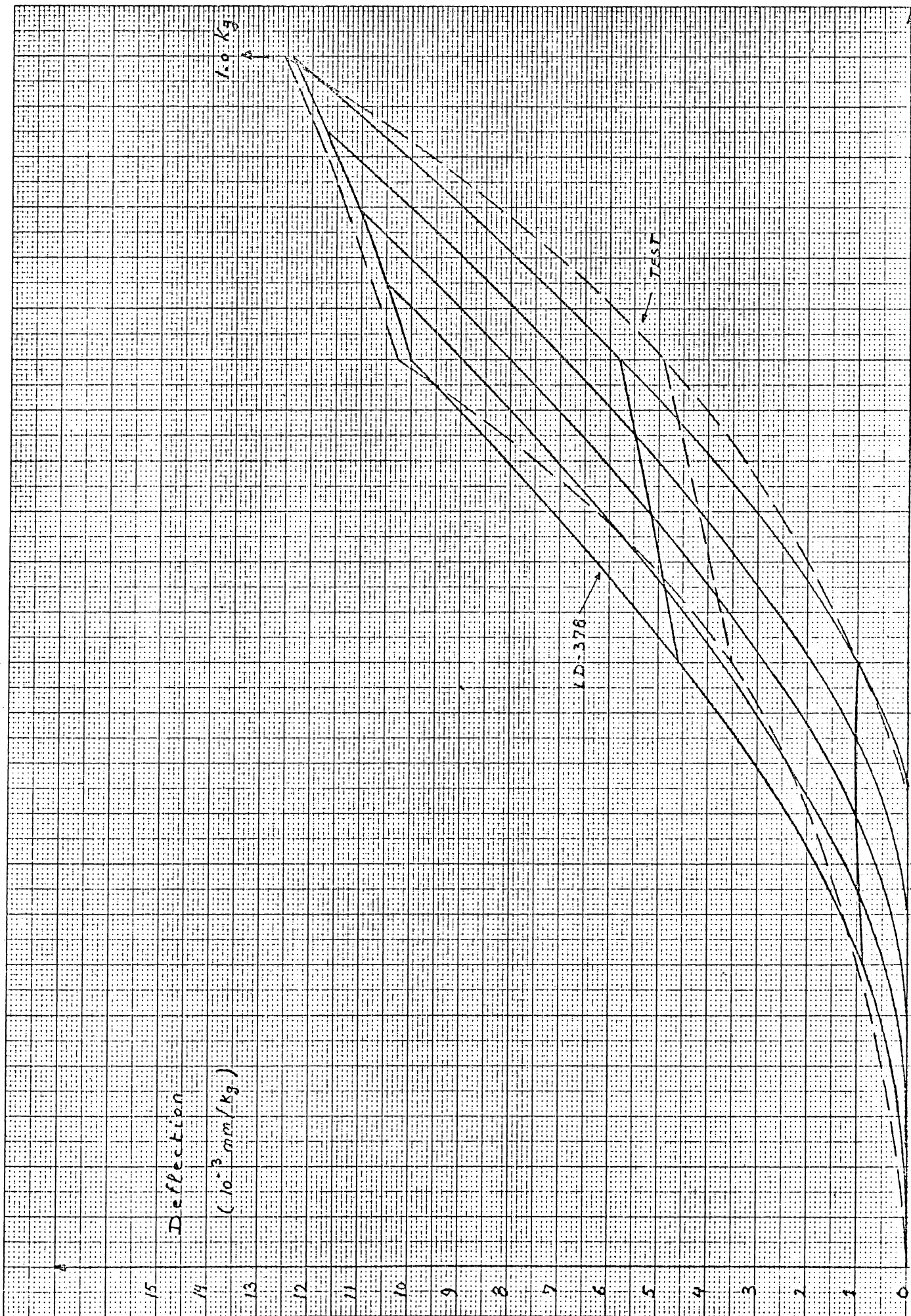


Figure F.3.90.

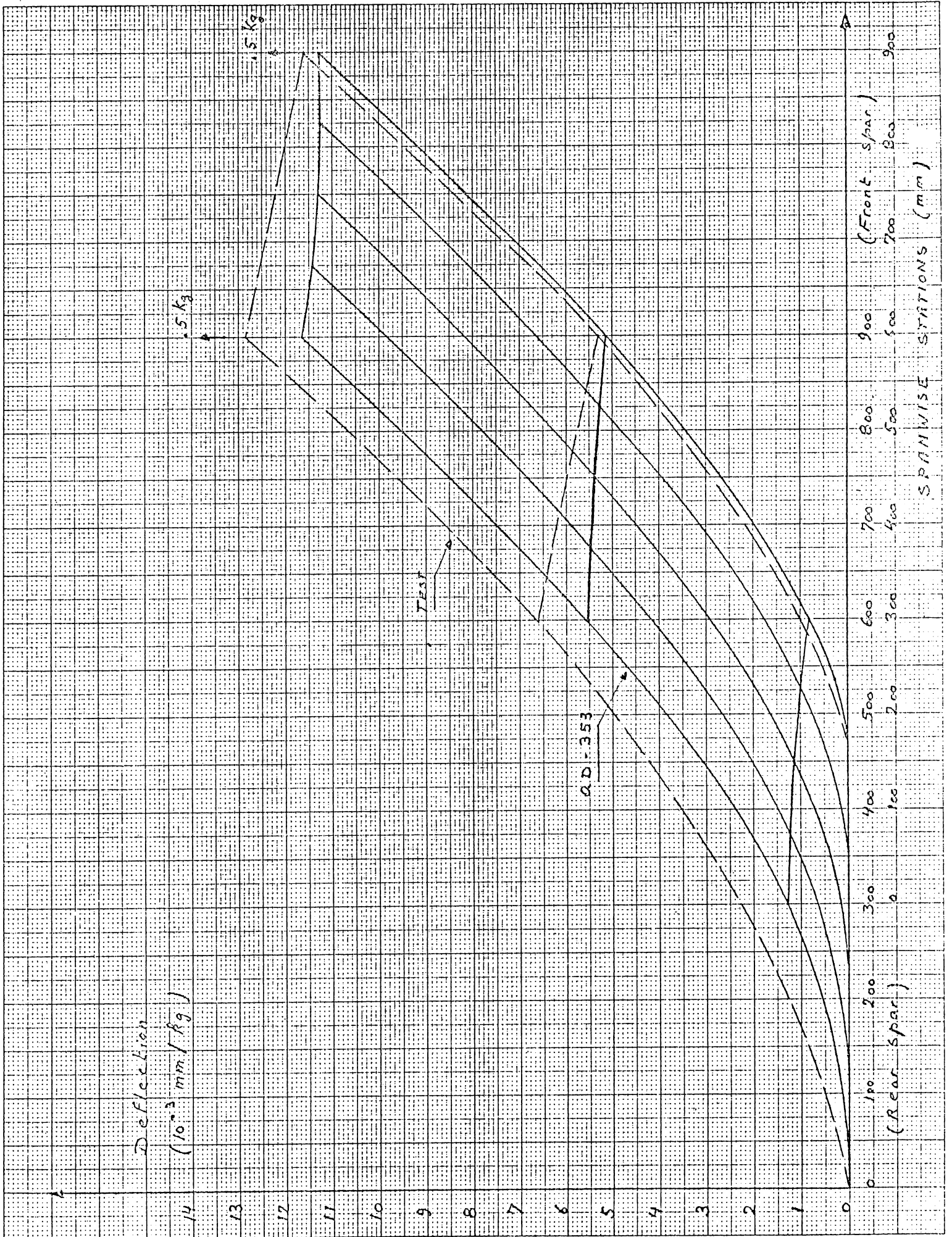


Figure F.3.91.

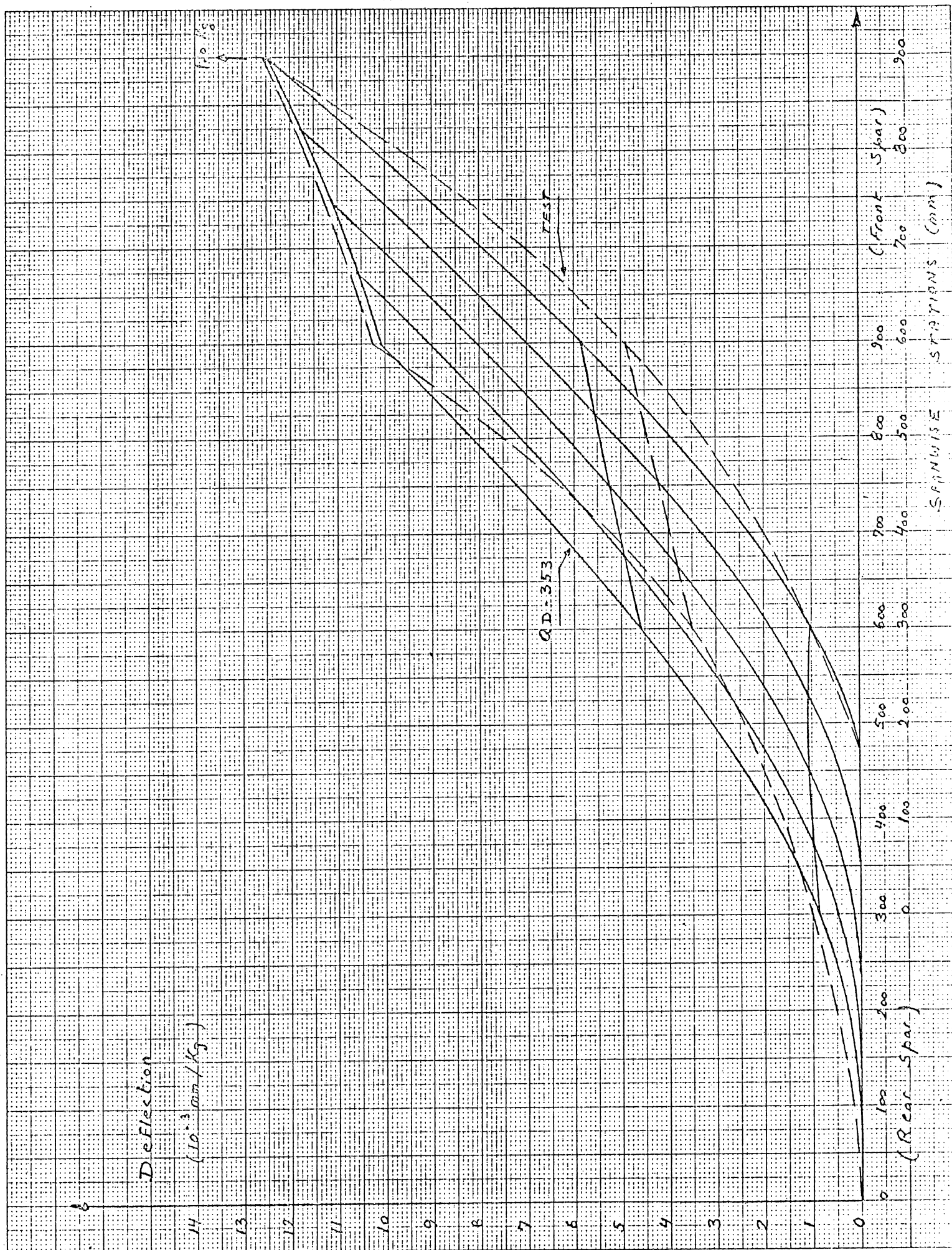


Figure F.3.92.

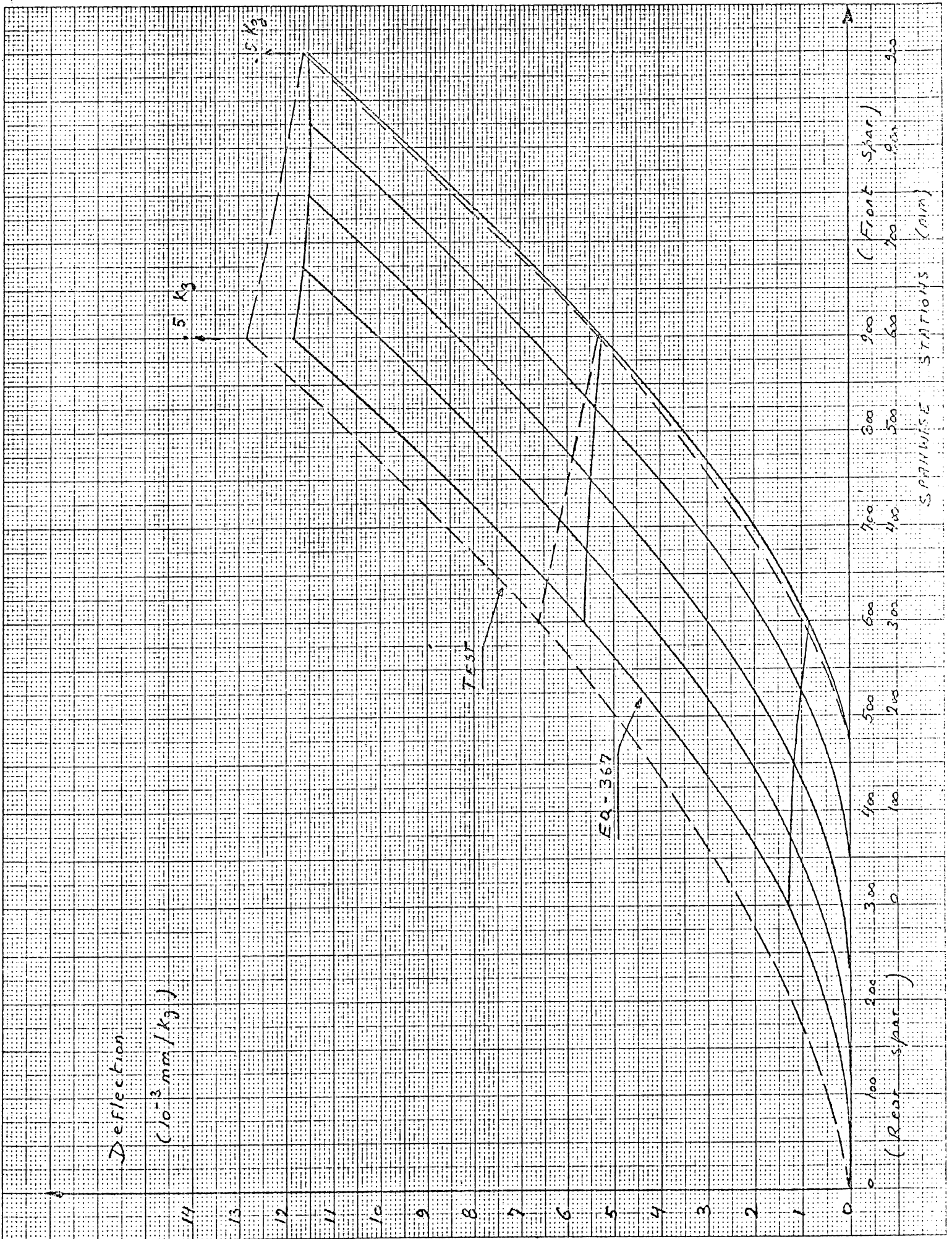


Figure F.3.93.

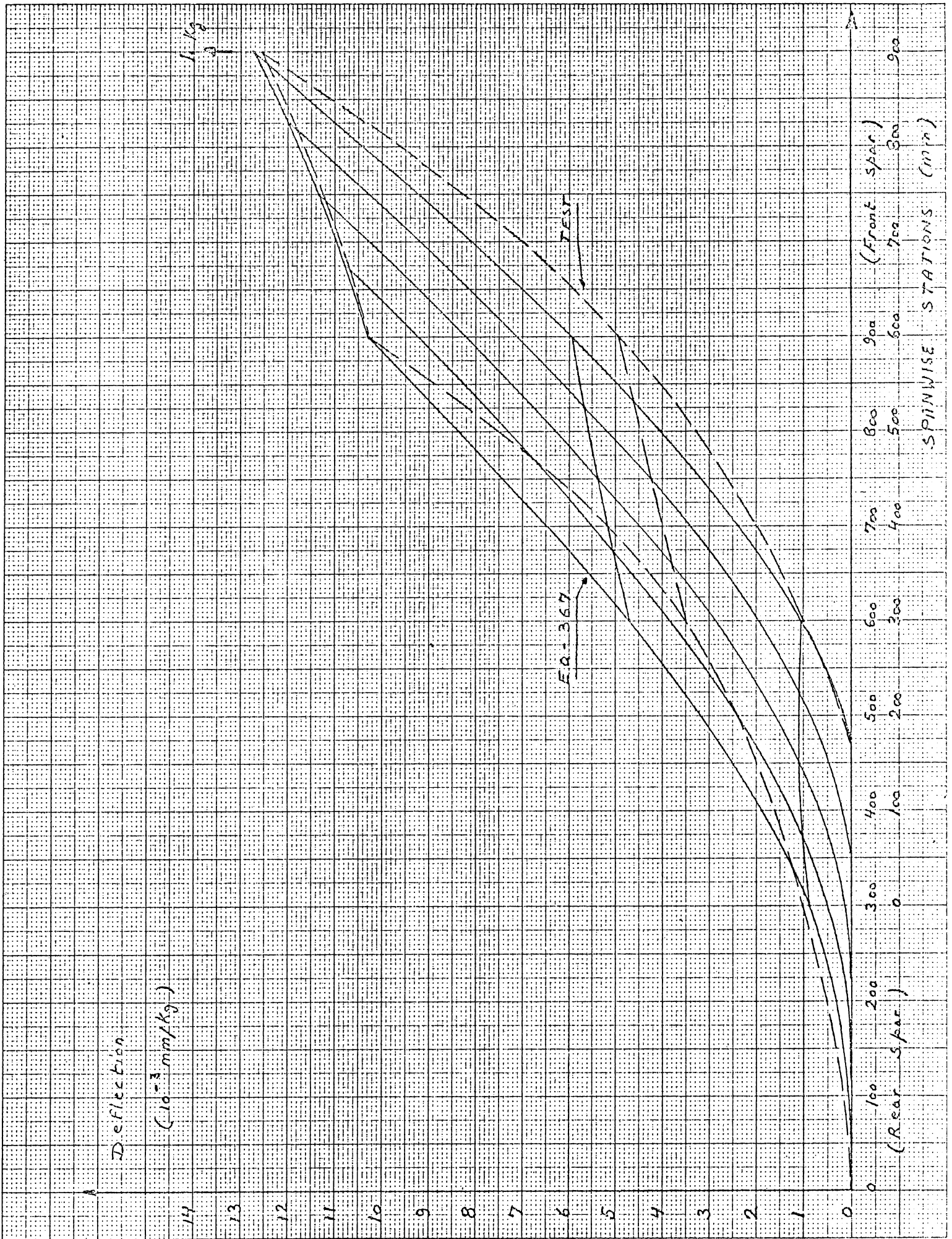
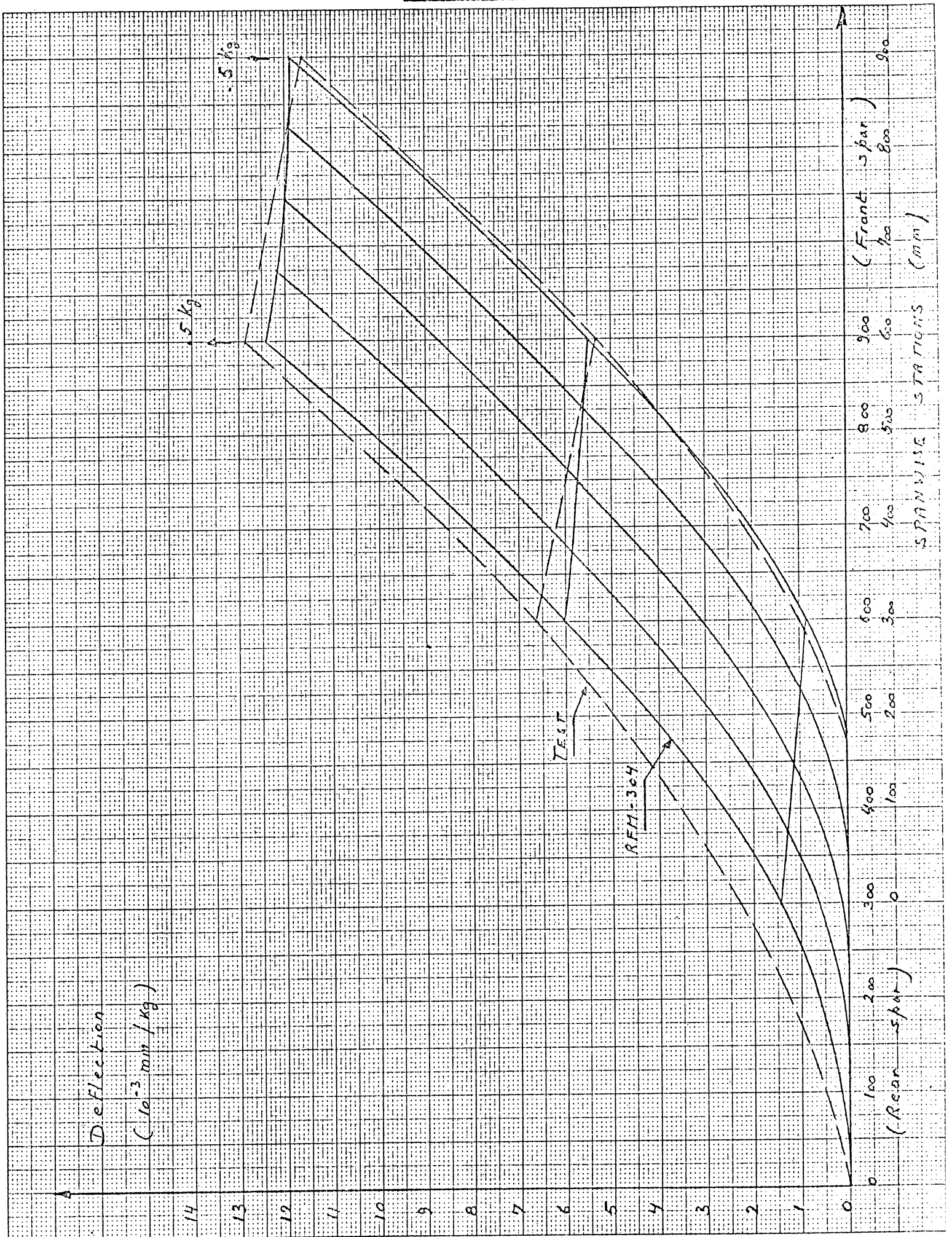


Figure F.3.94.



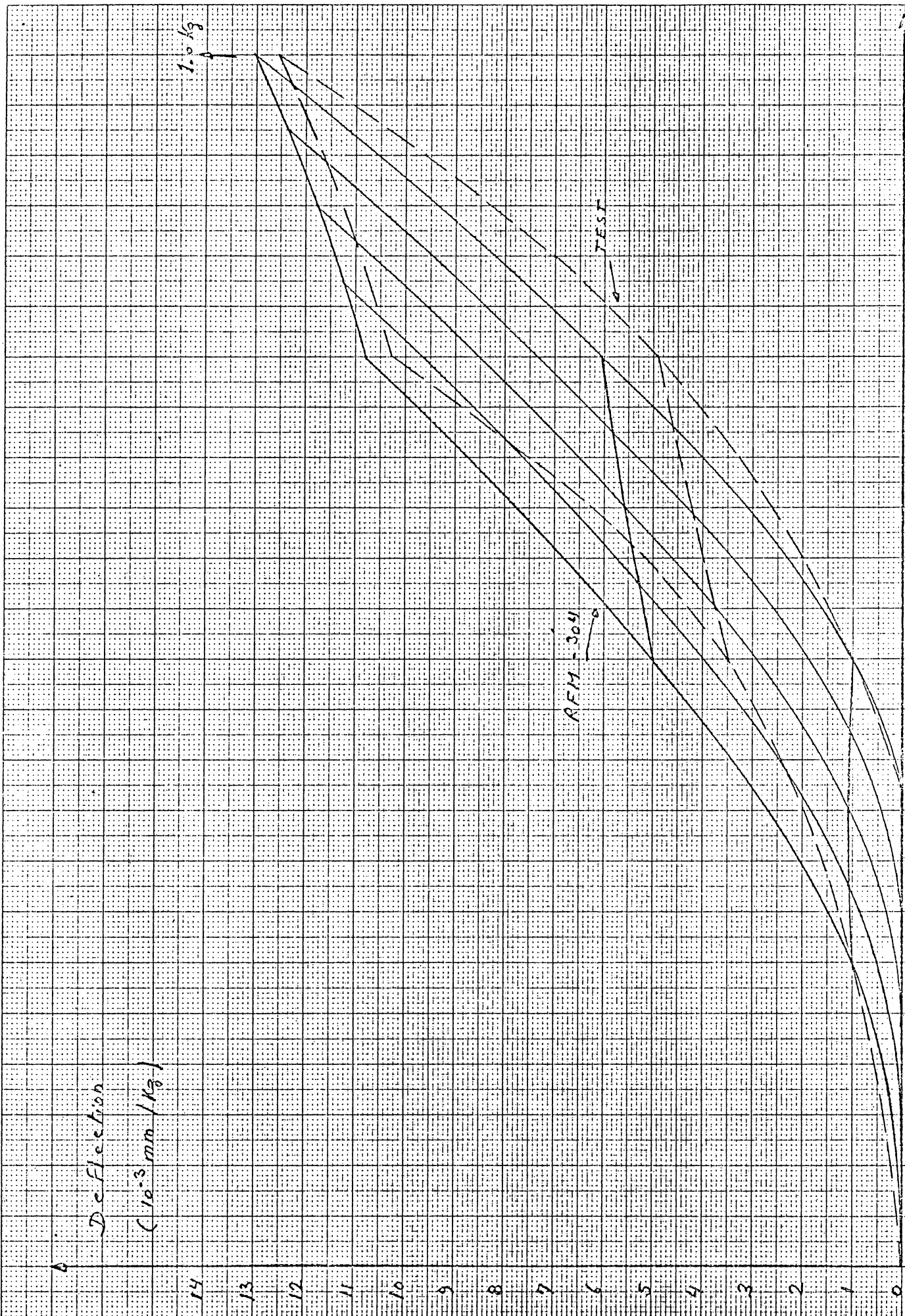


Figure F.3.96.

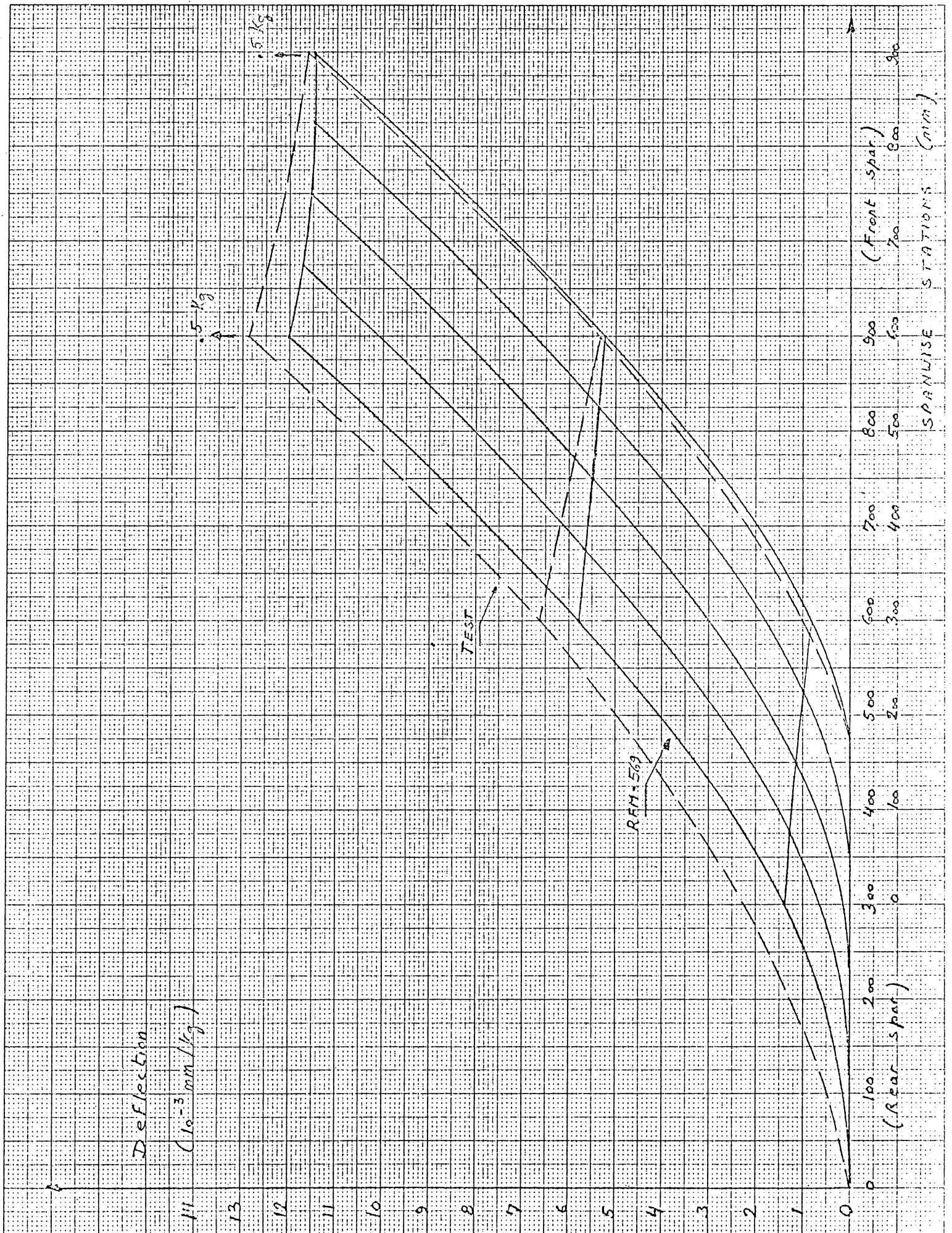


Figure F.3.97.

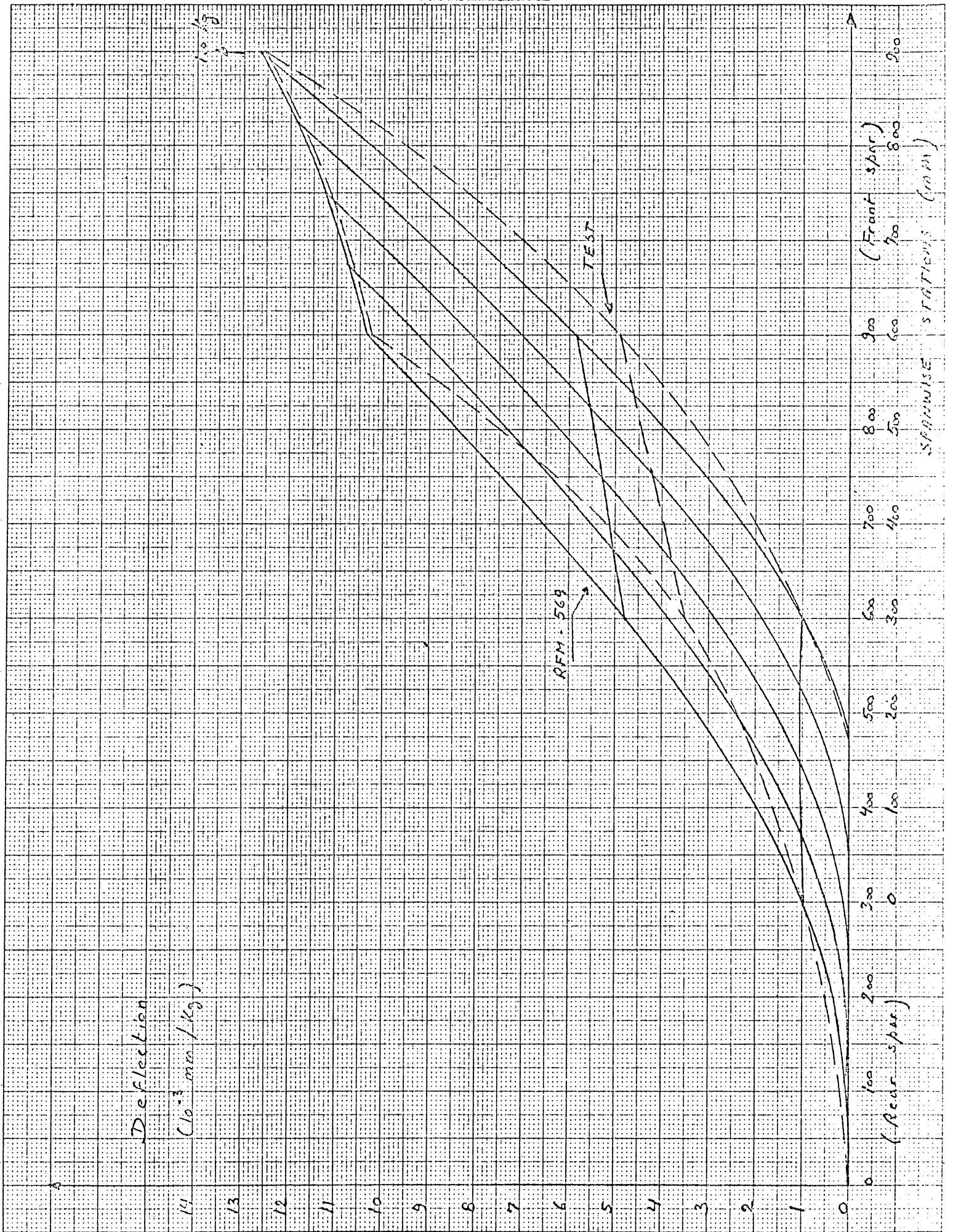


Figure F.3.98.

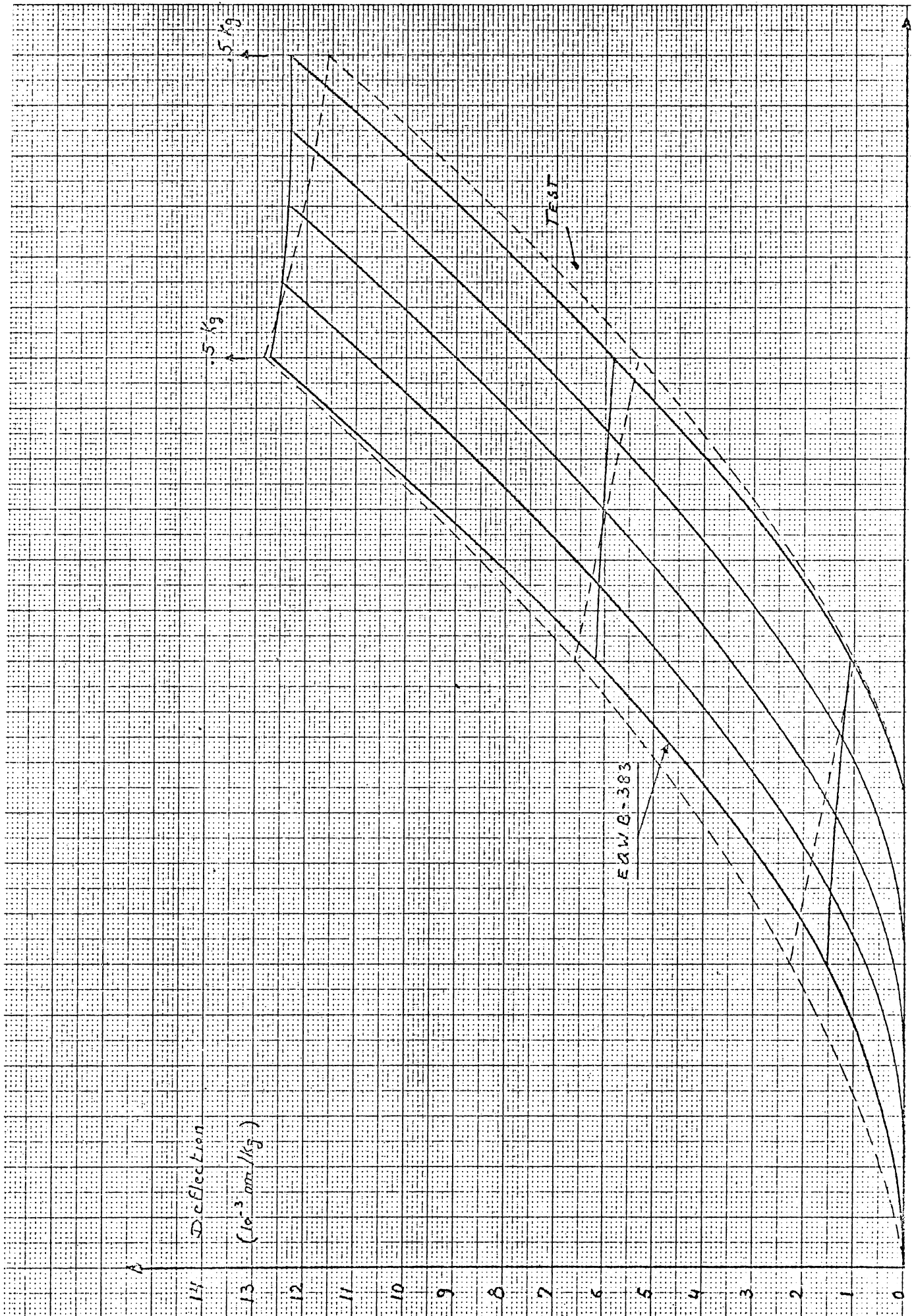


Figure F.3.99.

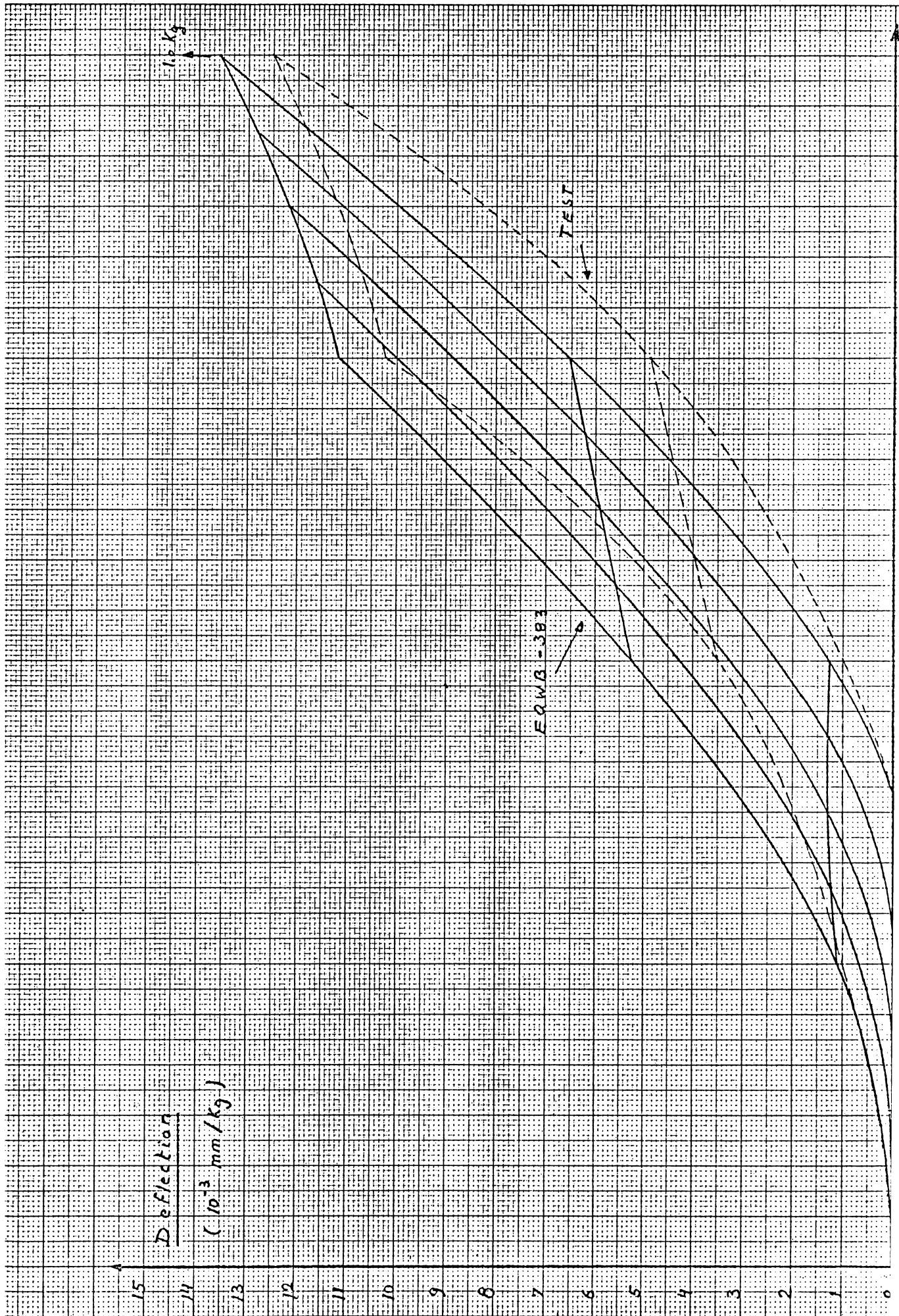


Figure F.3.100.

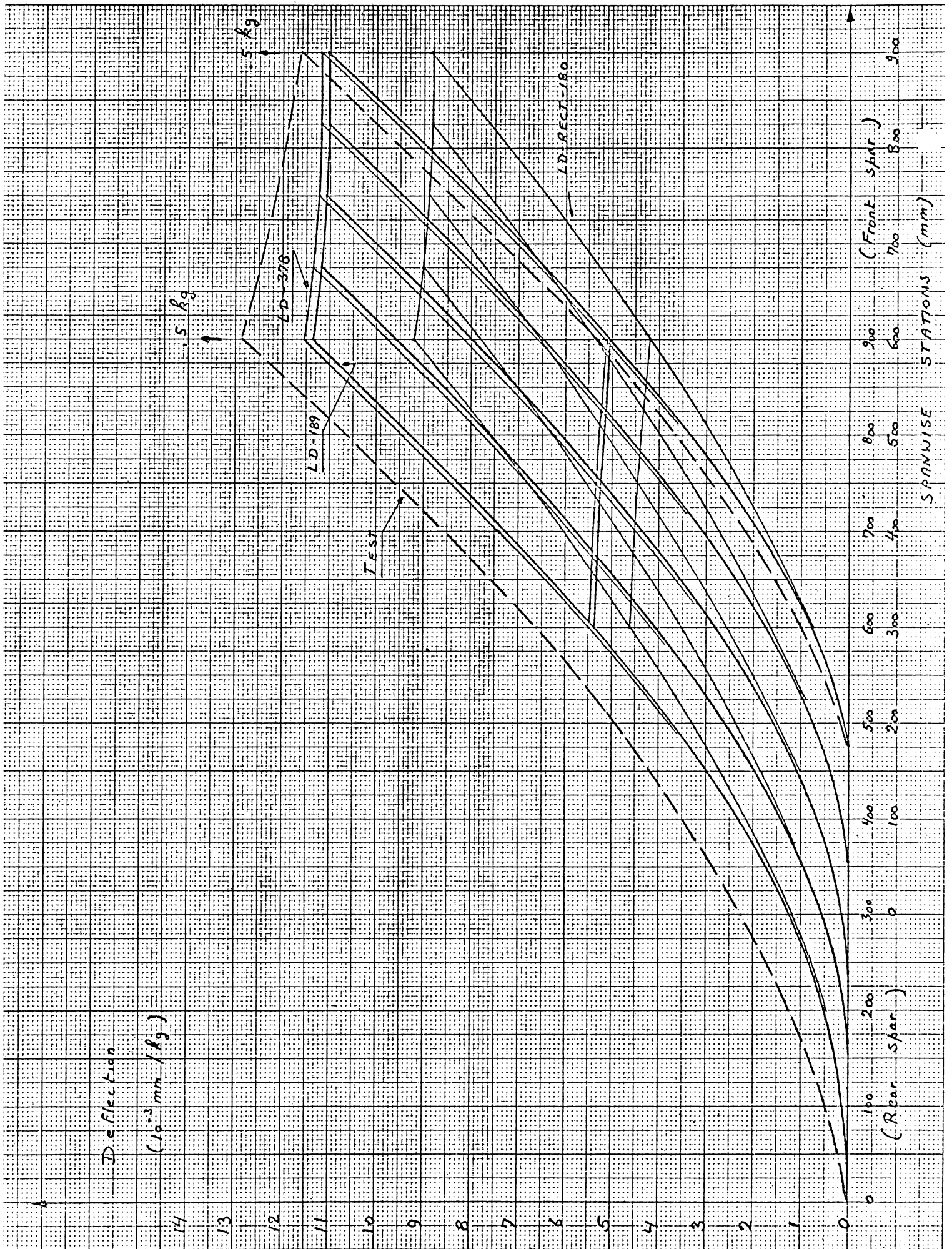


Figure F.3.101.

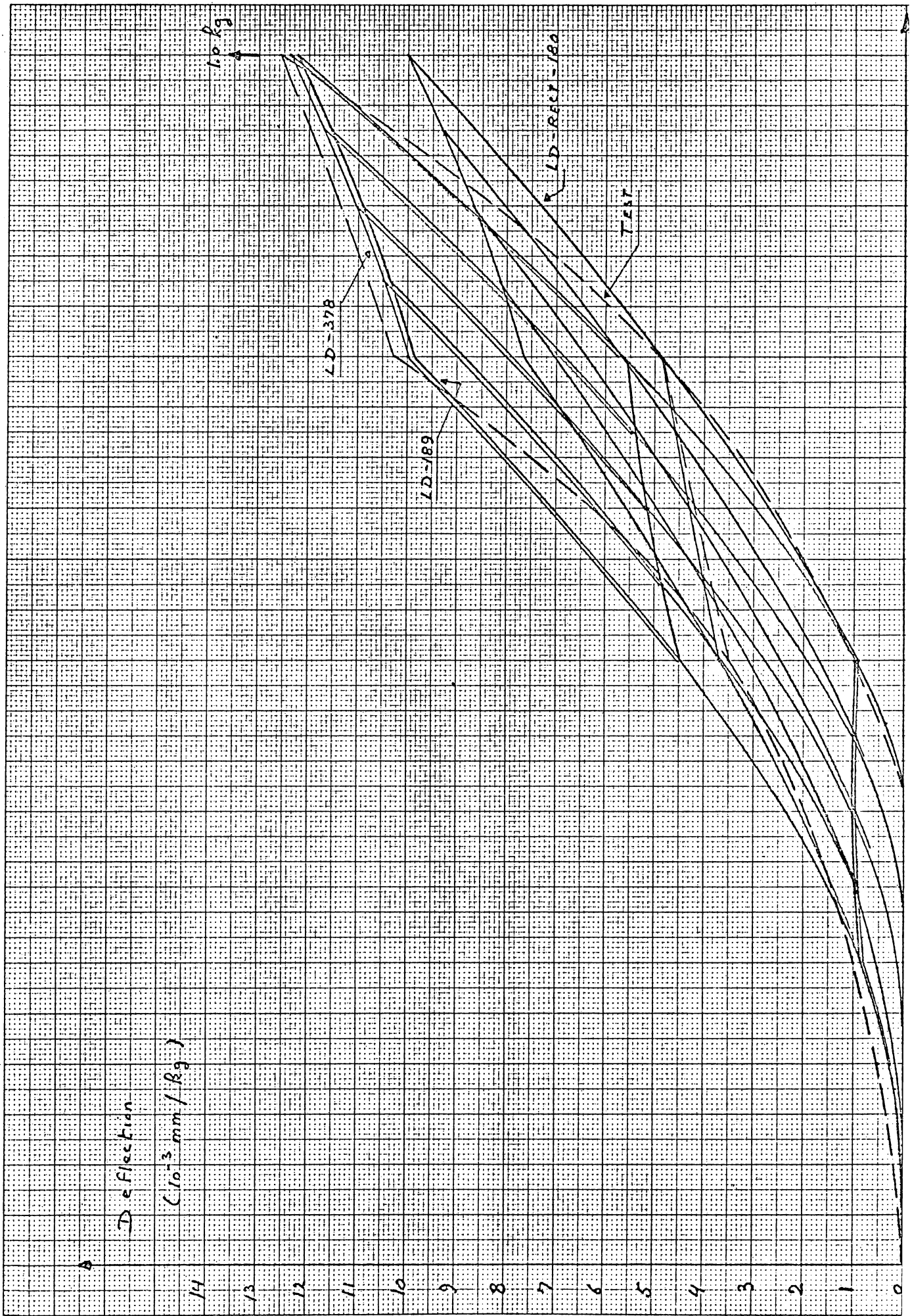
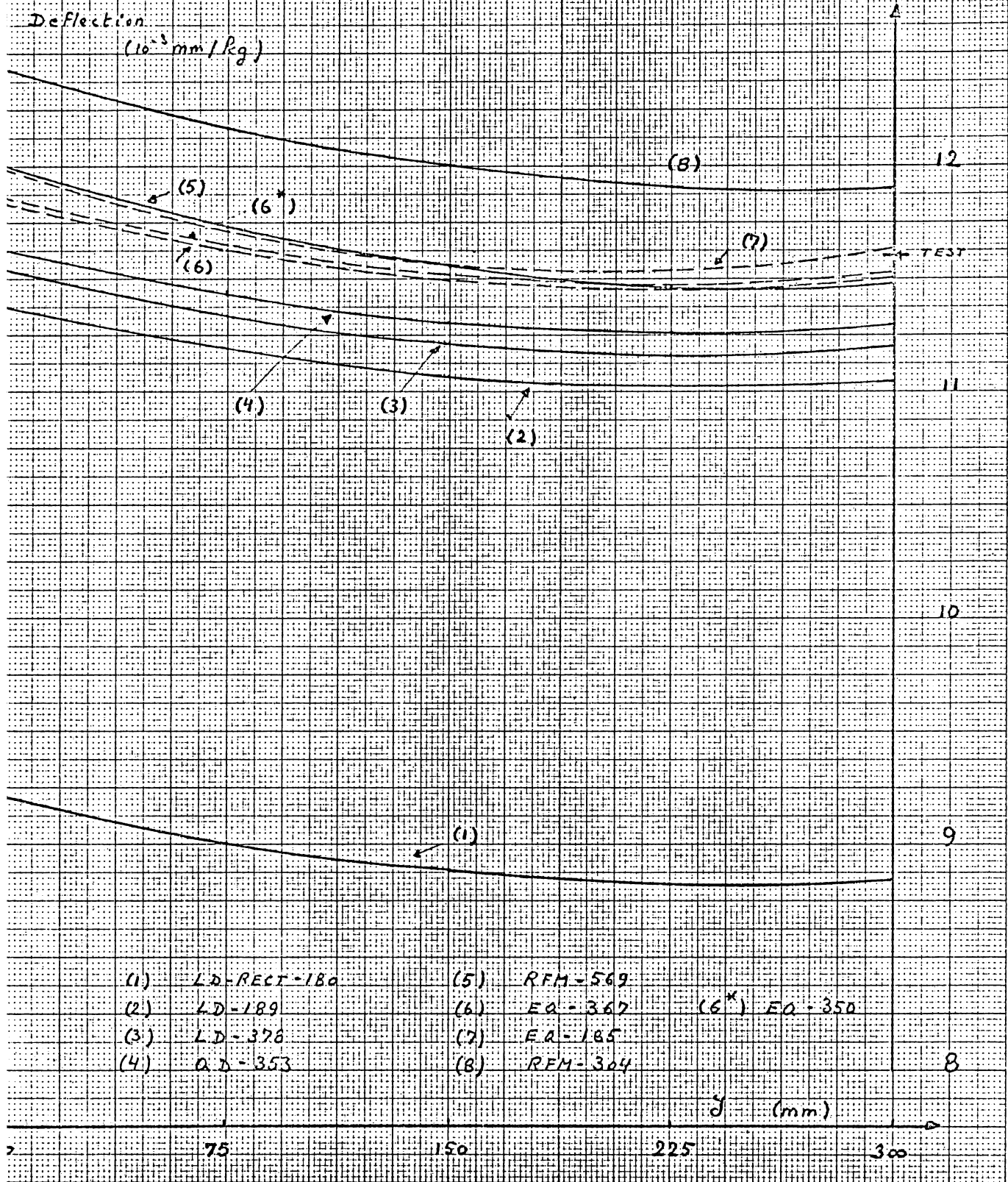




Figure E3.102

Rib 1 - Load 1



Rib 1 - Load 2

Deflection
 $\times 10^{-3}$ mm

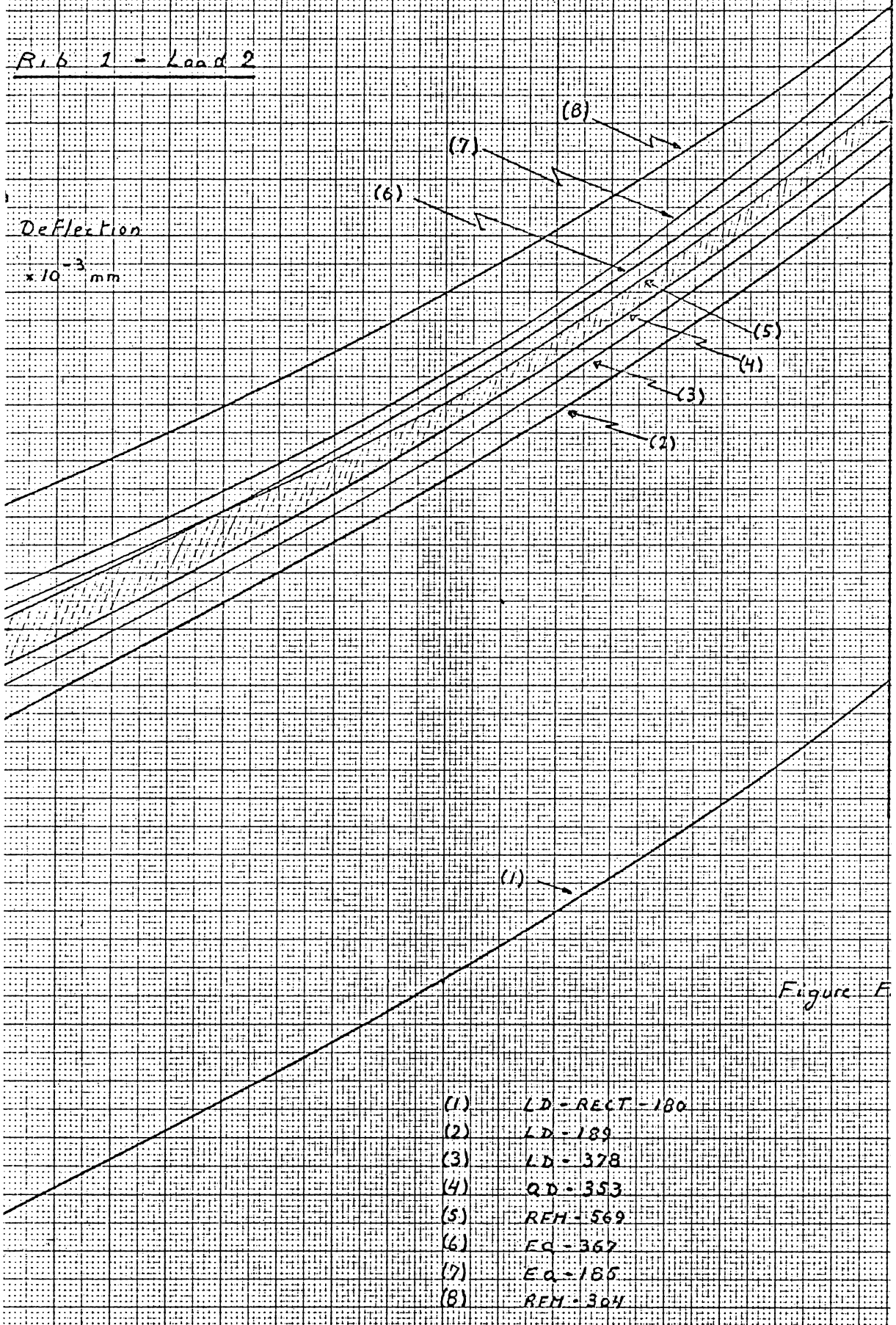
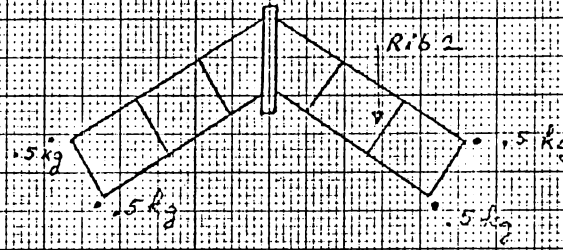


Figure F

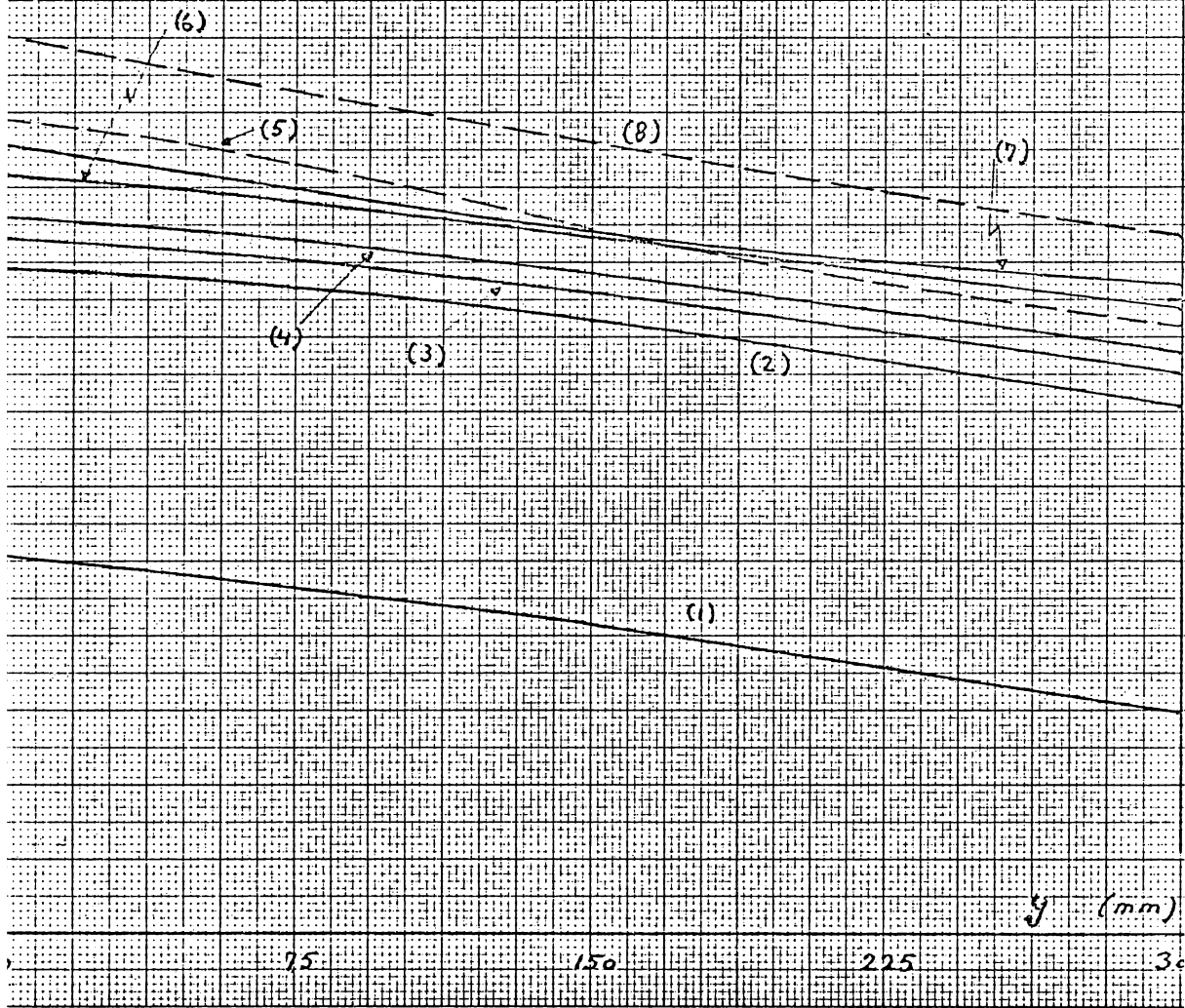
- (1) LD - RECT - 180
- (2) LD - 189
- (3) LD - 378
- (4) QD - 353
- (5) REH - 569
- (6) FC - 367
- (7) EQ - 186
- (8) REH - 304

Rib 2 - Load 1

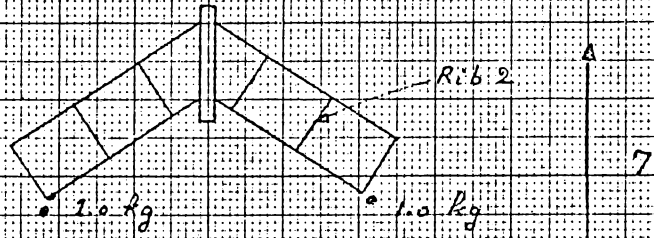
Deflection
(10^{-3} mm/kg)



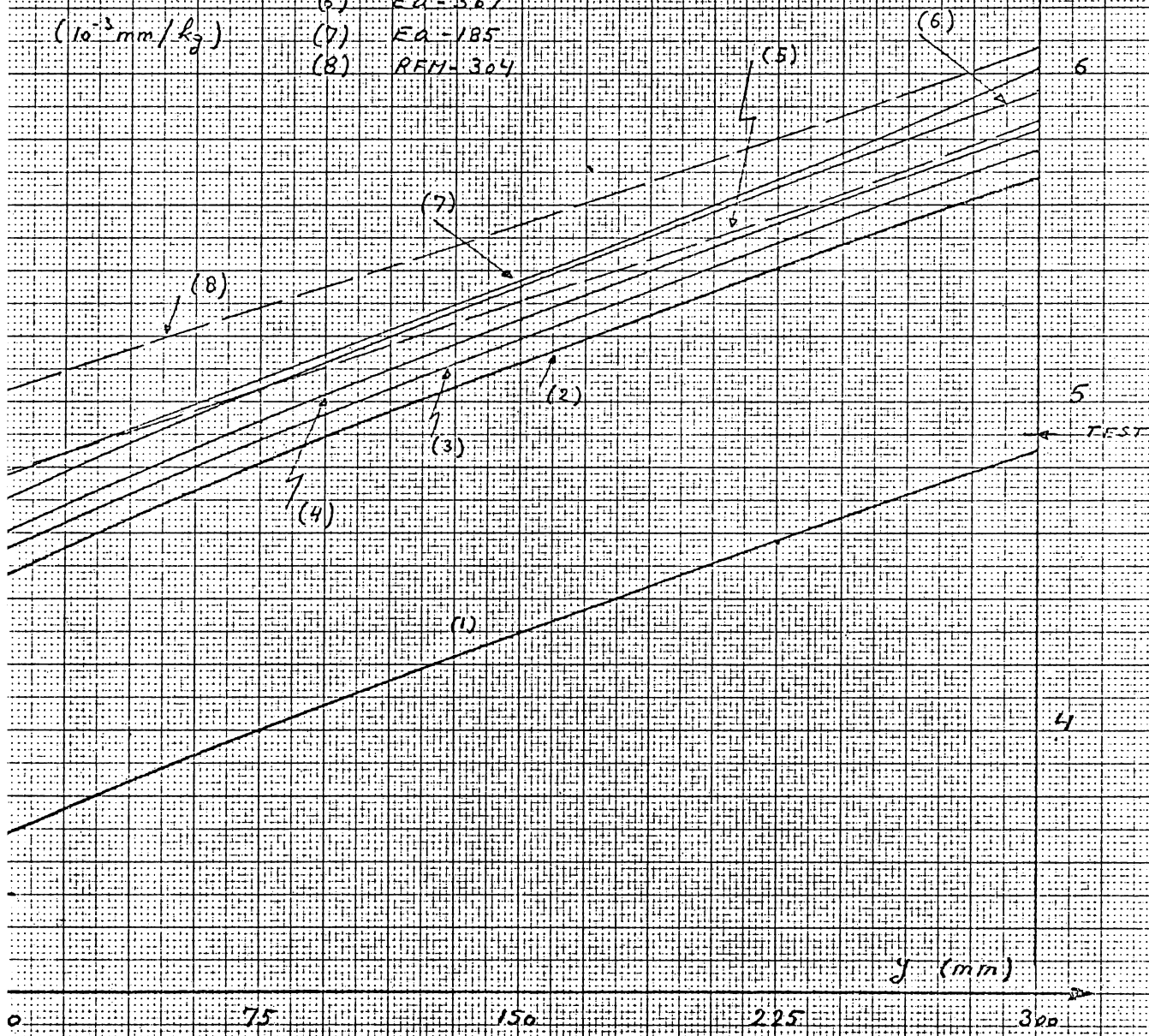
- (1) LD-RECT-180
- (2) LD-189
- (3) LD-378
- (4) QD-353
- (5) RFM-569
- (6) EQ-367
- (7) EQ-185
- (8) RFM-304



Rib 2 - Load 2



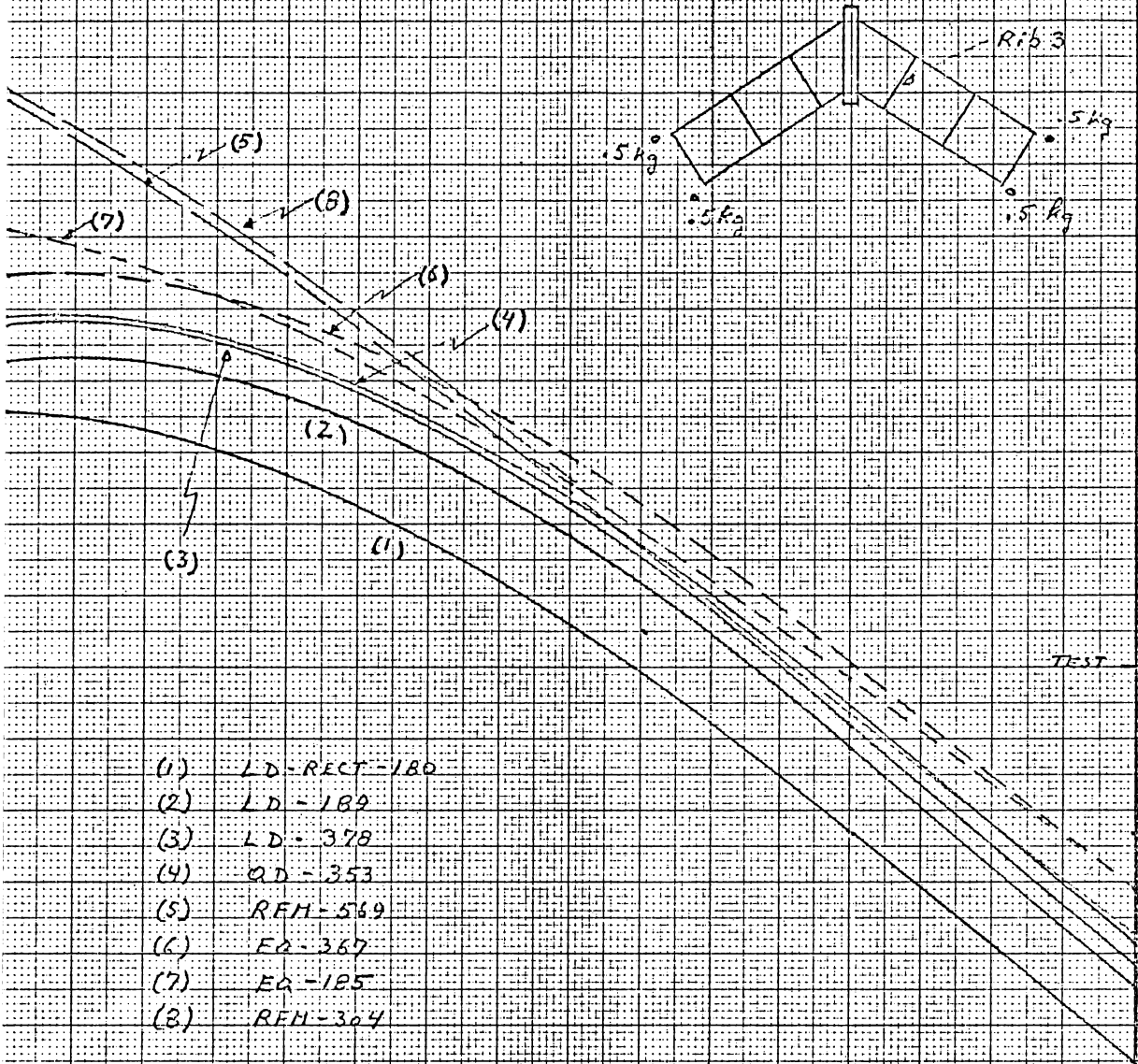
- Deflection
(10^{-3} mm/kg)
- (1) LD-RECT-180
 - (2) LD-189
 - (3) LD-378
 - (4) QD-353
 - (5) REM-569
 - (6) EA-367
 - (7) EA-185
 - (8) REM-304



Deflection

(10^{-3} mm/kg)

Figure E3.105

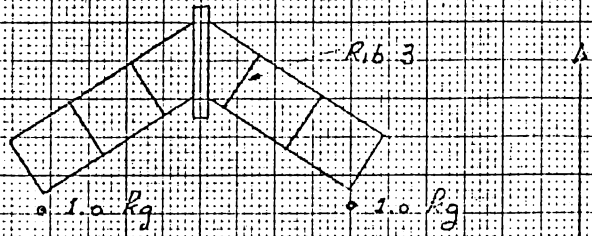


Rib 3 - Load 1

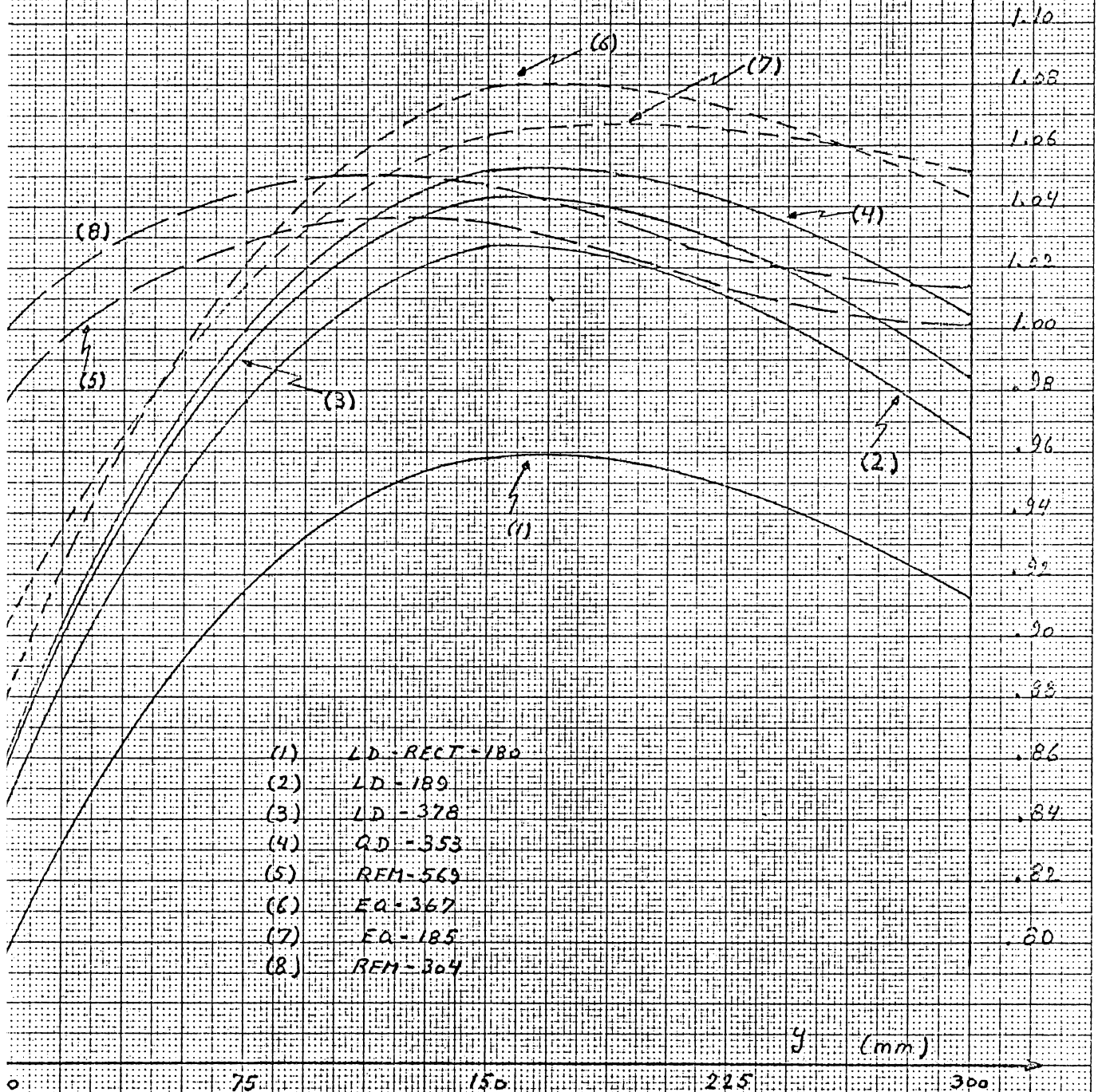
y (mm)

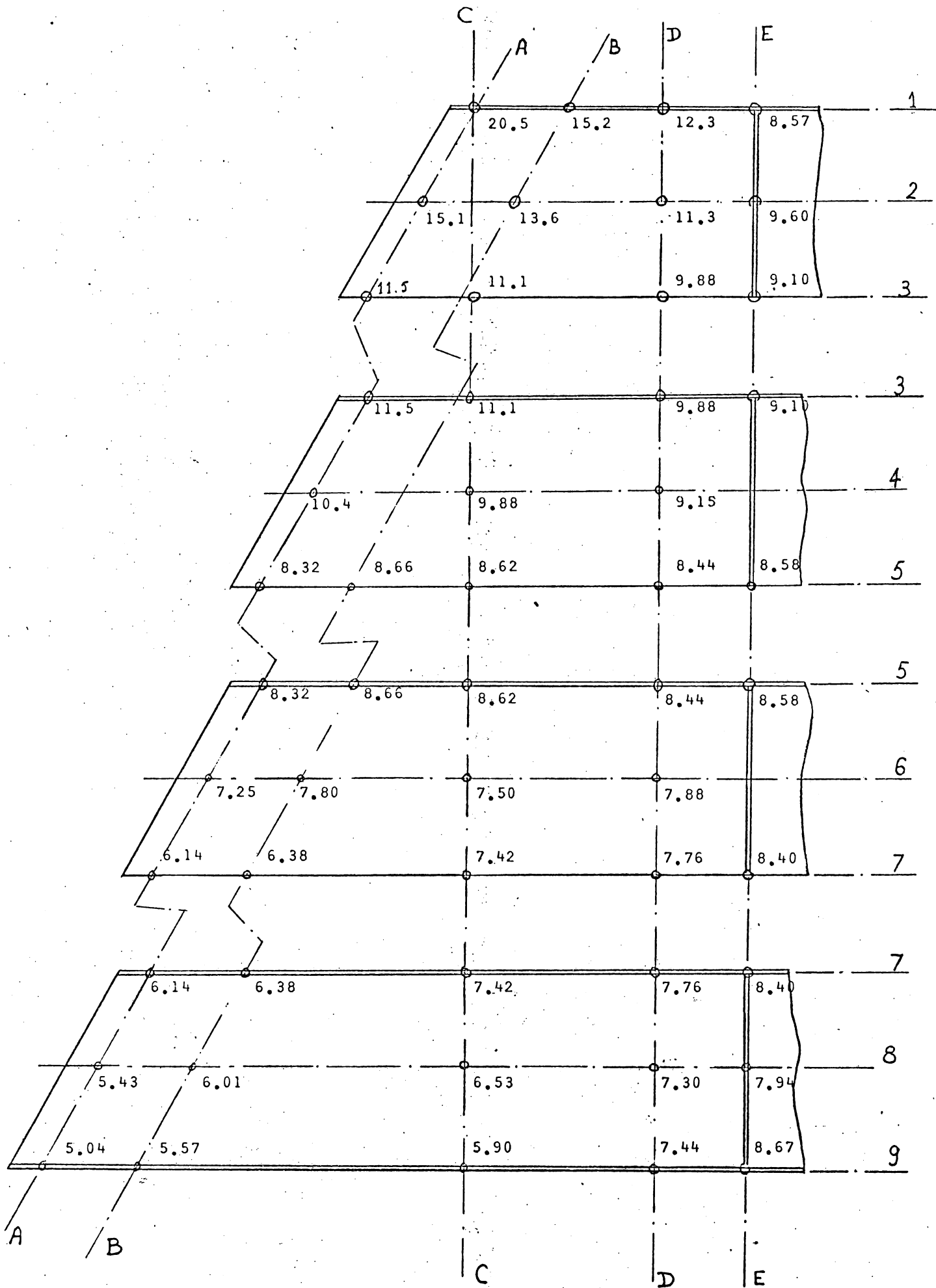
0 75 150 225 300

Rib 3 - Load 2



Deflection
(10^{-3} mm/kg)





N.B.: axis lines 1 to 9 and A to E refer to Figure F.3.69.

Figure F.3.108. Experimental σ_x stresses for load case nbr 2.

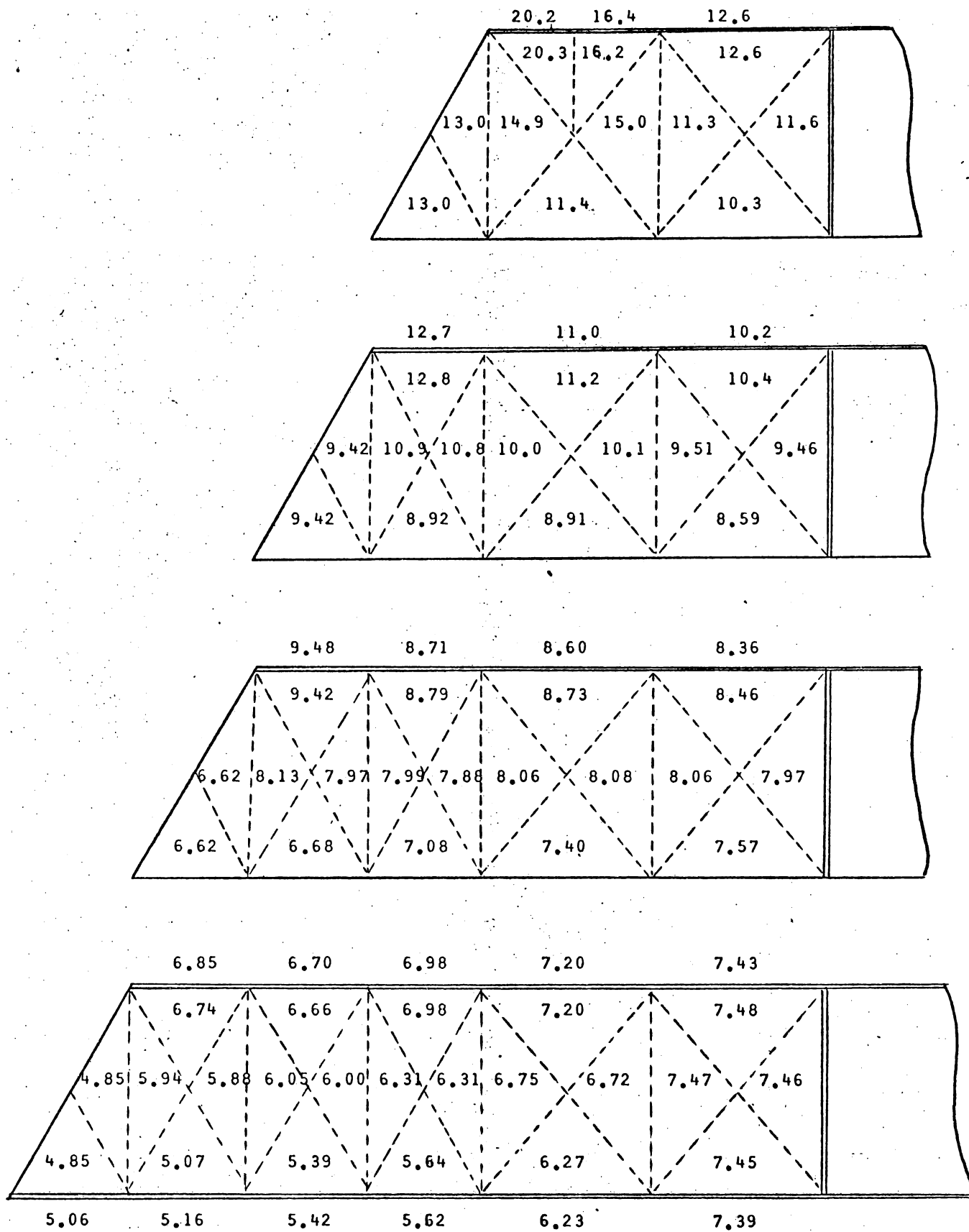


Figure F.3.I09. σ_x stress distribution for idealization LD-378 and load nbr 2.

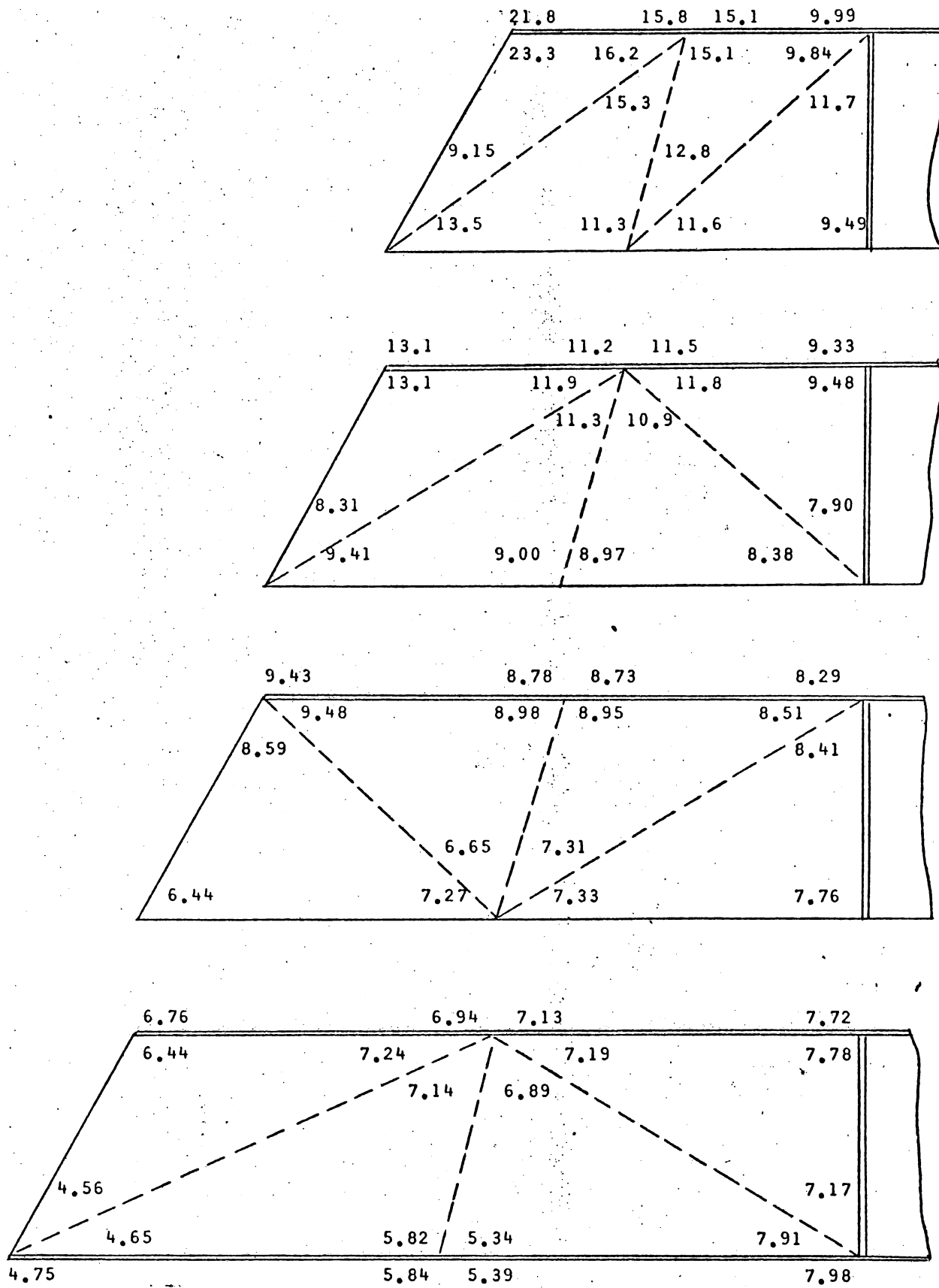


Figure F.3.II0. σ_x stress distribution for idealization QD-353 and load nbr 2.

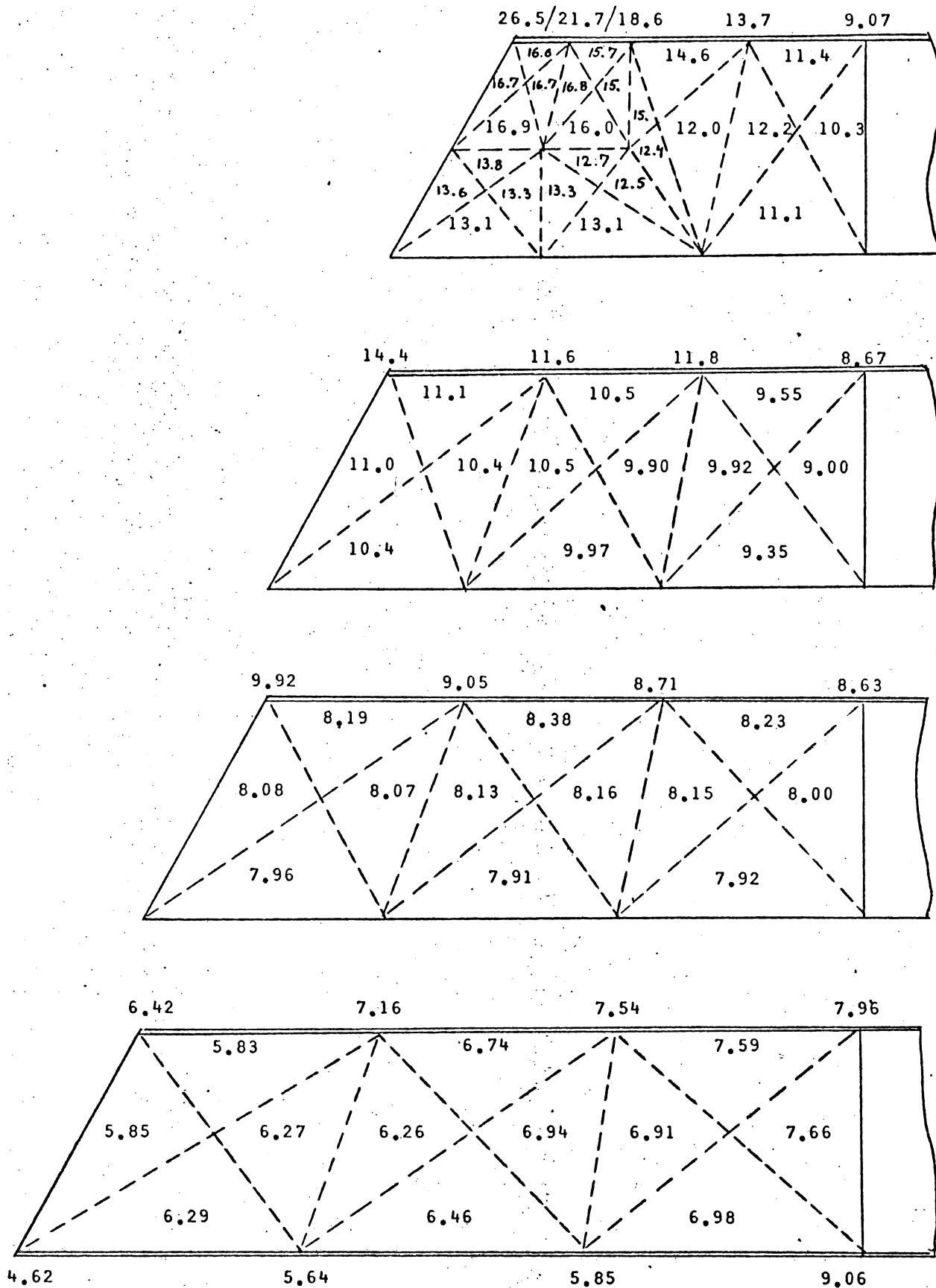


Figure F.3.III. σ_x stress distribution for idealization EQ-367 and load nbr 2.

Order of listing : σ_x
 σ_{max}

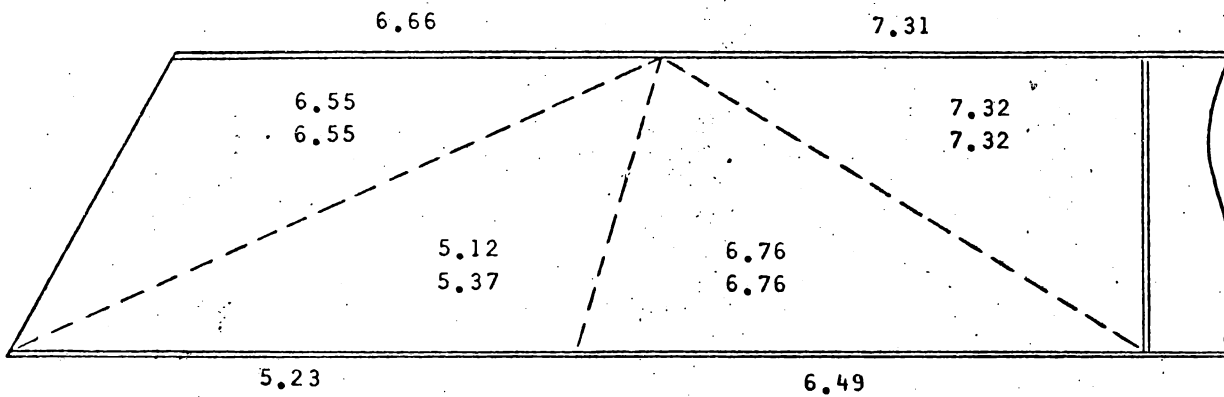
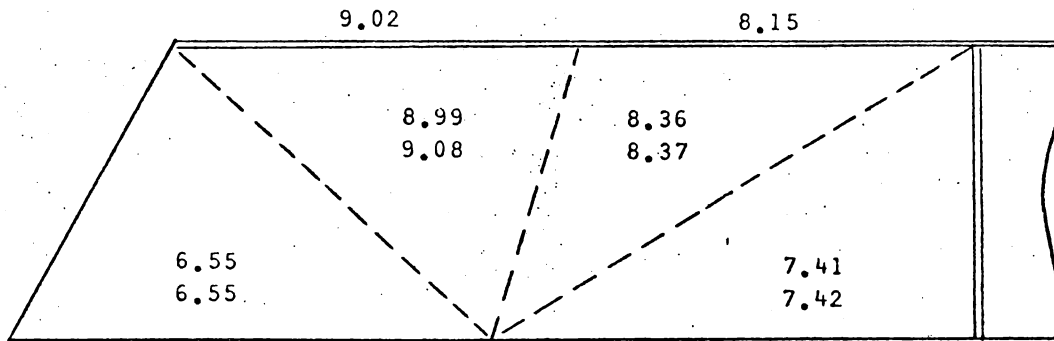
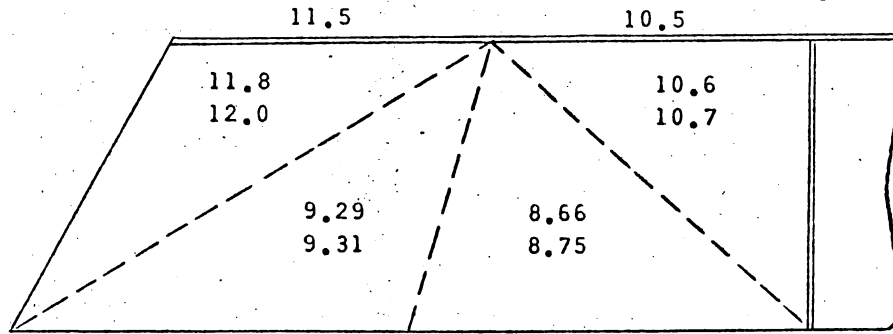
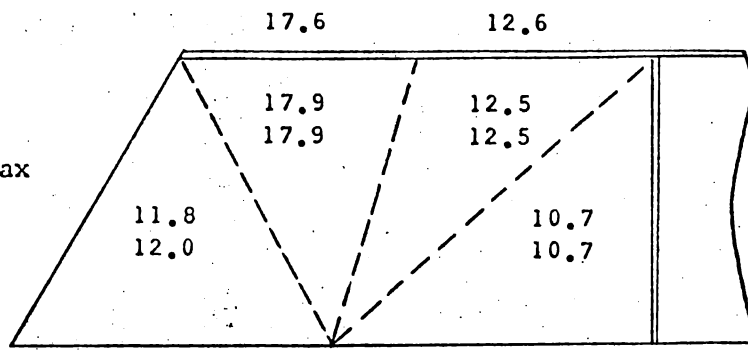


Figure F.3.II2. σ_x stress distribution for idealization LD-I85 and load nbr 2.

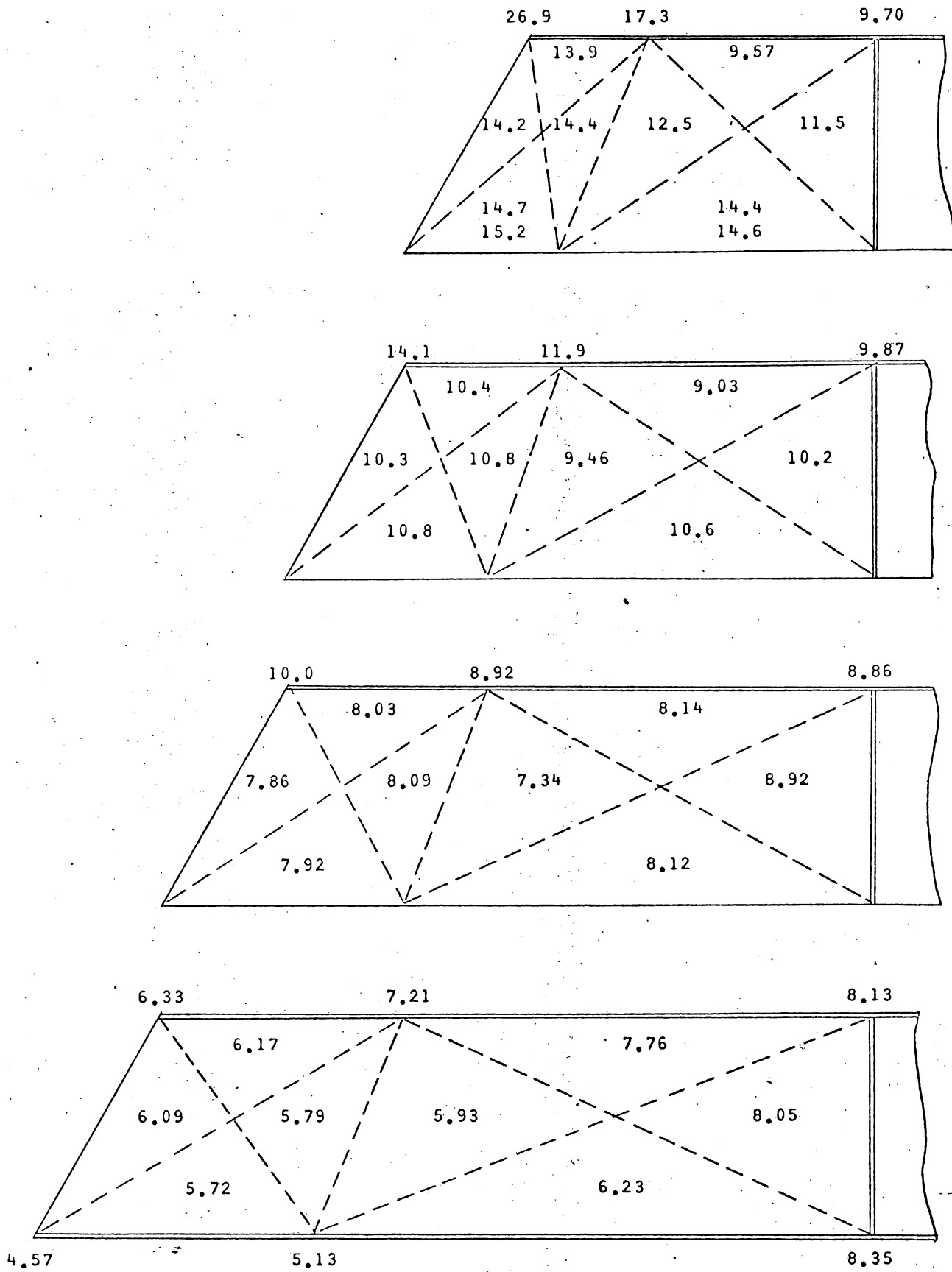
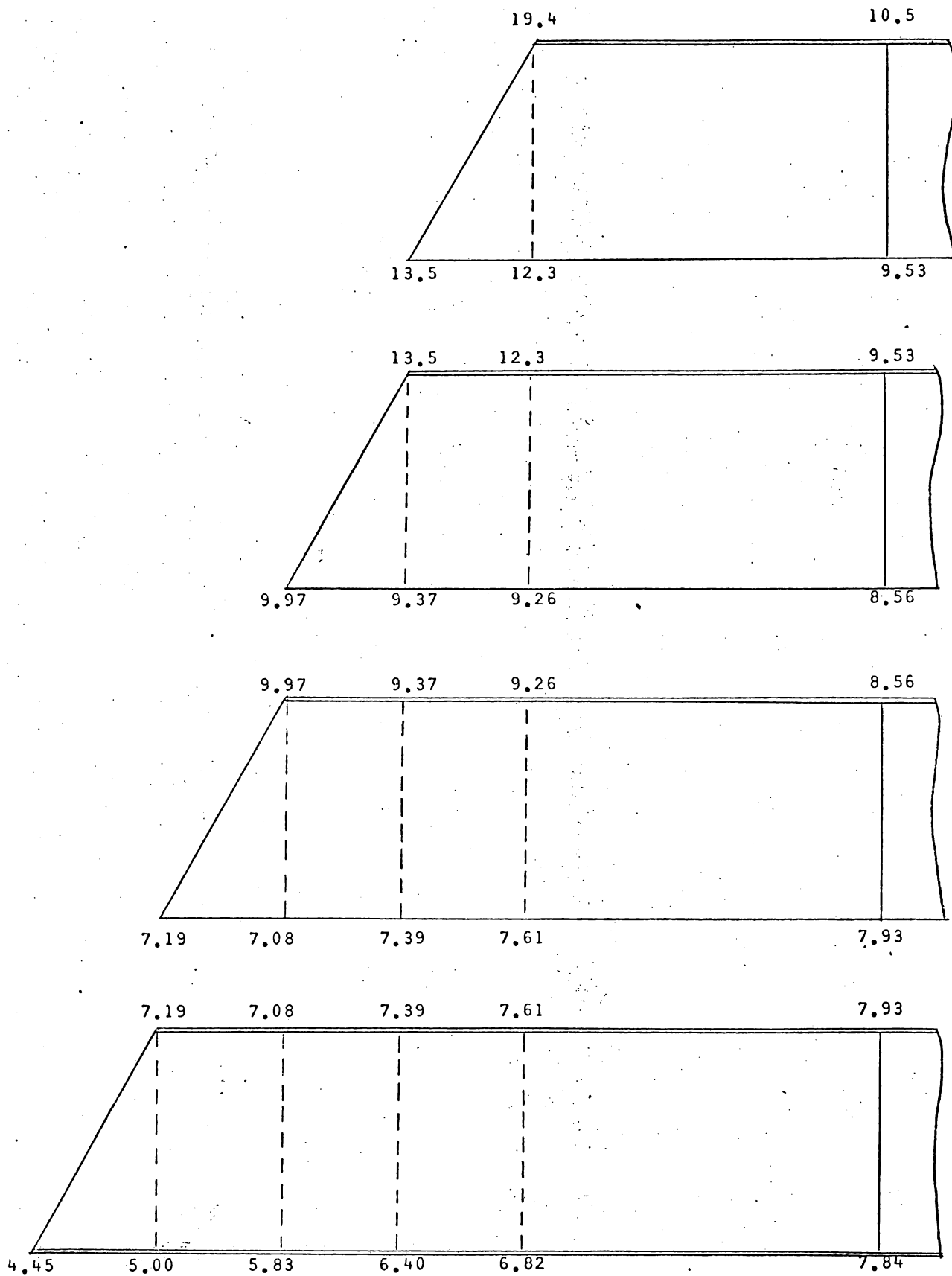
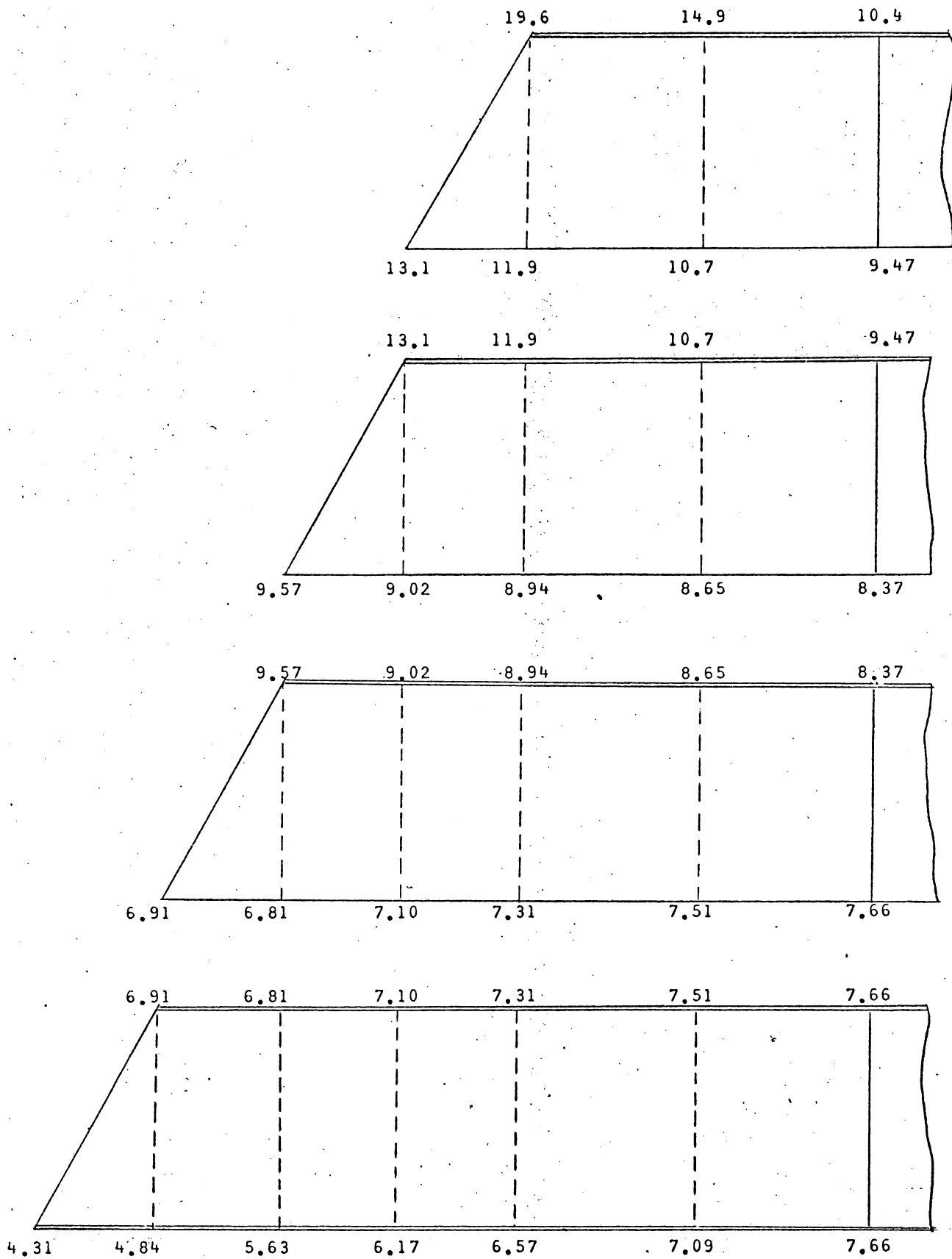


Figure F:3.II3. σ_x stress distribution for idealization EQ-I85 and load nbr 2.



N.B.: shear stresses are less than $.5 \text{ Kg/mm}^2$ in all the panels.

Figure F.3.II4. σ_x stress distribution for idealization RFM-304 and load nbr 2.



N.B.: shear stresses are less than $.5 \text{ Kg/mm}^2$ in all the panels.

Figure F.3.II5. σ_x stress distribution for idealization RFI-569 and load nbr 2.

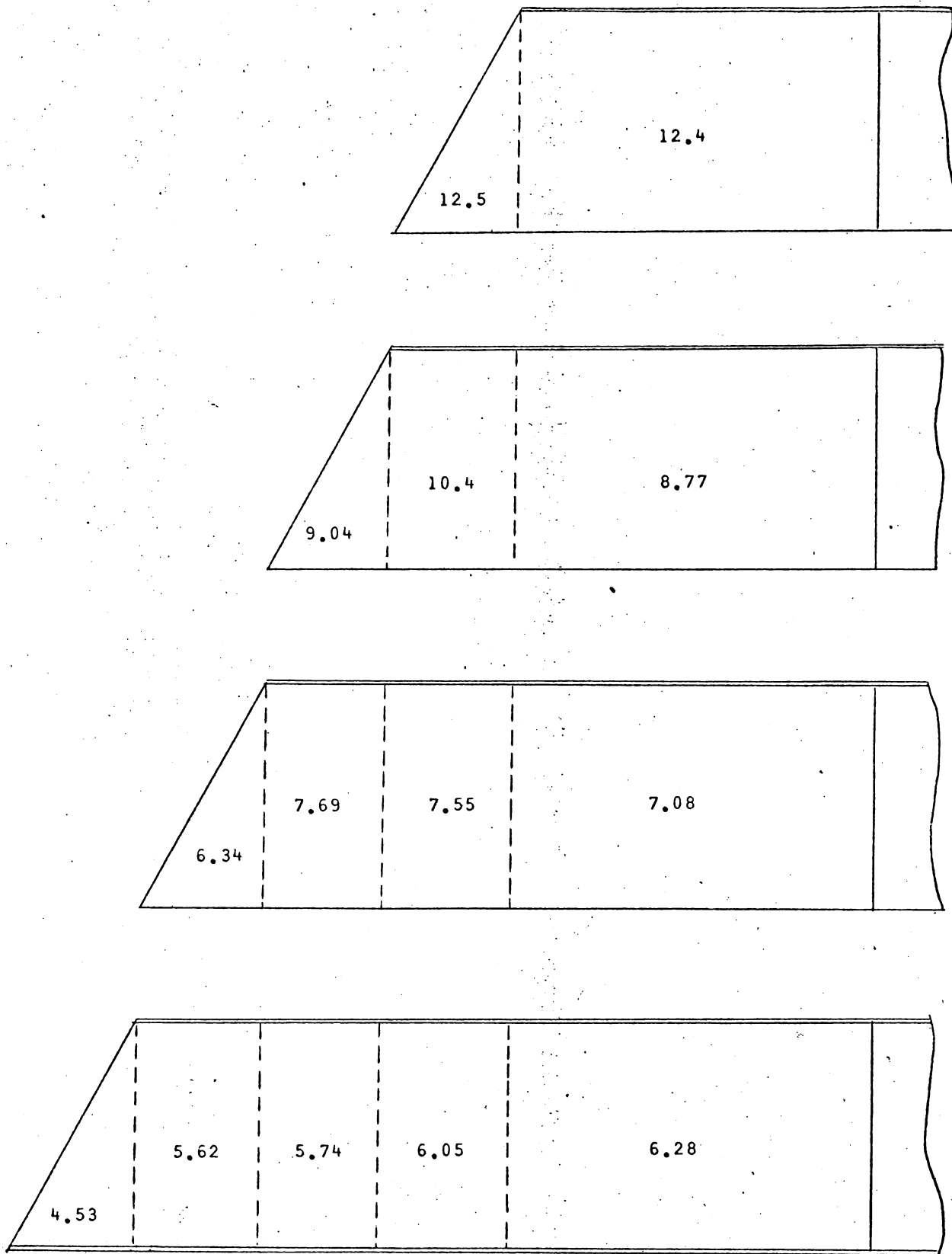
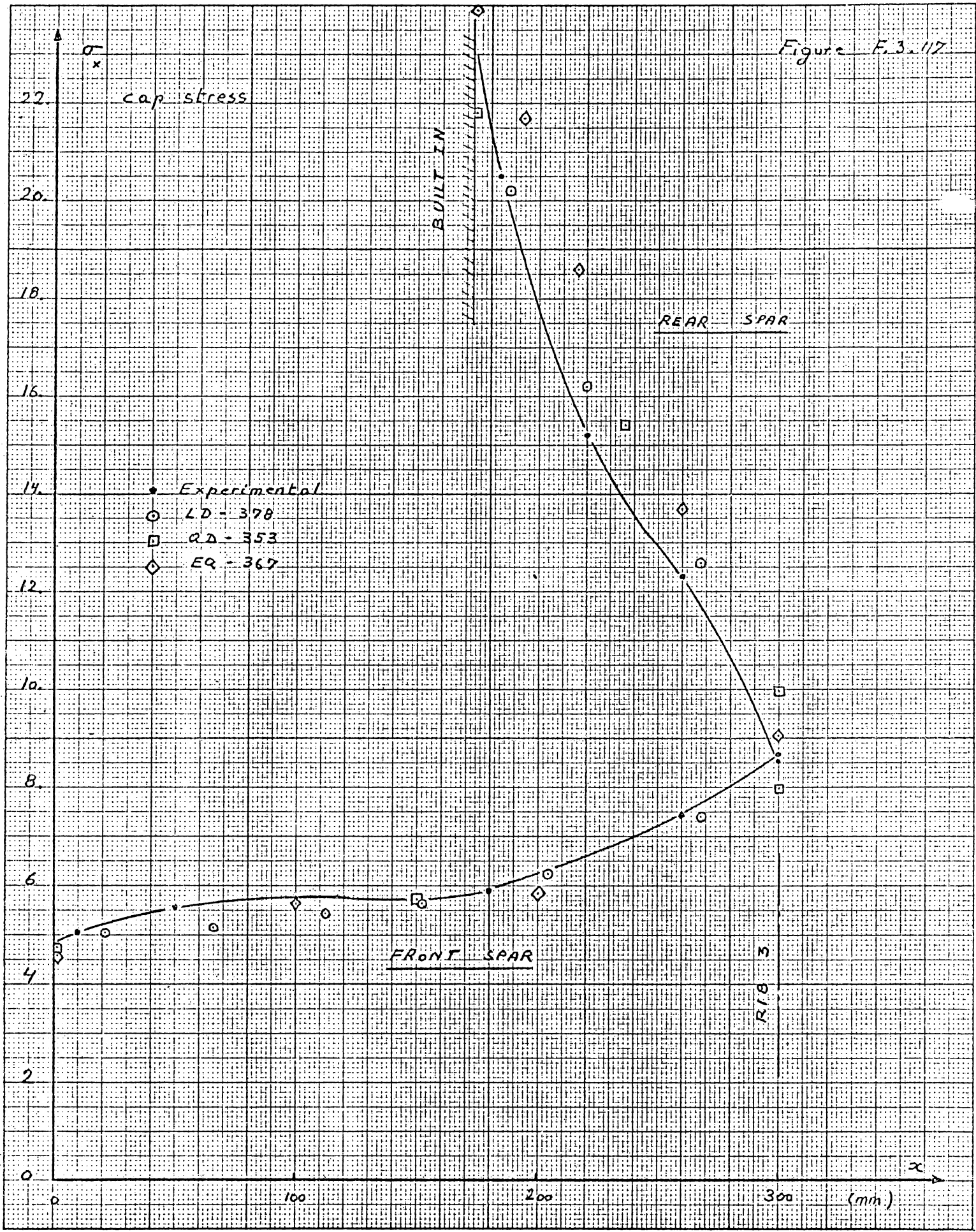
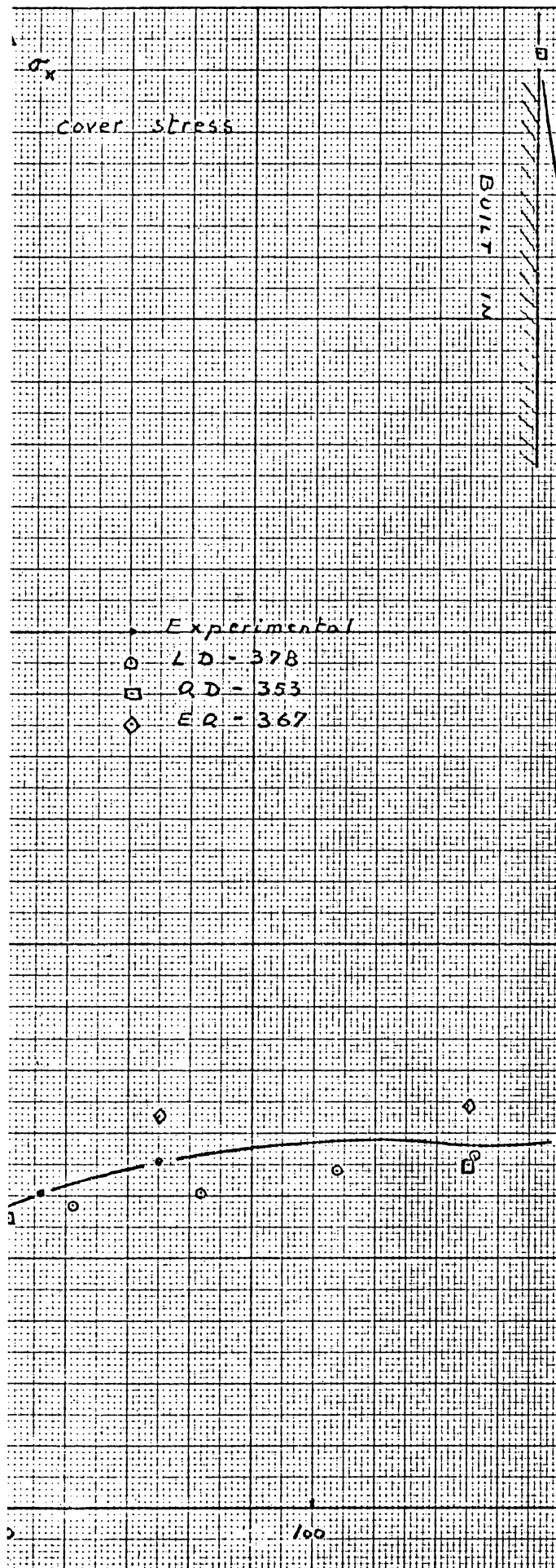


Figure F.3.II6. σ_x stress distribution for idealization LD-RECT-I80

and load nbr 2.

Figure F.3.17





SWEDISH WING MODEL

quadratic compatible analysis

353 gen. coord.

load nbr. 2

Principal stresses σ_{max}

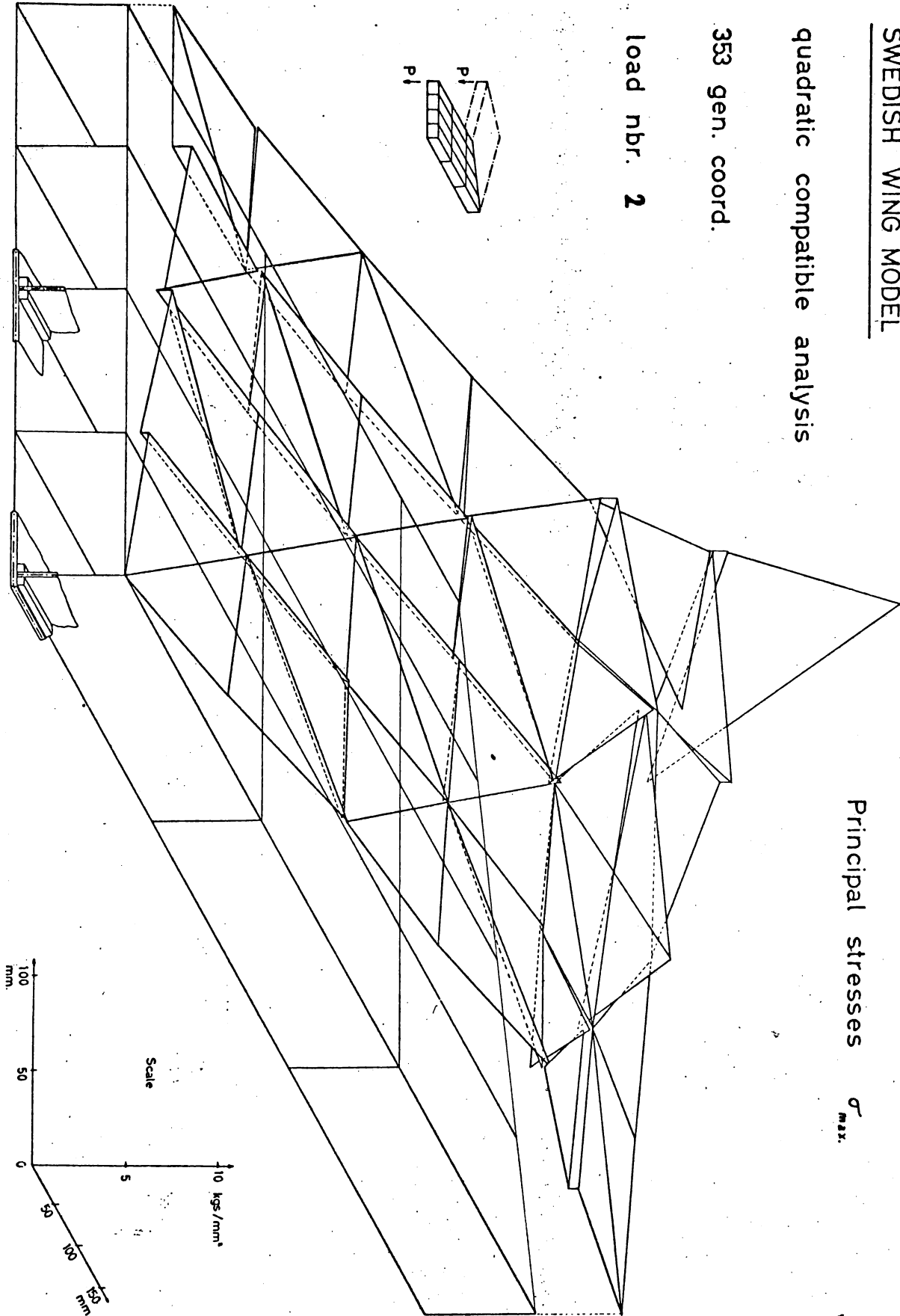


Figure F.3.120.

SWEDISH WING MODEL

linear compatible analysis

378 gen. coord.

load nbr. 2

Principal stresses σ_{max}

- Stress at a centroid of a triangle
- Test

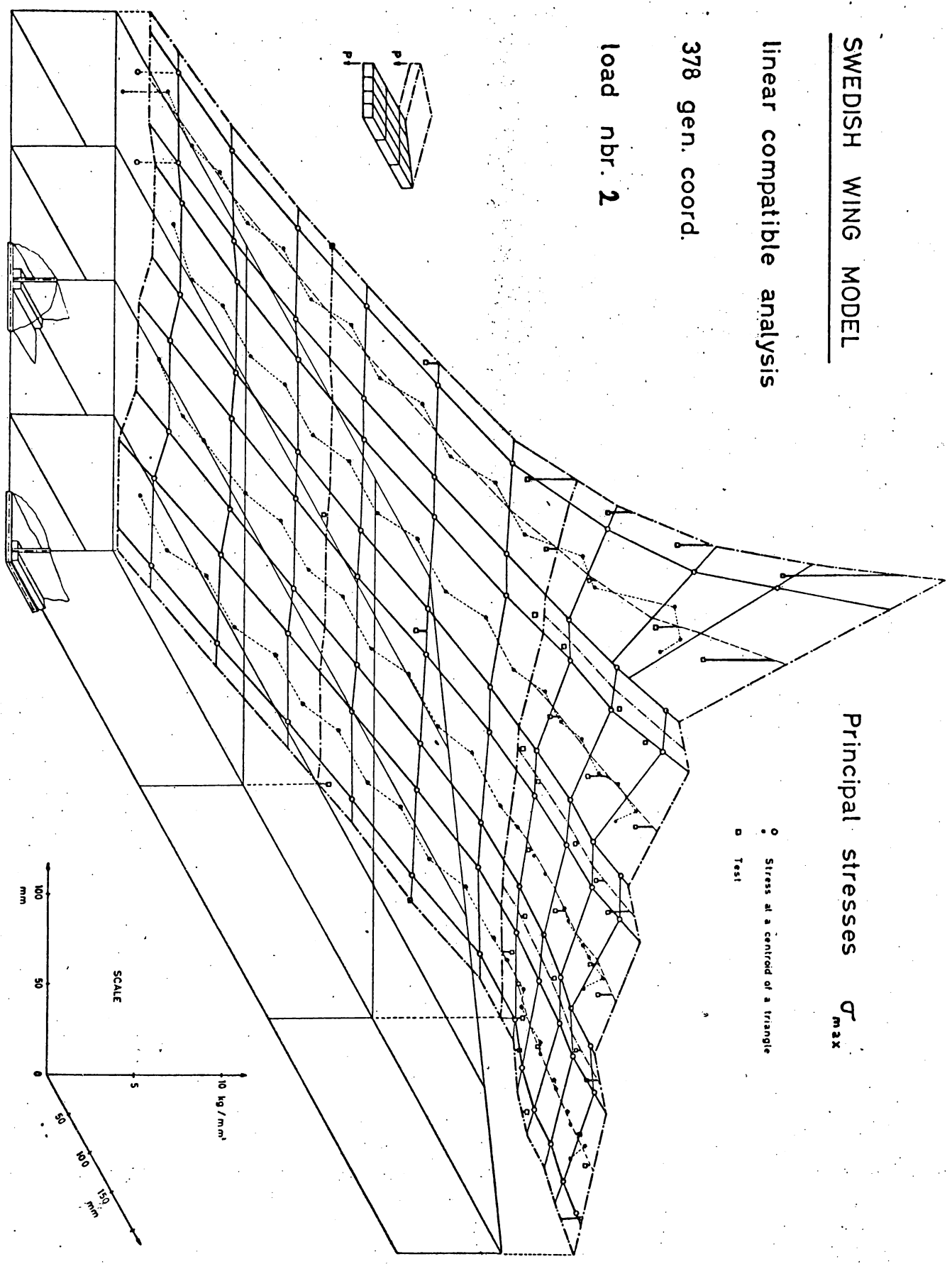


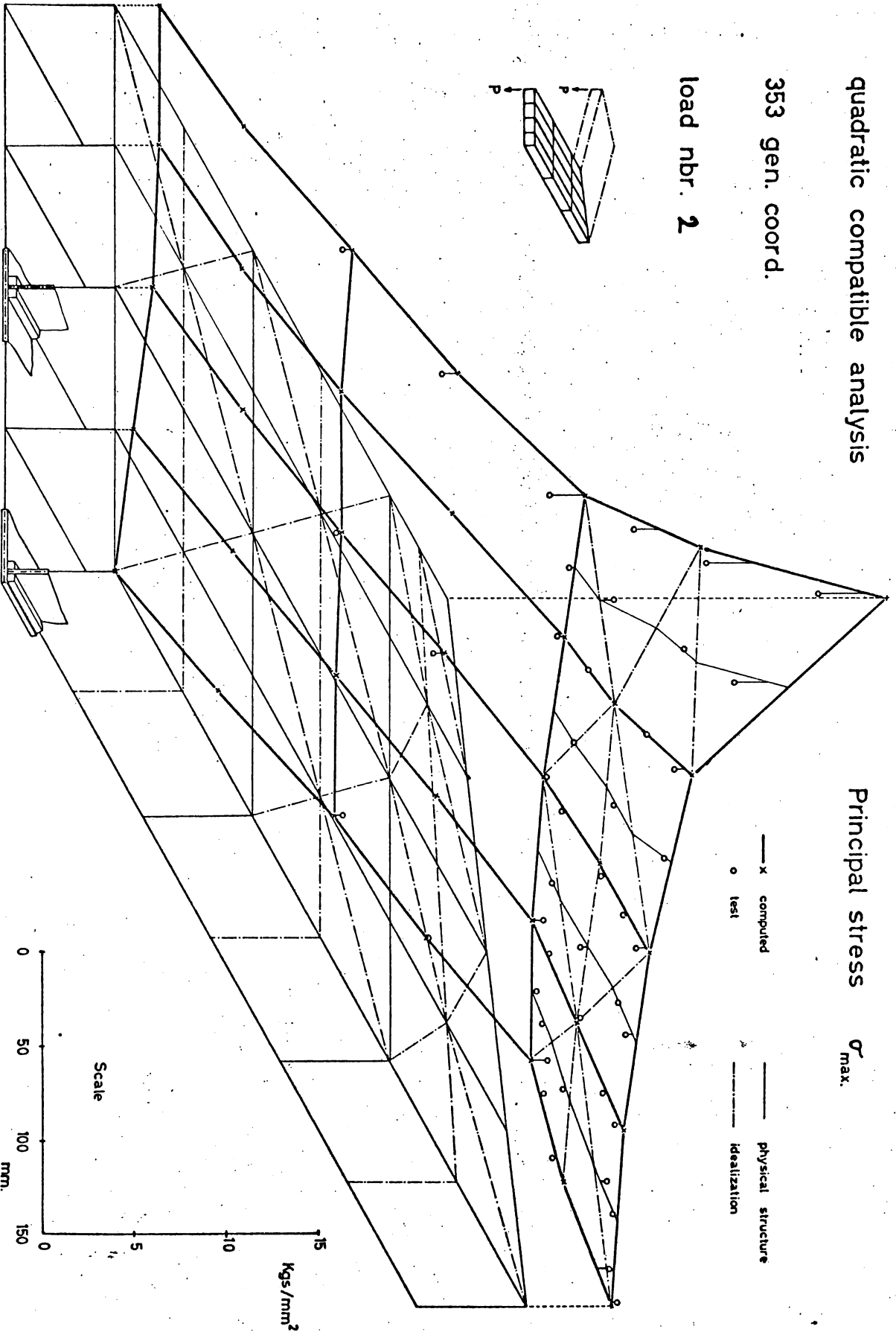
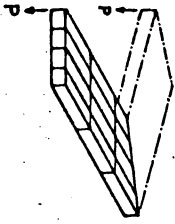
Figure F.3.121.

SWEDISH WING MODEL

quadratic compatible analysis

353 gen. coord.

load nbr. 2



SWEDISH WING MODEL

Principal stresses σ_{max}

linear compatible analysis

378 gen. coord.

load nbr. 2

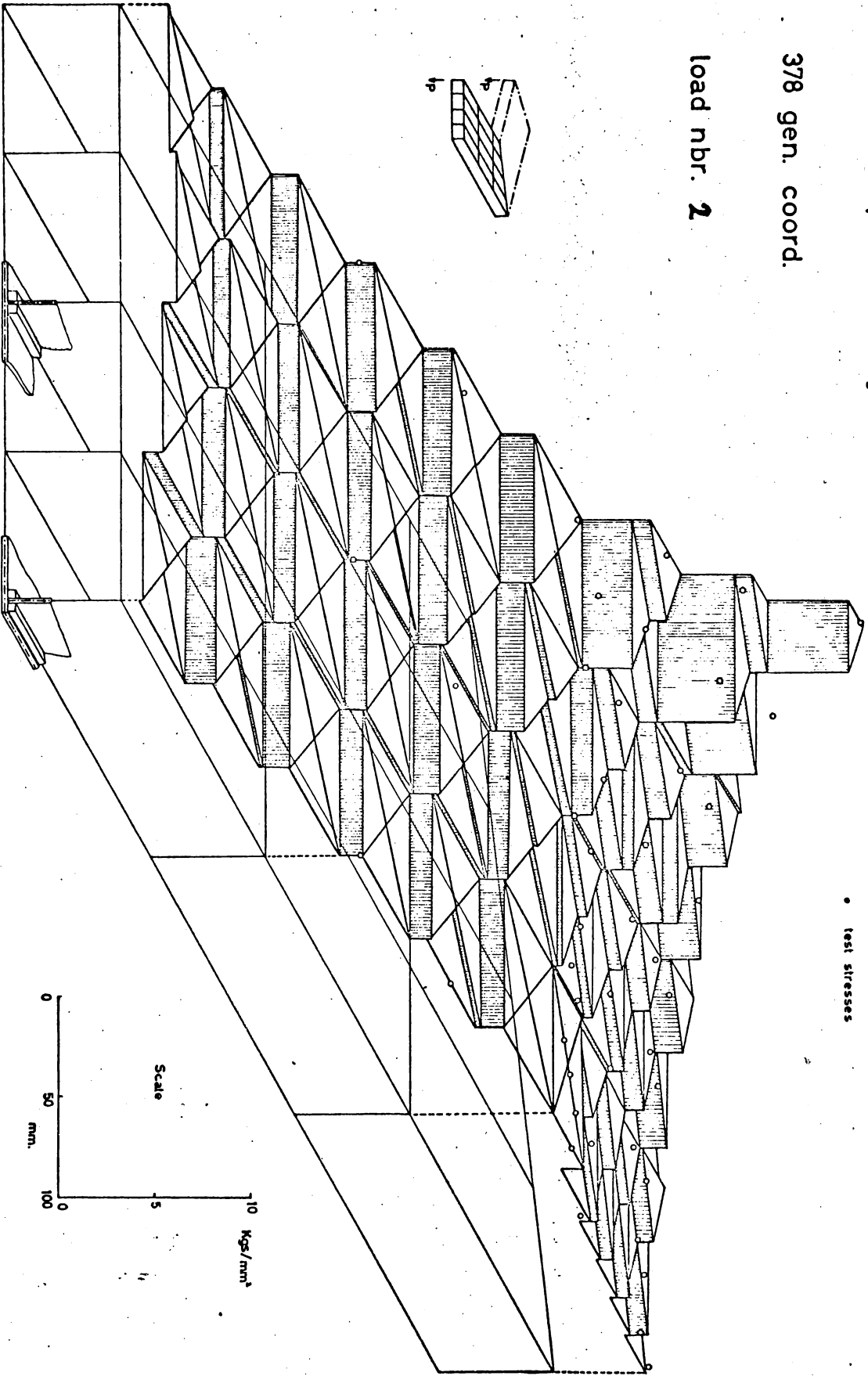


Figure P.3.II9.

Figure F.3.I23. Experimental shear stresses for load nbr 2.

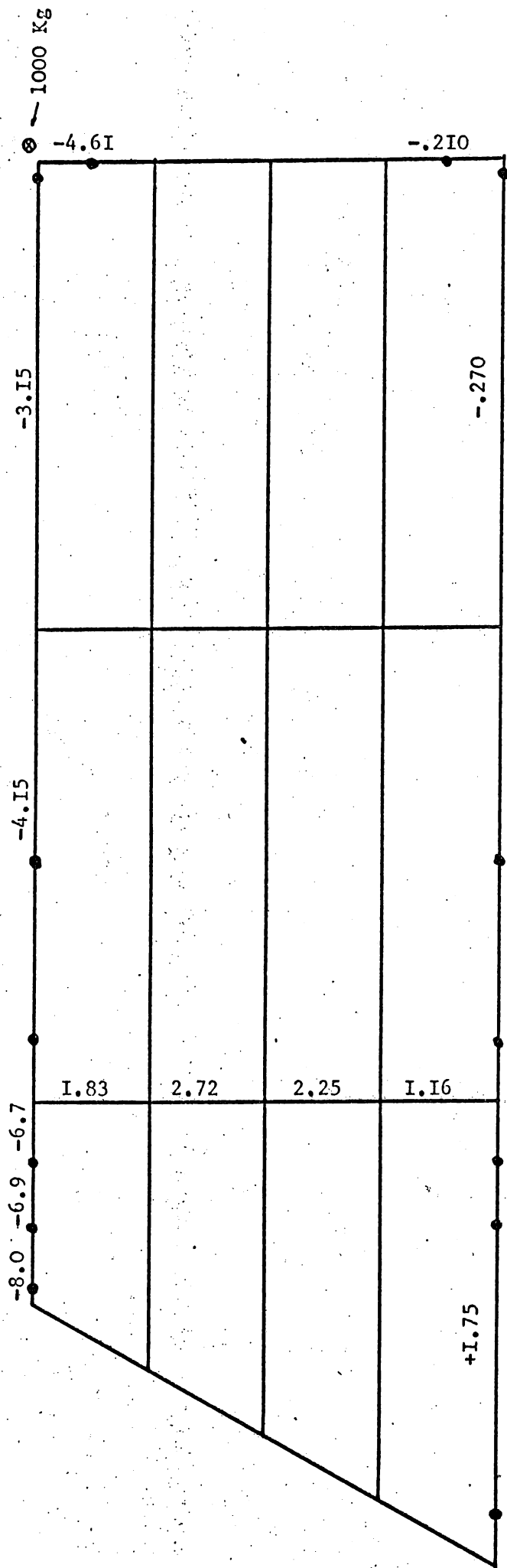


Figure F.3.124. Shear stresses for idealization LD-378 and load nbr 2.

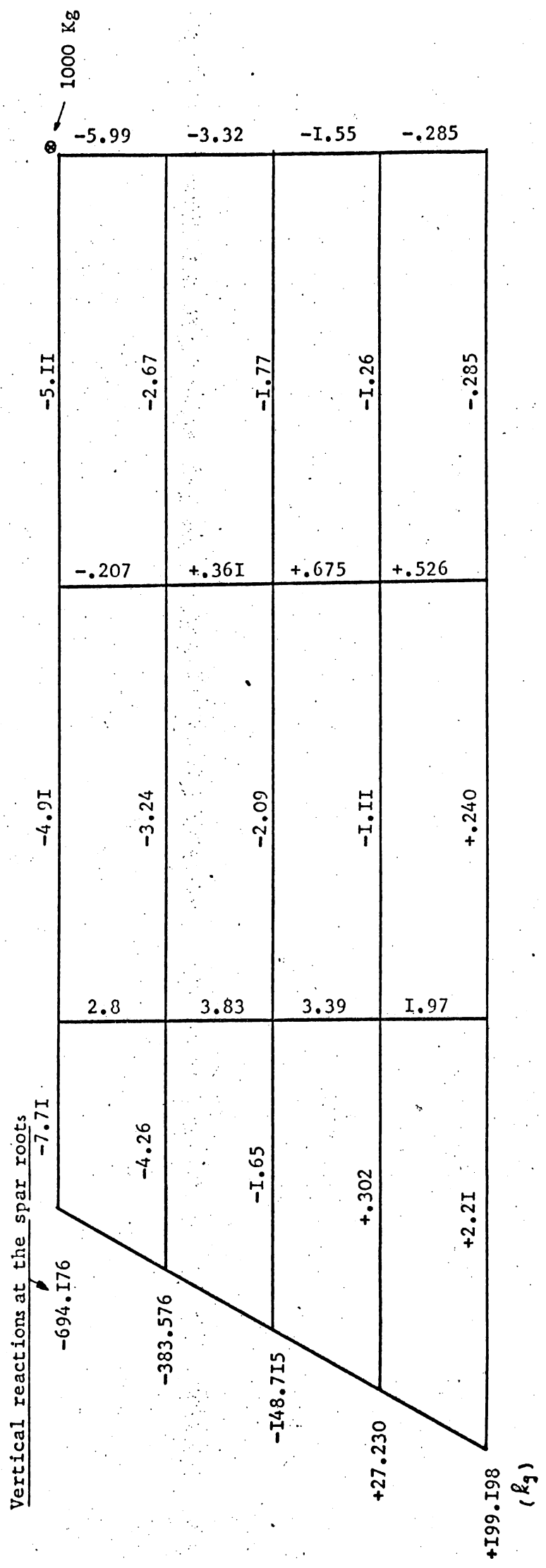


Figure F.3.I25. Shear stresses for idealization QD-353 and load nbr 2.

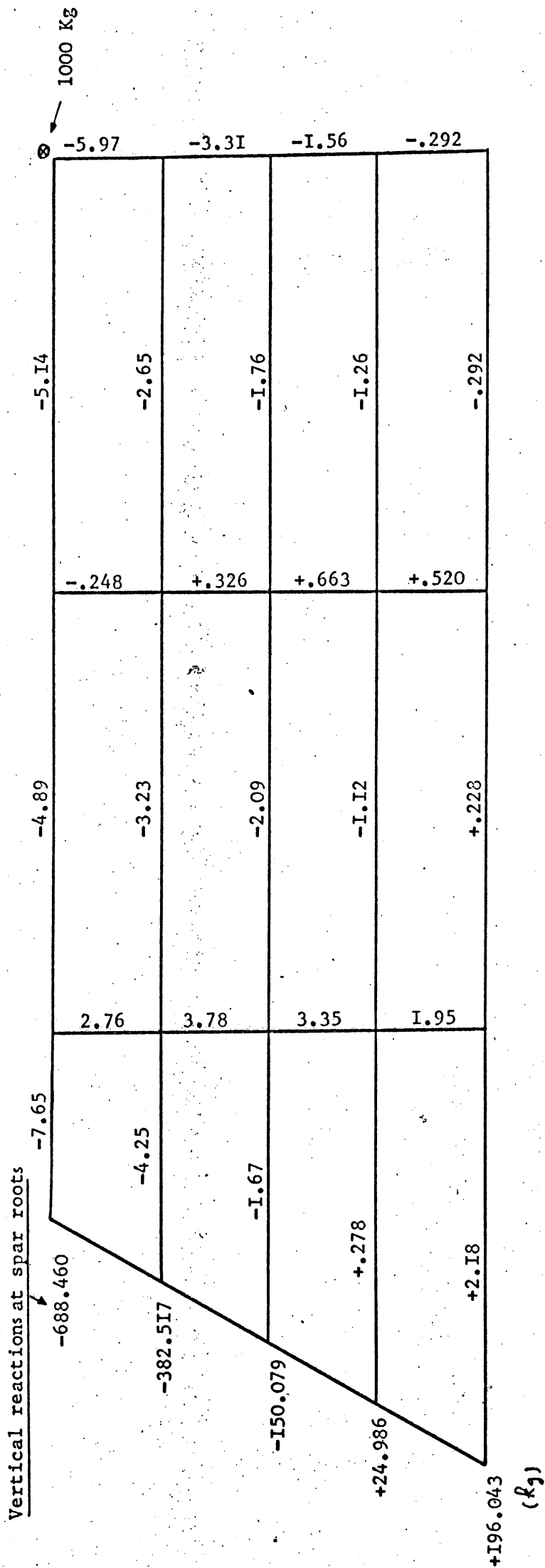


Figure F.3.126. τ_{xz} min and τ_{xz} max distribution for idealization EQ-367 and load nbr 2.

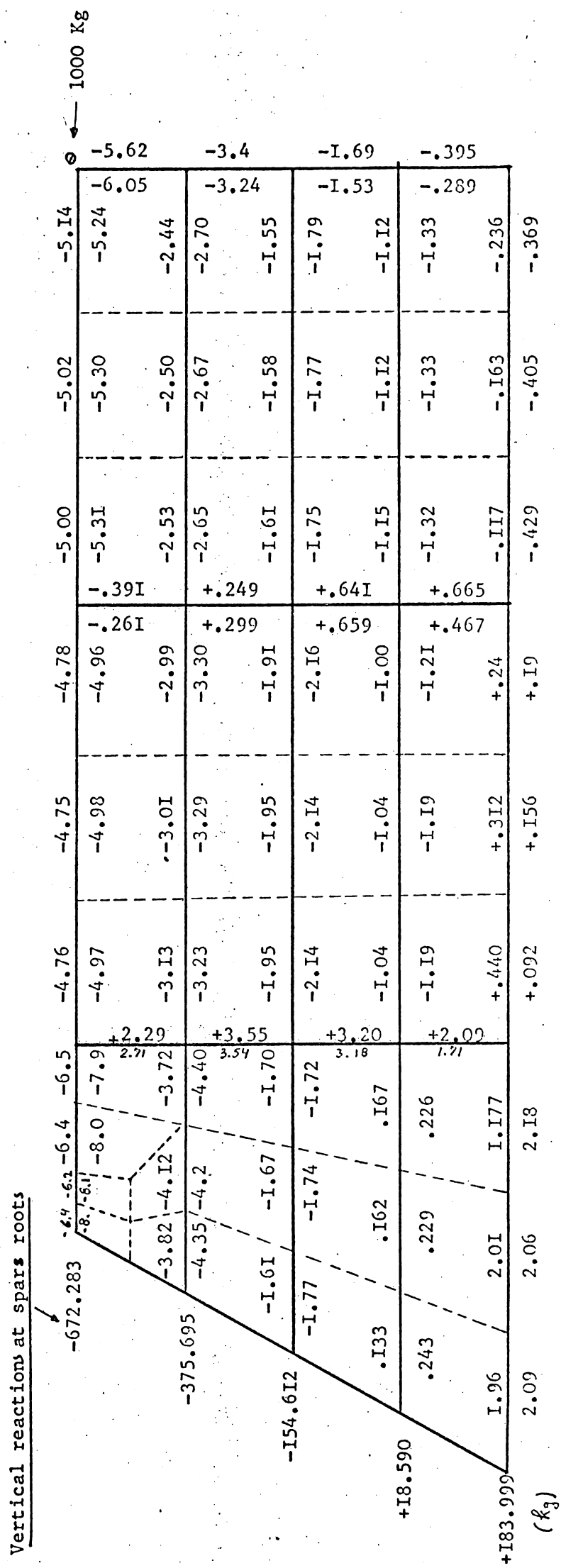


Figure F.3.127. Average shear stresses distribution for idealization EQ-367 and load nbr 2.

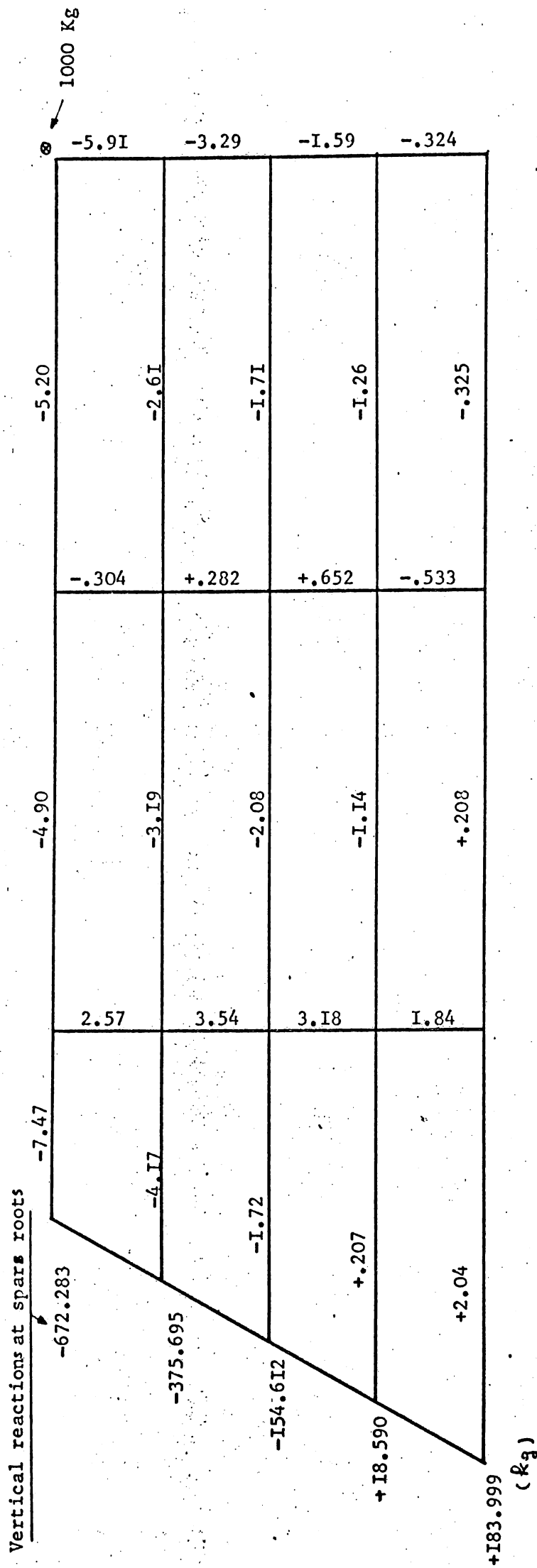


Figure F.3.128. Shear stresses distribution for idealization RFM-569 and load nbr 2.

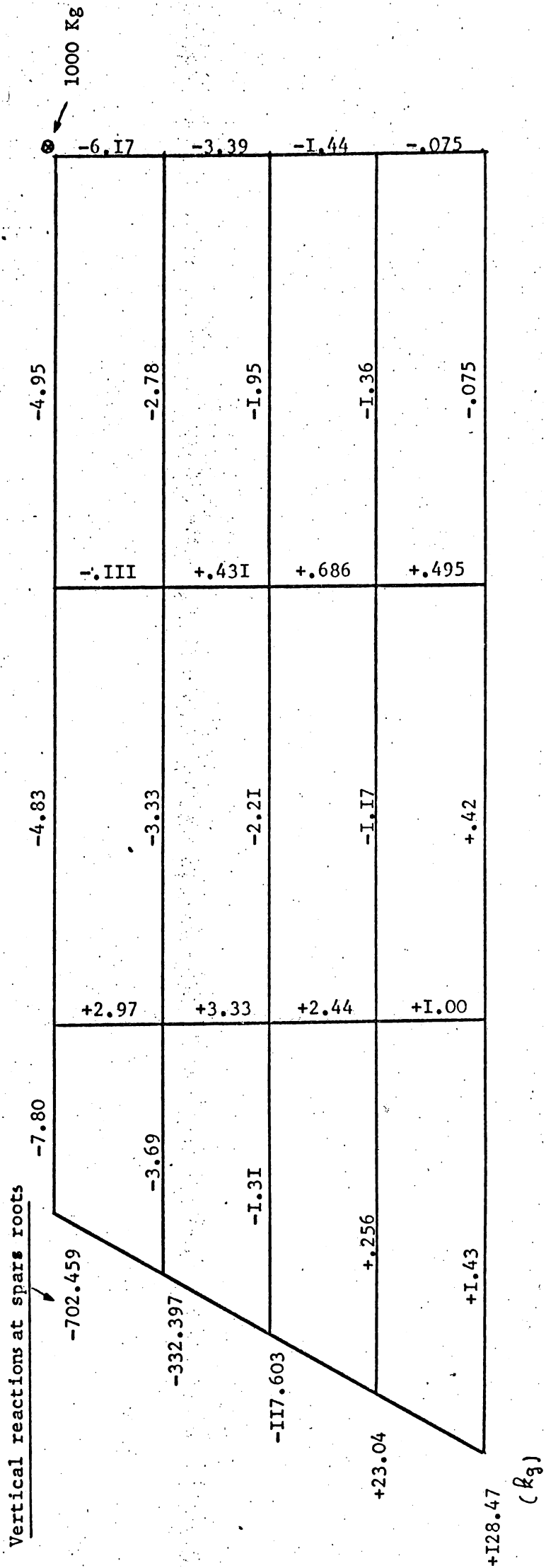


Figure F.3.I29. Shear stresses distribution for idealization LD-I89 and load nbr 2.

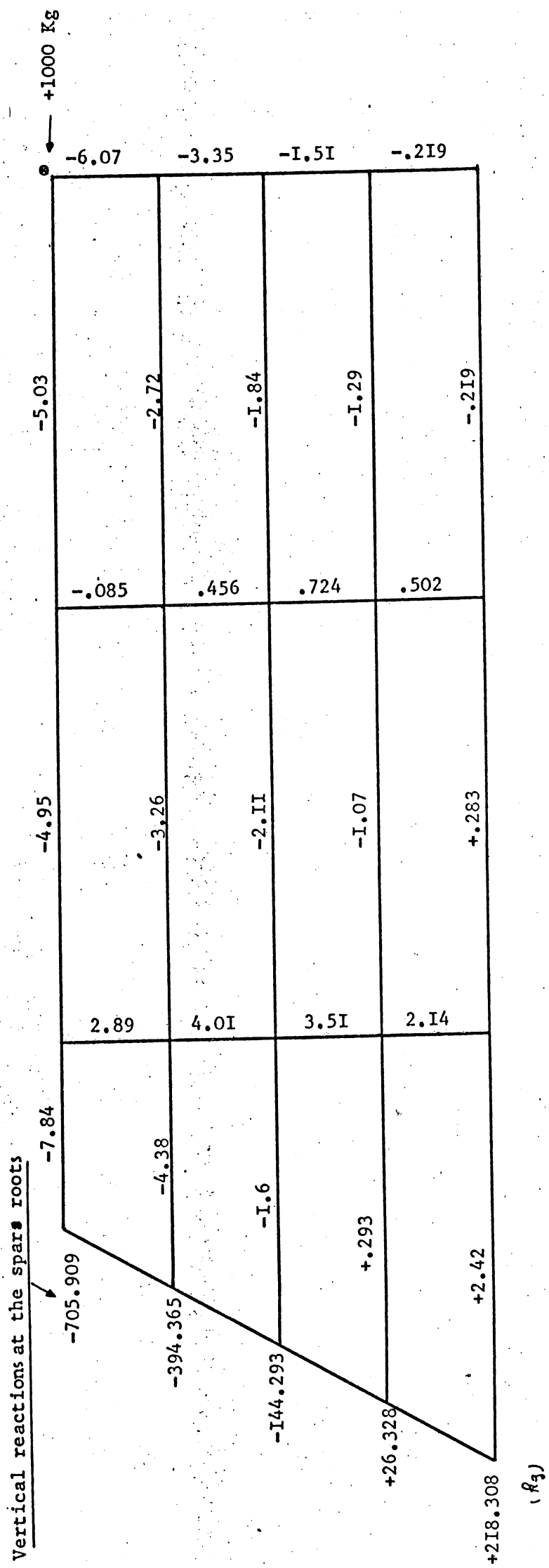


Figure F.3.131. Average shear stresses distribution for idealization EQ-I85 and load nbr 2.

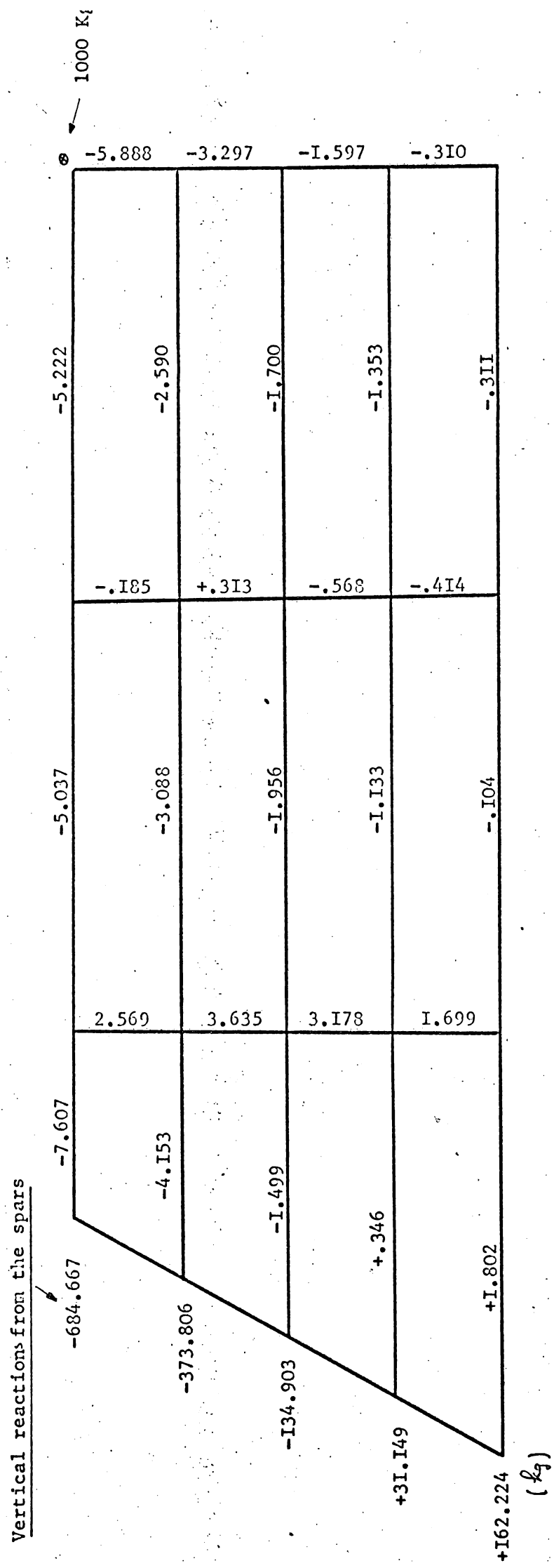


Figure F.3.132. Shear stresses distribution for idealization RfM-304 and load nbr 2.

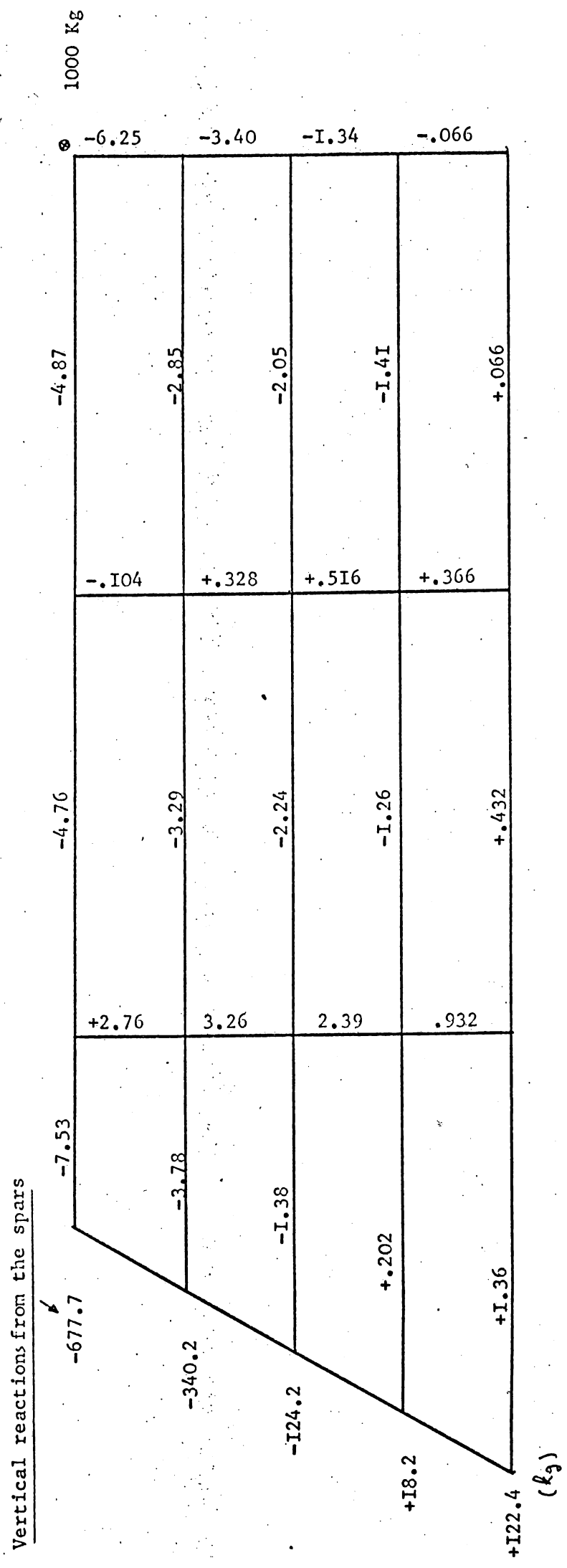
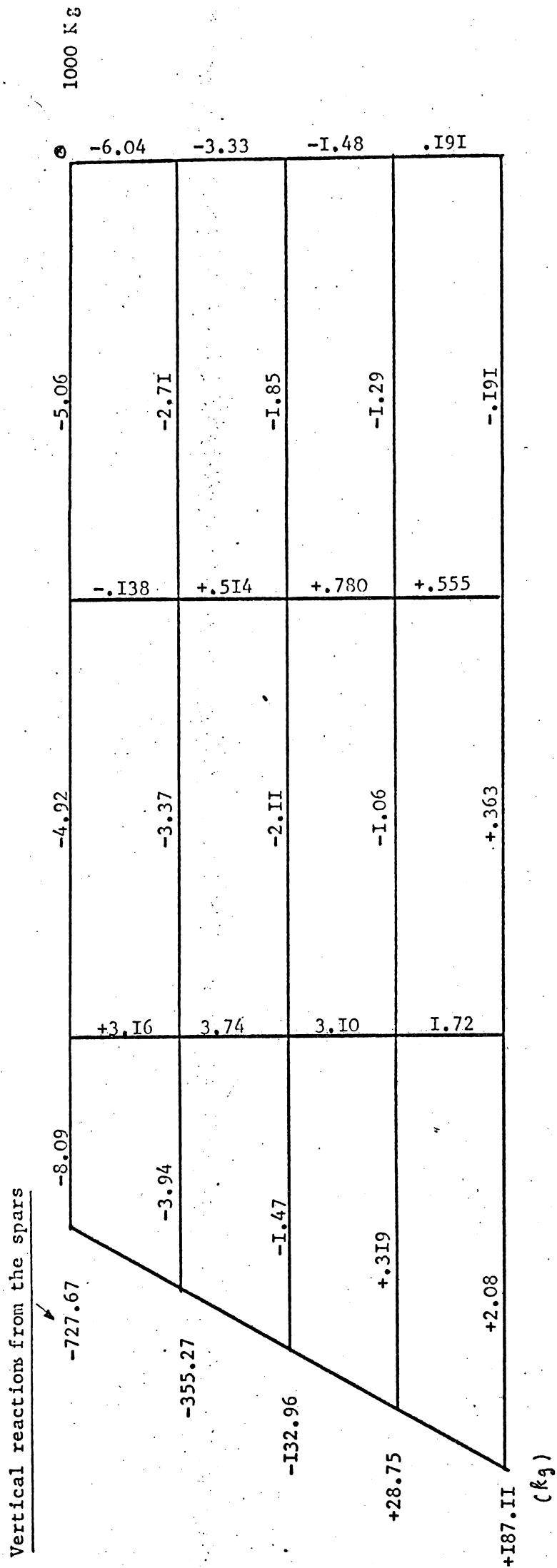
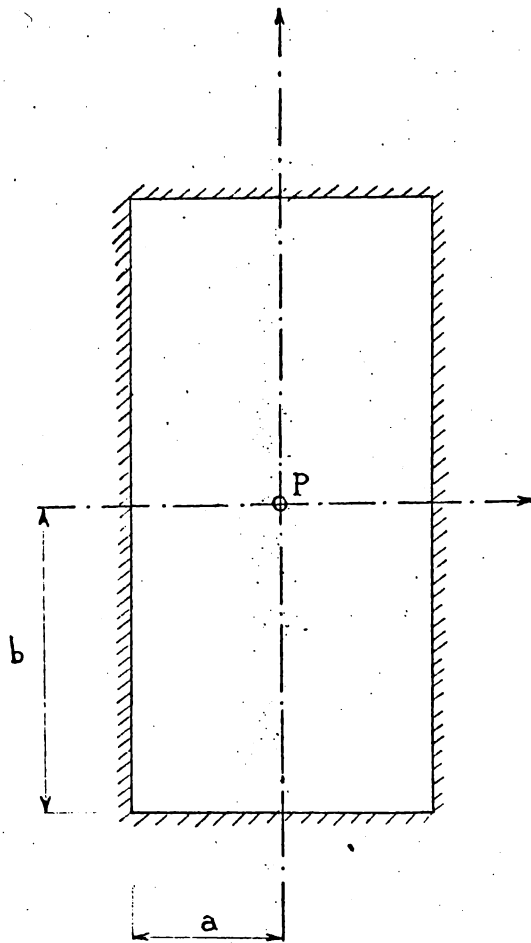


Figure F.3.I33. Shear stresses distribution for idealization LD-RECT-I80 and load nbr 2.

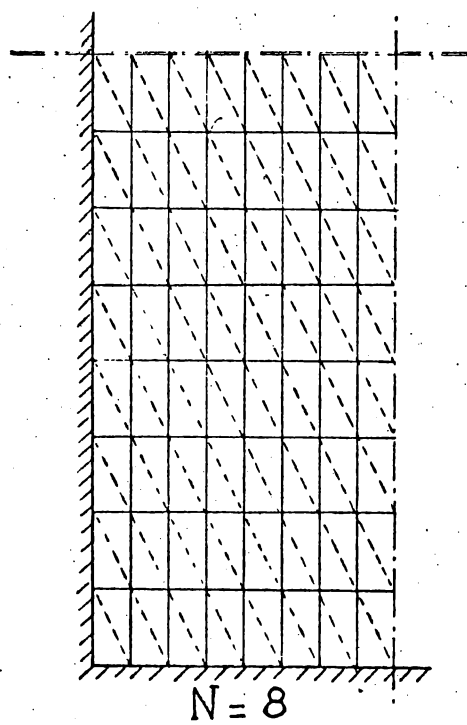
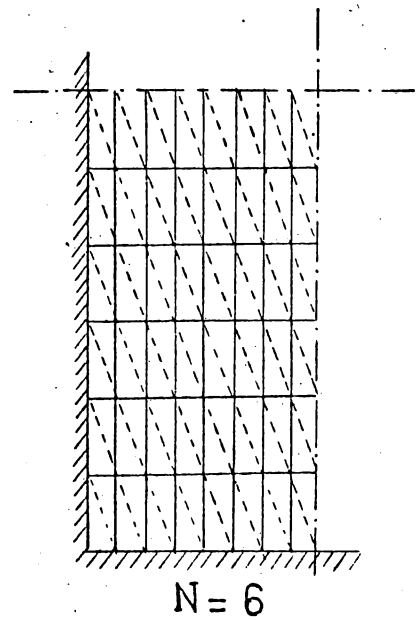
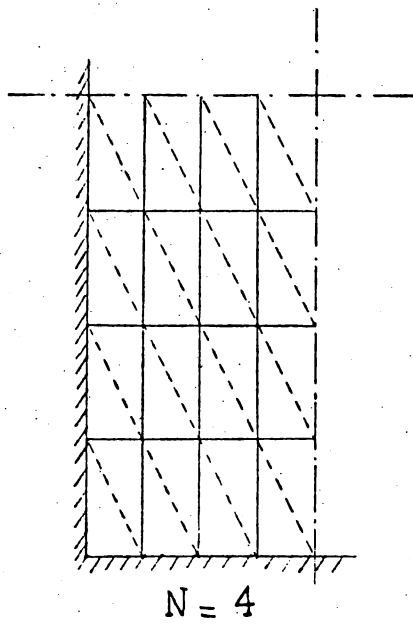
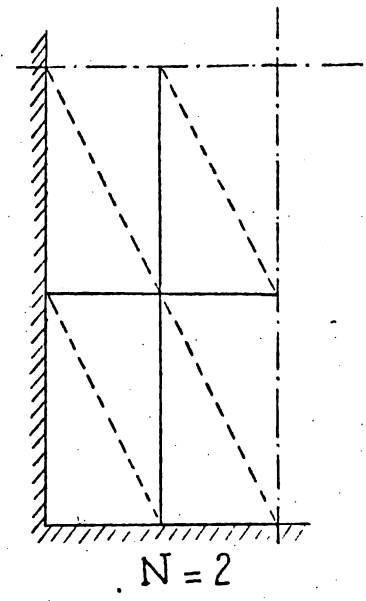
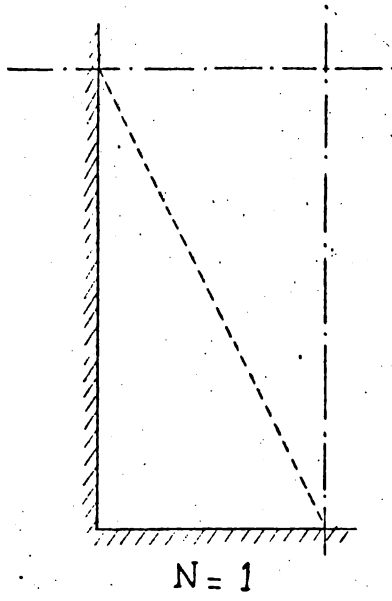




Case	$\frac{b}{a}$	Boundary Conditions
1	1	Simply supported
2	2	Simply supported
3	1	Clamped
4	2	Clamped

Figure F.3.I34.

Figure F.3.I35. Typical finite element idealization.



Case 1 : Square plate - Simply supported - Concentrated load in the center.

ANALYSIS	N = 1			N = 2			N = 4		
	N.G.C.	β	μ	N.G.C.	β	μ	N.G.C.	β	μ
	EXACT	—	11.6008	1.0	—	11.6008	1.0	—	11.6008
1 ACM	12	13.75	1.1853	27	12.30	1.0603	75	11.81	1.0180
2 M	12	12.10	1.0430	27	11.85	1.0215	75	11.66	1.0051
3 P	12	10.09	.8698	27	10.80	.9310	75	11.02	.9499
4 HCT	12	8.84	.7620	27	10.48	.9034	75	11.25	.9698
5 T	12	8.592	.7406	27	11.42	.9844	75	12.07	1.0404
6 T-10	12	16.62	1.4327	27	17.09	1.4732	75	17.23	1.4852
7 A	12	6.88	.5931	27	7.28	.6275	75	8.224	.7089
8 CQ	16	10.876	.9375	39	11.439	.9861	115	11.560	.9965
9 EQT	19	13.770	1.1870	57	12.124	1.0451	193	11.674	1.0063

β is defined by $v_c = \beta \frac{Pa^2}{D}$ (The Figures given are multiplied by a factor 10^3)

μ is defined by $\mu = \frac{\beta \text{ computed}}{\beta \text{ exact}}$

N.G.C. is the number of generalized coordinates

N is the mesh size number

Figure F.3.I36.

Case 1 : Square plate - Simply supported - Concentrated load in the center.

ANALYSIS	N = 6		N = 8	
	N.G.C.C.	β	N.G.C.C.	β
EXACT				
1 ACM	I47	II.6008	273	II.6008
2 M	I47	II.69	273	II.64
3 P	I47	II.61	273	II.6
4 HCT	I47	II.07	273	II.11
5 T	I47	II.44	273	II.48
6 T-10	I47	I2.I6	273	I2.I0
7 A	I47	I7.25	273	I7.33
8 CQ	231	8.544	273	8.7200
9 EQT	409	II.588	/	/
		II.656	/	/
				μ
				I.0
				I.0034
				.9999
				.9577
				.9896
				I.0430
				I.4939
				.7517
				/
				/

β is defined by $w_c = \beta \frac{Pa^2}{D}$ (The Figures given are multiplied by a factor 10^3)

μ is defined by $\mu = \frac{\beta \text{ computed}}{\beta \text{ exact}}$

N.G.C.C. is the number of generalized coordinates

N is the mesh size number

Figure F.3.I36-bis.

Case 2 : Rectangular plate ($\frac{b}{a} = 2$) - Simply supported - Concentrated load in the center.

ANALYSIS	N = 1			N = 2			N = 4		
	N.G.C.	β	μ	N.G.C.	β	μ	N.G.C.	β	μ
	EXACT	—	I6.5239	I.0	—	I6.5239	I.0	—	I6.5239
I ACM	I2	I8.487	I.II88	27	I7.579	I.0639	75	I6.919	I.0239
2 M	I2	I4.664	.8874	27	I6.476	.997I	75	I6.6I6	I.0056
3 P	I2	I4.536	.8797	27	I5.I99	.9I98	75	I5.485	.937I
4 HCT	I2	II.2I6	.6788	27	I3.60	.8230	75	I5.520	.9392
5 T	I2	IO.368	.6275	27	I6.5II	.9992	75	I8.656	I.I290
6 T-IO	I2	24.296	I.4704	27	26.896	I.6277	75	27.392	I.6577
7 A	I2	IO.064	.609I	27	IO.68	.6463	75	I2.4I6	.75I4
8 CQ	I6	I4.486	.8767	39	I6.000	.9683	II5	I6.400	.9925
9 EQT	I9	22.I77	I.342I	57	I7.878	I.08I9	I93	I6.804	I.OI69

β is defined by $w_c = \beta \frac{Pa^2}{D}$ (The Figures given are multiplied by a factor IO^3)

μ is defined by $\mu = \frac{\beta \text{ computed}}{\beta \text{ exact}}$

N.G.C. is the number of generalized coordinates

N is the mesh size number

Case 2 : Rectangular plate ($\frac{b}{a} = 2$) - Simply supported - Concentrated load in the center.

ANALYSIS	N = 6			N = 8		
	N.G.C.	β	μ	N.G.C.	B	μ
	EXACT	—	16.5239	1.0	—	16.5239
1 ACM	I47	16.745	1.0134	273	16.656	1.0080
2 M	I47	16.584	1.0036	273	16.570	1.0028
3 P	I47	15.597	.9439	273	15.650	.9471
4 HCT	I47	16.024	.9697	273	16.24	.9828
5 T	I47	19.12	1.1571	273	19.12	1.1571
6 T-10	I47	27.504	1.6645	273	27.520	1.6655
7 A	I47	13.016	.7877	273	13.184	.7979
8 CQ	231	16.477	.9972	—	/	/
9 EQT	409	16.666	1.0086	—	/	/

β is defined by $w_c = \beta \frac{Pa^2}{D}$ (The Figures given are multiplied by a factor 10^3)

μ is defined by $\mu = \frac{\beta_{\text{computed}}}{\beta_{\text{exact}}}$

N.G.C. is the number of generalized coordinates

N is the mesh size number

Figure F.3.137-bis.

Case 3 : Square plate - Clamped - Concentrated load in the center.

ANALYSIS	N = 1			N = 2			N = 4		
	N.G.C.C.	β	μ	N.G.C.C.	β	μ	N.G.C.C.	β	μ
	EXACT	—	5.605	1.0	—	5.605	1.0	—	5.605
1 ACH	12	5.919	1.0560	27	6.137	1.0949	75	5.807	1.0360
2 M	12	4.231	.7549	27	5.736	1.0234	75	5.688	1.0148
3 P	12	5.301	.9458	27	5.246	.9359	75	5.399	.9632
4 HCT	12	1.0	.1784	27	4.2400	.7565	75	5.192	.9263
5 T	12	5.264	.9392	27	5.896	1.0519	75	5.952	1.0619
6 T-10	12	7.864	1.4030	27	9.096	1.6228	75	9.072	1.6186
7 A	12	6.168	1.1004	27	5.0	.8921	75	5.0	.8921
8 CQ	16	5.208	.9292	39	5.430	.9638	115	5.5708	.9939
9 EQT	19	8.2565	1.4731	57	6.1939	1.1051	193	5.7557	1.0269

β is defined by $w_c = \beta \frac{Pa^2}{D}$ (The Figures given are multiplied by a factor 10^3)

μ is defined by $\mu = \frac{\beta \text{ computed}}{\beta \text{ exact}}$

N.G.C.C. is the number of generalized coordinates

N is the mesh size number

Figure F.3.136.

Case 3 : Square plate - Clamped - Concentrated load in the center.

ANALYSIS	N = 6			N = 8		
	N.G.C.	β	μ	N.G.C.	β	μ
EXACT		5.605	1.0		5.605	1.0
1 ACM	I47	5.704	I.0177	273	5.671	I.0118
2 M	I47	5.653	I.0086	273	5.640	I.0062
3 P	I47	5.439	.9704	273	5.461	.9743
4 HCT	I47	5.40	.9634	273	5.496	.9806
5 T	I47	5.936	I.0591	273	5.888	I.0505
6 T-10	I47	9.032	I.6114	273	9.024	I.6100
7 A	I47	5.0	.8921	273	5.0	.8921
8 CQ	231	5.5966	.9985		/	/
9 EQT	409	5.6712	I.0118		/	/

β is defined by $w_c = \beta \frac{Pa^2}{D}$ (The Figures given are multiplied by a factor 10^3)

μ is defined by $\mu = \frac{\beta \text{ computed}}{\beta \text{ exact}}$

N.G.C. is the number of generalized coordinates

N is the mesh size number

Figure F.3.138-bis.

Case 4 : Rectangular plate ($\frac{b}{a} = 2$) - Clamped - Concentrated load in the center.

ANALYSIS	N = 1		N = 2		N = 4				
	N.G.C.C.	β	μ	N.G.C.C.	β	μ	N.G.C.C.	β	μ
1 EXACT	-	7.215	1.0	-	7.215	1.0	-	7.215	1.0
2 AC1	12	6.3923	.8860	27	7.799	1.0809	75	7.5263	1.0431
3 M	12	2.1815	.3024	27	6.7742	.9389	75	7.2312	1.0022
4 P	12	5.7294	.7941	27	6.681	.9260	75	6.8653	.9515
5 HCT	12	1.1561	.1602	27	3.9546	.5481	75	6.1415	.8512
6 T	12	4.8838	.6769	27	6.8384	.9478	75	8.5287	1.1821
7 T-10	12	8.3578	1.1584	27	13.1936	1.8286	75	13.773	1.9089
8 A	12	4.8838	.6769	27	6.6302	.9189	75	6.8865	.9545
9 CQ	16	5.649	.7830	39	6.681	.9260	115	7.106	.9849
9 EQT	19	13.937	1.9317	57	8.7392	1.2113	193	7.5892	1.0519

β is defined by $v_c = \beta \frac{Pa^2}{D}$ (The Figures given are multiplied by a factor 10^3)

μ is defined by $\mu = \frac{\beta \text{ computed}}{\beta \text{ exact}}$

N.G.C.C. is the number of generalized coordinates

N is the mesh size number

Figure F.3.139.

Case 4 : Square plate. - Clamped - Concentrated load in the center.

ANALYSIS	N = 6			N = 8		
	N.G.C.	β'	μ	N.G.C.	β'	μ
EXACT	—	7.215	I.0	—	7.215	I.0
1 ACI	I47	7.3928	I.0246	273	7.3342	I.0165
2 H	I47	7.2538	I.0054	273	7.2490	I.0047
3 P	I47	6.9303	.9605	273	6.9592	.9645
4 HCT	I47	6.6943	.9278	273	6.8384	.9478
5 T	I47	8.7210	I.2087	273	8.6008	I.1921
6 T-10	I47	I3.853	I.9200	273	I3.805	I.9134
7 A	I47	6.8704	.9522	273	6.8384	.9478
8 CQ	231	7.1798	.9951	—	/	/
9 EQT	409	7.3786	I.0227	—	/	/

β is defined by $w_c = \beta \frac{Pa^2}{D}$ (The Figures given are multiplied by a factor 10^3)

μ is defined by $\mu = \frac{\beta \text{ computed}}{\beta \text{ exact}}$

N.G.C. is the number of generalized coordinates

N is the mesh size number

Figure F.3.139-bis.

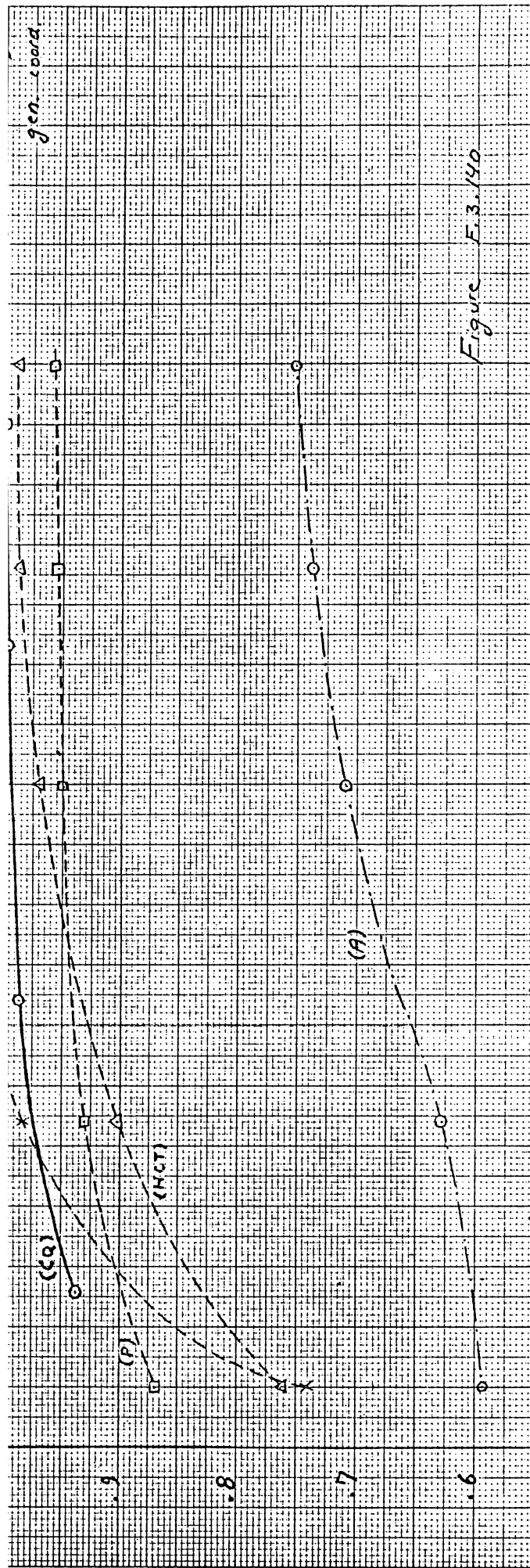
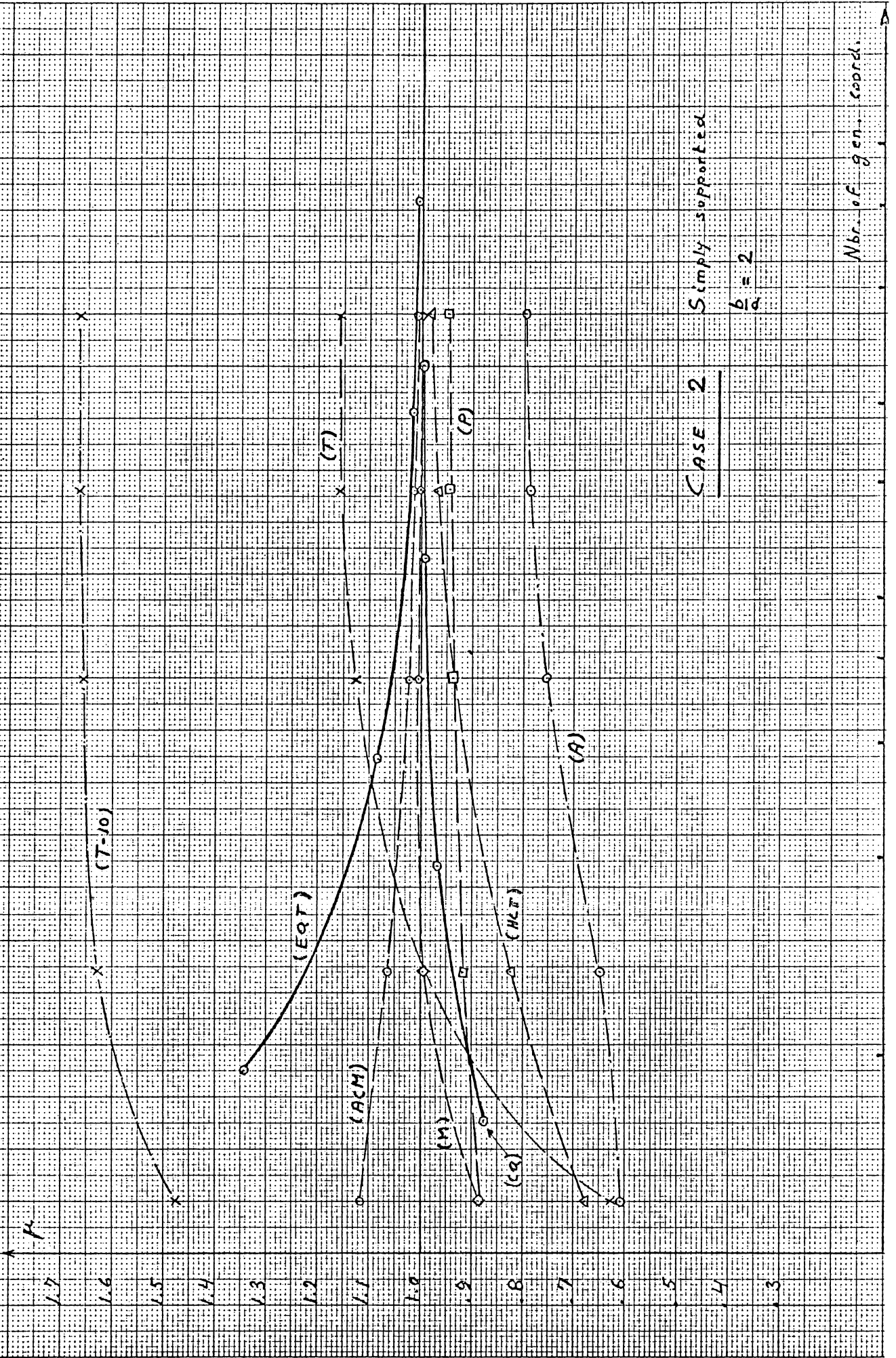
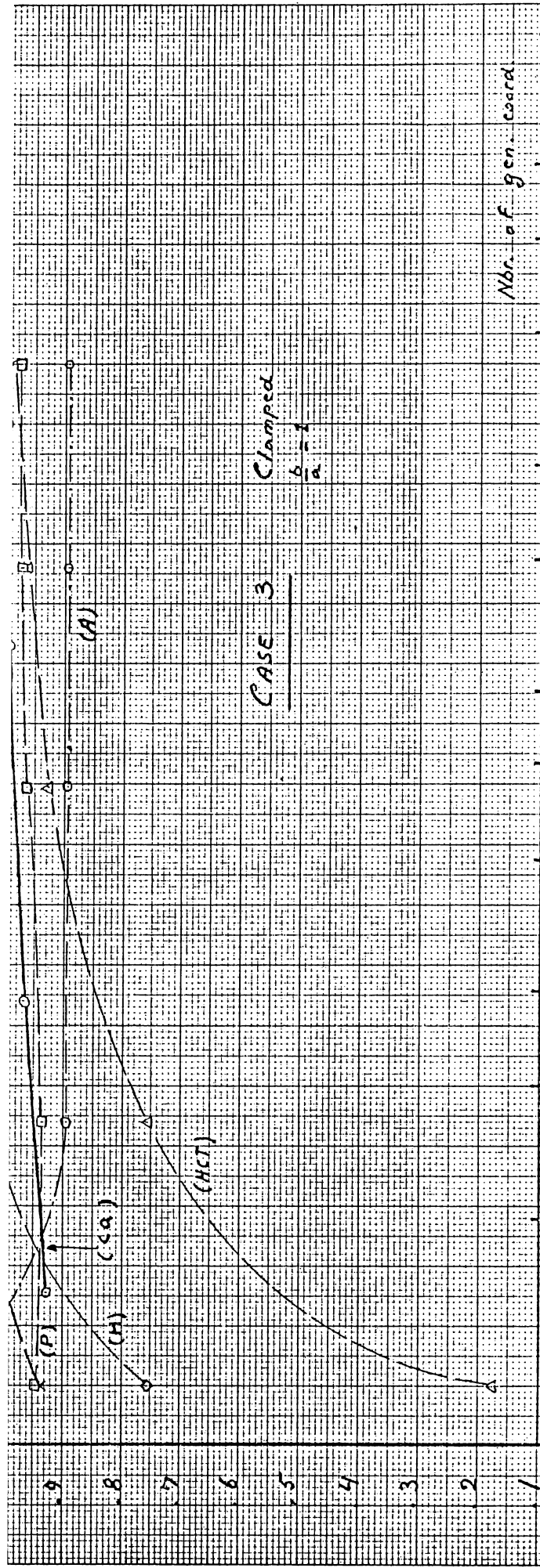
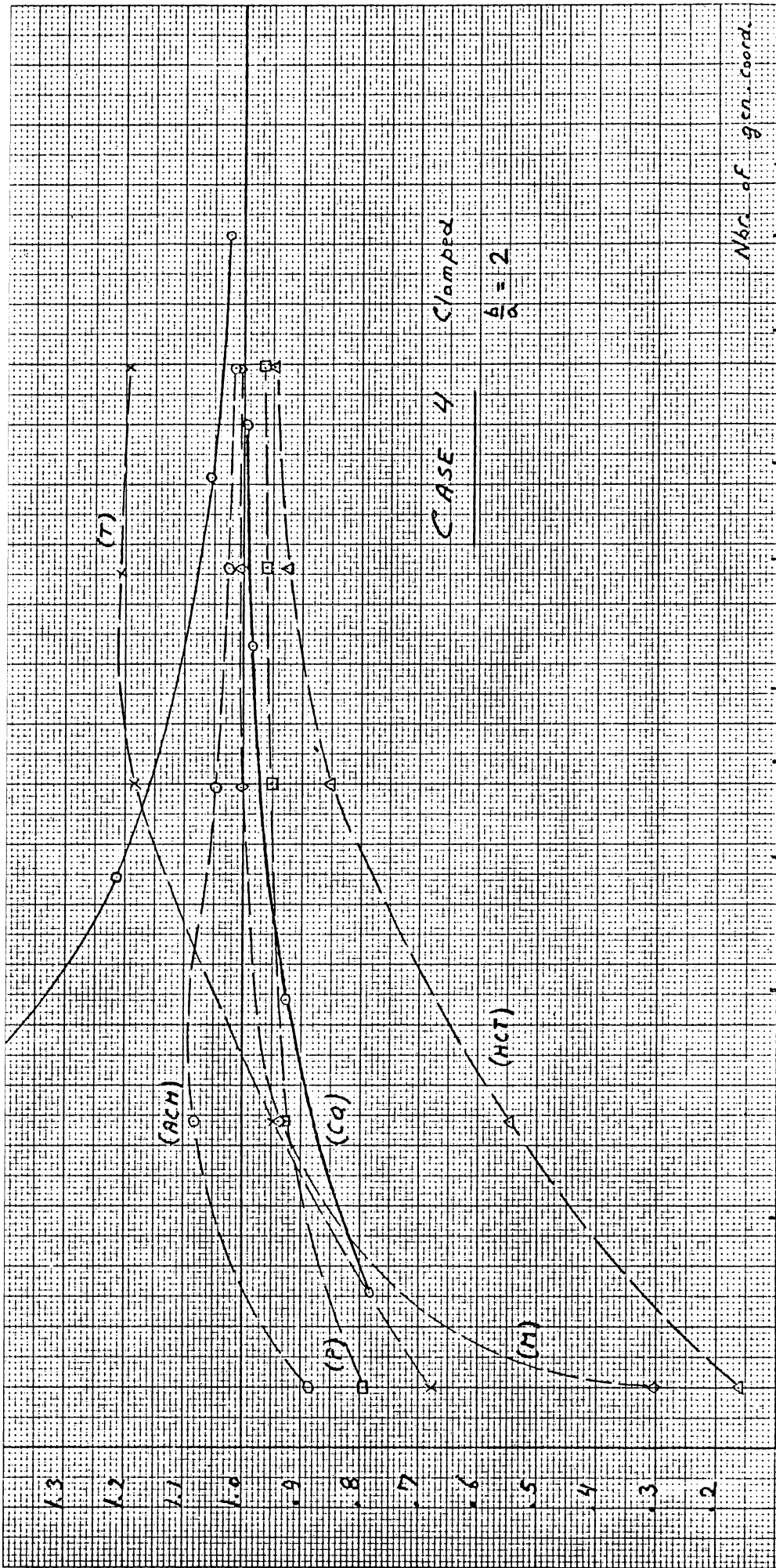
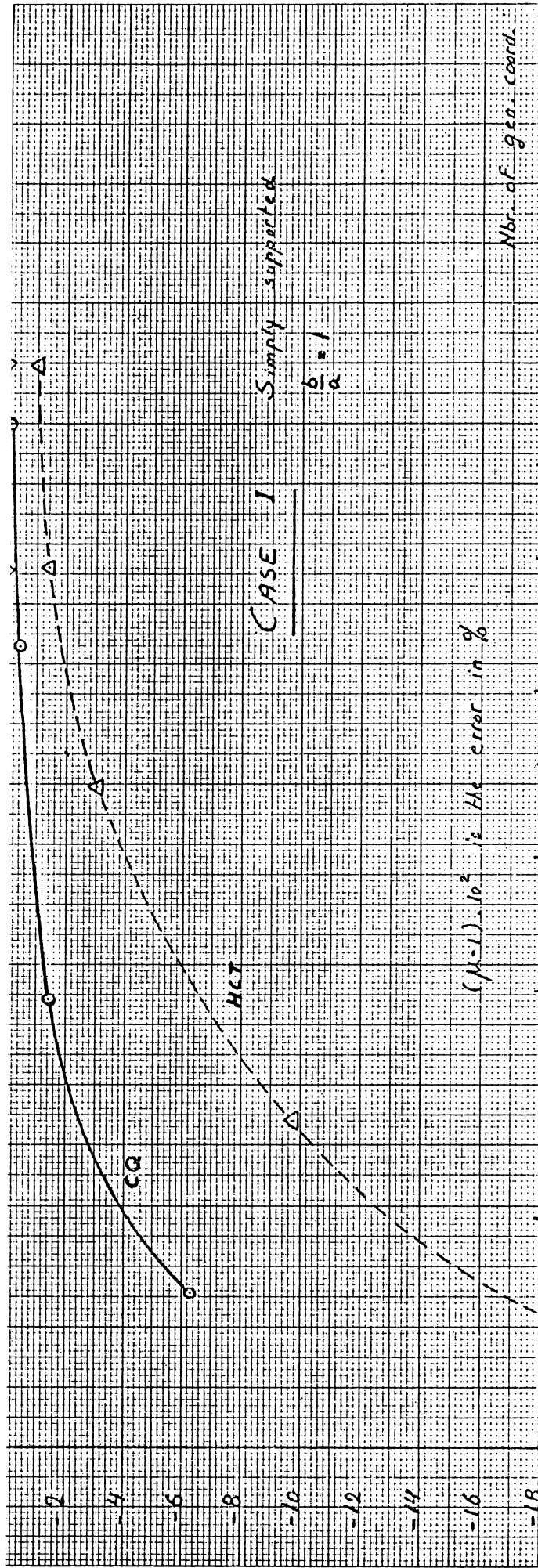


Figure E.3.141









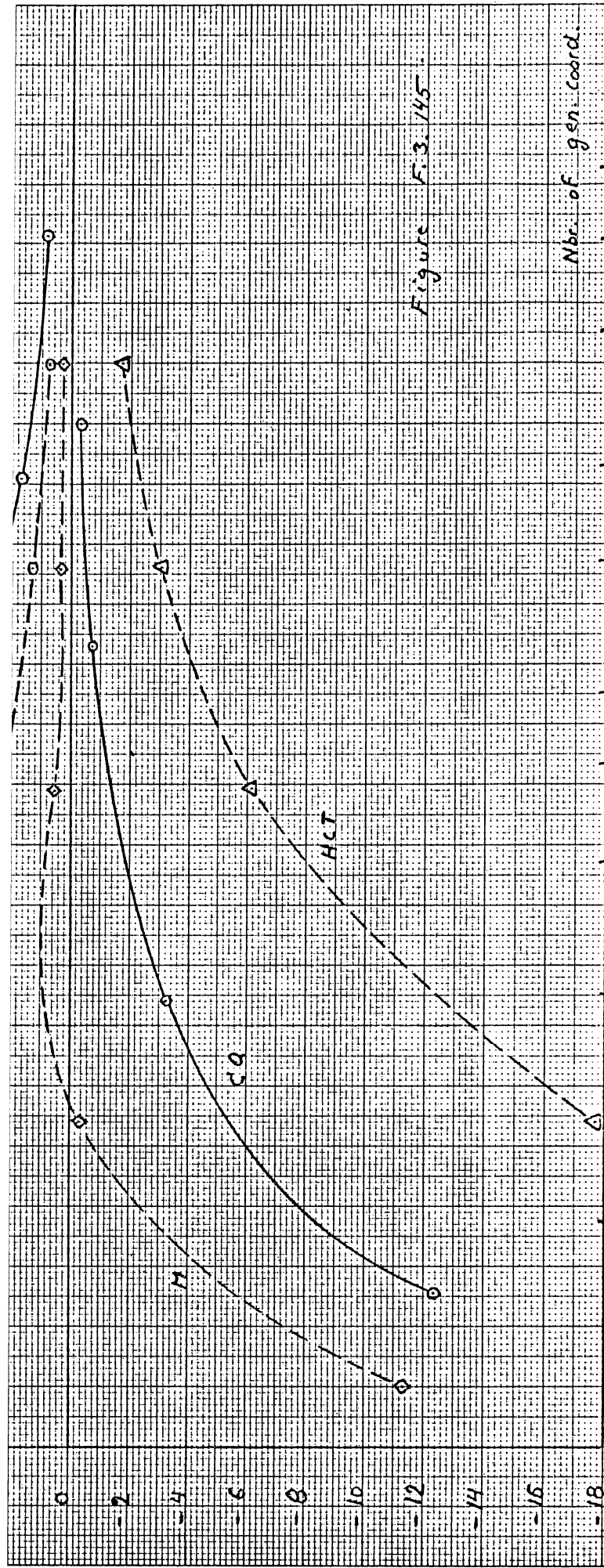


Figure F.3. 145

Nbc. of gen. coord.

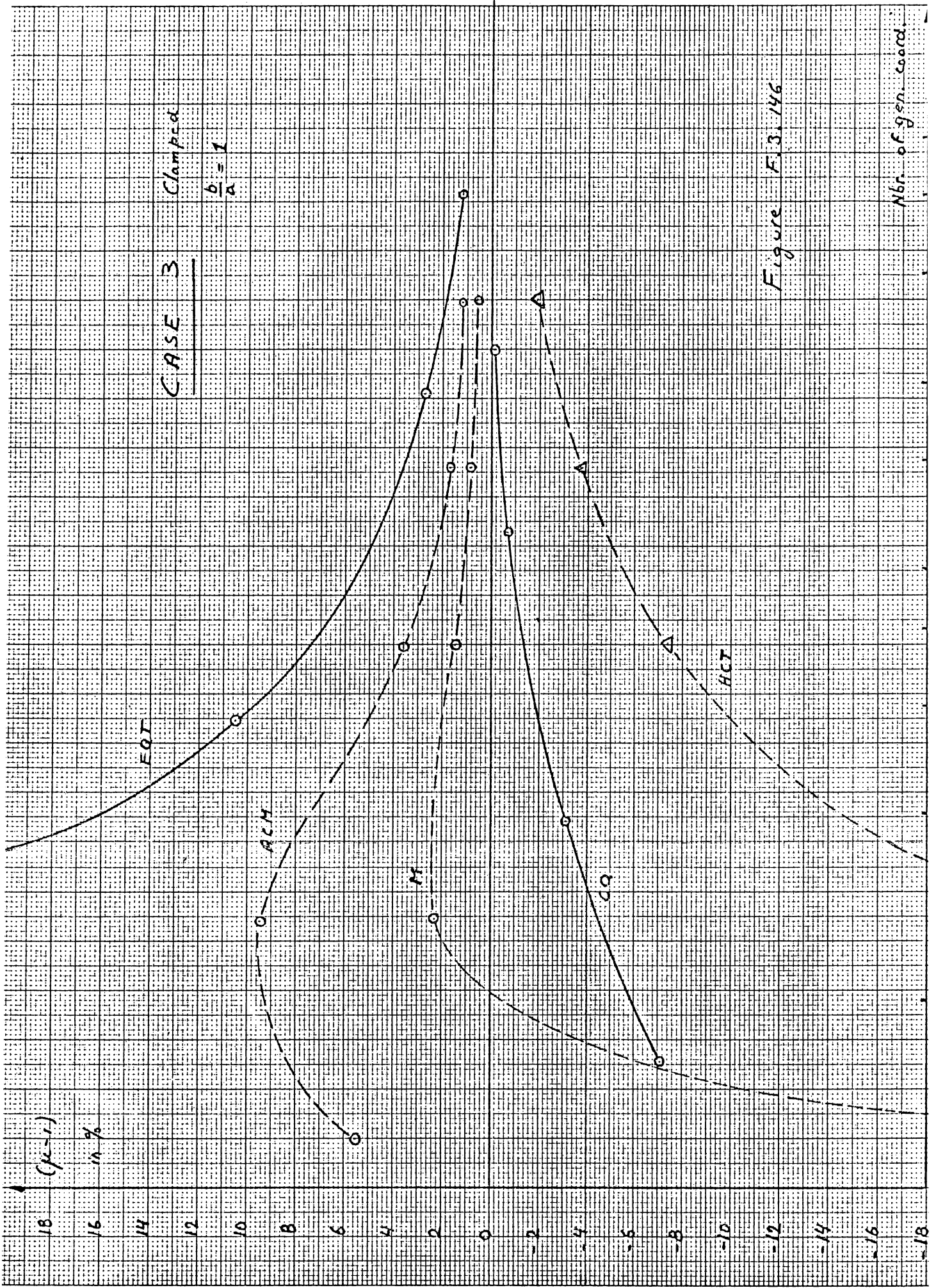


Figure F.3.146

Nbr. of gen. coord.

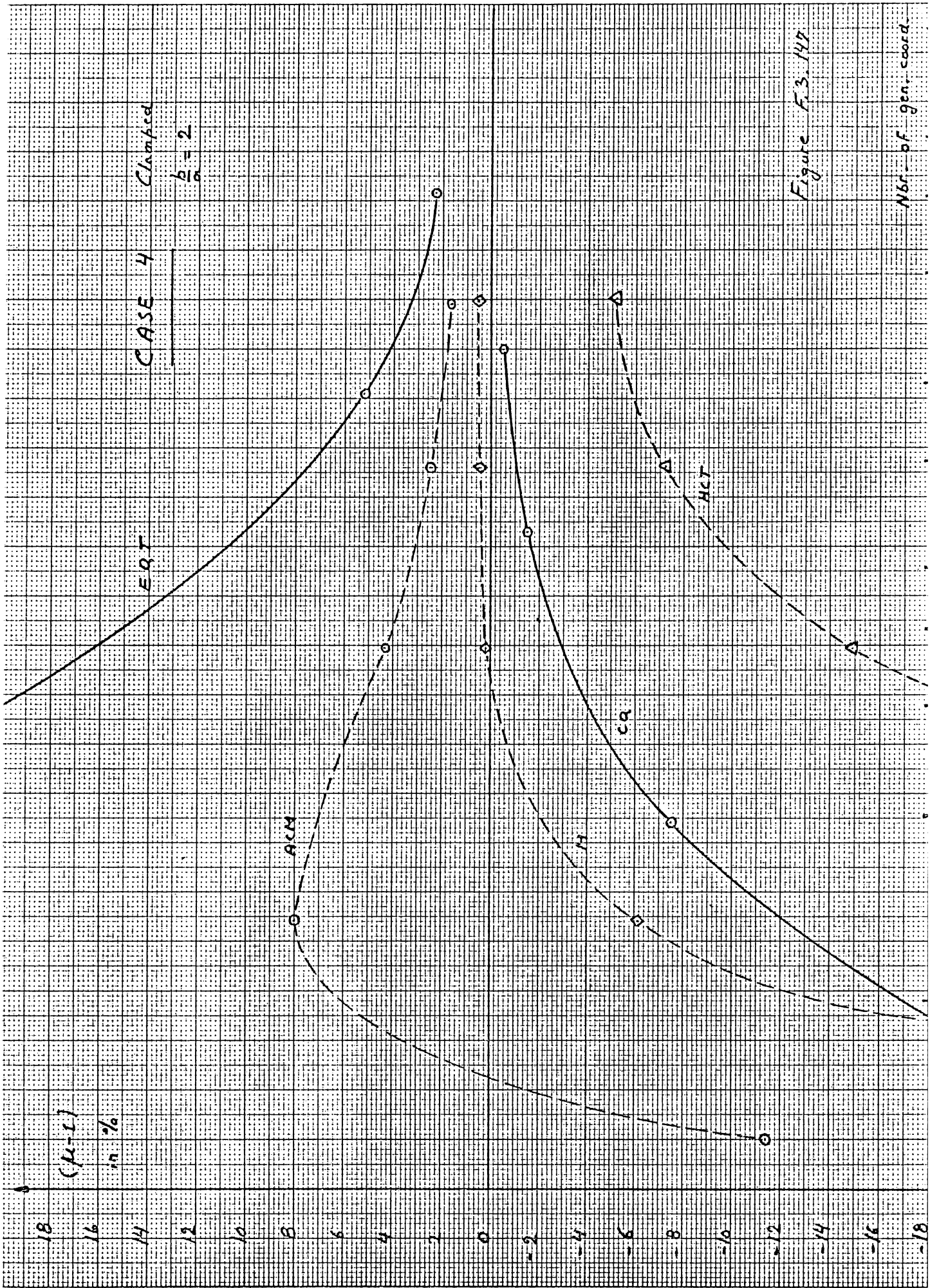
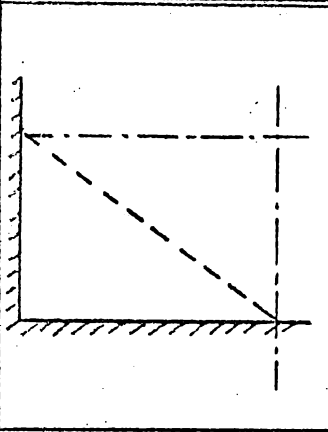
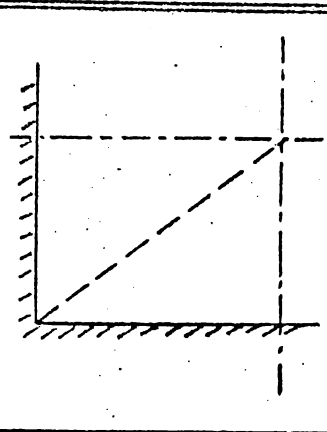


Figure F.3.147

Nbr. of gen. coord.

Displacement orientation		CV2E 1		CV2E 2		CV2E 3		CV2E 4	
B	h	B	h	B	h	B	h	B	h
	14.41	1.50	33.33	244.1	008.3	1.280	12.150	5.110	
	13.110	1.81	55.11	343.1	8.520	1.413	13.331	1.333	

B and h for mesh size M = 1

INFLUENCE OF SHEAR DEFORMATION

Mesh size is for $N = 2$

n in %	β	β*	ρ
C A S E 1			
2.5	I2.I2502	I2.I2567	I.000054
5	I2.I2502	I2.I267I	I.000I397
10	I2.I2502	I2.I3II7	I.0005075
20	I2.I2502	I2.I4936	I.002007
30	I2.I2502	I2.I7829	I.004394
40	I2.I2502	I2.2I727	I.007608
50	I2.I2502	I2.26437	I.0II49
100	I2.I2502	I2.56804	I.036538
250	I2.I2502	I3.33959	I.I00I7
C A S E 2			
20	I7.878896	I7.898564I	I.00II
C A S E 3			
20	6.I939202I	6.22I59707	I.0044683
C A S E 4			
20	8.7392757	8.7632454	I.002743

$$\eta = \frac{t}{2a}$$

β is defined by $w_c = \beta \frac{Pa^2}{D}$

β* includes shear deformation

$$\rho = \frac{\beta^*}{\beta}$$

for this mesh size

$\mu = 1.04510$	in case 1
$\mu = 1.0819$	in case 2
$\mu = 1.108$	in case 3
$\mu = 1.212$	in case 4

Figure F.3.I49.

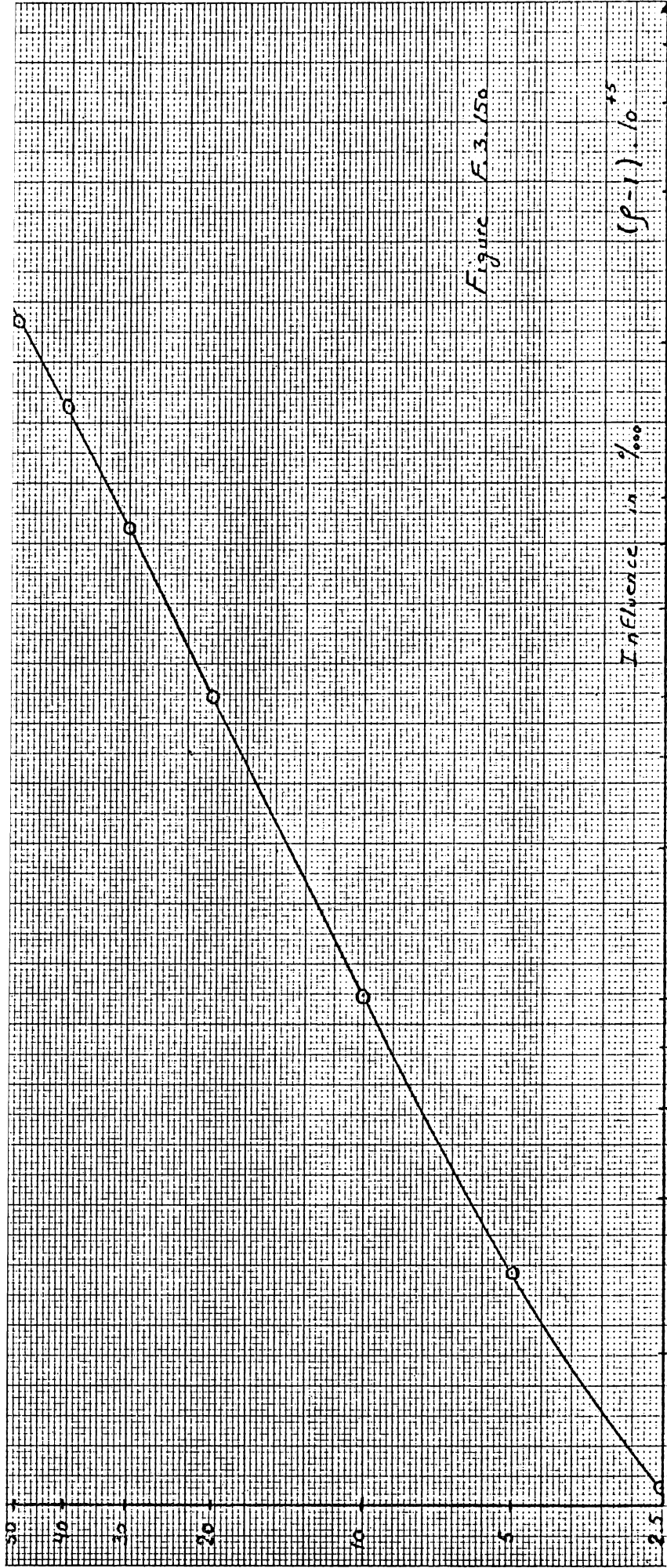


Figure F.3.15a

The A.S.E.F. Computer Program.

A.I- General description.

The A.S.E.F. computer program is an experimental Fortran IV program devised to investigate the practical value of dual structural analyses based on the finite elements developed at the laboratory during the last three years. In its present version it can draw on a library of 15 different elements and solve problems involving up to 500 effective unknowns. It was tailored to a 7040 IBM computer with 5 tapes and "in line" input-output. As a pilot program it does not exhaust all the theoretical possibilities offered by the equilibrium and displacement models, nor does it exhaust the capabilities of the computer itself. In a production version it should be rewritten with a more careful approach to input data preparation and reliability, consistency in the refinement level required from the various elements, accuracy of computation and versatility of use. However, as it stands, it can cope with any experimental job, thanks to some very flexible devices built in to this purpose.

A.2- Substructure technique.

When the dimensions of the master stiffness matrix exceed the available "in core" space of the computer, special treatment has to be provided for matrix inversion. The way it is achieved by the ASEP program consists in a substructure division, which is a form of the partitioning technique. The formulation is somewhat different from the usual one (see for instance reference R.A.1 or R.A.2) ^{and} has the advantage to allow any number of loading cases to be worked out simultaneously, the load components being introduced at the end of the process.

In counterpart, this limits to some extent the number of load components that can be treated.

If K_i are element stiffness matrices, pertaining to a substructure, the complete (master) stiffness matrix of the substructure $K_{s.str.}$ is obtained by suitable localization of the coefficients of the K_i matrices into the $K_{s.str.}$ matrix. This operation is usually written as :

$$K_{s.str.} = \sum_{i=1}^n L_i^T K_i L_i \quad (A.1)$$

n being the number of elements and L_i the localization matrices, which generate a trivial coordinate transformation and contain mostly zeros with a few unit coefficients. In practice the L_i matrices are never used; they are only convenient to describe mathematically the operation.

After localization, the matrix equation relating the stiffness properties of the substructure

$$g_{s.str.} = K_{s.str.} q_{s.str.} \quad (A.2)$$

is first partitioned as follows

$$\begin{vmatrix} g_{n.c} \\ g_c \end{vmatrix} = \begin{vmatrix} K_1 & K_2 \\ K_3 & K_4 \end{vmatrix} \begin{vmatrix} q_{n.c} \\ q_c \end{vmatrix} \quad (A.3)$$

where index $n.c.$ refers to non condensed displacements and index c to condensed displacements characterized by

$$g_c = 0 \quad (A.4)$$

This means that the displacements which can be eliminated are those which are externally unloaded and not required later to implement the boundary conditions. The second line of (A.3) can be solved for q_c :

$$q_c = -K_4^{-1} K_3 q_{n.c} = K_{b.s} q_{n.c} \quad (A.5)$$

$K_{b.s}$ being called the back substitution matrix of the condensation. Substituting this relation into the first line of (A.3) terminates the elimination of the q_c displacements :

$$g_{n.c} = (K_1 - K_2 K_4^{-1} K_3) q_{n.c} = K_c q_{n.c} \quad (A.6)$$

K_c is called the condensed stiffness matrix of the substructure.

This last relation is again partitioned in the form

$$\begin{vmatrix} g_r \\ g_b \end{vmatrix} = \begin{vmatrix} K_{c1} & K_{c2} \\ K_{c3} & K_{c4} \end{vmatrix} \begin{vmatrix} q_r \\ q_b \end{vmatrix} \quad (A.7)$$

where q_b are the displacements whose value is imposed and g_b are therefore reaction loads, while q_r are all other displacements : displacements connected to external loads in one of the loading cases to be solved and displacements needed to connect the adjacent substructures.

If one consider the particular case $q_b \equiv 0$, it follows that (A.7) can be written as

$$\begin{aligned} g_r &= K_{c1} q_r \\ g_b &= K_{c3} q_r \end{aligned} \quad (A.8)$$

where K_{c1} is called the condensed and fixed stiffness matrix of the substructure and K_{c3} is called the reaction matrix.

Using now the same partitioning for the $K_{b.s}$ matrix, it turns out that only part of that matrix is needed for back substitution under the assumption $q_b = 0$. If

$$q_c = \begin{vmatrix} K_{b.s.1} & K_{b.s.2} \end{vmatrix} \begin{vmatrix} q_r \\ q_b \end{vmatrix}$$

the assumption gives

$$q_c = K_{b.s.1} q_r \quad (A.9)$$

The matrices $K_{b.s.1}$ and K_{c3} are stored on tape, while the remaining stiffness matrix K_{c1} , of smaller order, can be assembled to the elements of the next substructure.

This second substructure's stiffness will be

$$K_{s.str_2} = L'_{c1} K_{c1} L_{c1} + \sum_{i=1}^n L'_i K_i L_i$$

to which the same treatment is applied.

As the last step, the q_r displacements are only loaded displacements and inversion of the K_{c1} matrix leads to

$$q_r = K_{c1}^{-1} g_r$$

Back substitution in the reverse order as that used in building the structure, allows computation of all the condensed displacements and reactions.

A.3- Description of the program.

The ASEF program works with the substructure technique described above. Another peculiarity is that only the effective displacements are handled by the computer. This means that, for instance, the out of plane displacements of a plane cover composed of membrane stressed elements are not considered by the computer. This is a more accurate and space saving procedure than to fix these displacements afterwards.

The number of substructures as well as the number of elements composing the structure are unlimited. Dimension limitations appear as follow : the total number of generalized displacements has to be less than 500, while the number of coordinates involved in a substructure has to be less than 115 and finally the total number of load components has also to be less than 115.

Computer time depends on the number of substructures; it is advisable to idealize the structure in such a way that this number be kept as small as possible.

The program runs as indicated by the flow diagram given in A.4 and can be summarized as follows :

- 1°) Compute all stiffness and stress matrices for all the elements of all the substructures.
- 2°) Assemble the element stiffness matrices of the first substructure according to the localization matrices (see details further).
- 3°) Condense and apply boundary conditions.
- 4°) Assemble the remaining part of the substructure to the elements of the next one and go again to point 3°) untill the last substructure is integrated.
- 5°) Solve the last condensed structure for the remaining displacements q_r .
- 6°) Achieve back substitution to find the condensed displacements q_c and boundary reactions q_b .
- 7°) Compute the stresses for the elements for which they are required.
- 8°) Solve for the next loading case if any.

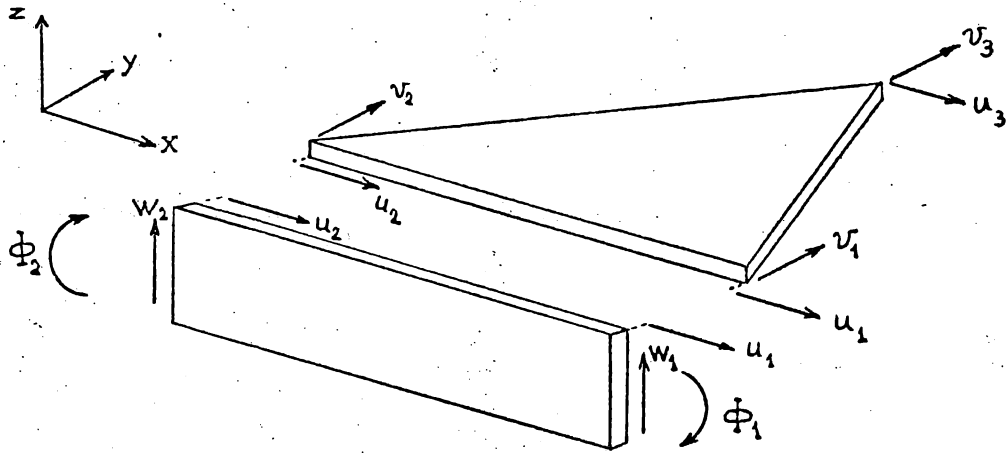
Element localization.

This paragraph describes the technique used to avoid the need of the L_i coordinate transformation matrices. The generalized displacements are sequenced in a fixed order by the subroutines building the element stiffness matrices. This sequence is indicated in the input data preparation section. The displacements of the whole structure q_i are numbered so that $1 \leq i \leq 500$ and the same index i may be use only for one displacement. The computer has therefore to identify the position in both sequences and a localization vector is used to indicate the correspondance. An example will

illustrate the point.

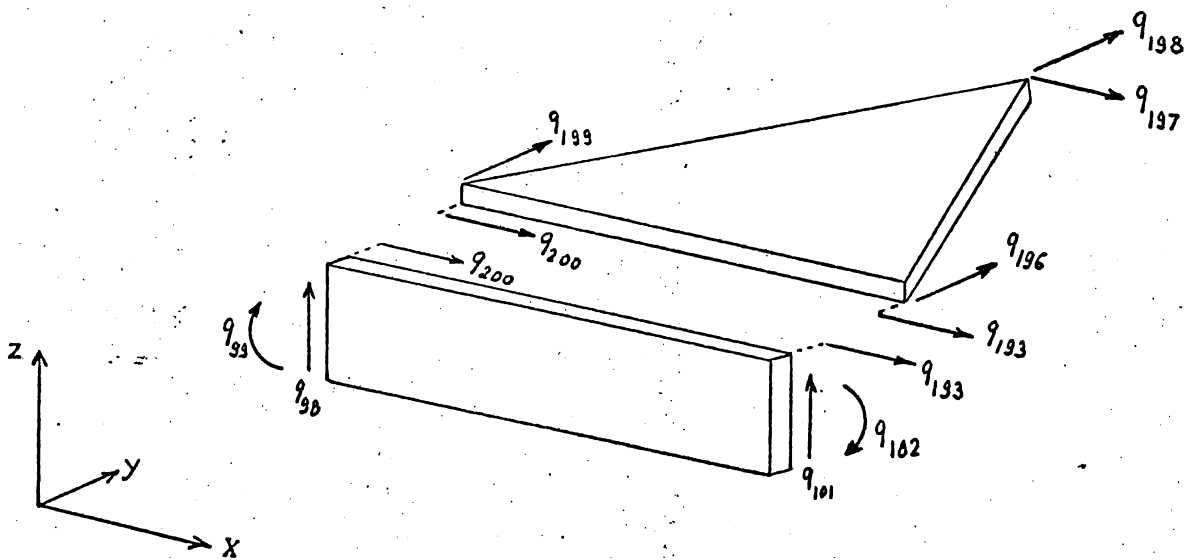
Using a triangular skin and a spar element of the linear displacement type as part of a substructure, the displacements required to describe the behaviour of the structure are indicated on Figure F.A.I.

Figure F.A.I.



These displacements are numbered as a part of the whole structure, for instance as in Figure F.A.2.

Figure F.A.2.



This means that w_1 in the spar element is displacement q_{101} in the final master stiffness matrix and so on. As the sequence of displacements for the triangular element is

$$q'_{tr.} = (u_1 \ v_1 \ w_1 \ u_2 \ v_2 \ w_2 \ u_3 \ v_3 \ w_3)$$

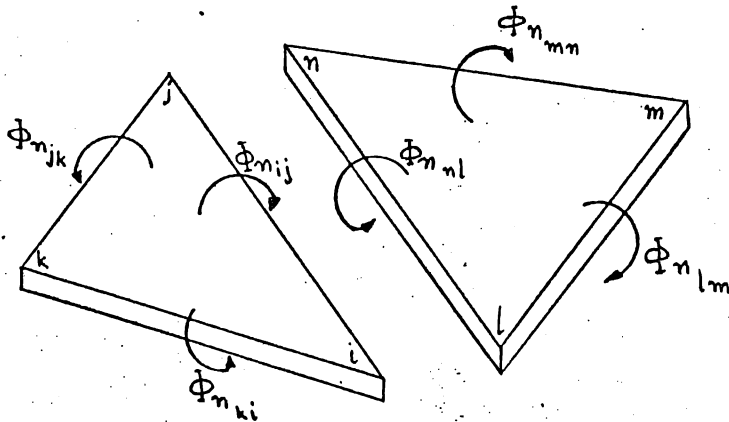
the localization vector is simply obtained by giving to the computer the subscripts i of the displacements q_i corresponding to $u_1 \ v_1 \dots w_3$ in the same sequence. The displacements which are not required - this means for which it is known a priori that zero stiffness coefficients will be generated - are numbered zero and will not be considered by the computer. This is the case for w_3 in our example if the triangle is only connected with other in plane membrane type elements, so that the localization vector for the triangle will be

$$LOCEL = (I93, I96, IOI, 200, I99, 98, I97, I98, 0)$$

Negative localization numbers are allowed and are used in plate elements. As the normal slopes in these elements are defined as indicated in Figure F.A.3., the connection has to be achieved so that

$$\phi_{nij} = -\phi_{njl}$$

Figure F.A.3.



To do so, a positive sense is given for ϕ_n along the interface. If this is, let us say, ϕ_{nij} then a positive localization number will be given to

$\phi_{n_{ij}}$ while for the opposite slope $\phi_{n_{nl}}$ the negative sign will be given to the same number.

This causes the program to change the sign of the off diagonal components of the element stiffness matrix, while assembling.

Substructure condensation and fixation.

The displacements - the number of which is indicated by NCS, with $0 < NCS \leq 115$ - pertaining to one substructure are subdivided into three types :

1) The displacements which will be loaded in any of the loading cases to be run with the current idealization plus the displacements which are to be identical at the interface with another substructure.

These displacements are called the remaining displacements the symbol of which is q_r and their number is indicated by NCR.

2) The unloaded displacements which have to be condensed.

Their symbol is q_c and their number is given by NCC (which may be 0). The forces corresponding to these displacements are $g_c \equiv 0$

3) The fixed displacements q_f . Only zero fixed displacements are allowed in this program, so that $q_f \equiv 0$. The forces corresponding to these displacements are the boundary reactions g_b .

While assembling the elements and substructures, a sequencing order has to be given for the displacements inside a substructure.

This is achieved by the LOC vector which is an array containing NCS numbers corresponding to the numbering of the displacements but such that the q_r displacements come first then the q_f and finally the q_c displacements.

The program checks that :

$$NCS = NCR + NCF + NCC$$

If this is not the case an error message is printed out and an optional return is taken.

Using this arrangement the master stiffness matrix of the substructure is automatically partitioned and processed so as to give :

1) the K_{c1} matrix which is an $NCR \times NCR$ matrix called the condensed and fixed matrix and which is stored on tape (1). At the next assembling step it will be used as an element stiffness matrix.

2) The K_{c3} matrix which is a $NCF \times NCR$ matrix called the reactions matrix and which is stored on tape (3).

3) The K_{bs1} matrix which is a $NCC \times NCR$ matrix called the back substitution matrix is also stored on tape (3).

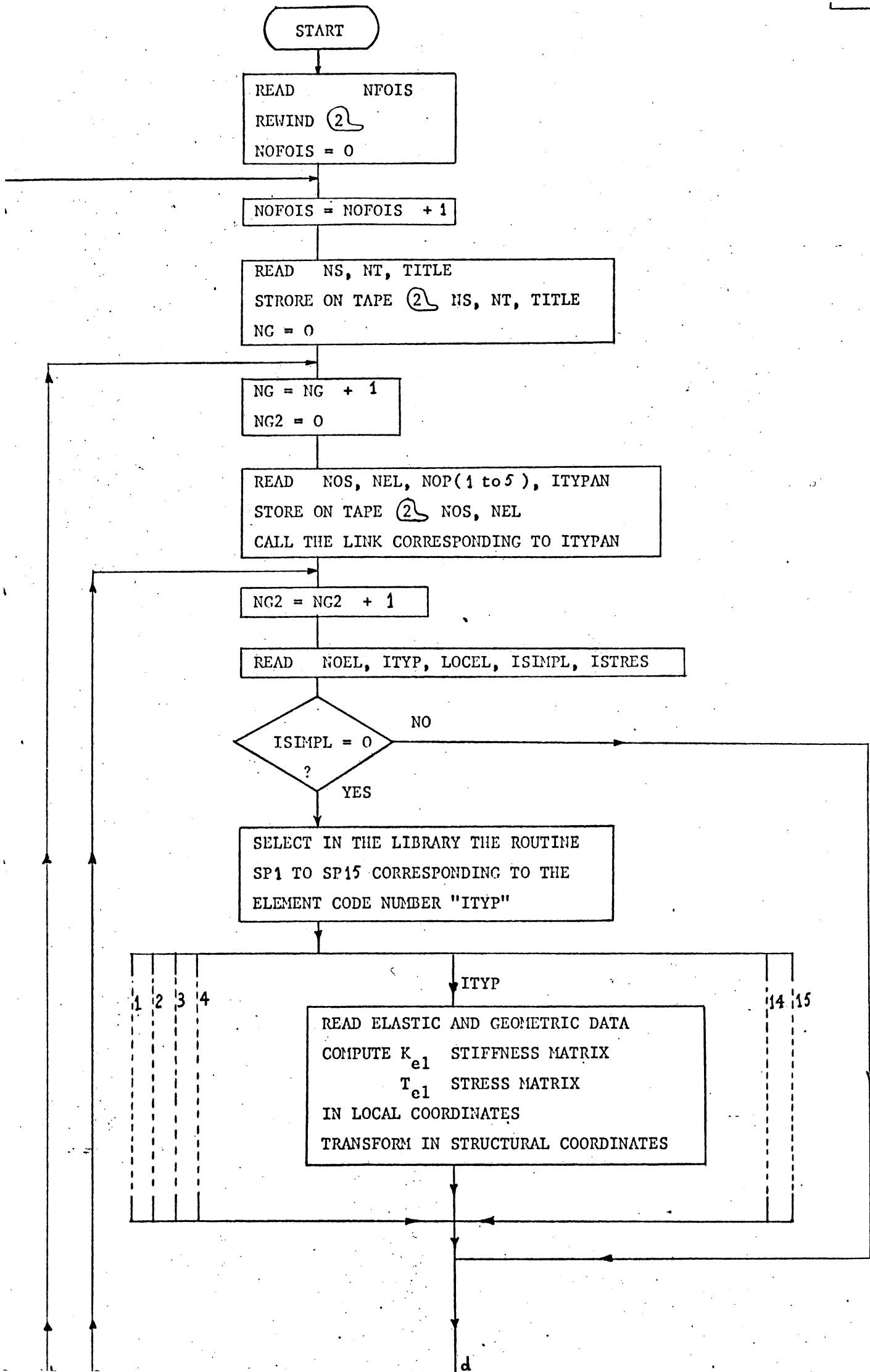
At the next substructure level, displacements coming from the K_{c1} matrix, and used previously only as boundary displacements between two substructures can be condensed if they are unloaded.

Variables used in the flow chart.

NFOIS	Number of problems to be solved in one run.
NOFOIS	Counter.
NS	Number of substructures in a problem.
NT	Total number of generalized coordinates in the structure.
TITLE	Any title to be printed in front of the output.
NG	Counter.
NOS	Numbering for the substructures (arbitrary).
NEL	Number of elements in a substructure.
NG2	Counter.
NOEL	Numbering for the elements (arbitrary).
ITYPAN	Code number defining the type of analysis to be selected ITYPAN = 1 for displacement elements (linear or quadratic) ITYPAN = 2 for equilibrium elements ITYPAN = 3 for plates (compatible or equilibrium). All the elements of a given substructure must belong to the same category and therefore have the same ITYPAN.
ITYP	Code number defining the type of element to be used ITYP causes the selection of the routine building the stiffness and stress matrices and the selection of the correct printing option for the stress output. If ITYP is not consistent with ITYPAN an error message is printed.
LOCEL	Localization vector of an element (see details under title "location"). LOCEL is a singly subscripted array dimensioned at 30.
ISIMPL	Option allowing to skip the computation of the element stiffness and stress matrices if it is known a priori that they will be identical to the one of the preceding element. The LOCEL is different - ISIMPL \neq 0 causes the skipping.
ISTRES	Option allowing to skip the stress computation sequence. If ISTRES \neq 0 stresses are not computed for that element.
K_{el}	Element stiffness matrix.
T_{el}	Element stress matrix.
NDIM	Dimension of the element stiffness matrix.
NBR TEN	Number of stresses (moments of forces) printed for that element.
NCS	Total number of displacements in a substructure.
NCC	Number of "condensed" displacements q_c in a substructure.

NCR	Number of "remaining" displacements q_r in a substructure.
NCF	Number of "fixed" displacements q_f in a substructure.
LOC	Localization vector of a substructure (see details under title "localization"). LOC is a singly subscripted array dimensioned at IIS.
K_{master}	Master stiffness matrix of a substructure.
K_{c1}	See details under title "condensation and fixation".
K_{c3}	
K_{bs1}	
NBCHAR	Number of loading cases to be solved in a problem.
MGB	Counter.
NC1	Counter.
$Q_{\text{s.str.}}$	Complete displacements vector for the whole structure. Contains NT components with NT less than 500. The displacements are numbered from 1 to NT.
$G_{\text{s.str.}}$	Complete loads and reactions vector (NT components).
g_2, q_2	"Remaining" forces and displacements.
g_b	Reactions. (See details).
q_c	Condensed displacements.
NC4	Counter.
NC5	Counter.
σ	Array containing the NBRTEN stresses printed for an element.

A.S.E.F. 3 FLOW DIAGRAM.



START

READ NFOIS
REWIND 2
NOFOIS = 0

NOFOIS = NOFOIS + 1

READ NS, NT, TITLE
STORE ON TAPE 2 NS, NT, TITLE
NG = 0

NG = NG + 1
NG2 = 0

READ NOS, NEL, NOP(1 to 5), ITYPAN
STORE ON TAPE 2 NOS, NEL
CALL THE LINK CORRESPONDING TO ITYPAN

NG2 = NG2 + 1

READ NOEL, ITYP, LOCEL, ISIMPL, ISTRES

ISIMPL = 0?

NO

YES

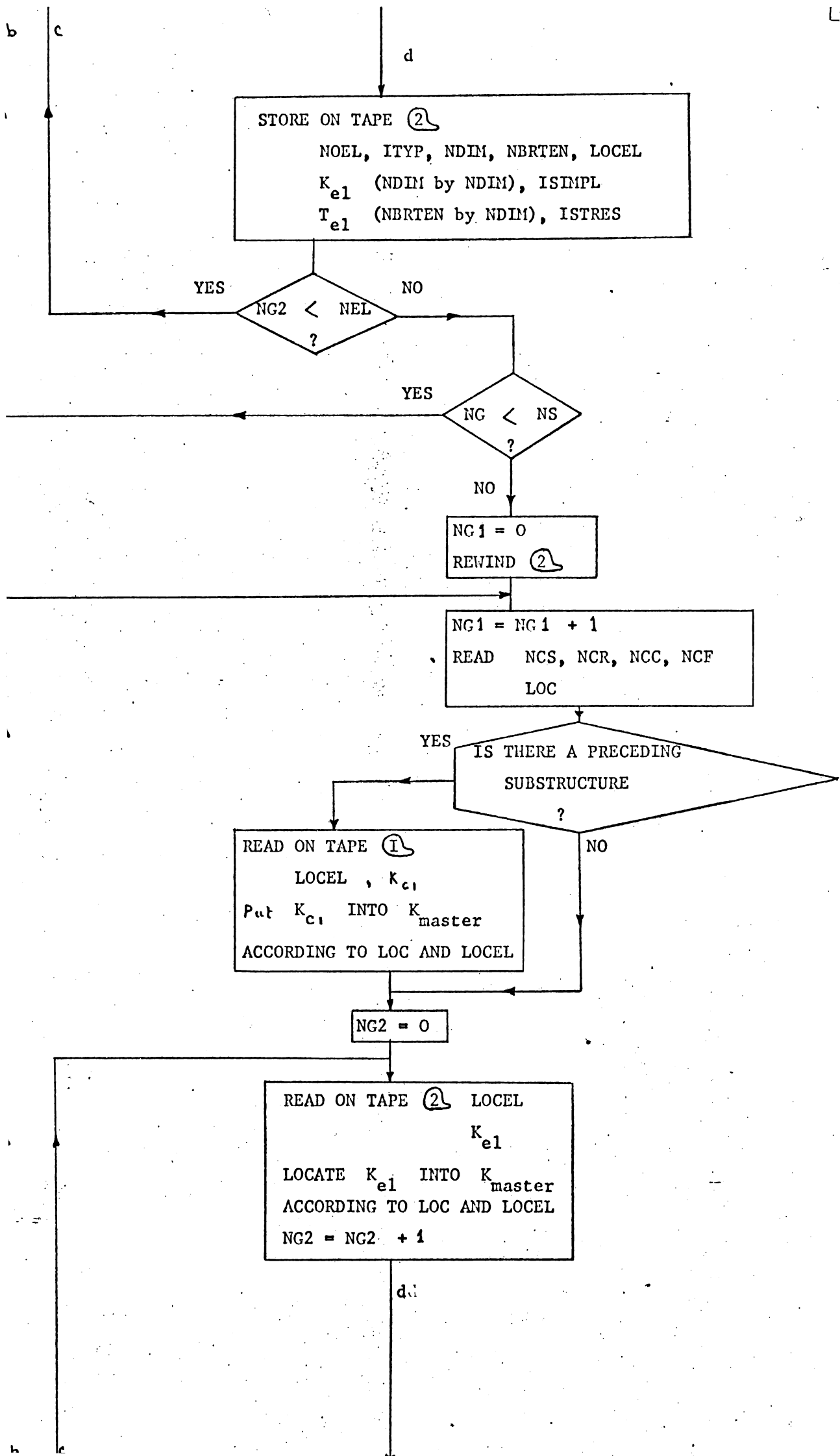
SELECT IN THE LIBRARY THE ROUTINE
SP1 TO SP15 CORRESPONDING TO THE
ELEMENT CODE NUMBER "ITYP"

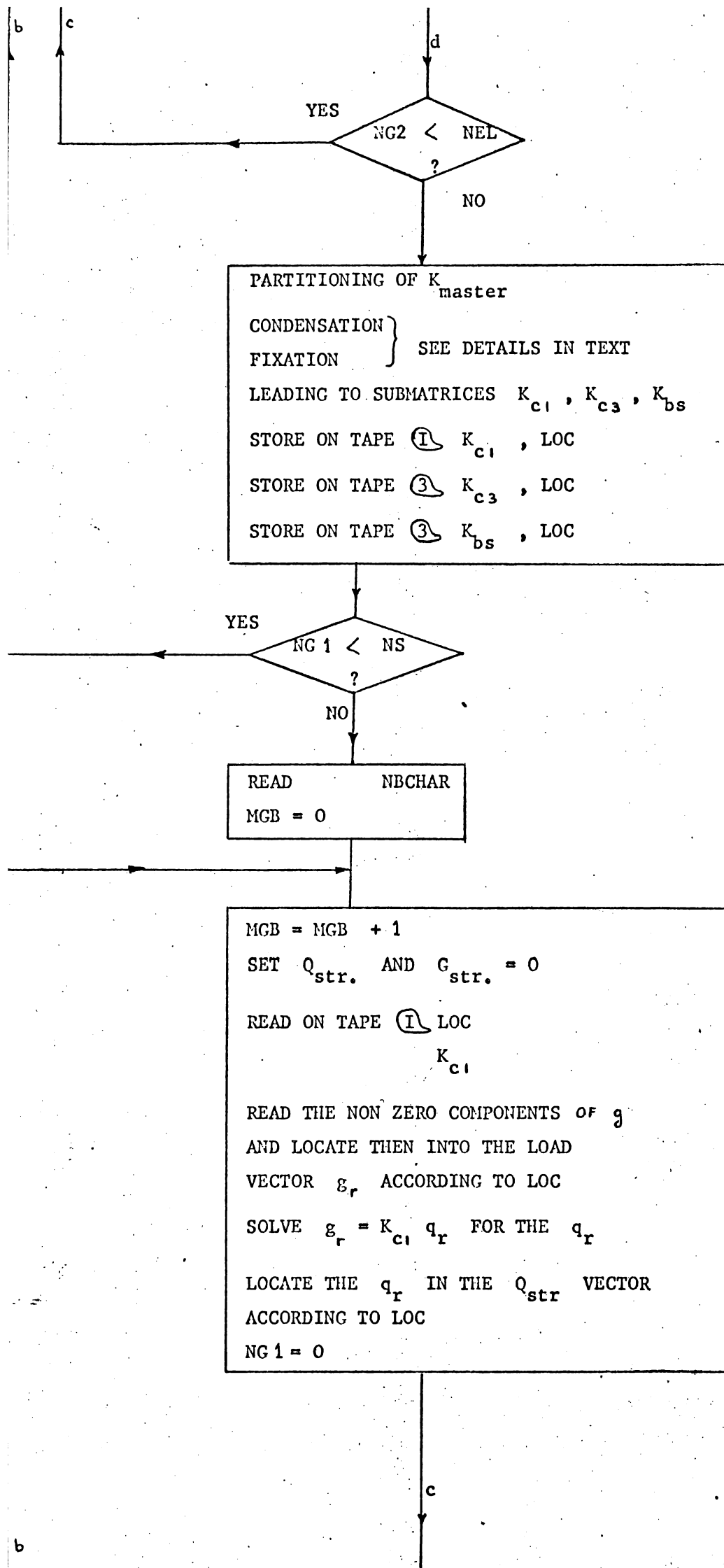
ITYP

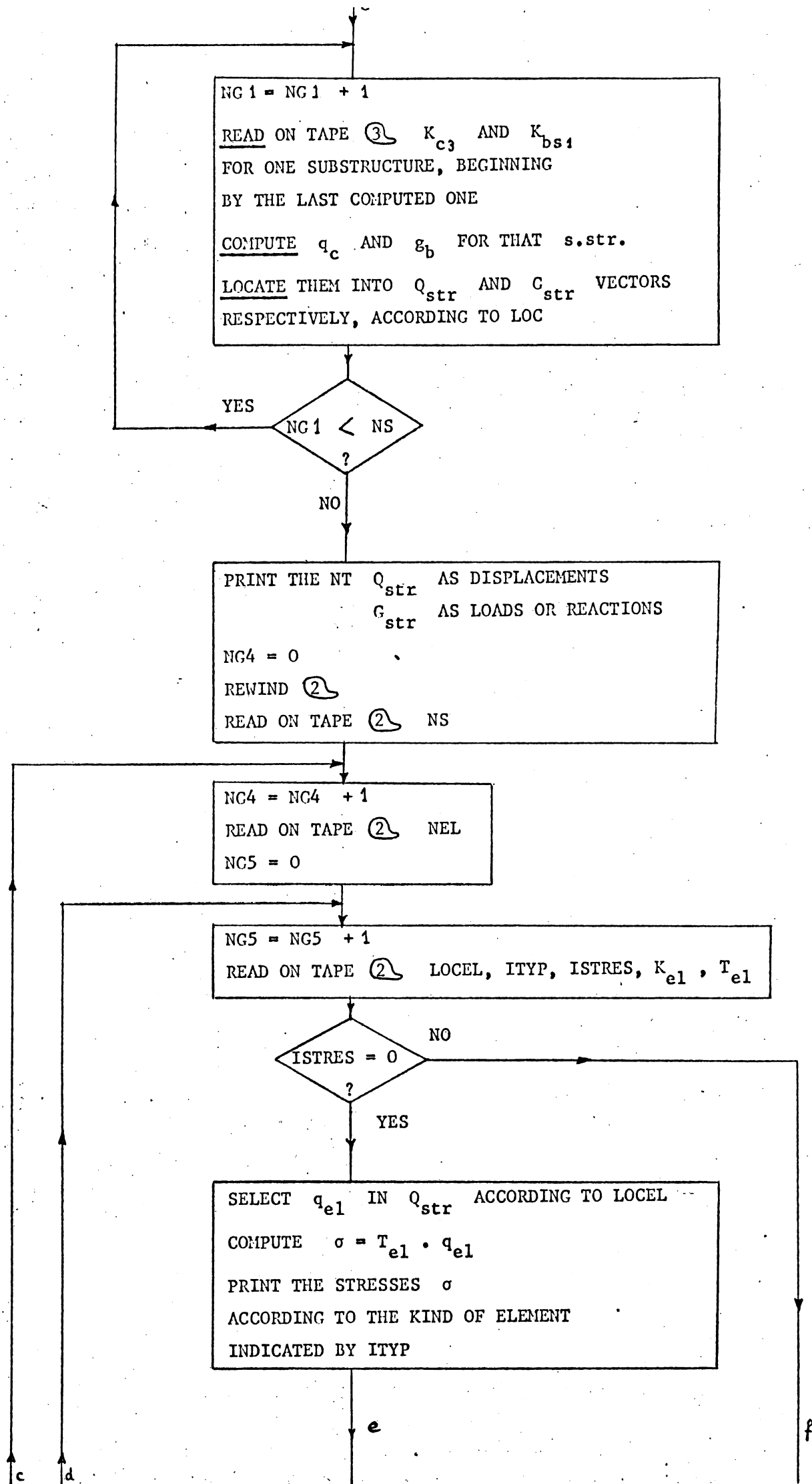
READ ELASTIC AND GEOMETRIC DATA
COMPUTE K_{e1} STIFFNESS MATRIX
 T_{e1} STRESS MATRIX
IN LOCAL COORDINATES
TRANSFORM IN STRUCTURAL COORDINATES

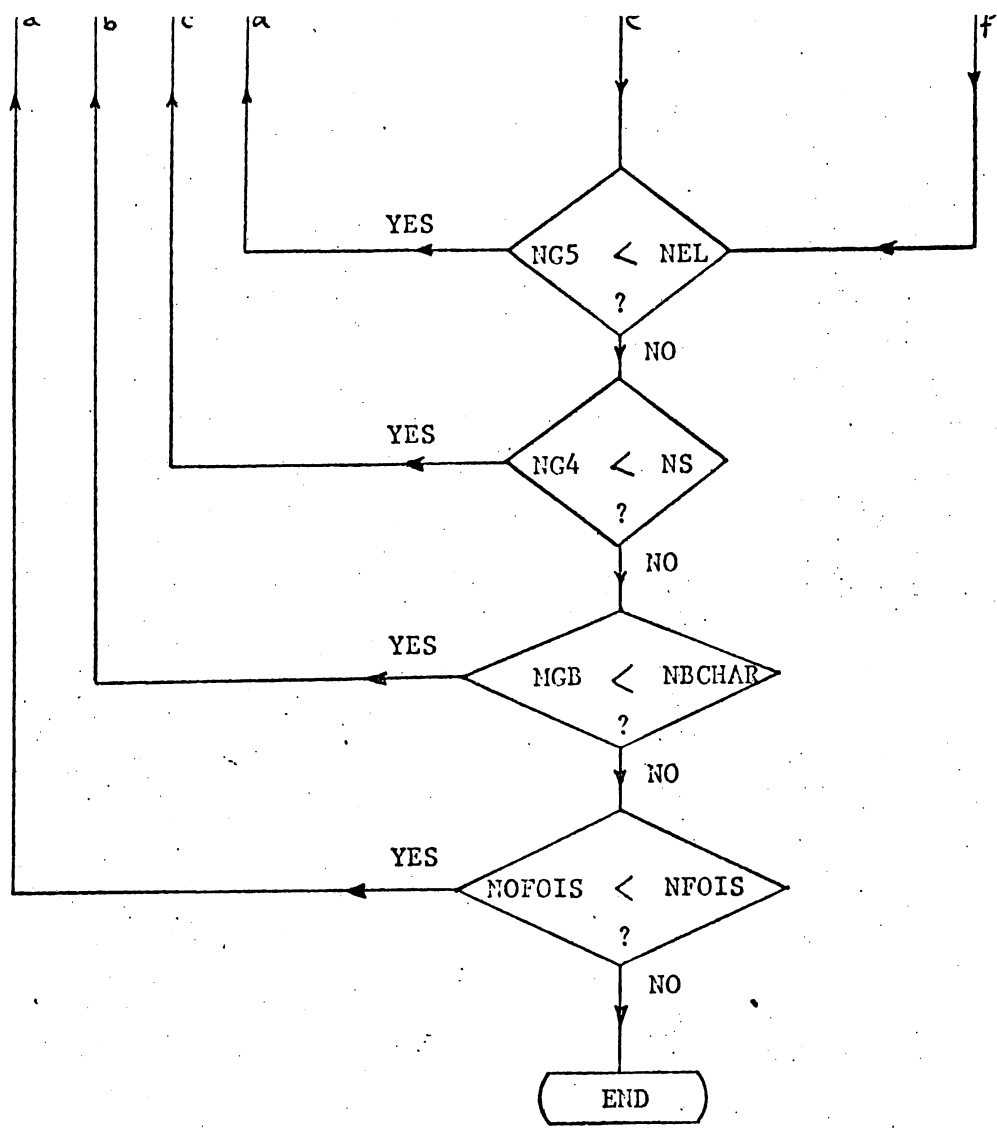
14 15

d









A.5- Input data preparation.

Starting with a structure idealized into a set of finite elements, the first step is to number the effective displacements so that each displacement q_i has an individual subscript between 1 and 500. It is recalled that an effective displacement is understood here as a displacement for which at least a non zero diagonal stiffness coefficient will be generated in the structural axes.

The largest Figure given to the subscript i during this numbering is to be taken as the total number of generalized coordinates NT even if some numbers are missing in the sequence. While printing the displacements the program starts at q_1 up to q_{NT} and prints zero for the displacements q_j which are not used in the numbering ($1 \leq j \leq NT$).

The second step is to subdivide the structure into substructures.

As already mentioned the smallest possible number of substructures should be used to have the best speed and accuracy. Having checked that the number of displacements of the first substructure is less than 115, these displacements have to be sorted in "remaining" displacements q_r , condensable displacements q_c or fixed displacements q_f as explained in section A.3. Then, assembling the elements of the next substructure, the loaded displacements of the preceding substructure (s) have to be taken as part of the new substructure and the number of displacements NCS has to include them.

It is therefore advisable in a structure, loaded only in one substructure, to end with the assembling of that one in order not to carry the loaded displacements all the way through the assembling procedure.

When dealing with a structure having a rather large number of loaded displacements, a certain amount of skill is required to subdivide into substructures in such a way that the number of elements added by a substructure is not too small due to the number of loaded displacements coming from previously assembled substructures. When the number of loaded displacements is coming close to the capacity of a substructure (115), two runs are required using the superposition principle.

Once the subdivision into substructures, including separation of the displacements into the 3 categories, is performed for the whole structure, filling the input data forms can be undertaken.

It is believed that these forms, in connection with the input data flow chart, the elements library informations and the worked examples given in the next chapter, should be sufficient to avoid most of the difficulties raised by the use of the program.

FORTRAN SYMBOLS USED IN THE INPUT DATA FORMS.

NFOIS Number of problems to be solved in the same run.

NS Number of substructures in one problem ($1 \leq NS \leq 999$).

NT Total number of generalized coordinates ($1 \leq NT \leq 500$).

TITLE Any title to be printed in front of the output.

NOS Numbering of the substructure ($1 \leq NOS \leq 999$).

NEL Number of elements in a substructure ($1 \leq NEL \leq 999$).

NOP(i) Printing options
NOP(1) = 0 no printing
NOP(1) = 1 prints elements data
NOP(1) = 4 prints elements data plus
 elements matrices
NOP(2) \neq 0 same effect as NOP(1)
NOP(3) to NOP(5) \neq 0 causes printing
 of substructures submatrices
 while assembling. Usually not
 required.

ITYPAN Code number to select the type of analysis and the subsequent
link to be charged`
ITYPAN = 1 for compatible membering elements
ITYPAN = 2 for equilibrium membering elements
ITYPAN = 3 for plate elements.

NOEL Numbering of the elements (dummy input).

ITYP Code number selecting the element subroutine. Given in the
elements library informations.

LOCEL Localization vector for an element.

ISIMPL Option allowing when $\neq 0$ to skip elements stiffness matrices
computation if they are known to be the same as the
preceeding element.

ISTRES Option which, if set $\neq 0$ skip stress computation for the
element.

NOS1 Substructure number. Must be the same as NOS.

NCS Total number of gen. coordinates pertaining to the substructure
including the loaded displacements coming from previously
assembled substructures ($1 \leq NCS \leq 115$).

NCC Number of gen. coordinates to be condensed, q_c . May be 0.

NCF Number of gen. coordinates to be fixed q_f . May be 0.

NCR Number of gen. coordinates to be kept for the next assembling
("Remaining" displacements q_r). May not be 0.
Check : $NCS = NCC + NCF + NCR$.

LOC Localization vector for a substructure.
Indices must be sorted in the order q_r , q_f , q_c .
0 is not allowed.

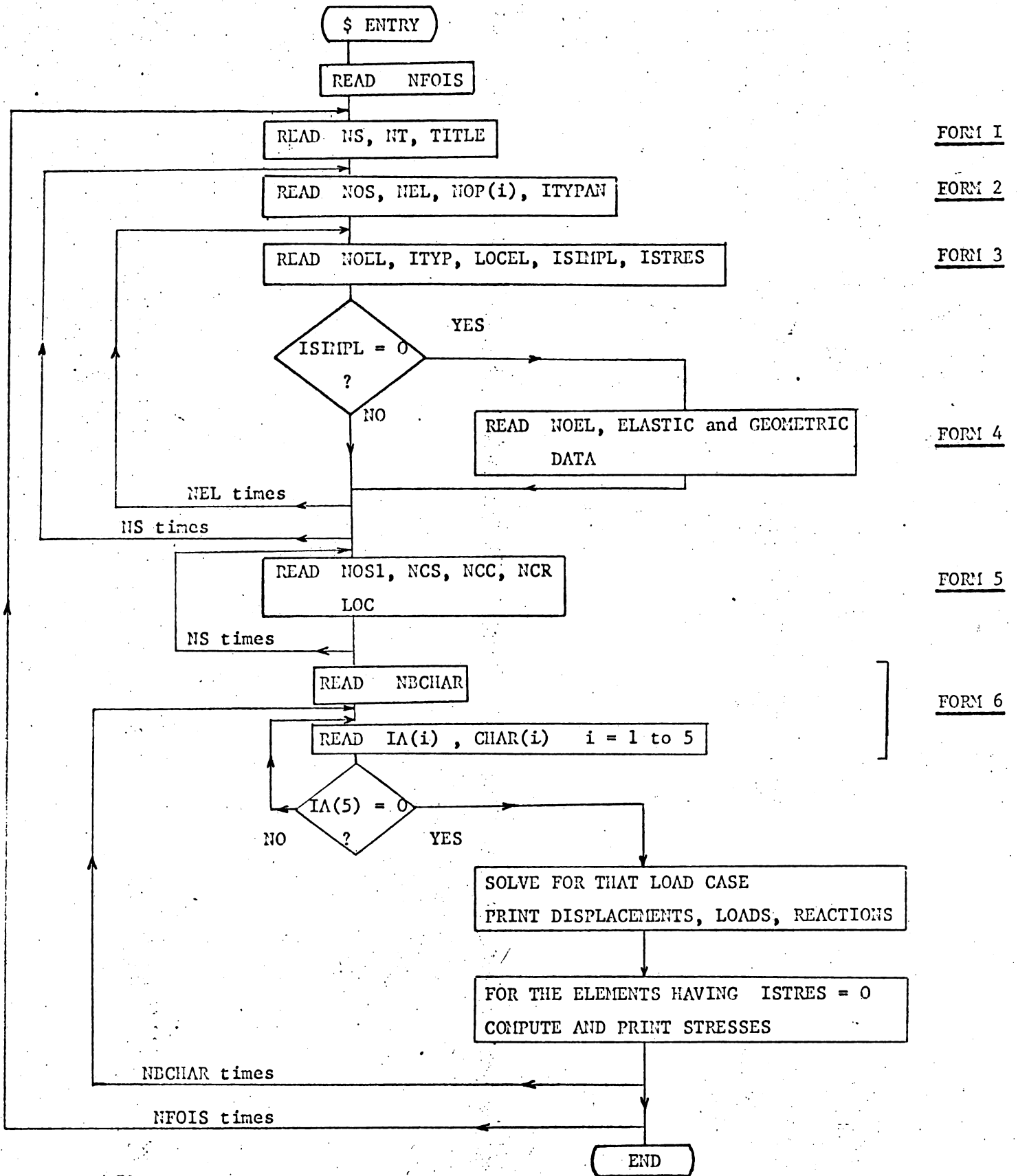
NBCHAR Number of loading cases.

IA(i) Index of a load component g_i .

A(i) Value of that load component g_i .

FLOW CHART GIVING

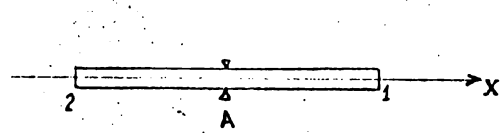
INPUT DATA SEQUENCE



Note : The indices of the displacements given in the local sequence refer to displacements in the structural axes at the corresponding points given in the elements drawings, while the local axes in which the stresses are expressed are also indicated on the drawing. The geometrical coordinates of the elements have to be expressed in the structural axes, if no other information is given.

ITYP = 1

LINEAR COMPATIBLE STRINGER or BAR



Displacement sequence

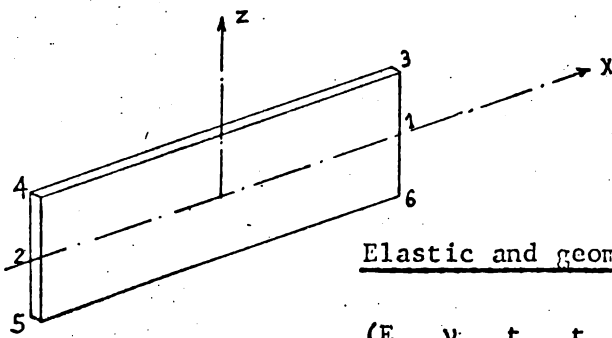
$$(u_1 \quad v_1 \quad w_1 \quad u_2 \quad v_2 \quad w_2)$$

Elastic and geometric data sequence

$$(E \quad \nu \quad A \quad x_1 \quad y_1 \quad z_1 \quad x_2 \quad y_2 \quad z_2)$$

ITYP = 2

LINEAR COMPATIBLE SPAR



Displacement sequence

$$(u_3 \quad v_3 \quad w_3 \quad \frac{\partial w}{\partial y_1} \quad \frac{\partial w}{\partial x_1} \quad 0 \quad u_4 \quad v_4 \quad w_4 \quad \frac{\partial w}{\partial y_2} \quad \frac{\partial w}{\partial x_2} \quad 0)$$

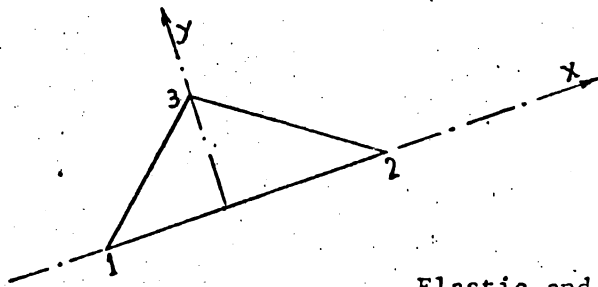
Elastic and geometric data sequence

$$(E \quad \nu \quad t_1 \quad t_2 \quad x_3 \quad y_3 \quad z_3 \quad x_4 \quad y_4 \quad z_4 \quad x_5 \quad y_5 \quad z_5 \quad x_6 \quad y_6 \quad z_6)$$

N.B. The structural z axis has to be parallel with the local z axis.

ITYP = 3

LINEAR COMPATIBLE TRIANGLE



Displacement sequence

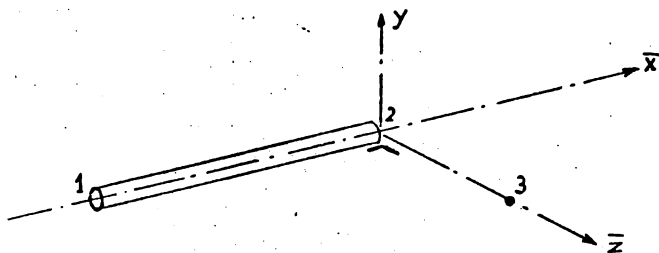
$(u_1 \ v_1 \ w_1 \ u_2 \ v_2 \ w_2 \ u_3 \ v_3 \ w_3)$

Elastic and geometric data sequence

$(E \ \nu \ x_1 \ y_1 \ z_1 \ t_1 \ x_2 \ y_2 \ z_2 \ t_2 \ x_3 \ y_3 \ z_3 \ t_3)$

ITYP = 4

FRAME ELEMENT



Displacement sequence

$(u_1 \ v_1 \ w_1 \ \phi_{x1} \ \phi_{y1} \ \phi_{z1} \ u_2 \ v_2 \ w_2 \ \phi_{x2} \ \phi_{y2} \ \phi_{z2})$

Elastic and geometric data sequence

$(x_1 \ y_1 \ z_1 \ x_2 \ y_2 \ z_2 \ x_3 \ y_3 \ z_3 \ A \ I_y \ I_z \ J \ E \ G)$

N.B. 1) The point 3 has to be given only if $I_y \neq I_z$. If not needed then set $x_3 \ y_3 \ z_3 > 10^{20}$. The routine chooses his own axes and print their direction cosines if $NOP(1) \neq 0$.

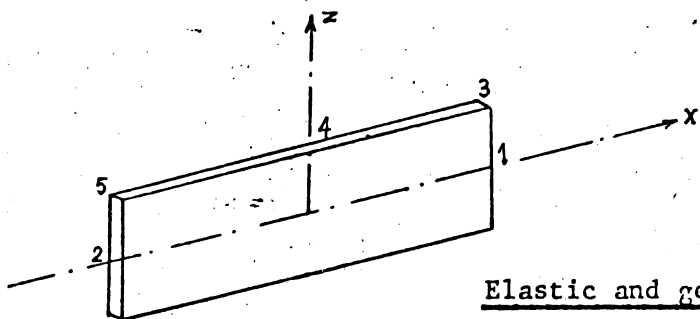
2) A is the cross section

$I_y \ I_z$ the moments of inertia

J the torsional rigidity

ITYP = 5

QUADRATIC COMPATIBLE SPAR



Displacement sequence

$(u_3 \ v_3 \ w_3 \ \frac{\partial w}{\partial x_1} \ \frac{\partial w}{\partial y_1} \ u_5 \ v_5 \ w_5 \ \frac{\partial w}{\partial x_2} \ \frac{\partial w}{\partial y_2} \ u_4 \ v_4)$

Elastic and geometric data sequence

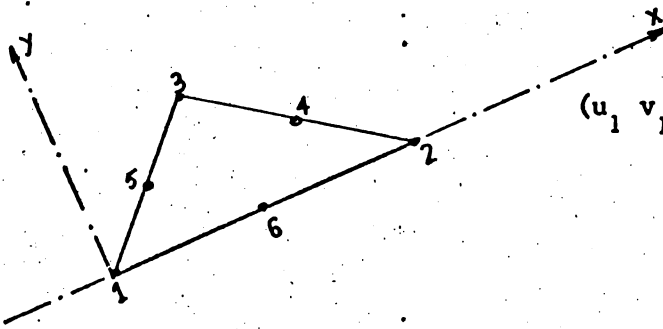
$(E \ \nu \ t \ H \ S \ x_1 \ y_1 \ x_3 \ y_3)$

Note : 1) local z axis have to be parallel to structural z axis

2) S is the cross section of one spar cap

ITYP = 6

QUADRATIC COMPATIBLE TRIANGLE



Displacement sequence

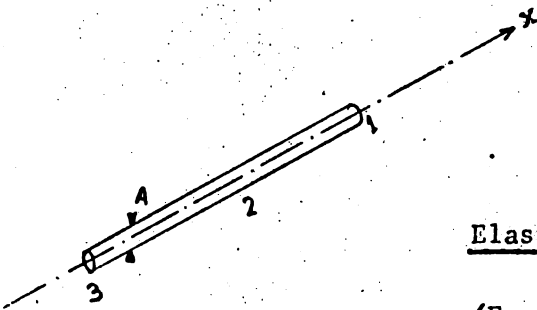
$(u_1 \ v_1 \ w_1 \ u_6 \ v_6 \ w_6 \ u_2 \ v_2 \ w_2 \ u_4 \ v_4 \ w_4 \ u_3 \ v_3 \ w_3 \ u_5 \ v_5 \ w_5)$

Elastic and geometric data sequence

$(E \ \nu \ t \ x_1 \ y_1 \ z_1 \ x_2 \ y_2 \ z_2 \ x_3 \ y_3 \ z_3)$

ITYP = 7

QUADRATIC COMPATIBLE BAR



Displacement sequence

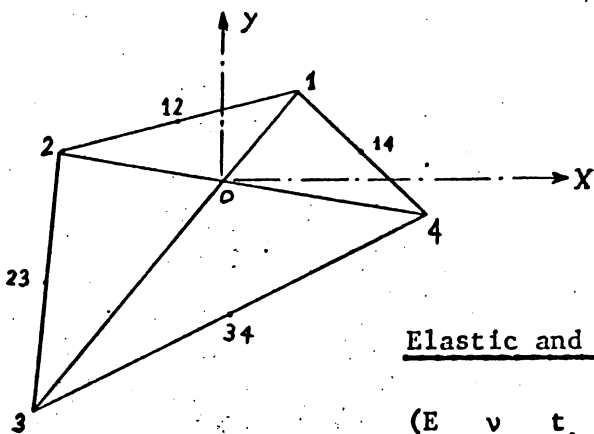
$(u_1 \ v_1 \ w_1 \ u_2 \ v_2 \ w_2 \ u_3 \ v_3 \ w_3)$

Elastic and geometric data sequence

$(E \ \nu \ A \ x_1 \ y_1 \ z_1 \ x_3 \ y_3 \ z_3)$

ITYP = 8

CONSTANT STRESS EQUILIBRIUM QUADRANGLE



Displacement sequence

$(\bar{v}_{14} \ \bar{u}_{14} \ \bar{v}_{12} \ \bar{u}_{12} \ \bar{v}_{23} \ \bar{u}_{23} \ \bar{v}_{34} \ \bar{u}_{34})$

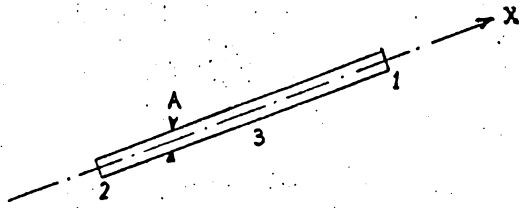
Elastic and geometric data sequence

$(E \ \nu \ t_{14} \ t_{12} \ t_{23} \ t_{34} \ x_1 \ x_2 \ x_3 \ x_4 \ y_1 \ y_2 \ y_3 \ y_4)$

- Restrictions :
- 1) The local xy plane has to coincide with the structural xy plane
 - 2) The geometric coordinates of points 1,2,3,4 have to be given in the local axes having their origin in point o
 - 3) This routine should not be used for element having an aspect ratio other 2 to 1

ITYP = 9

CONSTANT SHEAR BAR OR STRINGER



Displacements sequence

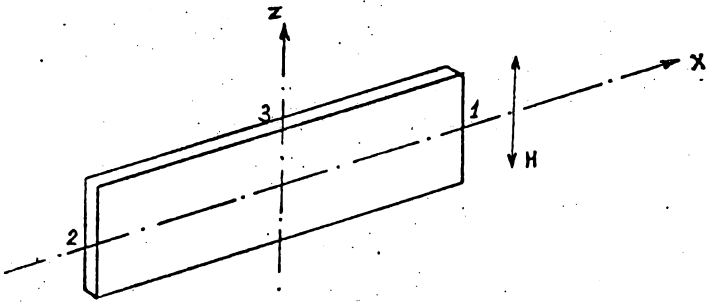
$(u_1 \ v_1 \ w_1 \ u_3 \ v_3 \ w_3 \ u_2 \ v_2 \ w_2)$

Elastic and geometric data sequence

$(E \ A \ x_1 \ y_1 \ z_1 \ x_2 \ y_2 \ z_2)$

ITYP = 10

EQUILIBRIUM SPAR - UPPER BOUND VERSION



Displacements sequence

$(w_1 \ \frac{\partial w}{\partial y}|_1 \ \frac{\partial w}{\partial x}|_1 \ w_2 \ \frac{\partial w}{\partial y}|_2 \ \frac{\partial w}{\partial x}|_2 \ u_3 \ v_3)$

Elastic and geometric data sequence

$(E \ \nu \ t \ H \ x_1 \ y_1 \ x_2 \ y_2)$

N.B. The local z axis has to be parallel to the structural z axis

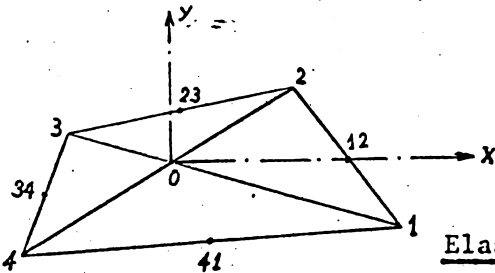
ITYP = 11

EQUILIBRIUM SPAR - DIRECT FORMULATION

Besides the theoretical differences, no other difference with the preceding element except ITYP = 11 instead of 10.

ITYP = 12

CONSTANT STRESS EQUILIBRIUM QUADRANGLE



Displacements sequence

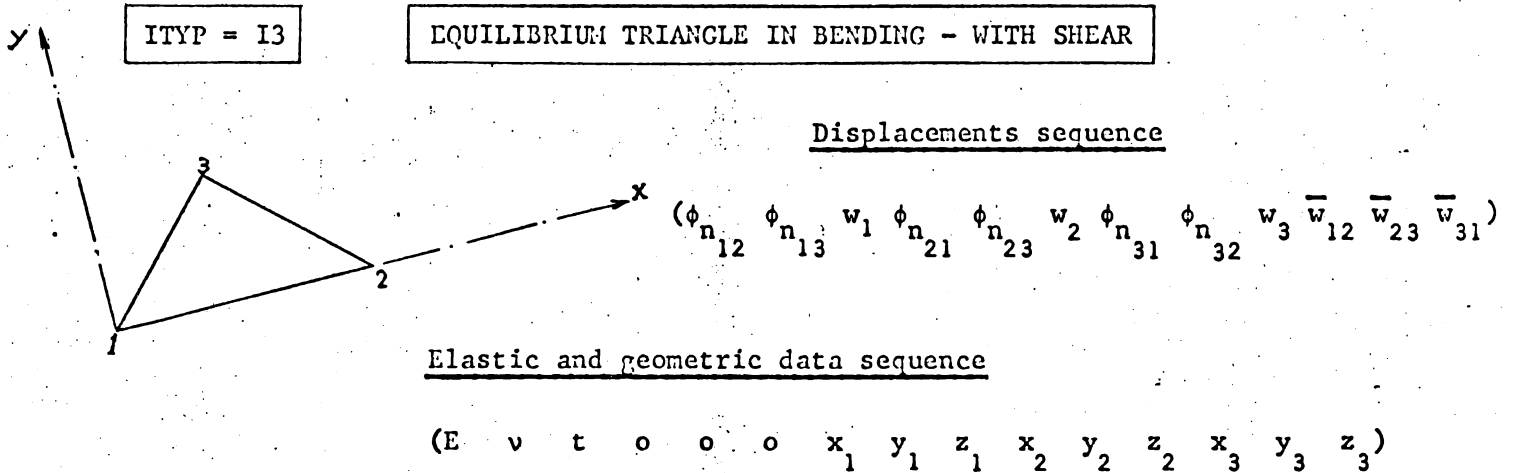
$(y_{12} \ x_{12} \ y_{23} \ x_{23} \ y_{34} \ x_{34} \ y_{41} \ x_{41})$

Elastic and geometric data sequence

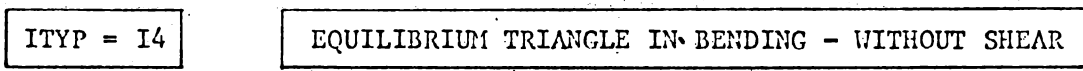
$(E \ \nu \ t_{12} \ t_{23} \ t_{34} \ t_{41} \ x_2 \ x_3 \ x_4 \ x_1 \ y_2 \ y_3 \ y_4 \ y_1)$

Note : 1) The local xy plane has to be parallel to the structural xy plane

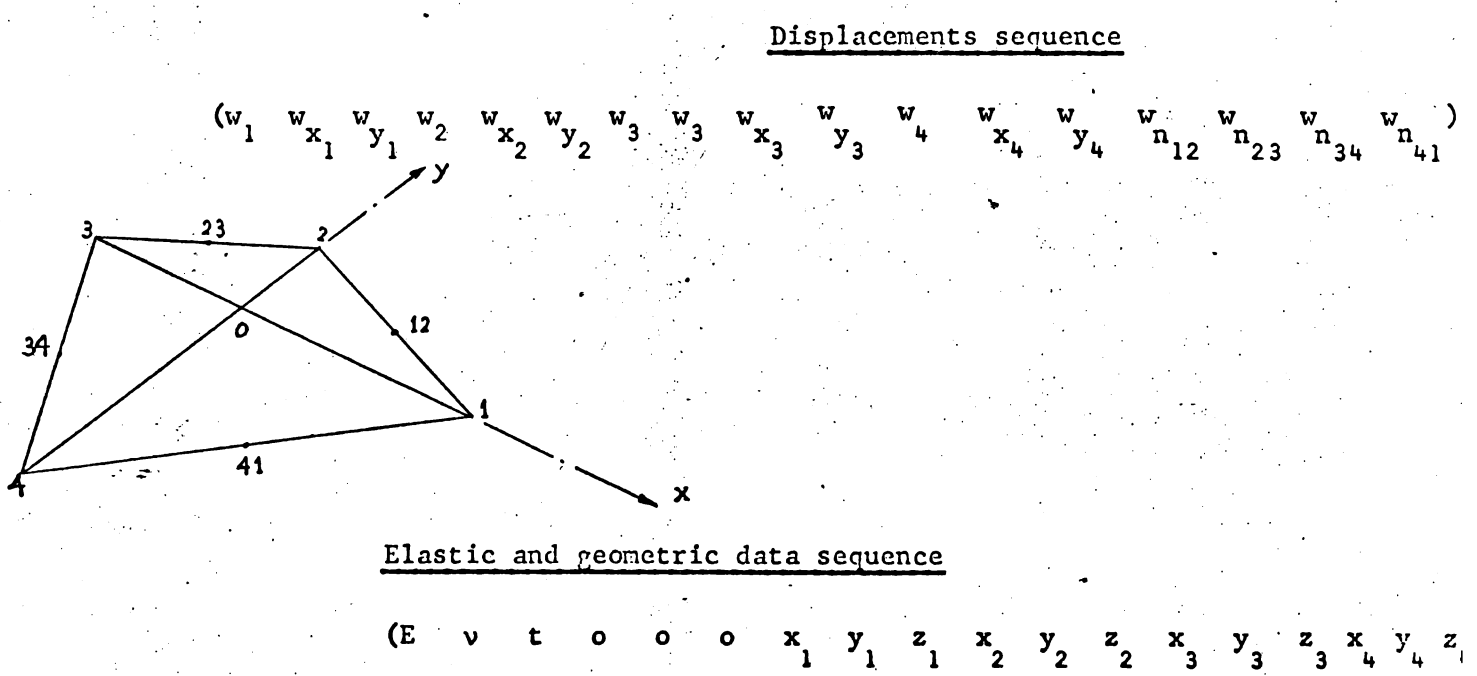
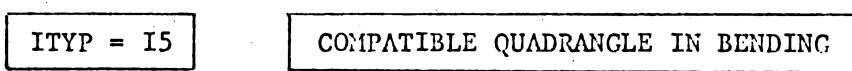
2) This routine is an improved version of ITYP = 8 working partially in double precision.



Note : in this element the energy due to the shearing stresses τ_{xz} τ_{yz} is included.



Note : this element is similar to the preceding one but the shear energy term is dropped out.



Remark for routines I3 - I4 - I5.

The z structural axis has to be parallel to the local z axis.

A.6- Worked examples.

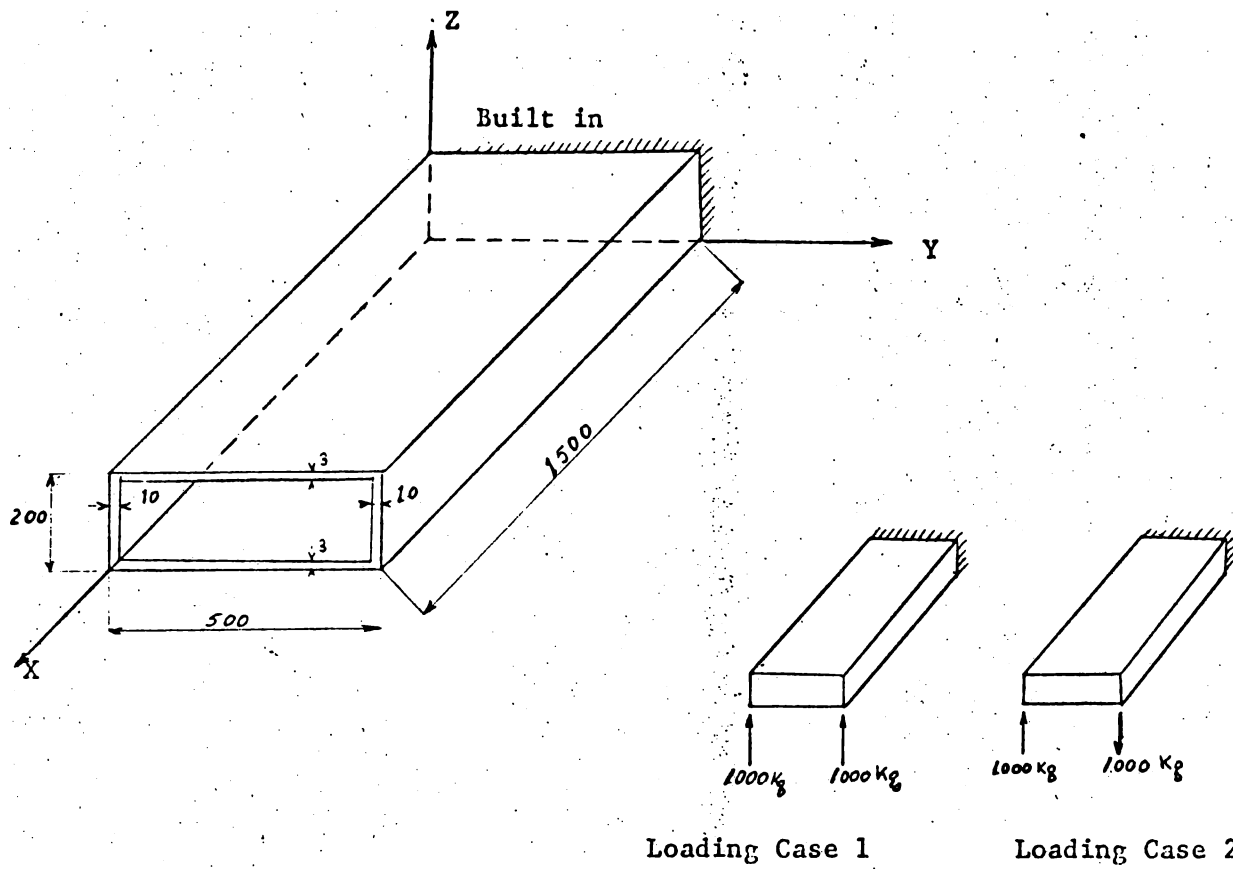
The simple box beam, illustrated in Figure F.A.4, is treated as an example of input data preparation. The selected idealization is indicated in Figures F.A.5 and F.A.6 using the quadratic compatible displacement field. 12 elements are used and 60 effective generalized displacements are necessary to describe the behaviour of the structure. The numbering of the displacements and of the elements is given in the Figure as well as local axes orientation. From these Figures input data forms have been filled and are given here after.

The same problem has been treated using 2 substructures for the sake of providing an example, as it is unnecessary for such a simple case.

The substructure subdivision is indicated in Figure F.A.7.

Using the same displacements and elements numbering as well as the same local axes localization, the corresponding input data sheet are given after the preceding ones.

The listing of input data cards ~~and output~~ for both cases is given next to the input data forms.



dimensions in mm.

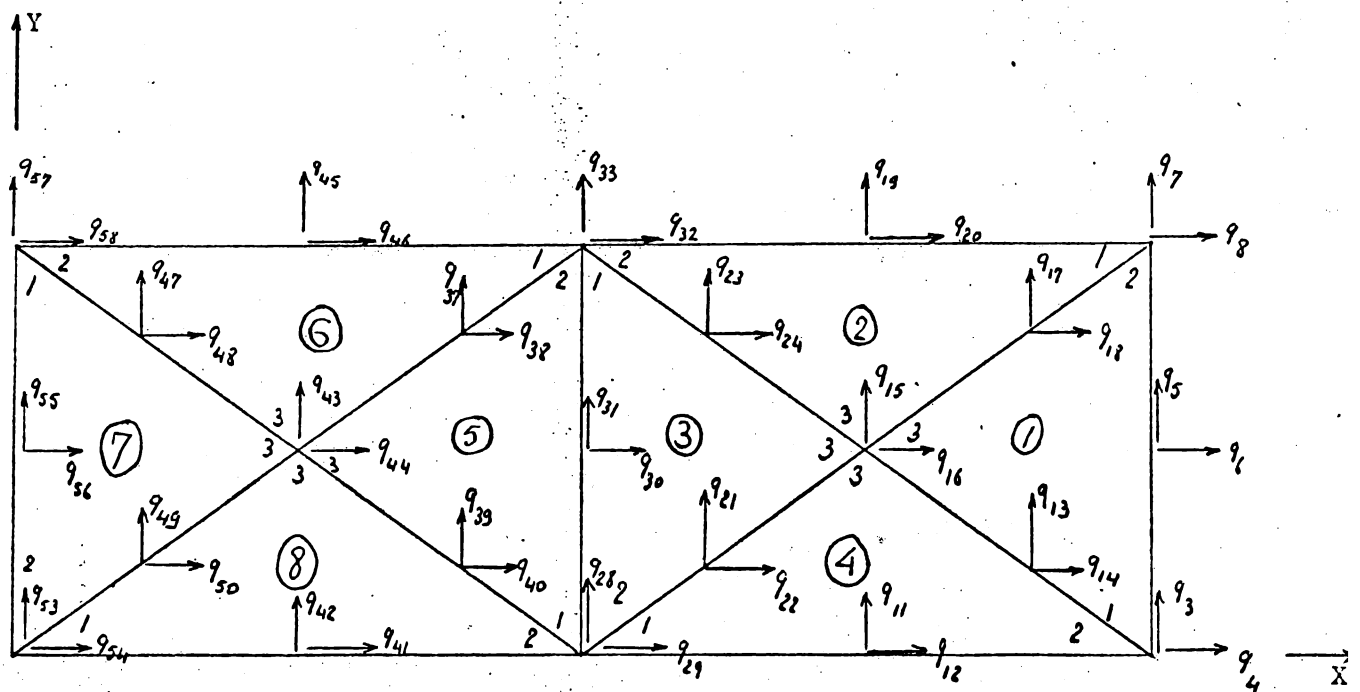
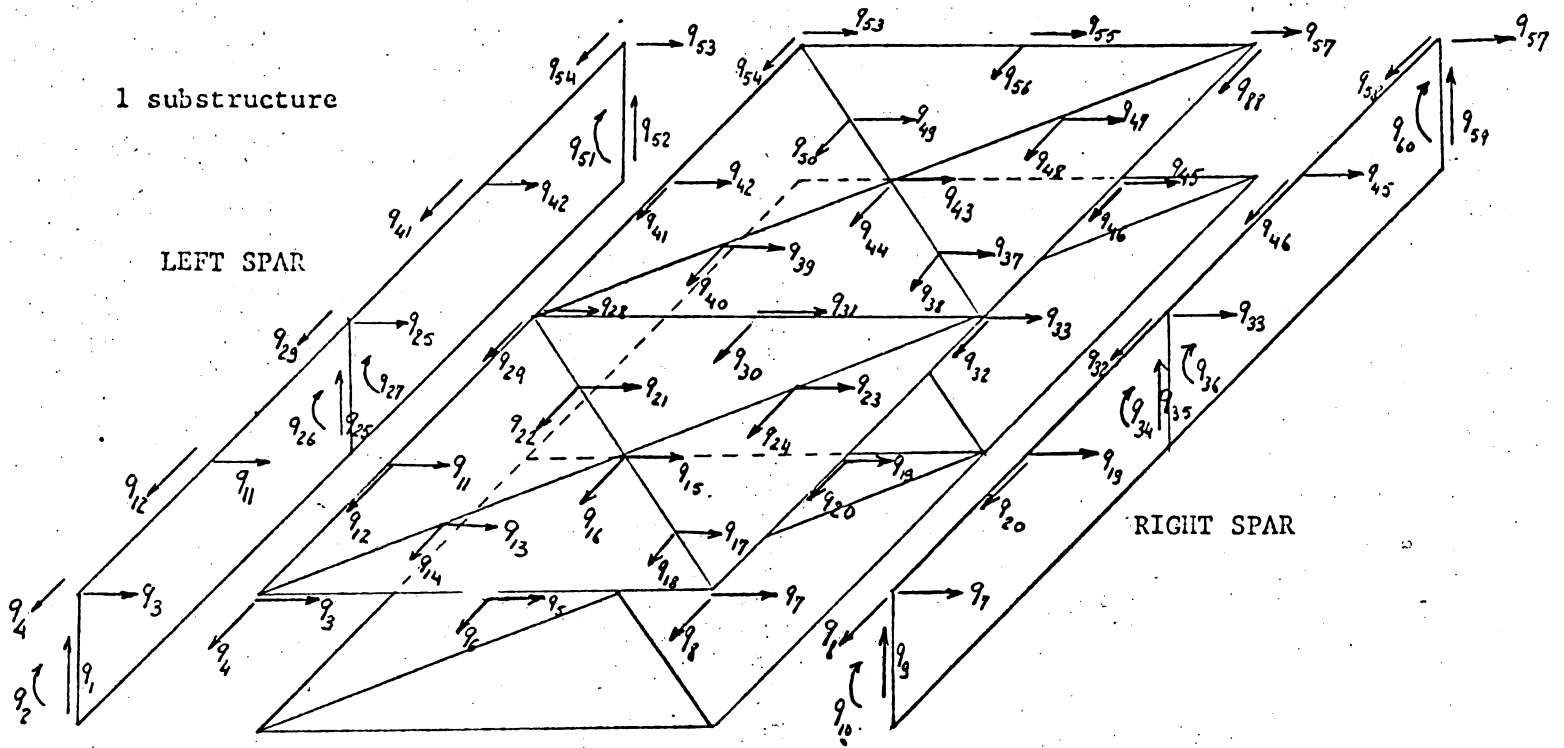
Elastic Properties

$$E = 7,500 \text{ Kg/mm}^2$$

$$\nu = .3$$

Figure F.A.4. The box beam used as input data preparation example.

IDEALIZATION



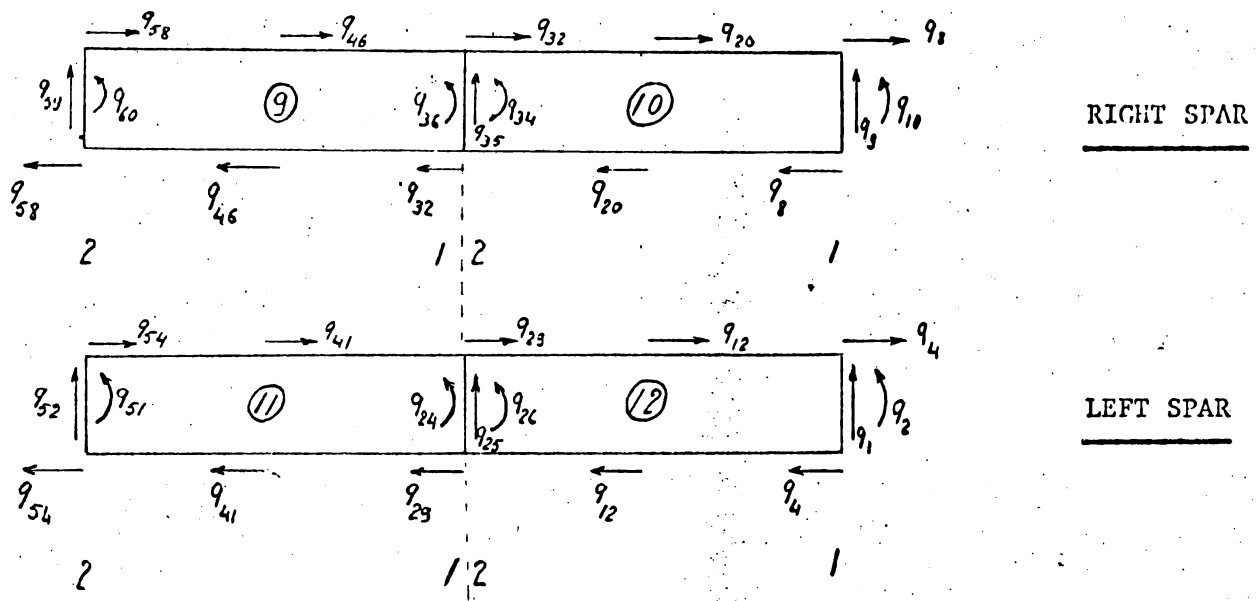
COVER

q_i gen. displacement number i

① element numbering

1.2.3. corner numbering inside a triangle; gives the orientation of local axes and stresses.

Figure F.A.5. Box beam idealization and displacements numbering.



q_i = gen. displacement number i

(12) = element numbering

1,2 = end of spar element numbering, gives the orientation of local axes and stresses

LOADS are applied on q_1 and q_{10}

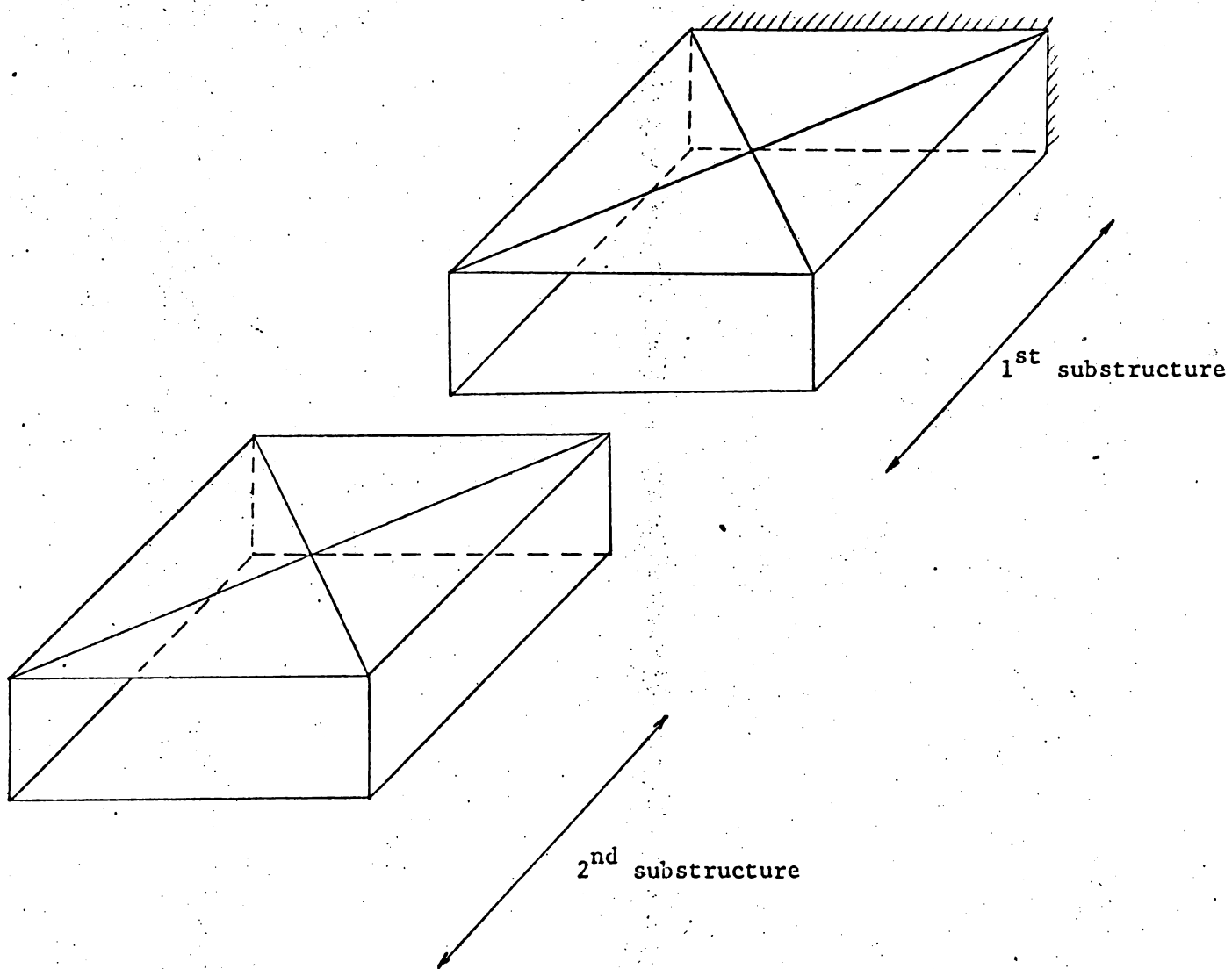
BOUNDARY CONDITIONS Built in at one edge.

This implies $q_{52}, q_{53}, q_{54}, q_{55}, q_{56}, q_{57}, q_{58}, q_{59} = 0$

Remark: q_{51} and q_{60} have to be left free (see spar theory).

Figure F.A.6. Box beam idealization and displacement numbering.

IDEALIZATION USING 2 SUBSTRUCTURES



the same numbering is used for the displacements and for the elements.

Figure F.A.7. Box beam idealization using 2 substructures.

References of Section A.

- R.A.1. J.S. PRZIEMIENIECKI, "Matrix Structural Analysis of Substructures",
Jour. Am. Inst. of Aeron. and Astron. - Vol. I, N° 1, Jan. 1963 -
pp. I38-I47.
- R.A.2. I.C. TAIG, "Automated Stress Analysis using Substructures",
Proc. of the Conf. on Matrix Methods in Structural Mechanics.
AF. Flight Dynamics Lab., Dayton, OHIO - October 1965.
- R.A.3. P.K. LIVESLEY, "Matrix Methods of Structural Analysis",
Pergamon Press, 1964.

1 60
 BOX BEAM ANALYSIS - 60 GEN. COORDINATES
 QUADRATIC COMPATIBLE DISPLACEMENT FIELD - 1 S.STR.

1 12 0 0 0 0 0 1
 1 6 4 3 0 6 5 0 8 7 0 18 17 0 16 15 0 0
 1 6 14 13 0
 1 +7.5000E+03 +0.3000E+00 +6.0000E+00 +1.5000E+03 +0.0000E+00 +2.0000E+02
 1 +1.5000E+03 +5.0000E+02 +2.0000E+02 +1.1250E+03 +2.5000E+02 +2.0000E+02
 1
 5 6 29 28 0 30 31 0 32 33 0 38 37 0 44 43 0 1
 5 6 40 39 0
 2 6 8 7 0 20 19 0 32 33 0 24 23 0 16 15 0 0
 2 6 18 17 0
 2 +7.5000E+03 +0.3000E+00 +6.0000E+00 +1.5000E+03 +5.0000E+02 +2.0000E+02
 2 +7.5000E+02 +5.0000E+02 +2.0000E+02 +1.1250E+03 +2.5000E+02 +2.0000E+02
 2
 6 6 32 33 0 46 45 0 58 57 0 48 47 0 44 43 0 1
 6 6 38 37 0
 3 6 32 33 0 30 31 0 29 28 0 22 21 0 16 15 0 0
 3 6 24 23 0
 3 +7.5000E+03 +0.3000E+00 +6.0000E+00 +7.5000E+02 +5.0000E+02 +2.0000E+02
 3 +7.5000E+02 +0.0000E+00 +2.0000E+02 +1.1250E+03 +2.5000E+02 +2.0000E+02
 3
 7 6 58 57 0 56 55 0 54 53 0 50 49 0 44 43 0 1
 7 6 48 47 0
 4 6 29 28 0 12 11 0 4 3 0 14 13 0 16 15 0 0
 4 6 22 21 0
 4 +7.5000E+03 +0.3000E+00 +6.0000E+00 +7.5000E+02 +0.0000E+00 +2.0000E+02
 4 +1.5000E+03 +0.0000E+00 +2.0000E+02 +1.1250E+03 +2.5000E+02 +2.0000E+02
 4
 8 6 54 53 0 41 42 0 29 28 0 40 39 0 44 43 0 1
 8 6 50 49 0
 9 5 32 0 35 0 36 58 0 59 0 60 46 0 0 0
 9
 9 +7.5000E+03 +0.3000E+00 +3.0000E+00 +2.0000E+02 +0.0000E+00 +7.5000E+02
 9 +5.0000E+02 +0.0000E+00 +5.0000E+02
 9
 10 5 8 0 9 0 10 32 0 35 0 34 20 0 0 1
 10
 11 5 29 0 25 0 27 54 0 52 0 51 41 0 0 1
 11
 12 5 4 0 1 0 2 29 0 25 0 26 12 0 0 1
 12

1 60 0 8 52
 1 2 3 4 5 6 7 8 9 10 11 12 13 14 15 16 17 18 19
 20 21 22 23 24 25 26 27 28 29 30 31 32 33 34 35 36 37 38
 39 40 41 42 43 44 45 46 47 48 49 50 51 60 52 53 54 55 56
 57 58 59

2
 1 +1.0000E+03 9 +1.0000E+03
 1 +1.0000E+03 9 -1.0000E+03

ASEF - 3

DATE 1-7-66
 PROBLEM NBR 1
 SHEET 1 OUT OF 6

FORM 1

FIRST EXAMPLE

BOX BEAM USING ONE SUBSTRUCTURE

DIMENSIONS AND TITLE			
NS =	1	NT =	60
TITLE	BOX BEAM ANALYSIS - 60 GEN. COORDINATES		
TITLE	QUADRATIC COMPATIBLE DISPLACEMENT FIELD - 1 S.STR.		
FORMAT (I3,IX,I3 / I3A6/I3A6)			

DATE
PROBLEM NBR
SHEET 2 out of 6

FORM 2

SUBSTRUCTURE NBR 1

SUBSTRUCTURE DIMENSIONS, PRINTING OPTIONS, TYPE OF ANALYSIS						
NOS	NEL	NOP(1)	NOP(2)	NOP(3)	NOP(4)	NOP(5) ITYPAN
1	12	0	0	0	0	1
FORMAT (I3, 3X, I3, 5(1X, I1), 3X, I3)						

DATE

PROBLEM NBR

FORM 3

SHEET: 3 OUT OF 6

LOCATION VECTORS FOR ELEMENTS OF SUBSTRUCTURE 1

NOEL	ITYP	LOCAL (I)												ISIMPL	ISTRRES																					
		8	12	15	16	19	20	23	24	27	28	31	32			35	36	39	40	43	44	47	48	51	52	55	56	59	60	63	64	67				
1	3	5	6	8	4	14	3	0	0	6	5	0	0	8	7	0	0	18	17	0	16	15	0	0	0	0	0	0	0	0	0	72	80			
1	6	6	6	8	14	13	0	0	0	0	0	0	0	32	33	0	0	38	37	0	44	43	0	0	0	0	0	0	0	0	0	0	0			
5	6	6	6	8	29	39	0	0	30	30	31	0	0	32	33	0	0	24	23	0	16	15	0	0	0	0	0	0	0	0	0	0	0			
2	6	6	6	8	40	7	0	0	20	19	19	0	0	32	33	0	0	24	23	0	16	15	0	0	0	0	0	0	0	0	0	0	0			
6	6	6	6	8	18	17	0	0	46	45	45	0	0	58	57	0	0	48	47	0	44	43	0	0	0	0	0	0	0	0	0	0	0	0		
6	6	6	6	8	32	33	0	0	0	0	0	0	0	58	57	0	0	48	47	0	44	43	0	0	0	0	0	0	0	0	0	0	0	0		
3	6	6	6	8	38	37	0	0	30	31	31	0	0	29	28	0	0	22	21	0	16	15	0	0	0	0	0	0	0	0	0	0	0	0		
3	6	6	6	8	32	33	0	0	30	31	31	0	0	29	28	0	0	22	21	0	16	15	0	0	0	0	0	0	0	0	0	0	0	0	0	
7	6	6	6	8	24	23	0	0	56	55	55	0	0	54	53	0	0	50	49	0	44	43	0	0	0	0	0	0	0	0	0	0	0	0	0	
7	6	6	6	8	58	57	0	0	0	0	0	0	0	54	53	0	0	50	49	0	44	43	0	0	0	0	0	0	0	0	0	0	0	0	0	
4	6	6	6	8	48	47	0	0	12	11	11	0	0	4	3	0	0	14	13	0	16	15	0	0	0	0	0	0	0	0	0	0	0	0	0	
4	6	6	6	8	29	28	0	0	0	0	0	0	0	4	3	0	0	14	13	0	16	15	0	0	0	0	0	0	0	0	0	0	0	0	0	0
8	6	6	6	8	22	21	0	0	41	42	42	0	0	29	28	0	0	40	39	0	44	43	0	0	0	0	0	0	0	0	0	0	0	0	0	0
8	6	6	6	8	54	53	0	0	0	0	0	0	0	29	28	0	0	40	39	0	44	43	0	0	0	0	0	0	0	0	0	0	0	0	0	0
9	5	5	5	8	50	49	0	0	0	0	0	0	0	0	0	0	0	60	46	0	0	0	0	0	0	0	0	0	0	0	0	0	0	0	0	0
9	5	5	5	8	32	0	35	0	0	0	36	58	0	0	59	0	0	60	46	0	0	0	0	0	0	0	0	0	0	0	0	0	0	0	0	0
10	5	5	5	8	8	0	9	0	0	0	10	32	0	0	35	0	0	34	20	0	0	0	0	0	0	0	0	0	0	0	0	0	0	0	0	0
10	5	5	5	8	0	0	9	0	0	0	10	32	0	0	35	0	0	34	20	0	0	0	0	0	0	0	0	0	0	0	0	0	0	0	0	0
11	5	5	5	8	29	0	25	0	0	0	27	54	0	0	52	0	0	51	41	0	0	0	0	0	0	0	0	0	0	0	0	0	0	0	0	0
11	5	5	5	8	0	0	25	0	0	0	27	54	0	0	52	0	0	51	41	0	0	0	0	0	0	0	0	0	0	0	0	0	0	0	0	0
12	5	5	5	8	4	0	1	0	0	0	2	29	0	0	25	0	0	26	12	0	0	0	0	0	0	0	0	0	0	0	0	0	0	0	0	0
12	5	5	5	8	0	0	1	0	0	0	2	29	0	0	25	0	0	26	12	0	0	0	0	0	0	0	0	0	0	0	0	0	0	0	0	0

FORMAT (I 3, I X, I 2, I X, 15(I 4), 4 X, I 1 / 7 X, 15(I 4), 12 X, I 1)

		E L A S T I C A N D G E O M E T R I C D A T A F O R S U B S T R U C T U R E N B R 1											
NOEL	15 17	27 29	D A T A				(S E E S E R V E N C I N G)				63 65	75	
			39 41	51 53	63 65	75	87 89	99 101	111 113	123 125			
1	7500.	.3	500.	3.	1500.	0.	200.	200.	200.				
	1500.	500.	200.	3.	1125.	250.	200.	200.	200.				
2	7500.	.3	500.	3.	1500.	500.	200.	200.	200.				
	750.	500.	200.	200.	1125.	250.	200.	200.	200.				
3	7500.	.3	500.	3.	750.	500.	200.	200.	200.				
	750.	0.	200.	200.	1125.	250.	200.	200.	200.				
4	7500.	.3	500.	3.	750.	0.	200.	200.	200.				
	1500.	0.	200.	200.	1125.	250.	200.	200.	200.				
9	7500.	.3	500.	3.	200.	0.	200.	200.	200.				
	500.	0.	500.	500.	200.	0.	750.	750.	750.				

FORMAT (3 X, 6 (IX, IPEII.4))

DATE _____ PROBLEM NBR _____ FORM 5 SHEET 5 OUT OF 6

SUBSTRUCTURE NBR 1

SUBSTRUCTURE FIXATION AND CONDENSATION				
NOS1	NCS	NCC	NCF	NCR
1	60	0	8	52
1	5	15	21	25
			31	35
			41	45

FORMAT (5(15,5X))

LOCATION VECTOR FOR A SUBSTRUCTURE																																					
	89	12	13	14	17	20	21	24	25	28	29	32	33	36	37	40	41	44	45	46	49	52	53	56	57	60	64	65	68	69	72	73	76	77	80		
1	2	3	4	5	6	7	8	9	10	11	12	13	14	15	16	17	18	19	20	21	22	23	24	25	26	27	28	29	30	31	32	33	34	35	36	37	38
20	21	22	23	24	25	26	27	28	29	30	31	32	33	34	35	36	37	38	39	40	41	42	43	44	45	46	47	48	49	50	51	52	53	54	55	56	
39	40	41	42	43	44	45	46	47	48	49	50	51	52	53	54	55	56	57	58	59																	
57	58	59																																			

FORMAT (4X, 1914)

DATE

PROBLEM NBR

FORM 6

SHEET

6 out of 6

NUMBER OF LOADING CASES	
NBCHAR	2
	4
	6

FORMAT (3X,I3)

LOADING CASES																			
IA(1)	A(1)	IA(2)	A(2)	IA(3)	A(3)	IA(4)	A(4)	IA(5)	A(5)										
1	3	5	15	17	19	21	31	33	35	37	47	49	51	53	63	65	67	69	79
1	+1000.	9	+1000.																
1	+1000.	9	-1000.																

FORMAT (5(I3,I3,I3,I3,I3))

2 60
 BOX BEAM ANALYSIS - 60 GEN. COORDINATES
 QUADRATIC COMPATIBLE DISPLACEMENT FIELD - 2 S.STR.

```

1      6 0 0 0 0 0      1 --- 1 ST. SUBSTRUCTURE ---
5 6   29 28  0 30 31  0 32 33  0 38 37  0 44 43  0  0
5 6   40 39  0
5 +7.5000E+03 +0.3000E+00 +6.0000E+00 +7.5000E+02 +0.0000E+00 +2.0000E+02
5 +7.5000E+02 +5.0000E+02 +2.0000E+02 +3.7500E+02 +2.5000E+02 +2.0000E+02
5
6 6   32 33  0 46 45  0 58 57  0 48 47  0 44 43  0  0
6 6   38 37  0
6 +7.5000E+03 +0.3000E+00 +6.0000E+00 +7.5000E+02 +5.0000E+02 +2.0000E+02
6 +0.0000E+00 +5.0000E+02 +2.0000E+02 +3.7500E+02 +2.5000E+02 +2.0000E+02
6
7 6   58 57  0 56 55  0 54 53  0 50 49  0 44 43  0  0
7 6   48 47  0
7 +7.5000E+03 +0.3000E+00 +6.0000E+00 +0.0000E+00 +5.0000E+02 +2.0000E+02
7 +0.0000E+00 +0.0000E+00 +2.0000E+02 +3.7500E+02 +2.5000E+02 +2.0000E+02
7
8 6   54 53  0 41 42  0 29 28  0 40 39  0 44 43  0  0
8 6   50 49  0
8 +7.5000E+03 +0.3000E+00 +6.0000E+00 +0.0000E+00 +0.0000E+00 +2.0000E+02
8 +7.5000E+02 +0.0000E+00 +2.0000E+02 +3.7500E+02 +2.5000E+02 +2.0000E+02
8
9 5   32  0 35  0 36 58  0 59  0 60 46  0  0
9
9 +7.5000E+03 +0.3000E+00 +3.0000E+00 +2.0000E+02 +0.0000E+00 +7.5000E+02
9 +5.0000E+02 +0.0000E+00 +5.0000E+02
9
11 5  29  0 25  0 27 54  0 52  0 51 41  0  1
11
2      6 0 0 0 0 0      1 --- 2 ND SUBSTRUCTURE ---
1 6   4  3  0  6  5  0  8  7  0 18 17  0 16 15  0  0
1 6   14 13  0
1 +7.5000E+03 +0.3000E+00 +6.0000E+00 +1.5000E+03 +0.0000E+00 +2.0000E+02
1 +1.5000E+03 +5.0000E+02 +2.0000E+02 +1.1250E+03 +2.5000E+02 +2.0000E+02
1
2 6   8  7  0 20 19  0 32 33  0 24 23  0 16 15  0  0
2 6   18 17  0
2 +7.5000E+03 +0.3000E+00 +6.0000E+00 +1.5000E+03 +5.0000E+02 +2.0000E+02
2 +7.5000E+02 +5.0000E+02 +2.0000E+02 +1.1250E+03 +2.5000E+02 +2.0000E+02
2
3 6   32 33  0 30 31  0 29 28  0 22 21  0 16 15  0  0
3 6   24 23  0
3 +7.5000E+03 +0.3000E+00 +6.0000E+00 +7.5000E+02 +5.0000E+02 +2.0000E+02
3 +7.5000E+02 +0.0000E+00 +2.0000E+02 +1.1250E+03 +2.5000E+02 +2.0000E+02
3
4 6   29 28  0 12 11  0  4  3  0 14 13  0 16 15  0  0
4 6   22 21  0
4 +7.5000E+03 +0.3000E+00 +6.0000E+00 +7.5000E+02 +0.0000E+00 +2.0000E+02
4 +1.5000E+03 +0.0000E+00 +2.0000E+02 +1.1250E+03 +2.5000E+02 +2.0000E+02
4
10 5   8  0  9  0 10 32  0 35  0 34 20  0  0
10
10 +7.5000E+03 +0.3000E+00 +3.0000E+00 +2.0000E+02 +0.0000E+00 +7.5000E+02
10 +5.0000E+02 +0.0000E+00 +5.0000E+02
10
12 5   4  0  1  0  2 29  0 25  0 26 12  0  1
12
1      34      18      8      8
28 29 30 31 32 33 25 35 53 54 55 56 57 58 52 59 27 36 37
38 39 40 41 42 43 44 45 46 47 48 49 50 51 60

```


A SEF - 3

DATE /

PROBLEM NBR 2

SHEET 1 out of 10

FORM 1

DIMENSIONS AND TITLE

NS = 2 NT = 60

TITLE BOX BEAM ANALYSIS - 60 GEN. COORDINATES

TITLE QUADRATIC COMPATIBLE DISPLACEMENT FIELD - 2 S. STR.

FORMAT (I3, IX, I3 / I3A6 / I3A6)

DATE
 PROBLEM NBR
 SHEET 2 out of 10

FORM 2

SUBSTRUCTURE NBR 1

SUBSTRUCTURE DIMENSIONS, PRINTING OPTIONS, TYPE OF ANALYSIS							
NOS	NEL	NOP(1)	NOP(2)	NOP(3)	NOP(4)	NOP(5)	ITYPNN
1	6	0	0	0	0	0	1
FORMAT (I3, 3X, I3, 5(1X, I1), 3X, I3)							

DATE		PROBLEM NBR		FORM 3		SHEET: 3 OUT OF 10																																	
NOEL		ITYP		LOCATION VECTORS FOR ELEMENTS OF SUBSTRUCTURE													ISIMPL		ISTRES																				
				LOCAL (I)																																			
				8	12	15	16	19	20	23	24	27	28	31	32	35	36	39	40	43	44	47	48	51	52	55	56	59	60	63	64	67	72	80					
1	3	5	6	8	12	15	16	19	20	23	24	27	28	31	32	35	36	39	40	43	44	47	48	51	52	55	56	59	60	63	64	67	72	80					
5	6	6	6	29	28	28	0	30	30	31	31	0	32	32	33	33	33	0	38	38	37	37	0	44	44	0	44	43	43	0	0	0	0	0	0				
6	6	6	6	40	39	39	0	46	46	45	45	0	58	58	57	57	0	48	48	47	47	0	44	44	0	44	43	43	0	0	0	0	0	0	0	0			
7	6	6	6	38	37	37	0	56	56	55	55	0	54	54	53	53	0	50	50	49	49	0	44	44	0	44	43	43	0	0	0	0	0	0	0	0	0		
8	6	6	6	54	53	53	0	41	41	42	42	0	29	29	28	28	0	40	40	39	39	0	44	44	0	44	43	43	0	0	0	0	0	0	0	0	0	0	
9	5	5	5	32	32	32	35	0	0	36	36	58	58	0	59	59	0	60	60	46	46	0																	
11	5	5	5	29	29	29	25	0	0	27	27	54	54	0	52	52	0	51	51	41	41	0																	

FORMAT (I 3, I X, I 2, I X, 15(I 4), 4 X, I 1 / 7 X, 15(I 4), 12 X, I 1)

DATE

PROBLEM NBR

FORM 5

SHEET 5

OUT OF 10

SUBSTRUCTURE NBR

1

SUBSTRUCTURE FIXATION AND CONDENSATION				
NOS1	NCS	NCC	NCF	NCR
1	34	18	8	8
5	11	15	21	25
			31	35
			41	45

FORMAT (5(15,5x))

LOCATION VECTOR FOR A SUBSTRUCTURE

	8	9	12	13	16	17	20	21	24	25	28	29	32	33	35	36	37	40	41	44	45	46	49	52	53	56	57	60	61	64	65	68	69	72	73	76	77	80		
28			29	30	31	32	33	35	36	37	40	41	44	45	46	49	52	53	56	57	60	61	64	65	68	69	72	73	76	77	80									
38			39	40	41	42	43	44	45	46	47	48	49	50	51	52	53	56	57	58	59	60	61	64	65	68	69	72	73	76	77	80								

FORMAT (4x, 1914)

DATE

PROBLEM NBR

SHEET 6 out of 10

FORM 2

SUBSTRUCTURE NBR

2

SUBSTRUCTURE DIMENSIONS, PRINTING OPTIONS, TYPE OF ANALYSIS

NOS	NEL	NOP(1)	NOP(2)	NOP(3)	NOP(4)	NOP(5)	ITYPAN
2	6	0	0	0	0	0	1

FORMAT (I3, 3X, I3, I3, 5(IX, I1), 3X, I3)

DATE

PROBLEM NBR

FORM 4

SHEET : 8

OUT OF 10

E L A S T I C A N D G E O M E T R I C D A T A F O R S U B S T R U C T U R E N B R 2

NOEL	15 17	27 29	D A T A	39 41	(SEE S E Q U E N C I N G S)	51 53	63 65	75
1	7500. 1500.	.3 500.	3. 200.	1500. 1125.	0. 250.	200. 200.		
2	7500. 750.	.3 500.	3. 200.	1500. 1125.	500. 250.	200. 200.		
3	7500. 750.	.3 0.	3. 200.	750. 1125.	500. 250.	200. 200.		
4	7500. 1500.	.3 0.	3. 200.	750. 1125.	0. 250.	200. 200.		
10	7500. 500.	.3 0.	3. 500.	200.	0.	750.		
/								
.								

FORMAT (3 X, 6 (IX, 1 P E 11.4))

DATE _____ PROBLEM NBR _____ FORM 5 SHEET 9 out of 10

SUBSTRUCTURE NBR 2

SUBSTRUCTURE FIXATION AND CONDENSATION				
NOS1	NCS	NCC	NCF	NCR
2	34	0	0	34
1	5 11 15 21	25 31	35 41	45

FORMAT (5(I5,SX))

LOCATION VECTOR FOR A SUBSTRUCTURE																																									
	8	9	12	13	16	17	20	21	24	25	28	29	32	33	36	37	40	41	44	45	48	49	52	53	56	57	60	61	64	65	68	69	72	73	76	77	80				
1	2	3	4	5	6	7	8	9	10	11	12	13	14	15	16	17	18	19	20	21	22	23	24	25	26	27	28	29	30	31	32	33	34	35	36	37	38	39	40		
20	21	22	23	24	25	26	27	28	29	30	31	32	33	34	35	36	37	38	39	40	41	42	43	44	45	46	47	48	49	50	51	52	53	54	55	56	57	58	59		

FORMAT (4X, 19I4)

ERRATA SHEET.

<u>Page</u>	<u>Line</u>	<u>Read</u>
II	I	$\sum_s \gamma_s P_s$
2-3	6	$U = \frac{1}{2} \int_{x_1}^{x_2} \epsilon_x \sigma_x S(x) dx = \frac{1}{2} q' K q$
2-I4	I6	$\tau_{xz} (+a) = E^o \frac{1-\nu}{2} \left(\frac{u_1}{h} + \phi_1 \right)$
2-I4	I7	$\tau_{xz} (o) = E^o \frac{1-\nu}{8} \left(2 \frac{u_1}{h} + 3 \frac{w_1}{a} - \phi_1 + 2 \frac{u_2}{h} - 3 \frac{w_2}{a} - \phi_2 \right)$
2-I4	I8	$\tau_{xz} (-a) = E^o \frac{1-\nu}{2} \left(\frac{u_2}{h} + \phi_2 \right)$
2-I5	3	

$$T = \frac{E}{1-\nu^2}$$

$\frac{1}{2a}$	$-\frac{1}{2a}$	o	o	o	o
$\frac{\nu}{2a}$	$-\frac{\nu}{2a}$	o	o	o	o
$\frac{1-\nu}{2h}$	o	o	o	$\frac{1-\nu}{2}$	o
$\frac{1-\nu}{4h}$	$\frac{1-\nu}{4h}$	$\frac{3(1-\nu)}{8a}$	$-\frac{3(1-\nu)}{8a}$	$\frac{\nu-1}{8}$	$\frac{\nu-1}{8}$
o	$\frac{1-\nu}{2h}$	o	o	o	$\frac{1-\nu}{2}$

2-40 20 $M_1 = \int_{-h}^{+h} (\sigma_x)_{x=+a} z dz = 4 h (\beta_1 + a \beta_2)$

2-40 2I $M_2 = \int_{-h}^{+h} (\sigma_x)_{x=-a} z dz = 4 h (-\beta_1 + a \beta_2)$

Page Line Read

2-4I I5

$$S = \begin{array}{|c|c|c|} \hline \frac{6z}{h^2} & \frac{6zx}{h^2} & 0 \\ \hline 0 & 0 & 0 \\ \hline 0 & -\frac{3z^2}{h^2} & 1 \\ \hline \end{array}$$

2-4I I9 $\frac{1}{2} \iint \sigma' M^{-1} \sigma \, dx dz = \frac{1}{2} b' F b$

2-4I 2I $F = \iint S' M^{-1} S \, dx dz$

Figure F.3.77. EQWB-383 idealization

In Appendix, second page of elements library informations, displacement sequence of quadratic compatible spar should read (line I9)

$$(u_3 \ v_3 \ w_1 \ \frac{\partial w}{\partial x_1} \ \frac{\partial w}{\partial y_1} \ u_5 \ v_5 \ w_2 \ \frac{\partial w}{\partial x_2} \ \frac{\partial w}{\partial y_2} \ u_4 \ v_4)$$

Figure F.A.4. The sense of one arrow should be change for loading case 2

Input data sheet of problem number 2 should be reordered

so that :

sheet 5 out of I0	becomes	sheet 8 out of I0
sheet 6 out of I0	becomes	sheet 5 out of I0
sheet 7 out of I0	becomes	sheet 6 out of I0
sheet 8 out of I0	becomes	sheet 7 out of I0 .